

# DISSERTATION

---

## Dicke superradiance as a nondestructive probe for optical lattices

---

Von der Fakultät für Physik  
der Universität Duisburg-Essen  
genehmigte Dissertation  
zur Erlangung des Grades  
Dr. rer. nat.  
von

**Dipl.-Phys. Nicolai ten Brinke**  
aus Krefeld

<b>Tag der Disputation:</b>	26. Oktober 2016
<b>Erstgutachter:</b>	Prof. Dr. Ralf Schützhold
<b>Zweitgutachter:</b>	Prof. Dr. Eric Akkermans
<b>Drittgutachter:</b>	Prof. Dr. Jürgen König
<b>Kommissionsvorsitzender:</b>	Prof. Dr. Uwe Bovensiepen
<b>weiterer Prüfer:</b>	Prof. Dr. Klaus Hornberger

Hiermit versichere ich, die vorliegende Dissertation selbstständig, ohne fremde Hilfe und ohne Benutzung anderer als den angegebenen Quellen angefertigt zu haben. Alle aus fremden Werken direkt oder indirekt übernommenen Stellen sind als solche gekennzeichnet. Die vorliegende Dissertation wurde in keinem anderen Promotionsverfahren eingereicht. Mit dieser Arbeit strebe ich die Erlangung des akademischen Grades "Doktor der Naturwissenschaften" (Dr. rer. nat.) an.

---

Datum

---

Nicolai ten Brinke



## List of publications

The following articles were published in peer-reviewed journals, based on results developed in this dissertation:

- [1] N. ten Brinke, R. Schützhold, “*Dicke superradiance as a nondestructive probe for quantum quenches in optical lattices*”, *Physical Review A* **92**, 013617 (2015).
- [2] N. ten Brinke, R. Schützhold, “*Dicke superradiance as nondestructive probe for the state of atoms in optical lattices*”, *European Physical Journal D* **70**, 102 (2016).

Beyond the scope of the work presented here, the following articles have been composed as part of the doctoral studies:

- [3] N. ten Brinke, R. Schützhold, D. Habs, “*Feasibility study of a nuclear exciton laser*”, *Physical Review A* **87**, 053814 (2013).
- [4] N. ten Brinke, M. Ligges, U. Bovensiepen, R. Schützhold, “*Multiple particle-hole pair creation in the Fermi-Hubbard model by a pump laser*”, submitted to *Physical Review B* (2016), arXiv:1602.00871.

For a complete overview over my scientific activities, please refer to my homepage at [udue.de/tenbrinke](http://udue.de/tenbrinke).



## Acknowledgments

First of all, I want to express my gratitude to my supervisor Ralf Schützhold for giving me the opportunity to work on research projects in the interdisciplinary field between quantum optics and ultracold quantum gases. His door was always open for scientific discussion, and his support and guidance at any time were invaluable assets to the creation of this Thesis. I was often amazed by his deep insights and in particular by his impressive intuitive understanding of complex physical phenomena.

Special appreciation goes to my colleagues Konstantin Krutitsky and Friedemann Queisser for many fruitful and enlightening discussions about the topics covered in this work. I also want to thank all the other current and former members of the research group, especially Malte Linder, Christian Schneider, Johannes Oertel, Sascha Lang, Andreas Osterloh, Nikodem Szpak, Piotr Marecki, Patrick Navez and Kay Eibl, for promoting an exceptional atmosphere of creativity and readiness to help. You all have been great fellows.

Furthermore, I appreciate the financial support from the Sonderforschungsbereich Transregio 12 “Symmetries and Universality in Mesoscopic Systems” of the Deutsche Forschungsgemeinschaft.

Also, I am indebted to Nigel Beckett for carefully proofreading the entire Thesis.

Finally, I want to express my sincere thanks to my family members and friends for their support and encouragement during my studies. In particular, I am deeply grateful to my “girls” Monika and Alina for their love, patience and continuous support in all non-scientific matters.

## Abstract

We develop a new, comprehensive method to nondestructively probe ultracold atoms in optical lattices, utilizing the unique features of Dicke superradiance. In particular, we propose a pump-and-probe scheme, in which a single photon is collectively and coherently absorbed, then stored for a variable period of time, and later collectively re-emitted by an ensemble of atoms in an optical lattice.

For an immovable collection of atoms, directed superradiant re-emission is predicted due to the coherence of the atomic Dicke state, which is created by the collective absorption of the photon. In contrast, we consider moving atoms in an optical lattice, modeled via the two most commonly studied lattice models – the Bose-Hubbard model and the Fermi-Hubbard model. In general, these lattice dynamics impair the spatial phase coherence of the Dicke state, which in turn modifies the superradiant emission characteristics. Conversely, measuring the emission characteristics allows to obtain information about the quantum state of the atoms in the optical lattice. As a main part of this Thesis, we study in detail the emission characteristics for different initial lattice states and discuss whether they can be distinguished using the suggested probing scheme. We find that it is possible to differentiate between excited states and the superfluid ground state in the case of bosonic atoms, while the Mott-Néel state can be distinguished from the metallic ground state in the case of fermions.

Furthermore, the pump-and-probe scheme is predestined to investigate nonequilibrium phenomena, such as quantum phase transitions. Thus, we explore whether an adiabatic phase transition from the Mott insulator phase to the superfluid or metallic phase, respectively, can be distinguished from a sudden quench.

As opposed to almost all commonly used detection techniques, such as time-of-flight measurements or in situ imaging, the proposed probing scheme can be considered nondestructive, as the coherent interaction with a single photon does not destroy the phase coherence of the optical lattice state.

Finally, we study a modified probing scheme employing classical laser fields instead of single-photon absorption and emission, demonstrating that it reproduces the features of the single-photon probe, while it is probably easier to implement experimentally. We give further suggestions on experimental realization.



## Zusammenfassung

Wir entwickeln eine neue, umfassende Methode zur zerstörungsfreien Messung ultrakalter Atome in optischen Gittern, die auf den spezifischen Eigenschaften von Dicke-Superradianz basiert. Insbesondere schlagen wir ein Pump-Probe-Schema vor, in dem ein einzelnes Photon von einem Ensemble von Atomen in einem optischen Gitter zunächst kollektiv und kohärent absorbiert, dann für eine variable Zeitspanne gespeichert, und schließlich kollektiv reemittiert wird.

Im Falle unbeweglicher Atome erwartet man gerichtete, superradiante Emission aufgrund der Kohärenz des atomaren Dicke-Zustands, der durch die kollektive Absorption des Photons erzeugt wird. Dementgegen betrachten wir jedoch bewegliche Atome in einem optischen Gitter, die wir durch die zwei am häufigsten betrachteten Modellsysteme beschreiben – das Bose-Hubbard-Modell und das Fermi-Hubbard-Modell. Im Allgemeinen beeinträchtigt die Gitterdynamik die räumliche Phasenkohärenz des Dicke-Zustands, wodurch wiederum die superradianten Emissionseigenschaften verändert werden. Umgekehrt können über die Messung der Emissionseigenschaften Rückschlüsse auf den Quantenzustand der Atome im optischen Gitter gezogen werden. Im Hauptteil der vorliegenden Dissertation untersuchen wir detailliert die Emissionseigenschaften für verschiedene Anfangszustände des Gitters und diskutieren ob diese mit der vorgestellten Messmethode unterschieden werden können. Dabei zeigen wir, dass im Falle von bosonischen Atomen zwischen angeregten Zuständen und dem superfluiden Grundzustand differenziert werden kann, während bei Fermionen der Mott-Néel-Zustand vom metallischen Grundzustand unterschieden werden kann.

Ferner ist das Pump-Probe-Schema prädestiniert zur Erforschung von Nichtgleichgewichts-Phänomenen, wie z.B. Quanten-Phasenübergängen. Deshalb untersuchen wir, inwiefern ein adiabatischer Phasenübergang von einem Mott-Isolator zur superfluiden bzw. metallischen Phase von einem abrupten (d.h. nichtadiabatischen) Übergang unterschieden werden kann.

Im Gegensatz zu fast allen gängigen Messmethoden, wie z.B. Time-of-Flight-Messungen oder In-situ-Abbildungen, kann die vorgestellte Messmethode als zerstörungsfrei angesehen werden, da die kohärente Interaktion mit einem einzelnen Photon nicht die Phasenkohärenz des Zustands des Gitters zerstört.

Zuletzt untersuchen wir eine abgewandelte Messmethode, die klassische Laserfelder anstatt einzelner Photonen einsetzt, und zeigen, dass diese vergleichbare Eigenschaften aufweist, während sie womöglich einfacher experimentell umzusetzen ist. Außerdem geben wir weitere Anregungen zur experimentellen Realisierung.



# Contents

<b>1. Introduction</b>	<b>13</b>
1.1. Preface . . . . .	13
1.2. Dicke superradiance . . . . .	22
1.2.1. Directed spontaneous emission . . . . .	22
1.2.2. Quasispin formalism . . . . .	25
1.2.3. Superradiance conditions . . . . .	27
1.3. Ultracold atoms in optical lattices . . . . .	29
1.3.1. Optical lattices . . . . .	29
1.3.2. Bose-Hubbard model . . . . .	31
1.3.3. Fermi-Hubbard model . . . . .	37
1.4. Synthesis: Lattice models coupled to light . . . . .	41
1.4.1. Hamiltonian description of the coupled system . . . . .	41
1.4.2. Description in the momentum space . . . . .	45
<b>2. Detection of stationary lattice states</b>	<b>51</b>
2.1. Single-photon probing scheme . . . . .	51
2.1.1. Initial state of the optical lattice . . . . .	51
2.1.2. Collective absorption of the probe photon . . . . .	52
2.1.3. Collective re-emission of the probe photon . . . . .	53
2.1.4. Combined emission probability density . . . . .	53
2.2. Detection in the separable state regime . . . . .	56
2.3. Detection in the weak interactions regime . . . . .	60
2.3.1. Bose-Hubbard model . . . . .	65
2.3.2. Fermi-Hubbard model . . . . .	74
2.4. Summary of the detection of stationary lattice states . . . . .	80
<b>3. Detection of quantum phase transitions</b>	<b>83</b>
3.1. Probing scheme to detect quantum phase transitions . . . . .	83
3.2. Absorption in the separable state regime . . . . .	85
3.3. Emission after a sudden phase transition . . . . .	86
3.4. Emission after an adiabatic phase transition . . . . .	91
3.4.1. Emission after adiabatic transition in the bosonic case . . . . .	91

3.4.2.	Emission after adiabatic transition in the fermionic case . . .	97
3.5.	Summary of the detection of phase transitions . . . . .	100
<b>4.</b>	<b>Detection via classical laser fields</b>	<b>101</b>
4.1.	Probing scheme employing classical laser fields . . . . .	101
4.2.	Hamiltonian and excitation process . . . . .	103
4.3.	De-excitation process with arbitrary wave vector . . . . .	105
4.3.1.	De-excitation dynamics applied to the $\hat{\Sigma}_\alpha^z$ operator . . . . .	105
4.3.2.	Interpretation and expectation values . . . . .	107
4.4.	De-excitation process after tunneling dynamics . . . . .	109
4.4.1.	Tunneling dynamics applied to the $\hat{\Sigma}_\alpha^z$ operator . . . . .	109
4.4.2.	De-excitation dynamics applied after tunneling . . . . .	110
4.4.3.	Interpretation and expectation values . . . . .	112
4.5.	Summary of the detection via classical laser fields . . . . .	117
<b>5.</b>	<b>Experimental realization</b>	<b>119</b>
<b>6.</b>	<b>Conclusions</b>	<b>125</b>
<b>A.</b>	<b>Appendix</b>	<b>129</b>
A.1.	$SU(2)$ algebra property of the quasispin operators . . . . .	129
A.2.	Angular momentum algebra of the Pauli operators . . . . .	130
A.3.	Four-point correlator in the lattice site basis . . . . .	132
A.4.	Matrix elements of the on-site repulsion term . . . . .	133
A.5.	Commutators of $\hat{\Sigma}^x(\boldsymbol{\kappa}_{\text{out}})$ and $\hat{\Sigma}^y(\boldsymbol{\kappa}_{\text{in}})$ . . . . .	135
A.6.	Commutators of $\hat{\Sigma}^x(\boldsymbol{\kappa}_{\text{in}})$ and $\hat{\Sigma}^y(\boldsymbol{\kappa}_{\text{in}})$ . . . . .	138
A.7.	Real and imaginary part of the phase sum . . . . .	141
	<b>Bibliography</b>	<b>142</b>

# 1. Introduction

## 1.1. Preface

### Ultracold atoms in optical lattices

Optical lattices are spatially periodic intensity patterns that emerge from the interference of counter-propagating laser beams [5, 6]. As such, regular arrays of microscopic potentials are formed, constituting an artificial crystal of light [6, 7]. The breakthrough discovery that optical lattices are able to confine ultracold neutral atoms via the interaction with an induced electric dipole moment [8, 9] opened up new possibilities to study many-body quantum physics with unprecedented clarity [6, 7, 10]. On the one hand, it is relatively easy to control the important parameters of these ideal model systems [11, 12], such as the periodic geometry, the lattice potential depth and the interaction between the atoms. On the other hand, the quantum gas in the optical lattice is well isolated from the environment and can be cooled down to very low (nanokelvin) temperatures [6, 7], which prevents unsolicited decoherence effects and allows to enter regimes which are not accessible via condensed matter systems [12, 13]. Therefore, not only do ultracold atoms in optical lattices [14] enable to perform a broad range of experiments to explore fundamental quantum many-body effects, but they do also constitute versatile quantum simulators [12] (e.g., for problems in condensed matter physics [13, 14]) in their originally conceived form [15–17] and are further considered in the field of quantum information processing [6, 12]. For example, it was shown that it is possible to efficiently create highly entangled cluster states of many atoms in optical lattices via controlled coherent collisions [18, 19], as a suitable resource for, e.g., a one-way quantum computer [20].

As a prototypical example of the fundamental quantum many-body phenomena which can be observed exceptionally well, quantum phase transitions [21] were explored in a wide range of bosonic and fermionic optical lattice configurations. In a seminal paper, D. Jaksch *et al.* [11] suggested that the (zero temperature) superfluid to Mott insulator transition of bosons with short-ranged repulsive interactions in periodic potentials, long-predicted by the Bose-Hubbard model [22], can be realized with ultracold bosonic atoms in optical lattices [23, 24]. For weak interactions and a shallow periodic potential, tunneling processes dominate (i.e., the on-

site number of bosons fluctuates) and all bosons condense into the same quantum ground state. In this superfluid phase, they form a macroscopic, phase-coherent matter wave, which spans the entire lattice. In the case of strong interactions and a deep periodic potential, on the other hand, the bosons localize at individual lattice sites in a Mott insulator state, which is characterized by a fixed (i.e., no fluctuations) and uniform number of bosons per lattice site, as well as by a gap in the excitation spectrum and zero compressibility. As a unique feature of optical lattices, the depth of the lattice potential can directly be controlled by varying the laser intensities [11,12], rendering it possible to routinely induce the superfluid to Mott insulator phase transition in optical lattice experiments [25–27]. This was first demonstrated in a three-dimensional optical lattice by M. Greiner *et al.* [25] – see Figure 1.1, and subsequently in one-dimensional [26] and two-dimensional optical lattices [27].

Fermions in periodic potentials, on the other hand, have long been studied in the context of condensed matter physics [28,29]. While originally developed to describe the motion of many electrons between the atoms of a crystalline solid [30], the famous (Fermi-)Hubbard model was rediscovered to be ideally realized via ultracold fermionic atoms in optical lattices [12, 31]. Similar to the Bose-Hubbard model, the Fermi-Hubbard model predicts the formation of a (Mott) insulator state in the case of strong repulsive interactions. But in the case of weak interactions, the fermions arrange in a metallic state, as a superfluid state is forbidden by the Pauli exclusion principle. Analogous to the superfluid to Mott insulator transition in the bosonic case, a metal-insulator transition [28,29] can thus be investigated with fermionic atoms in optical lattices. The Fermi-Hubbard model was realized experimentally, e.g., in a three-dimensional optical lattice [31,32]. Metallic, band-insulating [32,33] and Mott-insulating phases [34,35] have been observed experimentally – see Figure 1.2, for example.

### **Established measurement techniques**

Most prominently, the superfluid to Mott insulator phase transition was detected via time-of-flight measurements, where the periodic potential is suddenly switched off, such that the initial momentum is projected onto free particle states [25–27]. The expanding atom cloud then forms a matter-wave interference pattern, which can be detected via resonant absorption imaging. While the occurrence of sharp peaks in the interference pattern is generally interpreted as a signature of the phase-coherent superfluid state [25] (although not unambiguously so [36]), a broad max-

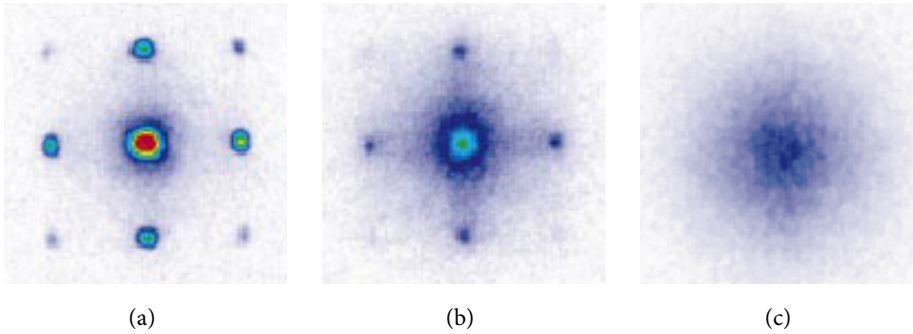


FIGURE 1.1. – Steps of the superfluid to Mott insulator phase transition observed via time-of-flight measurements. After suddenly releasing bosonic atoms from a three-dimensional cubic optical lattice, absorption images of the resulting matter-wave interference patterns are taken: for shallow potential depths (before the sudden release) the bosons are in the superfluid phase (a), which is accompanied by the occurrence of sharp peaks. Increasing the lattice potential depth to cross the quantum critical point (b), the sharp peaks disappear and a broad maximum indicates a Mott-insulating state (c). The figures were taken from [25].

imum is obtained for an incoherent Mott-insulating state – see Figure 1.1. The time-of-flight technique has also been combined with, e.g., momentum-resolved Bragg spectroscopy [37] to investigate the excitation spectra in the superfluid and the Mott-insulating regime [38, 39]. The observation of a broad continuum of excitations in the superfluid phase, as opposed to the discrete spectrum which characterizes the Mott insulator state, provides a complementary method to detect the quantum phase transition [25, 26]. Quite remarkably, time-of-flight measurements directly image the Fermi surface, i.e., the population within the first Brillouin zone, in the case of fermionic atoms in optical lattices [31, 32].

On the other hand, another well-established detection method is direct *in situ* imaging of bosonic [40–43] or fermionic [33, 35] atoms in optical lattices. While early attempts focused on observing the compressibility (which enables to distinguish between different quantum phases) of the atoms in the optical lattice via imaging the atomic cloud size [33, 40], recent experiments were able to detect the atom distribution with single-atom and single-site resolution [35, 41–43] – see Figure 1.2. Apart from visualizing the atom distribution for various quantum phases, the *in situ* images also allow to infer the temperature of the atomic cloud, e.g., via the radial occupation profile [35, 40, 42].

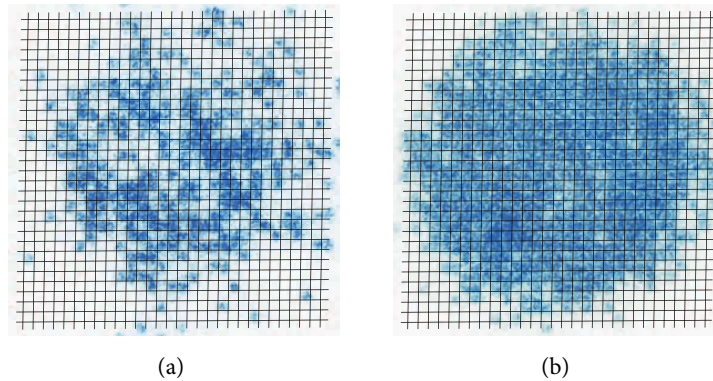


FIGURE 1.2. – Site-resolved *in situ* images of ultracold fermionic atoms in a two-dimensional quadratic optical lattice. Depending on the strength of the repulsive interactions between the fermionic atoms e.g. metallic phases (a) or Mott-insulating phases (b) can be observed. Note that double occupations appear as empty sites because of experimental limitations. The figures were taken from [35].

These two widely-used measurement schemes<sup>1</sup> provide extensive insights as they exhibit in detail either the momentum distribution (time-of-flight measurements, Figure 1.1) or the position distribution (*in situ* imaging, Figure 1.2) of the atoms in the optical lattice. However, in both cases, the measurement procedure irreversibly destroys the many-body quantum state. While the lattice potential is abruptly switched off for a time-of-flight measurement, it is deepened more than a hundred-fold (“frozen”) during *in situ* imaging in order to pin the atoms to the current lattice sites, while illuminating them with about  $10^3$ - $10^4$  photons per atom [35, 42, 43]. Of course, any phase coherence of the quantum state is lost after this procedure. For that reason, a number of alternative, less destructive measurement schemes were explored.

### **Nondestructive measurement proposals**

On the one hand, Bragg scattering in free space has been used as a diagnostic tool already in early studies on optical lattices with very low filling factors, e.g., to measure the fraction of atoms which have been trapped and their long-range spatial or-

<sup>1</sup>And also other, more exotic measurement schemes, such as high-resolution microwave spectroscopy to probe the spatial distribution of the atoms trapped in the optical lattice via density-dependent transition frequency shifts [44], or Bragg scattering of photons from the expanding atom cloud after switching off the periodic potential to probe the time evolution of the ground state atomic wave functions [45].



der [46, 47]. However, despite recent theoretical studies on the detection of different quantum phases [48, 49] and encouraging recent experiments [50, 51], the superfluid to Mott insulator phase transition has not yet been detected via free-space Bragg scattering, as far as we know. Closely related, off-resonant collective scattering of light from the atoms in a one-dimensional optical lattice into a *cavity* has also been investigated as a way to nondestructively monitor atom quantum statistics [52–54]. These proposals are based on the idea that scattering from different atomic quantum states creates different quantum states of the scattered light in the cavity – thus allowing to characterize the atomic quantum state only by measuring the cavity light field. For transverse probing, for example, no photons are scattered into the cavity from a Mott insulator state, while the number of scattered photons is proportional to the atom number in the case of a superfluid state. Comparable results were also obtained in a similar approach [55] by placing the optical lattice inside a ring resonator and studying the reflection of two counter-propagating modes. Quite recently, a corresponding nondestructive measurement of the dynamic structure factor of a quantum gas via light scattering into an optical cavity was realized experimentally [56] – evidencing the relevance of these quantum optical approaches. Inspired by the proposals on off-resonant scattering, resonant interactions between cavity photons and atoms in an optical lattice have also been considered lately as a tool for the nondestructive detection of superfluidity [57]. Resorting to the rich phase diagram of the two-band Bose-Hubbard model coupled to cavity light fields, which was previously elaborated on in [58–60], it was pointed out that Mott-insulating and superfluid phases are accompanied by different photon numbers, such that photon counting can be used to distinguish them.

On the other hand, a nondestructive, optical pump-and-probe detection scheme was put forward [61], which allows to extract information on the time evolution of atomic two-time correlations in fermionic optical lattices. As opposed to scattering, a coherent light pulse is *stored* in the quantum gas and retrieved at a later time after a variable interval, during which it is exposed to decoherence. Instead of the scattering or storage of light, also the interaction with matter was studied as a nondestructive probe for optical lattices [62–64]. For example, it was proposed that the interference of the trapped atoms with a reference Bose-Einstein condensate allows the measurement of space-time correlators of arbitrary order [62]. Otherwise, matter-wave scattering with slow atoms should allow to distinguish the many-body phases in an optical lattice, as they affect the inelastic scattering cross section [63, 64].

## Dicke superradiance

Independently of the advances in optical lattices, the intriguing effects of Dicke superradiance, as the collective and coherent spontaneous emission of radiation from an ensemble of excited two-level atoms, have been studied extensively since their first prediction [65]. In this seminal paper, R.H. Dicke investigated the emission of photons from a gas of large or small (compared to the emission wavelength) extent by regarding the whole gas as a single quantum many-body system which can be elegantly mapped to an angular momentum formalism. He discovered that in the case of coherent emission, the individual atoms cooperate such that the spontaneous radiation probabilities are enhanced by a factor which can be (at most) proportional to the square of the number of atoms involved, i.e., substantially larger than the incoherent radiation probabilities. As another astonishing effect, he showed that for a gas of large extent the (superradiant) emission occurs coherently only in one particular direction. The work of Dicke was then later generalized, e.g., to obtain the time evolution and details on the directional character of the radiated intensity for extended systems [66]. As an important result, a superradiant system excited by a plane wave always shows an emission maximum in the same direction as the exciting wave. While the previous work mostly included semiclassical approximations for a large number of excited atoms, Scully *et al.* sparked renewed interest in the field with their influential work on directed spontaneous emission [67], in which they focused on a fully quantum mechanical description of *single-photon* absorption and subsequent superradiant emission in the same direction. Important follow-ups [68, 69] studied correlated spontaneous emission between the fields of quantum optics (Dicke superradiance) and nuclear physics (forward scattering of  $\gamma$ -radiation, see also [70]), estimated the effect of virtual processes (e.g., Lamb shift) on the collective decay rate (which turned out to be small), or gave an intuitive physical explanation for the superradiance of states with no macroscopic dipole moment via a quantum multipath interference approach [71]. Recently, the enhanced emission probability due to single-photon superradiance was confirmed experimentally [72]. By controllably changing the number of atoms and direct measurement of the emission probability, the authors showed that the spontaneous decay rate is indeed proportional to the number of atoms in the ensemble, “presenting the last piece of evidence for the superradiant nature of such a process”.

### Dicke superradiance as a nondestructive probe

The idea which forms the basis of this dissertation is to employ the features of Dicke superradiance [65, 66, 73], i.e., the enhanced emission probability and directionality in coherent spontaneous emission [67–69], as a nondestructive probe for the quantum state of ultracold, bosonic or fermionic atoms in optical lattices. In anticipation of the upcoming detailed description and derivation in the course of this Thesis, let us briefly sketch the envisaged probing scheme, as its basic concept can be understood quite intuitively. The probing scheme consists of three steps, which are illustrated in Figure 1.3:

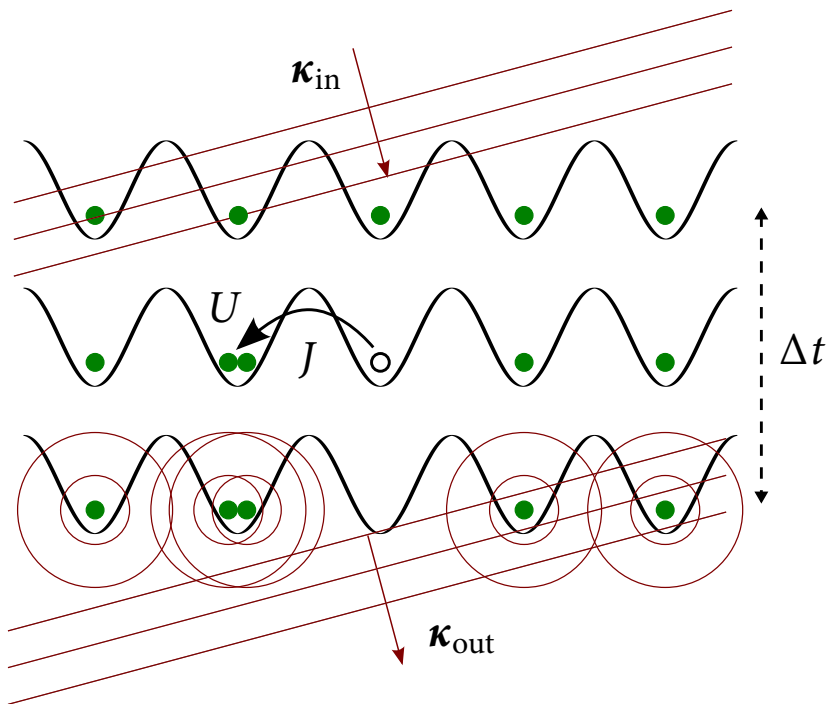


FIGURE 1.3. – Sketch of the envisaged probing sequence: In the first step, a probe photon with wave vector  $\kappa_{\text{in}}$  (red arrow with associated red wave fronts) is sent onto the optical lattice with an oblique incident angle. It is then absorbed by one of the atoms (green circles) in the optical lattice, “but we do not know which one” [67], resulting in collective absorption, i.e., a coherent superposition state with local spatial phases. Secondly, the atoms tunnel between different lattice sites (with the tunneling rate  $J$ , black arrow) and interact (with the on-site repulsion energy  $U$ ) according to the usual time evolution in the optical lattice during the waiting time  $\Delta t$ . As the tunneling of the atoms reduces the spatial phase coherence, the directed (i.e.,  $\kappa_{\text{out}} = \kappa_{\text{in}}$ ) spontaneous superradiant emission in the third step is presumably impaired.

*First of all*, an incoming probe photon with wave vector  $\kappa_{\text{in}}$  (depicted by a red arrow with associated red wave fronts) is absorbed collectively by an ensemble of atoms (green circles) in an optical lattice (black potential). According to the theory of directed spontaneous emission [67–69], this creates a “timed Dicke state” – a coherent superposition state which carries specific local phases depending on the atomic positions – among the atoms. Furthermore, if the atoms have not moved, the timed Dicke state decays via directed spontaneous (superradiant) emission in the same direction as the incoming photon  $\kappa_{\text{out}} = \kappa_{\text{in}}$ , which is a direct consequence of the coherence in their local spatial phases. In our case, on the contrary, the atoms in the optical lattice can tunnel between different lattice sites (black arrow) and interact (e.g., on-site repulsion of atoms at the same lattice site) during a waiting time  $\Delta t$  in the *second step*. Now, after the atoms have tunneled, their new positions do not match their local spatial phases anymore, thus reducing the coherence of the timed Dicke state – where the severity of this reduction is dependent on the initial quantum state and the overall parameters of the optical lattice (e.g., the tunneling rate  $J$  and the on-site repulsion energy  $U$ ). Thus, when the atoms finally collectively re-emit the photon in the *third step*, the emission characteristics from this tunneling-altered Dicke state are supposedly modified as compared to the case of immovable atoms. As a first guess, we would, e.g., assume a reduction in the directed (i.e., in the direction  $\kappa_{\text{out}} = \kappa_{\text{in}}$ ) superradiant emission probability, whose magnitude is proportional to the amount of tunneling that occurred during the waiting time  $\Delta t$  in between absorption and emission. Conversely, we could infer the amount of tunneling (or other information about the quantum state of the optical lattice and its parameters) from the measurement of the reduced superradiant emission probability. Generally, we want to address the question what can be learned about the quantum state of the optical lattice (or about quantum phase transitions) by observing the (decoherence-altered) emission characteristics.

In distinction from the previous proposals considering instantaneous off-resonant Bragg-type scattering into a cavity [52–56], we consider free-space superradiant absorption and (time-delayed) re-emission, employing a pump-and-probe scheme. Comparable to [61], our method is susceptible to time-resolved single-particle (and higher-order) correlation functions, which can provide additional information, e.g., of nonequilibrium dynamics. Going beyond [61], which focuses on fermions and the Bardeen-Cooper-Schrieffer state, we develop a general probing scheme utilizing Dicke superradiance in this Thesis, which enables to nondestructively probe both bosonic and fermionic optical lattices in a multitude of settings.

## Guide to the Thesis

This Thesis is structured as follows. In the remaining sections of the *first chapter*, we first give a brief introduction to the striking features of Dicke superradiance (section 1.2), on the one hand, and to the field of ultracold atoms in optical lattices, including the popular Bose- and Fermi-Hubbard models (section 1.3), on the other hand. The two ingredients are finally combined in section 1.4 when we introduce the basic model for the calculations in the following chapters. Among other important definitions and fundamental relations, the many-body Hamiltonian of the full system, i.e., incorporating both the full quantum mechanical description of the atom-field interaction as well as the lattice dynamics, is described in detail in this section. In the *second chapter*, we calculate a general expression for the emission probability in accordance with the situation depicted in Figure 1.3, i.e., after the collective absorption of a single photon and subsequent lattice dynamics during a waiting time  $\Delta t$  given by the (two-band) Bose-or Fermi-Hubbard model. We analyze the result for different parameter regimes of the optical lattice (i.e., strong or weak interactions) and for various initial states. Thereby we show that the proposed probing scheme allows to, e.g., distinguish thermal states from condensed states in the bosonic case or to differentiate between the Mott-Néel state and the metallic ground state in the case of fermions – thus enabling to infer the current parameter regime of the optical lattice. As another possible application, we explore in the *third chapter* if and how our single-photon probing scheme can detect signs of quantum phase transitions in the optical lattice. We find that it is possible to distinguish an adiabatic transition from a sudden transition in the bosonic case, but not in the case of fermionic atoms. In the *fourth chapter* we present a modified probing scheme, which replaces the single-photon absorption and directed spontaneous emission by the excitation and (stimulated) de-excitation via classical laser fields. The modified scheme is probably easier to implement experimentally, while it retains the key features. After giving suggestions for the experimental realization of the proposed probe in the *fifth chapter*, we eventually conclude and sum up the results of this Thesis in *chapter six*.

## 1.2. Dicke superradiance

As an indispensable ingredient of the nondestructive probing scheme which we will present in chapter 2, let us start with a brief introduction to Dicke superradiance. In short, Dicke superradiance [65] describes the collective and coherent absorption and spontaneous (re-)emission of (single) photons by an *ensemble* of atoms. In contrast to the case of a single atom, two astonishing effects arise due to the collective and coherent nature of the absorption and emission process [65, 66]. First, the spontaneous emission following the absorption of a single photon is *directed*, i.e., the photon is emitted predominantly with the same wave vector (and direction)  $\boldsymbol{\kappa}_{\text{out}} = \boldsymbol{\kappa}_{\text{in}}$  as the original photon [67, 68, 72]. Second, the *superradiant* spontaneous emission (i.e., the decay of the atomic excitation) happens much faster, or, in other words, the emission probability is significantly enhanced compared to the case of a single atom. Both effects and their origin will be explained in this section.

### 1.2.1. Directed spontaneous emission

The basic idea of directed spontaneous emission is illustrated in Figure 1.4. A single photon with wave vector  $\boldsymbol{\kappa}_{\text{in}}$  is absorbed collectively by an ensemble of  $S$  two-level atoms. Initially, all atoms are prepared in the ground state,  $|\sigma = 0\rangle = \prod_{\mu=1}^S |\text{gr}\rangle_{\mu}$ . A

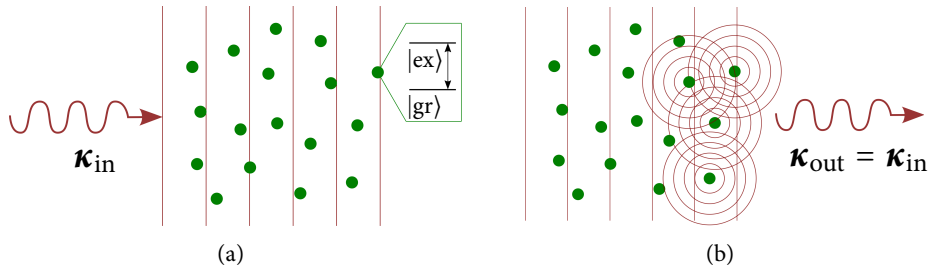


FIGURE 1.4. – Sketch of collective absorption (a), followed by directed spontaneous emission (b). First (a), an incident photon with wave vector  $\boldsymbol{\kappa}_{\text{in}}$  (red arrow with red wave fronts) is collectively absorbed by an ensemble of  $S \gg 1$  two-level atoms (green circles), which initially are all in the ground state  $|\text{gr}\rangle$ . After the absorption, one of the atoms is excited, “but we do not know which one” [67], generating a “timed Dicke” superposition state (1.4). When the atoms decay back to their ground state in a second step (b), their field amplitudes from spontaneous emission add up coherently in the same direction  $\boldsymbol{\kappa}_{\text{out}} = \boldsymbol{\kappa}_{\text{in}}$  of the original photon – leading to directed spontaneous emission. As a classical analog, one can think of the constructive interference of spherical waves (red circles) which are emitted from the individual atoms.

corresponding atom-field interaction Hamiltonian in the usual rotating-wave and

dipole approximation [74] is given by ( $\hbar = 1$ )

$$\hat{V}(t) = \sum_{\mu=1}^S \int d^3k g_k \hat{\sigma}_{\mu}^+ \hat{a}_{\mathbf{k}} e^{-i(\omega_k - \omega)t} \exp\{i\mathbf{k} \cdot \mathbf{r}_{\mu}\} + \text{H.c.} \quad (1.1)$$

This consists of a coupling constant  $g_k$ , the raising operator for the  $\mu$ -th atom  $\hat{\sigma}_{\mu}^+ = |\text{ex}\rangle_{\mu} \langle \text{gr}|_{\mu}$ , the annihilation operator  $\hat{a}_{\mathbf{k}}$  for a photon with wave vector  $\mathbf{k}$  and frequency  $\omega_k$  and – importantly – of a spatial phase factor depending on the wave vector  $\mathbf{k}$  and the position  $\mathbf{r}_{\mu}$  of the  $\mu$ -th atom. Furthermore,  $\omega$  denotes the energy difference between the two atomic levels  $|\text{gr}\rangle$  and  $|\text{ex}\rangle$ . The interaction Hamiltonian (1.1) can be understood as the sum over the individual atom-light interaction Hamiltonians for each single atom  $\mu$ . Assuming small coupling, we can regard the time evolution in first-order perturbation theory

$$\hat{U}(\tau_A) = \mathcal{T} \exp\left\{-i \int_0^{\tau_A} dt \hat{V}(t)\right\} \approx 1 - i \int_0^{\tau_A} dt \hat{V}(t). \quad (1.2)$$

Now we apply the time evolution to the initial state composed of the atoms in the ground state  $|\sigma = 0\rangle$  and the incident photon  $\hat{a}_{\kappa_{\text{in}}}^{\dagger} |0\rangle$ , assuming that the incident photon is in resonance with the atomic transition,  $\omega_{\text{in}} = \omega$ , for simplicity. We find for the first order term

$$|\Psi_{\text{abs}}\rangle = [\hat{U}(\tau_A) - 1] |\sigma = 0\rangle \otimes \hat{a}_{\kappa_{\text{in}}}^{\dagger} |0\rangle \approx -i\tau_A g_{\kappa_{\text{in}}} \sqrt{S} |\sigma = 1\rangle \otimes |0\rangle, \quad (1.3)$$

where  $|\sigma = 1\rangle$  is a normalized, coherent superposition of all the basis states where one atom is excited and the other  $S - 1$  atoms are in the ground state,

$$\begin{aligned} |\sigma = 1\rangle &= \frac{1}{\sqrt{S}} \sum_{\mu=1}^S \hat{\sigma}_{\mu}^+ \exp\{i\kappa_{\text{in}} \cdot \mathbf{r}_{\mu}\} |\sigma = 0\rangle = \frac{1}{\sqrt{S}} \sum_{\mu=1}^S \exp\{i\kappa_{\text{in}} \cdot \mathbf{r}_{\mu}\} |\text{ex}\rangle_{\mu} \prod_{v \neq \mu}^S |\text{gr}\rangle_v \\ &= \frac{1}{\sqrt{S}} \sum_{\mu=1}^S \exp\{i\kappa_{\text{in}} \cdot \mathbf{r}_{\mu}\} |\text{gr}\rangle_1 |\text{gr}\rangle_2 \dots |\text{ex}\rangle_{\mu} \dots |\text{gr}\rangle_{S-1} |\text{gr}\rangle_S. \end{aligned} \quad (1.4)$$

The coherent superposition state (1.4) is also called “timed Dicke state”<sup>2</sup> in the literature [67–69], where the adjunct “timed” refers to the local spatial phase factors  $\exp\{i\boldsymbol{\kappa}_{\text{in}} \cdot \mathbf{r}_\mu\}$ , which relate to the timing of the excitation of atoms located at position  $\mathbf{r}_\mu$ . The importance of these spatial phase factors cannot be stressed enough, as they allow the state to remember the wave vector  $\boldsymbol{\kappa}_{\text{in}}$  of the incoming photon and are thus ultimately responsible for the *directed* spontaneous emission.

Let us now corroborate this assertion by straightforwardly calculating the emission from the timed Dicke state (1.4), again in first-order perturbation theory,

$$|\Psi_{\text{emi}}\rangle = [\hat{U}(\tau_E) - 1] |\Psi_{\text{abs}}\rangle \approx -\tau_A g_{\boldsymbol{\kappa}_{\text{in}}} \int_0^{\tau_E} dt \int d^3k g_{\mathbf{k}}^* \hat{a}_{\mathbf{k}}^\dagger e^{i(\omega_{\mathbf{k}} - \omega)t} \times \sum_{\mu=1}^S \exp\{i(\boldsymbol{\kappa}_{\text{in}} - \mathbf{k}) \cdot \mathbf{r}_\mu\} |\sigma = 0\rangle \otimes |0\rangle. \quad (1.5)$$

Note that the first line alone is proportional to the well-known problem of (single-atom) spontaneous emission into a continuum of modes, which can be treated using Weisskopf-Wigner theory [67, 74]. The sum over the atoms  $\mu$  in the second line, however, leads to an enhancement of the amplitude (and thus the emission probability) when the emission wave vector  $\mathbf{k}$  is close to  $\boldsymbol{\kappa}_{\text{in}}$ . In the case that  $\mathbf{k} = \boldsymbol{\kappa}_{\text{in}}$ , for example, the sum yields a factor  $S$  in the amplitude, resulting in an emission probability (density) which is enhanced by a factor  $S^2$  in this direction, as compared to the single-atom case. Note that one factor of  $S$  is simply the result of  $S$  atoms absorbing the photon more likely than one atom, but the other factor  $S$  is the enhancement due to single-photon directed spontaneous (superradiant) emission. Consequently, for  $\mathbf{k} \neq \boldsymbol{\kappa}_{\text{in}}$ , the absolute value of the sum yields  $\sqrt{S}$  on average (as the sum then corresponds to a two-dimensional random walk), yielding only the first trivial factor  $S$ , but no superradiant enhancement. After having discussed directed spontaneous emission from an ensemble of  $S$  two-level atoms prepared by the absorption of a single photon – also known as *single-photon* Dicke superradiance [69], we will consider the case of multiple excitations in the next section via the famous quasispin formalism [65, 70, 73].

---

<sup>2</sup>As opposed to the “timed” Dicke state, Dicke first considered a situation where the *whole ensemble* of atoms is confined in a volume whose size is small compared to the radiation wavelength. In this case, the local spatial phases are negligible, as  $\boldsymbol{\kappa}_{\text{in}} \cdot \mathbf{r}_\mu \ll 1$ , and the (still superradiant) emission is not directed. Throughout this Thesis, however, we always assume the opposite limit of a “gas of large extent”, i.e., the size of the optical lattice should be large compared to the probe photon wavelength  $\lambda_{\text{probe}}$ , such that the spatial phases are not negligible. Concrete numbers will be provided in chapter 5.



### 1.2.2. Quasispin formalism

In the previous section on (single-photon) directed spontaneous emission, we only dealt with timed Dicke states where either no atom was excited,  $|\sigma = 0\rangle$ , or one atom was excited while the other  $S - 1$  atoms were in the ground state,  $|\sigma = 1\rangle$ . This formalism can be generalized to the case of multiple excitations, i.e. to generalized (timed) Dicke states  $|\sigma\rangle$  in which  $\sigma$  atoms are coherently (i.e., with the same wave vector) excited while the remaining  $S - \sigma$  atoms are in the ground state. The quasispin formalism, which was detailed in [65, 70], then provides an elegant way to calculate the transition amplitudes between generalized Dicke states with a different number of excitations. For this purpose, we define the quasispin raising operator  $\hat{\Sigma}^+(\mathbf{k})$  and its Hermitian conjugate counterpart, the quasispin lowering operator  $\hat{\Sigma}^-(\mathbf{k}) = [\hat{\Sigma}^+(\mathbf{k})]^\dagger$ , via

$$\hat{\Sigma}^\pm(\mathbf{k}) = \sum_{\mu=1}^S \hat{\sigma}_\mu^\pm \exp\{\pm i\mathbf{k} \cdot \mathbf{r}_\mu\}. \quad (1.6)$$

The Hamiltonian (1.1) can then be written as  $\hat{V}(t) = \int d^3k g_{\mathbf{k}} \hat{a}_{\mathbf{k}} e^{-i(\omega_{\mathbf{k}} - \omega)t} \hat{\Sigma}^+(\mathbf{k}) + \text{H.c.}$ , i.e., whenever a photon is absorbed, a collective excitation is created among the atom ensemble via  $\hat{\Sigma}^+(\mathbf{k})$ , and vice versa. A generalized Dicke state with  $\sigma$  excitations can in principle (ignoring the spontaneous decay and higher order effects) be created by repeated absorption of successive photons with the same wave vector  $\mathbf{k}$ , i.e., by repeatedly applying the quasispin raising operator,  $|\sigma\rangle \propto [\hat{\Sigma}^+(\mathbf{k})]^\sigma |\sigma = 0\rangle$ . In the following, we want to understand the  $S$  two-level atoms as  $S$  spin-1/2 systems, where we identify the ground state with spin down,  $s_z = -1/2$ , and the excited state with spin up,  $s_z = +1/2$ . In other words, the state of each atom is described by a two-component spinor. Accordingly, the atomic transition operators  $\hat{\sigma}_\mu^\pm$  are equivalent to ladder operators consisting of Pauli matrices,  $\hat{\sigma}_\mu^\pm = (\hat{\sigma}_\mu^x \pm i\hat{\sigma}_\mu^y)/2$ , which feature the angular momentum algebra

$$[\hat{\sigma}_\mu^\ell, \hat{\sigma}_\nu^m] = \sum_n 2i\epsilon_{lmn} \hat{\sigma}_\mu^n \delta_{\mu\nu}. \quad (1.7)$$

The idea of the quasispin formalism is now that the number of atomic excitations is represented by a (macroscopic) quasispin quantum number  $\sigma$  – whose raising and lowering operators (1.6) comprise the  $S$  (microscopic) individual spin-1/2 systems.

Based on this notion, we can also construct quasispin  $X$  and  $Y$  operators via

$$\hat{\Sigma}^{\pm}(\mathbf{k}) = \hat{\Sigma}^x(\mathbf{k}) \pm i\hat{\Sigma}^y(\mathbf{k}), \quad (1.8)$$

and also a quasispin  $Z$  operator via

$$\hat{\Sigma}^z = \frac{1}{2} [\hat{\Sigma}^+(\mathbf{k}), \hat{\Sigma}^-(\mathbf{k})] = \frac{1}{2} \sum_{\mu, \nu=1}^S \exp\{i\mathbf{k} \cdot (\mathbf{r}_{\mu} - \mathbf{r}_{\nu})\} [\hat{\sigma}_{\mu}^+, \hat{\sigma}_{\nu}^-] = \frac{1}{2} \sum_{\mu=1}^S \hat{\sigma}_{\mu}^z, \quad (1.9)$$

where the properties of the Pauli matrices (1.7) were used. With these definitions, the operators  $\hat{\Sigma}^x(\mathbf{k})$ ,  $\hat{\Sigma}^y(\mathbf{k})$  and  $\hat{\Sigma}^z$  form an  $SU(2)$  algebra [70], i.e.,

$$[\hat{\Sigma}^{\ell}, \hat{\Sigma}^m] = \sum_n i\epsilon_{\ell mn} \hat{\Sigma}^n. \quad (1.10)$$

A detailed proof of the  $SU(2)$  algebra property is given in Appendix A.1. It should be stated that the corresponding operators form a  $SU(2)$  algebra for any *fixed* value of the wave vector  $\mathbf{k}$ . Two quasispin operators with different wave vectors  $\mathbf{k}$  and  $\mathbf{k}'$ , however, in general do not obey simple commutation rules. Furthermore, we know from textbook quantum mechanics [75] that the quantization of angular momentum (in a prevalent notation),

$$\hat{\mathbf{J}}^2 |j, m\rangle = j(j+1) |j, m\rangle, \quad (1.11)$$

$$\hat{J}_z |j, m\rangle = m |j, m\rangle, \quad (1.12)$$

(where the quantum number  $m$  can take values from  $-j$  to  $j$  in unit steps) together with the respective matrix elements of the ladder operators,

$$\hat{J}_+ |j, m\rangle = \sqrt{(j-m)(j+m+1)} |j, m+1\rangle, \quad (1.13)$$

$$\hat{J}_- |j, m\rangle = \sqrt{(j+m)(j-m+1)} |j, m-1\rangle, \quad (1.14)$$

is a direct consequence of the  $SU(2)$  algebra property  $[\hat{J}_{\ell}, \hat{J}_m] = \sum_n i\epsilon_{\ell mn} \hat{J}_n$ . Thus, the same derivation is feasible for the quasispin operators (1.8) and (1.9), and the results from the angular momentum formalism can be adopted. With a shifted definition of the quantum numbers via<sup>3</sup>  $S = 2j$  and  $\sigma = m + S/2$  (where the quantum

<sup>3</sup>Technically, the angular quantum number  $j$  can assume smaller values than the maximum of  $j = S/2$ . If it takes a low value of  $|m| < j \ll S/2$ , for example, the underlying many-body quantum state is highly correlated as well, but exhibits the opposite effect to superradiance called subradi-

number  $\sigma$  consequently ranges from 0 to  $S$ ), but apart from that in complete analogy, we obtain the matrix elements

$$\hat{\Sigma}^+(\mathbf{k})|\sigma\rangle = \sqrt{(S-\sigma)(\sigma+1)}|\sigma+1\rangle, \quad (1.15)$$

$$\hat{\Sigma}^-(\mathbf{k})|\sigma\rangle = \sqrt{(S-\sigma+1)\sigma}|\sigma-1\rangle, \quad (1.16)$$

for the quasispin raising and lowering operators from (1.10). In the context of the coherent emission (or absorption) of a photon, which coincides with the action of the quasispin lowering (raising) operator  $\hat{\Sigma}^-(\mathbf{k})$  on a quasispin state  $|\sigma\rangle$ , the emission (absorption) probability scales roughly with the number of atoms  $S$  *times* the number of excitations<sup>4</sup>  $\sigma$ . The highest emission (absorption) probability is obtained for a state where half of the atoms are in a coherently excited state, i.e.  $\sigma = S/2$ . In this case, the emission probability is enhanced by factor  $(S/2+1)S/2 \approx S^2/4$ . To sum up, the coherent emission (absorption) probability is drastically enhanced in comparison to individual single-atom incoherent emission (or absorption). Please be aware, however, that we primarily consider the case of *single-photon* superradiance throughout this Thesis, where the absorption ( $\sigma = 0$ ) and directed spontaneous emission ( $\sigma = 1$ ) probabilities are both enhanced by a factor  $S$ .

### 1.2.3. Superradiance conditions

Last but not least, let us briefly discuss the requirements placed on the system parameters which have to be met in order to obtain superradiance. Therefore, it is useful to compare the time scale of the usual, incoherent spontaneous emission  $\tau_{\text{single}}$  with the time scale  $\tau_{\text{sp}}$  of the coherent spontaneous (superradiant) emission – when the latter is much smaller than the former, i.e.  $\tau_{\text{sp}} \ll \tau_{\text{single}}$ , superradiant emission is

---

ance, i.e., it has abnormally low emission probabilities [65]. Throughout this Thesis, however, we only deal with the superradiant case. This becomes clear when considering that the initial state  $|\sigma = 0\rangle$  possesses the angular quantum number  $j = S/2$ , as can be deduced from the eigenvalue equation  $(\hat{\Sigma})^2|\sigma = 0\rangle = [(\hat{\Sigma}^x)^2 + (\hat{\Sigma}^y)^2 + (\hat{\Sigma}^z)^2]|\sigma = 0\rangle = (S/2)(S/2 + 1)|\sigma = 0\rangle$ . As the quasispin raising/lowering operator(s)  $\hat{\Sigma}^\pm(\mathbf{k})$ , which are consecutively applied to the initial state, only change the magnetic quantum number  $m$ , the angular quantum number  $j = S/2$  is conserved.

<sup>4</sup>Please note that there are two enhancement mechanisms at work here [70]. The first one, which enhances the emission probability by a factor  $S$ , is attributable to the constructive interference of the amplitudes for the emission of a photon by the different atoms, and was already encountered in section 1.2.1 for the case of a single excitation,  $|\sigma = 1\rangle$ . The second enhancement mechanism relies on the existence of more than one excitation in the generalized Dicke state  $|\sigma\rangle$  and boosts the emission probability by an additional factor  $\sigma$ . The term superradiance is ambiguously used in the literature regardless of whether the second enhancement mechanism is in play, as the emission probability is significantly enhanced either way.

the dominant decay channel. In reference [3], we derived the corresponding time scales from the time-dependent intensity profile of the superradiant emission. The resulting condition reads

$$\frac{\tau_{\text{sp}}}{\tau_{\text{single}}} = 64\pi^2 \frac{L_{\perp}^2}{\lambda_{\text{probe}}^2} \frac{1}{N} = \left( 8\pi \frac{\ell}{\lambda_{\text{probe}}} \right)^2 \ll 1, \quad (1.17)$$

where  $\lambda_{\text{probe}}$  is the wavelength of the emitted photon,  $N$  is the number of atoms and  $L_{\perp}^2$  denotes the transversal cross-section area of the atom ensemble. In a second step, we have assumed that the atoms are enclosed in a two-dimensional, quadratic optical lattice with  $N$  lattice sites and lattice spacing of  $\ell$ , which results in a cross-section area of  $L_{\perp}^2 = N\ell^2$ . Please note that the analytical derivation of (1.17) is based on a range of major simplifications, such as the introduction of a cutoff function and classical treatment of the quasispin operators (for details see reference [3]). Therefore, this should be interpreted mainly as a *qualitative* result: it is important that the photon wavelength  $\lambda_{\text{probe}}$  is large in comparison to the typical distances in the atom ensemble, which in our case are determined by the lattice spacing  $\ell$ .

*Quantitatively*, the latest calculations [76] and experimental results [77] indicate that atoms in a periodic two-dimensional lattice already respond cooperatively (rather than independently) for a lattice spacing  $\ell$  which is of the same order (e.g., slightly smaller) than the probe-photon wavelength  $\lambda_{\text{probe}}$ .

Aside from the temporal condition (1.17), the atomic recoil due to the absorption or emission of the photon needs to be negligible. Due to their larger wavelength and lower momentum (compared to the visible range), *infrared* photons seem to be best suited for our purpose. Specific example values will be put forward in chapter 5, which is devoted to scenarios for experimental realization.

## 1.3. Ultracold atoms in optical lattices

In this section we will first briefly introduce the concept of trapping ultracold quantum gases in optical lattices [5, 6]. Starting from the Hamiltonian for a gas of interacting bosons, we derive the Bose-Hubbard Hamiltonian [22] in section 1.3.2, which describes the dynamics of ultracold bosonic atoms in optical lattices [11]. We discuss its important ground states, the Mott insulator state and the superfluid ground state, as well as the quantum phase transition between these states [22, 23]. Following the discussion of bosonic systems, we analogously introduce and discuss the Fermi-Hubbard Hamiltonian [30] in section 1.3.3. Note that only a brief summary is given, in order to prepare the research conducted in this Thesis. More comprehensive overviews on ultracold atoms in optical lattices can, e.g., be found in [10, 14, 24, 31].

### 1.3.1. Optical lattices

Optical lattices [5, 6] are periodic structures made of light which can confine ultracold neutral atoms [8, 9] – thereby creating artificial crystals, named in analogy to (real) atomic crystals in solid-state physics. To understand the striking ability to trap ultracold atoms in these periodic intensity patterns of light [6, 7], let us consider the situation of a single atom in an oscillating electric field  $\mathbf{E}(\mathbf{r}, t)$  as, e.g., provided by a laser. Assuming that the laser field frequency  $\omega_{\text{lat}}$  is far detuned from atomic resonance frequencies, a similarly oscillating electric dipole moment is induced in the atom,

$$\mathbf{p}(t) = \alpha(\omega_{\text{lat}})\mathbf{E}(\mathbf{r}, t), \quad (1.18)$$

where  $\alpha(\omega_{\text{lat}})$  denotes the polarizability of the atom. Note that we assume that the polarizability is a scalar, for simplicity, which implies that the dipole moment aligns parallel to the electric field. The interaction of the induced dipole moment with the original laser field  $\mathbf{E}(\mathbf{r}, t)$  then again leads to an energy shift proportional to the square of the electric field amplitude (AC Stark effect),

$$V_{\text{lat}}(\mathbf{r}) = -\mathbf{p}(t) \cdot \mathbf{E}(\mathbf{r}, t) \propto \alpha(\omega_{\text{lat}}) |\mathbf{E}(\mathbf{r}, t)|^2 \propto I(\mathbf{r}, t), \quad (1.19)$$

i.e., proportional to the intensity  $I(\mathbf{r}, t)$  of the laser field at position  $\mathbf{r}$  and time  $t$ . The polarizability  $\alpha(\omega_{\text{lat}})$  generally depends on the level scheme of the atom in

conjunction with the laser frequency [14]. In particular, its sign is determined by the detuning between the laser frequency and the excited state which is closest to resonance. If the laser frequency  $\omega_{\text{lat}}$  is smaller than the particular atomic resonance frequency (red-detuned lattice), the atoms are attracted by the intensity maxima. Conversely, the atoms are attracted to the regions of minimum intensity when the laser frequency is larger than the resonance frequency (blue-detuned lattice).

In conclusion, the atoms are exposed to an optical potential which is directly proportional to the spatial pattern of the laser-field intensity [14]. This remarkable result has two obvious, but far-reaching implications. Firstly, the depth of the optical potential can be conveniently controlled simply by slowly varying the laser intensities [11, 12], which has been beautifully demonstrated, e.g., in experiments [25–27] on the superfluid to Mott insulator phase transition (see below). Secondly, the geometry of an optical potential solely depends on the specific laser setup. In the simplest case, a one-dimensional standing-wave periodic intensity pattern is created by the interference of two counter-propagating laser beams,

$$V(x) = V_0 \sin^2(kx), \quad (1.20)$$

as depicted in Figure 1.6 on page 34. The depth  $V_0$  of the optical lattice potential, which is proportional to the atomic polarizability times the laser intensity and thus easily tunable (see above), is often expressed in units of the recoil energy  $E_R^{\text{lat}} = (\hbar k)^2/(2m)$ . With the wave number of the lasers  $k = 2\pi/\lambda_{\text{lat}}$ , where  $\lambda_{\text{lat}}$  denotes their wavelength, and the atomic mass  $m$ , the recoil energy represents the kinetic energy of an atom which has the momentum of a lattice photon, and establishes a

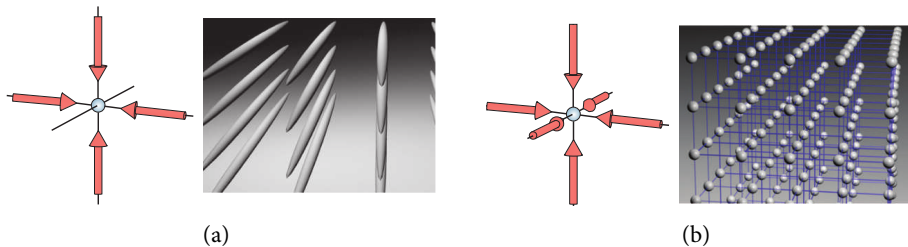


FIGURE 1.5. – Sketch of optical lattice potentials created by the interference of four or six counter-propagating laser beams, i.e., two or three orthogonal standing waves: (a) A two-dimensional array of tightly confining one-dimensional potential tubes and (b) a three-dimensional simple cubic lattice. The figures were taken from [7].

natural energy scale. Accordingly, the spacing between two adjacent nodes (or antinodes) in (1.20) defines the lattice spacing  $\ell = \lambda_{\text{lat}}/2$ . Apart from one-dimensional lattice potentials, also two- and three-dimensional lattice potentials can be created by interfering four or six counter-propagating laser beams respectively, as depicted in Figure 1.5. In the latter case, an isotropic 3D simple cubic crystal can be obtained,

$$V(x, y, z) = V_0 \left( \sin^2(kx) + \sin^2(ky) + \sin^2(kz) \right), \quad (1.21)$$

for example. Of course, optical lattices are not restricted to rectangular layouts. More sophisticated lattice geometries [12, 78, 79] are attainable, e.g., by changing the angle between the interfering laser beams. Please be aware, however, that we only consider two-dimensional, quadratic optical lattices throughout this Thesis.

Because of their unique controllability and the (virtual) absence of defects, decoherence or temperature effects [6, 7], ultracold atoms in optical lattices constitute an invaluable tool to investigate many-body quantum physics [12, 13]. Via the mechanism described above, optical lattices are able to confine bosonic as well as fermionic neutral atoms, and thus simulate the physics of the Bose-Hubbard model [11, 22] and Fermi-Hubbard model [30, 31], which will be introduced in the following two sections 1.3.2 and 1.3.3 respectively.

### 1.3.2. Bose-Hubbard model

Following the seminal proposal of D. Jaksch *et al.* [11], we derive the Bose-Hubbard Hamiltonian [22] from the many-body Hamiltonian for a gas of  $N$  interacting bosonic atoms, which are exposed to an external potential  $V_{\text{ext}}(\mathbf{r})$ , as given, e.g., by the lattice potential (1.21). In second quantized form, with  $\hat{\psi}^\dagger(\mathbf{r})$  and  $\hat{\psi}(\mathbf{r})$  the usual bosonic creation and annihilation field operators satisfying the commutator relations

$$\left[ \hat{\psi}(\mathbf{r}), \hat{\psi}^\dagger(\tilde{\mathbf{r}}) \right] = \delta^3(\mathbf{r} - \tilde{\mathbf{r}}), \quad \left[ \hat{\psi}(\mathbf{r}), \hat{\psi}(\tilde{\mathbf{r}}) \right] = \left[ \hat{\psi}^\dagger(\mathbf{r}), \hat{\psi}^\dagger(\tilde{\mathbf{r}}) \right] = 0, \quad (1.22)$$

the Hamiltonian reads

$$\begin{aligned} \hat{H}_{\text{gas}} = & \int d^3r \hat{\psi}^\dagger(\mathbf{r}) \left[ -\frac{\nabla^2}{2m} + V_{\text{ext}}(\mathbf{r}) \right] \hat{\psi}(\mathbf{r}) + \\ & + \frac{1}{2} \int d^3r d^3\tilde{r} \hat{\psi}^\dagger(\mathbf{r}) \hat{\psi}^\dagger(\tilde{\mathbf{r}}) V(\mathbf{r} - \tilde{\mathbf{r}}) \hat{\psi}(\mathbf{r}) \hat{\psi}(\tilde{\mathbf{r}}). \end{aligned} \quad (1.23)$$

Note that we (throughout the whole Thesis) set  $\hbar = 1$ , for simplicity. Apart from the external potential  $V_{\text{ext}}(\mathbf{r})$ , the Hamiltonian (1.23) consists of a kinetic term with the atomic mass  $m$ , and a two-boson interaction term depending on the interaction potential  $V(\mathbf{r} - \tilde{\mathbf{r}})$ . In the case of ultracold neutral atoms in an optical lattice, the de Broglie wavelength and the lattice spacing  $\lambda_{\text{lat}}/2$  are both much larger than the effective range of the actual interaction potential, so that only short-range two-body collisions are relevant [14]. The low-energy collisions are dominated by  $s$ -wave scattering [80, 81], i.e., the interaction potential between the atoms is approximated by the short-range pseudopotential

$$V(\mathbf{r} - \tilde{\mathbf{r}}) = \frac{4\pi a_s}{m} \delta^3(\mathbf{r} - \tilde{\mathbf{r}}), \quad (1.24)$$

where the  $s$ -wave scattering length  $a_s$  characterizes the strength and sign of the interatomic interaction. While we only consider repulsive collisions, which are described by a positive  $s$ -wave scattering length, a negative  $s$ -wave scattering length would correspond to attractive interactions.

A single atom which is exposed to a periodic potential is usually described via the well-known Bloch wave functions, which can be expressed as a product of a plane wave times a periodic function [82, 83],

$$\Phi_{\mathbf{k}}(\mathbf{r}) = u_{\mathbf{k}}(\mathbf{r}) \exp\{i\mathbf{k} \cdot \mathbf{r}\}, \quad (1.25)$$

where the periodic function  $u_{\mathbf{k}}(\mathbf{r})$  exhibits the same periodicity as the potential, i.e.,  $u_{\mathbf{k}}(\mathbf{r}) = u_{\mathbf{k}}(\mathbf{r} + \mathbf{R})$  for any lattice vector  $\mathbf{R}$ . Note that we only consider the lowest Bloch band, as higher vibrational states are usually negligible in the case of *ultracold* atoms [14].

For a deep optical potential and low temperatures, we expect that the bosons localize on individual lattice sites. Thus, it is not convenient to describe the bosons in the basis of Bloch waves, which extend over the entire lattice. As an alternative, we consider localized Wannier functions, which can be written as a superposition of Bloch waves, and form a complete set of orthonormal functions [83],

$$w(\mathbf{r} - \mathbf{r}_\nu) = \frac{1}{\sqrt{N}} \sum_{\mathbf{k}} \Phi_{\mathbf{k}}(\mathbf{r}) \exp\{-i\mathbf{k} \cdot \mathbf{r}_\nu\}, \quad (1.26)$$

with  $\mathbf{r}_\nu$  the position of the lattice site  $\nu$  and  $N$  the number of lattice sites, for normalization. As a convention throughout this Thesis, any sum over reciprocal lattice



vectors, such as the sum over  $\mathbf{k}$  in this case, is intended to be taken over all values of  $\mathbf{k}$  in the first Brillouin zone, unless otherwise noted. In conclusion, we can expand the bosonic field operators in the basis of localized Wannier functions for sufficiently deep optical potentials,

$$\hat{\psi}(\mathbf{r}) = \sum_{\nu} \hat{b}_{\nu} w(\mathbf{r} - \mathbf{r}_{\nu}), \quad \hat{\psi}^{\dagger}(\mathbf{r}) = \sum_{\mu} \hat{b}_{\mu}^{\dagger} w^{*}(\mathbf{r} - \mathbf{r}_{\mu}), \quad (1.27)$$

with  $\hat{b}_{\mu}^{\dagger}$  and  $\hat{b}_{\nu}$  the creation and annihilation operators of bosons localized at lattice sites  $\mu$  and  $\nu$  respectively. As another convention, sums involving lattice site indices such as  $\nu$  or  $\mu$  run over *all* lattice sites, unless otherwise specified. Using the back transformation corresponding to (1.27), one can derive the canonical commutation relations of the creation and annihilation operators from (1.22),

$$[\hat{b}_{\nu}, \hat{b}_{\mu}^{\dagger}] = \delta_{\mu\nu}, \quad [\hat{b}_{\nu}, \hat{b}_{\mu}] = [\hat{b}_{\nu}^{\dagger}, \hat{b}_{\mu}^{\dagger}] = 0. \quad (1.28)$$

Inserting the Wannier basis expansion (1.27) into the general many-body Hamiltonian of  $N$  interacting bosons (1.23), we immediately obtain

$$\hat{H}_{\text{lat}}(t) = - \sum_{\mu\nu} J_{\mu\nu} \hat{b}_{\mu}^{\dagger} \hat{b}_{\nu} + \frac{1}{2} \sum_{\mu\nu\rho\eta} U_{\mu\nu\rho\eta} \hat{b}_{\mu}^{\dagger} \hat{b}_{\nu}^{\dagger} \hat{b}_{\rho} \hat{b}_{\eta}, \quad (1.29)$$

with the tunneling matrix element between two arbitrary lattice sites  $\mu$  and  $\nu$ ,

$$J_{\mu\nu} = - \int d^3r w^{*}(\mathbf{r} - \mathbf{r}_{\mu}) \left[ -\frac{\nabla^2}{2m} + V_{\text{ext}}(\mathbf{r}) \right] w(\mathbf{r} - \mathbf{r}_{\nu}), \quad (1.30)$$

and the interaction matrix element, which involves Wannier functions centered at four different lattice sites in general,

$$U_{\mu\nu\rho\eta} = \frac{4\pi a_s}{m} \int d^3r w^{*}(\mathbf{r} - \mathbf{r}_{\mu}) w^{*}(\mathbf{r} - \mathbf{r}_{\nu}) w(\mathbf{r} - \mathbf{r}_{\rho}) w(\mathbf{r} - \mathbf{r}_{\eta}). \quad (1.31)$$

Starting from the lattice Hamiltonian (1.29), we now consider the following additional approximations. Notably, the tunneling matrix element (1.30) and the interaction matrix element (1.31) both contain products of Wannier functions, which are well localized at (in general) different lattice sites. As a first approximation regarding the tunneling matrix element (1.30), we hence assume that meaningful tunneling only occurs between nearest-neighbor lattice sites. For example, the next-

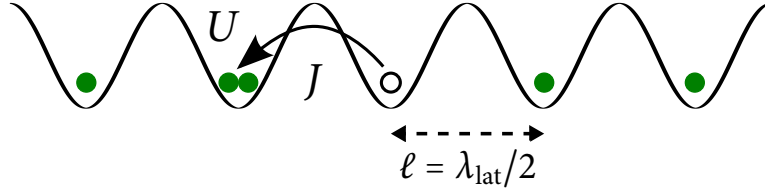


FIGURE 1.6. – Sketch of a one-dimensional optical lattice potential realizing the Bose-Hubbard model: The atoms (green circles) can tunnel between different lattice sites with the tunneling rate  $J$  (black arrow) and interact with the on-site repulsion energy  $U$ .

nearest neighbor amplitudes are typically two orders of magnitude smaller and can thus be neglected [11, 12]. Formally, we therefore introduce the adjacency matrix  $T_{\mu\nu}$  which is unity when  $\mu$  and  $\nu$  are nearest neighbors and zero otherwise in the first summation in (1.29). As a second approximation, we suppose that the external optical potential  $V_{\text{ext}}(\mathbf{r})$  is homogeneous and isotropic, such that the (remaining) tunneling matrix elements between adjacent lattice sites do not depend on the position or the direction,  $J_{\mu\nu} = J/Z$ . By convention, the coordination number  $Z = \sum_{\nu} T_{\mu\nu}$  was introduced here. Thirdly, we analogously approximate the sum over the interaction matrix elements (1.31). For the same reason as before, i.e., the product of well localized Wannier functions, the off-site interaction matrix elements  $U_{\mu\nu\rho\eta}$  (where not all indices are the same) are much smaller than the on-site repulsion strength  $U_{\mu\mu\mu\mu}$ , and are thus omitted [11, 12]. Assuming again a homogeneous lattice, the on-site repulsion strength then is equal on all lattice sites  $\mu$ ,  $U_{\mu\mu\mu\mu} = U$ . In conclusion, we arrive at the famous Bose-Hubbard Hamiltonian [12, 22], describing a gas of interacting bosons in a periodic potential,

$$\hat{H}_{\text{BH}} = -\frac{J}{Z} \sum_{\mu\nu} T_{\mu\nu} \hat{b}_{\mu}^{\dagger} \hat{b}_{\nu} + \frac{U}{2} \sum_{\mu} \hat{n}_{\mu} (\hat{n}_{\mu} - 1), \quad (1.32)$$

where  $\hat{n}_{\mu} = \hat{b}_{\mu}^{\dagger} \hat{b}_{\mu}$  denotes the number operator for bosonic atoms at lattice site  $\mu$ . The Bose-Hubbard Hamiltonian (1.32) consists of two competing terms, which are represented by the tunneling rate  $J$  and the on-site repulsion strength  $U$  respectively – see Figure 1.6. The tunneling term describes the tunneling of bosons to nearest-neighbor lattice sites according to the tunneling rate  $J$ , the coordination number  $Z$  and the adjacency matrix  $T_{\mu\nu}$ . The minus sign thereby indicates a gain in kinetic energy, guided by the tunneling rate  $J$ , due to nearest-neighbor tunneling. The on-site repulsion term, on the other hand, disfavors configurations where two (or more)

bosons occupy the same lattice site via an energy penalty  $U$ .

If not otherwise specified, we always assume the case of unit filling of one boson per lattice site, on average, i.e.,  $\langle \hat{n}_\mu \rangle = 1$ . In this case, the Bose-Hubbard Hamiltonian (1.32) features a quantum phase transition [21] between two fundamentally different quantum phases, depending on the ratio between the tunneling rate  $J$  and the on-site repulsion strength  $U$ . In the following, we discuss these quantum phases and the transition between them, starting with the Mott insulator state.

**Mott insulator state** In the situation of a deep periodic potential, i.e., when the on-site repulsion term dominates over the tunneling term,  $U \gg J$ , the atoms are fixed to their lattice sites, while atom-number fluctuations are strongly suppressed. In general, the atoms are well localized in the Mott insulator phase, and the many-particle ground state is approximately given by a product of local Fock states. In the extremal limit of  $U/J \rightarrow \infty$ , and for a commensurate filling with  $N$  atoms and lattice sites, the ground state is given by the Mott insulator state,

$$|\Psi\rangle_{\text{Mo}}^{J=0} = \prod_{\mu=1}^N \hat{b}_\mu^\dagger |0\rangle = \bigotimes_{\mu=1}^N |1\rangle_\mu. \quad (1.33)$$

Clearly, the Mott insulator state shows no correlations between (different) lattice sites, as  $\langle \hat{b}_\mu^\dagger \hat{b}_\nu \rangle_{\text{Mo}} = \delta_{\mu\nu}$ . Furthermore, starting from the Mott insulator state (1.33), the first excited state is created by the tunneling of a single boson, which leads to an increase in the energy by an amount  $U$ . Hence, there is a gap of (roughly)  $U$  in the excitation spectrum in the Mott insulator phase (also for nonzero but small  $J$ ). In addition, any attempt to compress the Mott insulator state involves increasing the number of atoms at given lattice sites, i.e., it would need to overcome this energy gap. Thus, the Mott insulator state is characterized by zero compressibility.

If we start in the Mott insulator state (1.33) and then increase the tunneling rate  $J$  from zero to a value which is still small in comparison with the on-site repulsion strength  $U$ , the atoms begin to tunnel and the atom-number fluctuations at individual lattice sites become nonzero. However, as the gain in kinetic energy due to the hopping  $J$  is smaller than the price  $U$  which has to be paid for double occupancy, the atoms remain localized, although the ground state is not a simple product state (1.33) anymore [23]. Increasing  $J$  further to the order of  $U$ , a delocalized state becomes energetically favorable, when the gain in kinetic energy outweighs the en-

ergy penalty due to double occupations [23]. In three dimensions, for example, this quantum critical point is expected at a ratio of  $U/J = 5.8 Z$ , according to mean-field calculations [22]. Finally, for  $J \gg U$ , the kinetic energy totally dominates and the system is characterized by the superfluid phase.

**Superfluid phase** In the setting of weak interactions and a shallow periodic potential, i.e., when the tunneling term dominates over the on-site repulsion term,  $J \gg U$ , the many-particle system is in the superfluid phase. In this case, the atoms can move freely across the entire optical lattice, which leads to large fluctuations in the on-site number of particles. As a result, and antipodal to the Mott insulator phase, the superfluid ground state exhibits a high degree of uncertainty in the atomic number distribution, as each atom is completely delocalized over the whole lattice. In the limit  $J/U \rightarrow \infty$ , and for  $N$  atoms and lattice sites, all atoms occupy the identical ( $\mathbf{k} = \mathbf{0}$ ) Bloch state of the lowest band. In normalized form, the superfluid ground state reads

$$|\Psi\rangle_{\text{sf}}^{U=0} = \frac{1}{\sqrt{N!}} (\hat{b}_{\mathbf{k}=\mathbf{0}}^\dagger)^N |0\rangle = \frac{1}{\sqrt{N!}} \left( \frac{1}{\sqrt{N}} \sum_{\mu=1}^N \hat{b}_\mu^\dagger \right)^N |0\rangle. \quad (1.34)$$

In contrast to the Mott insulator phase, the superfluid phase features first-order long-range off-diagonal correlations,  $\langle \hat{b}_\mu^\dagger \hat{b}_\nu \rangle_{\text{sf}} = 1$ , and a broad continuum of excitations [11,22]. In fact, the appearance of an energy gap when crossing the quantum critical point towards the Mott insulator phase is an essential feature (and a clear experimental signature) of the described quantum phase transition – see e.g. [25,26].

Please remember that the superfluid to Mott insulator phase transition portrayed here can be induced simply by varying the laser intensity which creates the optical lattice [11, 12]. Increasing the laser intensity, for example, deepens the periodic potential and thus leads to an increase in the on-site repulsion strength  $U$ , as two particles become more compressed on the same lattice sites, and to a decrease in the tunneling rate  $J$  due to higher barriers between different lattice sites [11, 12]. This dependency is exemplarily shown in Figure 1.7. As a consequence, the transition was demonstrated experimentally in a three-dimensional optical lattice by M. Greiner *et al.* [25], and subsequently in one-dimensional [26] and two-dimensional optical lattices [27].

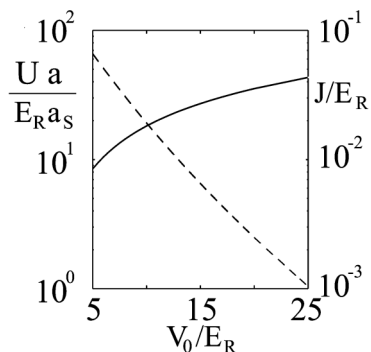


FIGURE 1.7. – Plot of numerically calculated values for the tunneling rate  $J$  (dashed line, right axis) and the on-site repulsion strength  $U$  (solid line, left axis) as a function of the optical lattice potential depth  $V_0$  for a three-dimensional cubic lattice. The recoil energy  $E_R = (\hbar k)^2/(2m)$  with  $k = 2\pi/\lambda_{\text{lat}}$ , the  $s$ -wave scattering length  $a_s$  and the lattice spacing  $a = \lambda_{\text{lat}}/2$  appear for reasons of scaling. An increase in the laser intensity (i.e.,  $V_0$ ) deepens the periodic potential and thus leads to an increase in the on-site repulsion strength  $U$ . On the other hand, the tunneling rate  $J$  decreases due to higher barriers between the lattice sites. The figure was taken from [12].

### 1.3.3. Fermi-Hubbard model

After having discussed the Bose-Hubbard model, which describes the lattice dynamics of (spinless) bosonic ultracold atoms in optical lattices, let us now briefly introduce the equivalent for fermionic ultracold atoms (with spin) – the Fermi-Hubbard model [12, 30]. Instead of a derivation from first principles [14], we adapt the Bose-Hubbard Hamiltonian (1.32) appropriately, placing special emphasis on the differences which arise when dealing with fermions.

First of all, we assume that the fermionic atoms can have different spin orientations, which we denote by an additional spin label  $s \in \{\uparrow, \downarrow\}$ . However, there is no reason why the tunneling dynamics of a fermionic atom (with a specific spin orientation) should differ from the tunneling dynamics of a spinless boson. Thus, we only include (a summation over) the spin index  $s$  in the tunneling term (see below). Regarding the on-site repulsion term, let us first recall that in the bosonic case, an arbitrary number of atoms can occupy the same lattice site (i.e., coincide in all quantum numbers). The on-site penalty for two atoms is given by  $U$ , for three atoms by  $3U$ , and so forth (1.32). In the fermionic case, however, two atoms cannot occupy the same quantum state simultaneously, according to the Pauli exclusion principle. Hence, the only way to have two atoms sitting on the same lattice site is when their spin differs. Analogous to the Bose-Hubbard Hamiltonian (1.32), the

energy penalty for this situation should be  $U$ . In conclusion, the Fermi-Hubbard Hamiltonian [12, 30] is given by

$$\hat{H}_{\text{FH}} = -\frac{J}{Z} \sum_{\mu\nu,s} T_{\mu\nu} \hat{c}_{\mu,s}^\dagger \hat{c}_{\nu,s} + U \sum_{\mu} \hat{n}_{\mu,\uparrow} \hat{n}_{\mu,\downarrow}, \quad (1.35)$$

where  $\hat{c}_{\mu,s}^\dagger$  and  $\hat{c}_{\nu,s}$  denote creation and annihilation operators of fermionic atoms at lattice sites  $\mu$  and  $\nu$  with spin  $s$ , while  $\hat{n}_{\mu,s} = \hat{c}_{\mu,s}^\dagger \hat{c}_{\mu,s}$  is the corresponding number operator.

Unless otherwise specified, we consider the case of half-filling  $\langle \hat{n}_{\mu,\uparrow} + \hat{n}_{\mu,\downarrow} \rangle = 1$ , where half (i.e.,  $N/2$ ) of the atoms are in the  $s = \uparrow$  state and the other half are in the  $s = \downarrow$  state. In this case, the Fermi-Hubbard model describes a transition [28, 29] between the Mott insulator phase and a metallic phase, depending on the ratio between the tunneling rate  $J$  and the on-site repulsion strength  $U$ . We will now discuss the ground states of the two parameter regimes.

**Mott-Néel state** In analogy to the bosonic case, let us first regard the situation when the on-site repulsion term dominates, i.e.  $U \gg J$ . Obviously, the interaction energy in (1.35) again is minimized for a ground state with one particle per lattice site, as it was in the Mott insulator state (1.33). In the fermionic case, however, we have the additional degree of freedom in the spin quantum number, such that the ground state is highly degenerate for  $J = 0$ . In order to circumvent this complication, we consider the square lattice as a bipartite lattice. That is, we can divide the total lattice into two sublattices  $\mathcal{A}$  and  $\mathcal{B}$  in such a way that for each site  $\mu \in \mathcal{A}$ , all the nearest-neighboring sites  $\nu$  belong to  $\mathcal{B}$ , and vice versa. As a consequence, all fermions on one sublattice are connected only to fermions on the other sublattice via the tunneling term of the Fermi-Hubbard Hamiltonian (1.35). For small but nonzero tunneling rate  $J \ll U$ , where the degeneracy does not apply, the approximate ground state is thus given by the antiferromagnetic Mott-Néel state [14],

$$|\Psi\rangle_{\text{Néel}}^{J=0} = \prod_{\mu \in \mathcal{A}} \hat{c}_{\mu,\uparrow}^\dagger \prod_{\nu \in \mathcal{B}} \hat{c}_{\nu,\downarrow}^\dagger |0\rangle = \bigotimes_{\mu \in \mathcal{A}} |\uparrow\rangle_{\mu} \bigotimes_{\nu \in \mathcal{B}} |\downarrow\rangle_{\nu}, \quad (1.36)$$

which is characterized by the fact that nearest-neighboring fermions always have opposite spin (checkerboard pattern).

**Metallic ground state** When the tunneling term dominates, i.e.,  $J \gg U$ , the situation is completely different in the case of fermions. Because of the Pauli exclusion principle, a superfluid state (1.34) is impossible. Instead, the fermionic atoms occupy the energetically lowest lying states in momentum space<sup>5</sup> in pairs. The metallic ground state, which is also known from solid-state physics [83], reads

$$|\Psi\rangle_{\text{me}}^{U=0} = \prod_{E_{\mathbf{k}} < E_F, s} \hat{c}_{\mathbf{k},s}^\dagger |0\rangle. \quad (1.37)$$

The product contains all  $\mathbf{k}$ -modes in momentum space whose energy eigenvalues  $E_{\mathbf{k}}$  are smaller than the so-called Fermi energy  $E_F$  – and of course all spin orientations  $s \in \{\uparrow, \downarrow\}$ . As we will see in section 1.4.2, the dispersion relation of the Fermi-Hubbard model (1.35) for  $U = 0$  is given by  $E_{\mathbf{k}} = -J/Z T_{\mathbf{k}}$  with  $T_{\mathbf{k}} = 2[\cos(k_x \ell) + \cos(k_y \ell)]$  the Fourier transform of the adjacency matrix  $T_{\mu\nu}$ .

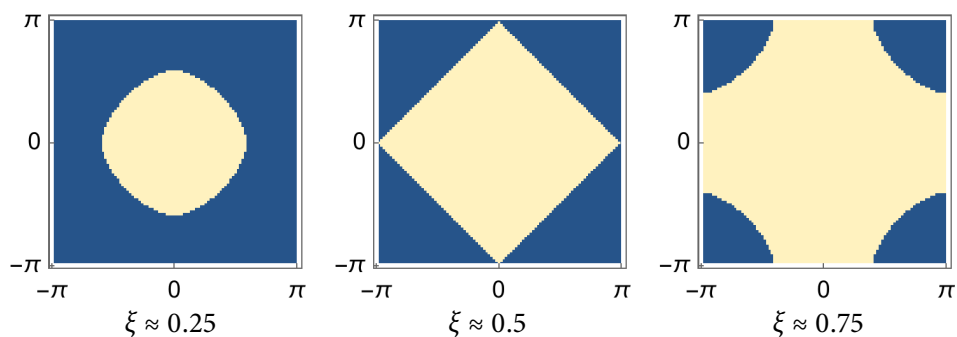


FIGURE 1.8. – Fermi surfaces for different fillings of (from left to right)  $N_\Psi = 4994$ ,  $N_\Psi = 9802$  and  $N_\Psi = 14990$  fermions (equal mixture of spin-up and spin-down) in a two-dimensional reciprocal quadratic lattice with  $N = L^2 = 10000$  lattice sites. Plotted is the first Brillouin zone, i.e., the values for  $k_x \ell$  (x-axis) and  $k_y \ell$  (y-axis) range from  $-\pi$  to  $\pi$ . The numbers of fermions are chosen such that the resulting ground states are nondegenerate (see footnote 6) and correspond to filling factors of  $\xi = N_\Psi/(2N) \approx 0.25$ ,  $\xi \approx 0.5$  and  $\xi \approx 0.75$  respectively. In the case of half-filling,  $\xi \approx 0.5$ , we obtain a diamond-shaped Fermi surface, which can be described via the expectation value (1.38).

Fermi surfaces of different numbers of fermions in a two-dimensional (reciprocal) quadratic lattice are exemplarily shown in Figure 1.8. We consider the case of half-filling, which corresponds to a diamond-shaped Fermi surface [84]. Thus, we can write the expectation value of the number operator in the mode  $\mathbf{k}$  with spin

<sup>5</sup>The transformation to the momentum space, including the corresponding creation operators such as  $\hat{c}_{\mathbf{k},s}^\dagger$ , will be explained in detail in section 1.4.2.

s approximately<sup>6</sup> as

$${}_{\text{me}}^{U=0}\langle\Psi|\hat{n}_{\mathbf{k},s}|\Psi\rangle_{\text{me}}^{U=0} = \begin{cases} 1, & \text{if } |k_x| + |k_y| < \pi/\ell, \\ 0, & \text{otherwise.} \end{cases} \quad (1.38)$$

Although the Fermi-Hubbard model [30] was originally developed in the context of solid-state physics [28, 29], ultracold fermionic atoms in optical lattices constitute an ideal model system for its study [12, 31]. Consequently, the Fermi-Hubbard model was realized, e.g., in a three-dimensional optical lattice [31, 32], and the described metallic phase as well as the Mott-insulating phase have been evidenced [33–35].

---

<sup>6</sup>In fact, the metallic ground state (1.37) is degenerate for a finite lattice with exactly  $N$  fermionic atoms on  $N = L^2$  lattice sites (i.e., half-filling). Considering, e.g., that  $L$  is even, there are only  $2(L - 1)$  atoms left to populate the outer edge of the diamond-shaped Fermi surface, which, however, offers  $4(L - 1)$   $\mathbf{k}$ -modes of equal energy eigenvalue  $E_{\mathbf{k}}$ . Therefore, we will employ the expectation value (1.38), which describes the exact metallic ground state for a reduced (as indicated by the less-than sign in the definition) number of  $N - 2(L - 1)$  atoms. As we always consider  $L \gg 1$ , and thus  $N \gg L$ , the deviation of the atom number is negligible, i.e.,  $N - 2(L - 1) \approx N$ .



## 1.4. Synthesis: Lattice models coupled to light

The two topics presented in the previous sections – Dicke superradiance in section 1.2 on the one hand and ultracold atoms in optical lattices in section 1.3 on the other – have both been studied in great detail independently from each other. As outlined in the preface (section 1.1), the basic idea of this Thesis is to create a nondestructive probing scheme for ultracold atoms in optical lattices by utilizing the effects of Dicke superradiance – i.e., to combine these two initially unrelated topics. To this end, we are going to prepare the necessary formalism as well as important tools in this section. Subsequent chapters will often refer back to important definitions and relations which are worked out here.

### 1.4.1. Hamiltonian description of the coupled system

#### General lattice Hamiltonian

As described above, the lattice dynamics are either guided by the Bose-Hubbard Hamiltonian (1.32) in the case of bosonic atoms, or by the Fermi-Hubbard Hamiltonian (1.35) in the case of fermionic atoms. To avoid writing similar equations twice, we are going to treat the two classes of particles together in this Thesis wherever possible. Therefore, we are going to describe the lattice dynamics via universal (bosonic or fermionic) creation and annihilation operators  $\hat{a}_{\mu,s}^{\lambda\dagger}$  and  $\hat{a}_{\nu,s}^{\lambda}$  for atoms at lattice sites  $\mu$  and  $\nu$  (with spin  $s$ ) respectively. The corresponding number operator is given by  $\hat{n}_{\mu,s}^{\lambda} = \hat{a}_{\mu,s}^{\lambda\dagger} \hat{a}_{\mu,s}^{\lambda}$ . The universal operators obey either bosonic commutation relations (1.39) or fermionic anticommutation relations (1.40),

$$\left[ \hat{a}_{\mu,s_1}^{\lambda}, \hat{a}_{\nu,s_2}^{\lambda\dagger} \right] = \delta_{\mu\nu} \delta_{s_1 s_2}, \quad \left[ \hat{a}_{\mu,s_1}^{\lambda}, \hat{a}_{\nu,s_2}^{\lambda} \right] = \left[ \hat{a}_{\mu,s_1}^{\lambda\dagger}, \hat{a}_{\nu,s_2}^{\lambda\dagger} \right] = 0, \quad (1.39)$$

$$\left\{ \hat{a}_{\mu,s_1}^{\lambda}, \hat{a}_{\nu,s_2}^{\lambda\dagger} \right\} = \delta_{\mu\nu} \delta_{s_1 s_2}, \quad \left\{ \hat{a}_{\mu,s_1}^{\lambda}, \hat{a}_{\nu,s_2}^{\lambda} \right\} = \left\{ \hat{a}_{\mu,s_1}^{\lambda\dagger}, \hat{a}_{\nu,s_2}^{\lambda\dagger} \right\} = 0. \quad (1.40)$$

The left part can be condensed into a useful single equation,

$$\hat{a}_{\mu,s_1}^{\lambda} \hat{a}_{\nu,s_2}^{\lambda\dagger} \mp \hat{a}_{\nu,s_2}^{\lambda\dagger} \hat{a}_{\mu,s_1}^{\lambda} = \delta_{\mu\nu} \delta_{s_1 s_2}, \quad (1.41)$$

where the upper written sign represents the bosonic case, while the lower written sign describes the fermionic case. Very importantly, the atoms in the optical lattice should be able to (collectively) absorb and re-emit photons to enable the proposed probing scheme. Thus, we additionally distinguish between (at least) two internal

levels of the atoms [57, 59] via the superscript index  $\lambda \in \{\text{gr}, \text{ex}\}$ . Of course, operators corresponding to different species  $\lambda$  do always commute, irregardless of their class, bosonic or fermionic. In conclusion, we describe the lattice dynamics via a general lattice Hamiltonian, which incorporates the Bose-Hubbard Hamiltonian as well as the Fermi-Hubbard Hamiltonian. This reads

$$\hat{H}_{\text{lat}} = -\frac{J}{Z} \sum_{\mu\nu, s, \lambda} T_{\mu\nu} \hat{a}_{\mu, s}^{\lambda\dagger} \hat{a}_{\nu, s}^{\lambda} + \frac{U}{2} \sum_{\mu} \left( \sum_{s, \lambda} \hat{n}_{\mu, s}^{\lambda} \right) \left( \sum_{s, \lambda} \hat{n}_{\mu, s}^{\lambda} - 1 \right), \quad (1.42)$$

and models the behavior of ultracold bosonic or fermionic atoms in an optical lattice, assuming lowest band occupation only and neglecting long-range interactions<sup>7</sup>. The tunneling term with the tunneling rate  $J$ , the coordination number  $Z$  and the adjacency matrix  $T_{\mu\nu}$ , as well as the on-site repulsion term with the interaction strength  $U$ , are defined equivalently as in the Bose- and Fermi-Hubbard model. For simplicity, we assume identical lattice dynamics for both the ground-state atoms and the excited-state atoms in (1.42), as indicated by the summation over  $\lambda \in \{\text{gr}, \text{ex}\}$ . If not otherwise specified, we always assume a two-dimensional, quadratic lattice with  $Z = \sum_{\nu} T_{\mu\nu} = 4$  and  $N = \sum_{\mu}$  lattice sites and atoms. Please note that this corresponds to unit filling in the bosonic case,  $\langle \hat{n}_{\mu} \rangle = 1$ , but half-filling in the fermionic case,  $\langle \hat{n}_{\mu, \uparrow} + \hat{n}_{\mu, \downarrow} \rangle = 1$ .

A two-species Bose-Hubbard Hamiltonian<sup>8</sup> is retrieved from the general lattice Hamiltonian (1.42) when we discard the spin index  $s$  (and its summation) and identify *bosonic* creation and annihilation operators via  $\hat{a}_{\mu, s}^{\lambda\dagger} = \hat{b}_{\mu}^{\lambda\dagger}$  and  $\hat{a}_{\nu, s}^{\lambda} = \hat{b}_{\nu}^{\lambda}$ , i.e.,

$$\hat{H}_{\text{BH}}^{2\text{sp}} = -\frac{J}{Z} \sum_{\mu\nu, \lambda} T_{\mu\nu} \hat{b}_{\mu}^{\lambda\dagger} \hat{b}_{\nu}^{\lambda} + \frac{U}{2} \sum_{\mu} \left( \sum_{\lambda} \hat{n}_{\mu}^{\lambda} \right) \left( \sum_{\lambda} \hat{n}_{\mu}^{\lambda} - 1 \right), \quad (1.43)$$

<sup>7</sup>Possible long-range interactions include Coulomb forces and dipole-dipole interactions. While the former do not occur in the case of neutral atoms, the latter can be neglected, as dipole-dipole interactions are usually two orders of magnitude weaker than on-site forces [11, 14].

<sup>8</sup>The two-species (or two-band) Bose-Hubbard model coupled to a cavity field was studied, e.g., in [57–60]. In the most general case, the two species  $\lambda \in \{\text{gr}, \text{ex}\}$  of bosons can have different tunneling rates  $J_{\text{gr/ex}}$  and on-site repulsion strengths  $U_{\text{gr/ex/gr-ex}}$ , i.e., a great many parameters. For simplicity, we assume that the tunneling rate  $J$  and on-site repulsion strength  $U$  are identical for both species (1.42). However, the qualitative results which will be derived in this Thesis should also hold true in the general case. For example, the atoms would be equally fixed to their lattice sites in the separable state regime when the on-site repulsion strengths differ, as long as they are all large compared to the tunneling rates ( $U_{\text{gr/ex/gr-ex}} \gg J_{\text{gr/ex}}$ ). Also in the weak interactions regime, two different tunneling rates ( $J_{\text{gr/ex}} \gg U_{\text{gr/ex/gr-ex}}$ ) would lead to decoherence of the superradiance peak analogous to the simplified case (see chapter 2 below).

while the usual Bose-Hubbard Hamiltonian (1.32) is obtained as a special case when we also drop the species index  $\lambda$ . On the other hand, we can read the general lattice Hamiltonian (1.42) as a two-species Fermi-Hubbard Hamiltonian when we maintain the spin quantum number  $s \in \{\uparrow, \downarrow\}$  and identify *fermionic* creation and annihilation operators via  $\hat{a}_{\mu,s}^{\lambda\dagger} = \hat{c}_{\mu,s}^{\lambda\dagger}$  and  $\hat{a}_{\nu,s}^{\lambda} = \hat{c}_{\nu,s}^{\lambda}$ , i.e.,

$$\hat{H}_{\text{FH}}^{2\text{sp}} = -\frac{J}{Z} \sum_{\mu\nu,s,\lambda} T_{\mu\nu} \hat{c}_{\mu,s}^{\lambda\dagger} \hat{c}_{\nu,s}^{\lambda} + U \sum_{\mu} \left( \sum_{\lambda} \hat{n}_{\mu,\uparrow}^{\lambda} \hat{n}_{\mu,\downarrow}^{\lambda} + \sum_{s_1 s_2} \hat{n}_{\mu,s_1}^{\text{gr}} \hat{n}_{\mu,s_2}^{\text{ex}} \right), \quad (1.44)$$

where the on-site repulsion term has been rearranged to a form more intuitive for fermions. Again, the usual Fermi-Hubbard Hamiltonian (1.35) is recovered as a special case if we additionally drop the species index  $\lambda$ .

### Atom-field interaction Hamiltonian and total system Hamiltonian

The general lattice Hamiltonian (1.42), which comprehensively describes the lattice dynamics of ground-state atoms as well as excited-state atoms of either class (bosons/fermions), constitutes only a part of the total system Hamiltonian. In order to have the (collective) absorption and emission of photons included, we need to add an atom-field interaction Hamiltonian, which couples the internal state of the atoms to the electromagnetic field. Closely following section 1.2.1, the perturbation Hamiltonian (in rotating-wave and dipole approximation [74]) for the on-site atom-field coupling is given by

$$\hat{V} = \int d^3k g_{\mathbf{k}}(t) \hat{a}_{\mathbf{k}} \hat{\Sigma}^+(\mathbf{k}) + \text{H.c.}, \quad (1.45)$$

where the time dependency of the small coupling constant  $g_{\mathbf{k}}(t)$  will be explained later. Note that we assume equal coupling of all atoms to the electromagnetic field (1.45), as the coupling constant is not space-dependent [61]. Besides,  $\hat{a}_{\mathbf{k}}$  and  $\hat{a}_{\mathbf{k}}^{\dagger}$  denote the usual annihilation and creation operators for photons with wave vector  $\mathbf{k}$ , satisfying the commutation relation

$$[\hat{a}_{\mathbf{k}}, \hat{a}_{\mathbf{p}}^{\dagger}] = \delta^3(\mathbf{k} - \mathbf{p}). \quad (1.46)$$

Finally, the exciton creation operator is defined as

$$\hat{\Sigma}^+(\mathbf{k}) = \sum_{\mu,s} \hat{a}_{\mu,s}^{\text{ex}\dagger} \hat{a}_{\mu,s}^{\text{gr}} \exp\{i\mathbf{k} \cdot \mathbf{r}_{\mu}\}, \quad (1.47)$$

where each summand represents the excitation of a single atom at lattice site  $\mu$  (and spin  $s$ ) with the corresponding local spatial phase factor, which depends on the wave vector  $\mathbf{k}$  and the position vector  $\mathbf{r}_\mu$  of the lattice site. Via the sum over all lattice sites, the exciton creation operator (1.47) effectively generates an entangled W-type superposition state, where one atom is excited, “but we do not know which one” [67]. Note that previous related models of atom–field coupling in optical lattices, e.g. [57–60], mostly consider a single-mode field in a cavity instead of the free-space situation we suggest. Moreover, they usually assume that the interatomic distances are much smaller than the wavelength – i.e., they neglect the local spatial phases in (1.47), which are essential for directed superradiance.

The exciton creation operator (1.47) and its complex conjugate counterpart, the exciton annihilation operator  $\hat{\Sigma}^-(\mathbf{k}) = [\hat{\Sigma}^+(\mathbf{k})]^\dagger$ , are closely related to the quasi-spin raising and lowering operators (1.6) in section 1.2.2. In comparison, we can define  $\hat{\sigma}_\mu^+ := \sum_s \hat{a}_{\mu,s}^{\text{ex}\dagger} \hat{a}_{\mu,s}^{\text{gr}}$ ,  $\hat{\sigma}_\mu^- := [\hat{\sigma}_\mu^+]^\dagger$  and the corresponding  $x$  and  $y$  operators via  $\hat{\sigma}_\mu^\pm = (\hat{\sigma}_\mu^x \pm i\hat{\sigma}_\mu^y)/2$ . As is explicitly shown in Appendix A.2, the resulting operators  $\hat{\sigma}_\mu^{x/y}$  analogously satisfy the angular momentum algebra (1.7) of the Pauli matrices together with  $\hat{\sigma}_\mu^z = \sum_s (\hat{n}_{\mu,s}^{\text{ex}} - \hat{n}_{\mu,s}^{\text{gr}})$ . Hence, the very same reasoning as in section 1.2.2 applies. In particular, the matrix elements of the exciton creation (1.47) and annihilation operators are also given by (1.15) – indicating that Dicke superradiance is included in the description of the system. For the sake of completeness (and for later reference), we list the resulting quasispin  $X$ ,  $Y$  and  $Z$  operators

$$\hat{\Sigma}^x(\mathbf{k}) = \frac{1}{2} \sum_{\mu,s} (\hat{a}_{\mu,s}^{\text{ex}\dagger} \hat{a}_{\mu,s}^{\text{gr}} \exp\{i\mathbf{k} \cdot \mathbf{r}_\mu\} + \text{H.c.}), \quad (1.48)$$

$$\hat{\Sigma}^y(\mathbf{k}) = \frac{1}{2i} \sum_{\mu,s} (\hat{a}_{\mu,s}^{\text{ex}\dagger} \hat{a}_{\mu,s}^{\text{gr}} \exp\{i\mathbf{k} \cdot \mathbf{r}_\mu\} - \text{H.c.}), \quad (1.49)$$

and

$$\hat{\Sigma}^z = \frac{1}{2} [\hat{\Sigma}^+(\mathbf{k}), \hat{\Sigma}^-(\mathbf{k})] = \frac{1}{2} \sum_{\mu,s} (\hat{n}_{\mu,s}^{\text{ex}} - \hat{n}_{\mu,s}^{\text{gr}}), \quad (1.50)$$

which satisfy the  $SU(2)$  algebra (1.10).

Apart from the general lattice Hamiltonian (1.42) and the atom–field interaction Hamiltonian (1.45), we also need to add the energy counting terms for the excited-state atoms and for the free-space electromagnetic field respectively. When the energy gap between the ground state and the excited state in the atomic level scheme

is denoted by  $\omega$  ( $\hbar = 1$ ), the full Hamiltonian of the total system is thus given by

$$\hat{H} = \hat{H}_{\text{lat}} + \omega \sum_{\mu,s} \hat{n}_{\mu,s}^{\text{ex}} + \int d^3k \omega_{\mathbf{k}} \hat{a}_{\mathbf{k}}^{\dagger} \hat{a}_{\mathbf{k}} + \hat{V}. \quad (1.51)$$

Finally, please note again that the summation over the spin quantum number  $s$  in (1.42), (1.47) and (1.51) implies that the orientation of the internal spin of a fermionic atom has no influence on its hopping, interaction and excitation dynamics.

## 1.4.2. Description in the momentum space

### Discrete Fourier transform

On numerous occasions it will be convenient to perform calculations in the momentum space. We can transform from the lattice site basis to the momentum space  $\mathbf{k}$ -basis via the discrete Fourier transformation

$$\hat{a}_{\mu,s}^{\lambda\dagger} = \frac{1}{\sqrt{N}} \sum_{\mathbf{k}} \hat{a}_{\mathbf{k},s}^{\lambda\dagger} \exp\{-i\mathbf{k} \cdot \mathbf{r}_{\mu}\}, \quad (1.52)$$

where the summation runs over the (discretized) first Brillouin zone, i.e., over all reciprocal lattice vectors  $\mathbf{k} = 2\pi/(L\ell) \cdot \{n, m\}$  with  $n, m \in \{-L/2 + 1, \dots, L/2\}$ , and  $L$  the number of lattice sites per dimension,  $L^2 = N$ . As before,  $\mathbf{r}_{\mu}$  denotes the position vector of the lattice site  $\mu$ . The corresponding back transformation reads

$$\hat{a}_{\mathbf{k},s}^{\lambda\dagger} = \frac{1}{\sqrt{N}} \sum_{\mu} \hat{a}_{\mu,s}^{\lambda\dagger} \exp\{i\mathbf{k} \cdot \mathbf{r}_{\mu}\}. \quad (1.53)$$

The reader can verify that transformations (1.52) and (1.53) are inverse to each other by applying the two essential relations

$$\sum_{\mu} \exp\{i(\mathbf{p} - \mathbf{k}) \cdot \mathbf{r}_{\mu}\} = N\delta_{\mathbf{k}\mathbf{p}}, \quad (1.54)$$

$$\sum_{\mathbf{k}} \exp\{i\mathbf{k} \cdot (\mathbf{r}_v - \mathbf{r}_{\mu})\} = N\delta_{\mu v}, \quad (1.55)$$

which can be derived using geometric summation with the reciprocal lattice vectors  $\mathbf{k}$  and  $\mathbf{p}$  and the lattice site positions  $\mathbf{r}_{\mu}$  and  $\mathbf{r}_v$ .

### General lattice Hamiltonian in the momentum space $k$ -basis

Let us now express the general lattice Hamiltonian (1.42) in the momentum space. For reasons of clarity and comprehensibility, we will consider the tunneling term and the on-site repulsion term separately, i.e.,  $\hat{H}_{\text{lat}} = \hat{H}_J + \hat{H}_U$ .

**Tunneling term** Applying transformation (1.52) to the tunneling term, we immediately obtain

$$\begin{aligned}\hat{H}_J &= -\frac{J}{Z} \sum_{\mu\nu,s,\lambda} T_{\mu\nu} \hat{a}_{\mu,s}^{\lambda\dagger} \hat{a}_{\nu,s}^{\lambda} \\ &= -\frac{J}{NZ} \sum_{\mu\nu\mathbf{k}\mathbf{p},s,\lambda} T_{\mu\nu} \hat{a}_{\mathbf{k},s}^{\lambda\dagger} \hat{a}_{\mathbf{p},s}^{\lambda} \exp\{-i\mathbf{k}\cdot\mathbf{r}_{\mu}\} \exp\{i\mathbf{p}\cdot\mathbf{r}_{\nu}\}.\end{aligned}\quad (1.56)$$

In a two-dimensional lattice, the adjacency matrix  $T_{\mu\nu}$  is unity if  $\mu$  and  $\nu$  are nearest neighbors, and zero otherwise. Considering the summation over the four nearest neighbors  $\nu$  of the lattice site  $\mu$  explicitly, we can thus write

$$\sum_{\nu} T_{\mu\nu} \exp\{i\mathbf{p}\cdot\mathbf{r}_{\nu}\} = T_{\mathbf{p}} \exp\{i\mathbf{p}\cdot\mathbf{r}_{\mu}\}, \quad (1.57)$$

via the Fourier transform of the adjacency matrix,

$$T_{\mathbf{p}} = 2 [\cos(p_x \ell) + \cos(p_y \ell)]. \quad (1.58)$$

In conclusion, we can describe the tunneling term of the general lattice Hamiltonian (1.42) in the  $\mathbf{k}$ -basis,

$$\begin{aligned}\hat{H}_J &= -\frac{J}{NZ} \sum_{\mu\mathbf{k}\mathbf{p},s,\lambda} T_{\mathbf{p}} \hat{a}_{\mathbf{k},s}^{\lambda\dagger} \hat{a}_{\mathbf{p},s}^{\lambda} \exp\{i(\mathbf{p}-\mathbf{k})\cdot\mathbf{r}_{\mu}\} \\ &= -\frac{J}{Z} \sum_{\mathbf{k},s,\lambda} T_{\mathbf{k}} \hat{a}_{\mathbf{k},s}^{\lambda\dagger} \hat{a}_{\mathbf{k},s}^{\lambda} = -\frac{J}{Z} \sum_{\mathbf{k},s,\lambda} T_{\mathbf{k}} \hat{n}_{\mathbf{k},s},\end{aligned}\quad (1.59)$$

where the relation (1.54) was employed, yielding a nonzero result only if the reciprocal lattice vectors are equal, i.e.,  $\mathbf{p} = \mathbf{k}$ . Evidently, the tunneling term of the general lattice Hamiltonian is diagonal in the momentum space  $\mathbf{k}$ -basis – which will prove particularly helpful in the limit of weak interactions ( $J \gg U$ ), where the interaction term (which is nondiagonal in the  $\mathbf{k}$ -basis, as we will see below) can be neglected.

**On-site repulsion term** In preparation for the transformation of the on-site repulsion term of the general lattice Hamiltonian (1.42), we express it in the following form:

$$\begin{aligned}
\hat{H}_U &= \frac{U}{2} \sum_{\mu} \left( \sum_{s,\lambda} \hat{n}_{\mu,s}^{\lambda} \right) \left( \sum_{s,\lambda} \hat{n}_{\mu,s}^{\lambda} - 1 \right) \\
&= \frac{U}{2} \sum_{\mu} \left[ \sum_{s_1 s_2, \lambda_1 \lambda_2} \hat{a}_{\mu,s_1}^{\lambda_1 \dagger} \hat{a}_{\mu,s_1}^{\lambda_1} \hat{a}_{\mu,s_2}^{\lambda_2 \dagger} \hat{a}_{\mu,s_2}^{\lambda_2} - \sum_{s,\lambda} \hat{a}_{\mu,s}^{\lambda \dagger} \hat{a}_{\mu,s}^{\lambda} \right] \\
&= \frac{U}{2} \sum_{\mu} \left[ \sum_{s_1 s_2, \lambda} \hat{a}_{\mu,s_1}^{\lambda \dagger} \hat{a}_{\mu,s_2}^{\lambda \dagger} \hat{a}_{\mu,s_2}^{\lambda} \hat{a}_{\mu,s_1}^{\lambda} + 2 \sum_{s_1 s_2} \hat{a}_{\mu,s_1}^{\text{gr} \dagger} \hat{a}_{\mu,s_2}^{\text{ex} \dagger} \hat{a}_{\mu,s_2}^{\text{ex}} \hat{a}_{\mu,s_1}^{\text{gr}} \right], \quad (1.60)
\end{aligned}$$

where in the second step, the cases of equal  $\lambda = \lambda_1 = \lambda_2$  and different  $\lambda_1 \neq \lambda_2$  have been separated. In the first term, (anti)commutation relations (1.39) or (1.40) have then been applied to rearrange the fermionic or bosonic operators, while the second term follows immediately. Now the on-site repulsion term (1.60) can be easily transformed to the  $\mathbf{k}$ -basis via the discrete Fourier transform (1.52),

$$\begin{aligned}
\hat{H}_U &= \frac{U}{2N^2} \sum_{\mu \mathbf{k}_1 \mathbf{k}_2 \mathbf{k}_3 \mathbf{k}_4, s_1 s_2} \left[ \sum_{\lambda} \hat{a}_{\mathbf{k}_1, s_1}^{\lambda \dagger} \hat{a}_{\mathbf{k}_2, s_2}^{\lambda \dagger} \hat{a}_{\mathbf{k}_3, s_2}^{\lambda} \hat{a}_{\mathbf{k}_4, s_1}^{\lambda} + 2 \hat{a}_{\mathbf{k}_1, s_1}^{\text{gr} \dagger} \hat{a}_{\mathbf{k}_2, s_2}^{\text{ex} \dagger} \hat{a}_{\mathbf{k}_3, s_2}^{\text{ex}} \hat{a}_{\mathbf{k}_4, s_1}^{\text{gr}} \right] \\
&\quad \times \exp\{i(\mathbf{k}_3 + \mathbf{k}_4 - \mathbf{k}_1 - \mathbf{k}_2) \cdot \mathbf{r}_{\mu}\}. \quad (1.61)
\end{aligned}$$

Using again the relation (1.54), we finally obtain the following expression for the on-site repulsion term of the general lattice Hamiltonian (1.42) in the momentum space  $\mathbf{k}$ -basis:

$$\begin{aligned}
\hat{H}_U &= \frac{U}{2N} \sum_{\mathbf{k}_1 \mathbf{k}_2 \mathbf{k}_3 \mathbf{k}_4, s_1 s_2} \delta_{\mathbf{k}_1 + \mathbf{k}_2, \mathbf{k}_3 + \mathbf{k}_4} \left[ \sum_{\lambda} \hat{a}_{\mathbf{k}_1, s_1}^{\lambda \dagger} \hat{a}_{\mathbf{k}_2, s_2}^{\lambda \dagger} \hat{a}_{\mathbf{k}_3, s_2}^{\lambda} \hat{a}_{\mathbf{k}_4, s_1}^{\lambda} + 2 \hat{a}_{\mathbf{k}_1, s_1}^{\text{gr} \dagger} \hat{a}_{\mathbf{k}_2, s_2}^{\text{ex} \dagger} \hat{a}_{\mathbf{k}_3, s_2}^{\text{ex}} \hat{a}_{\mathbf{k}_4, s_1}^{\text{gr}} \right] \\
&= \frac{U}{2N} \sum_{\mathbf{k}_2 \mathbf{k}_3 \mathbf{k}_4, s_1 s_2} \left[ \sum_{\lambda} \hat{a}_{\mathbf{k}_3 + \mathbf{k}_4 - \mathbf{k}_2, s_1}^{\lambda \dagger} \hat{a}_{\mathbf{k}_2, s_2}^{\lambda \dagger} \hat{a}_{\mathbf{k}_3, s_2}^{\lambda} \hat{a}_{\mathbf{k}_4, s_1}^{\lambda} + 2 \hat{a}_{\mathbf{k}_3 + \mathbf{k}_4 - \mathbf{k}_2, s_1}^{\text{gr} \dagger} \hat{a}_{\mathbf{k}_2, s_2}^{\text{ex} \dagger} \hat{a}_{\mathbf{k}_3, s_2}^{\text{ex}} \hat{a}_{\mathbf{k}_4, s_1}^{\text{gr}} \right]. \quad (1.62)
\end{aligned}$$

### Atom-field interaction and total system Hamiltonian in the $\mathbf{k}$ -basis

The exciton creation operator (1.47) can be transformed in a similar fashion via the discrete Fourier transform (1.52) and the summation relation (1.54),

$$\begin{aligned}\hat{\Sigma}^+(\mathbf{k}) &= \sum_{\mu,s} \hat{a}_{\mu,s}^{\text{ex}\dagger} \hat{a}_{\mu,s}^{\text{gr}} \exp\{i\mathbf{k} \cdot \mathbf{r}_\mu\} = \frac{1}{N} \sum_{\mu \mathbf{p} \mathbf{q},s} \hat{a}_{\mathbf{p},s}^{\text{ex}\dagger} \hat{a}_{\mathbf{q},s}^{\text{gr}} \exp\{i(\mathbf{k} - \mathbf{p} + \mathbf{q}) \cdot \mathbf{r}_\mu\} \\ &= \sum_{\mathbf{p},s} \hat{a}_{\mathbf{p},s}^{\text{ex}\dagger} \hat{a}_{\mathbf{p}-\mathbf{k},s}^{\text{gr}}.\end{aligned}\quad (1.63)$$

However, note that we required here that  $\mathbf{k}$  is a reciprocal lattice vector, and will continue to do so for any wave-vector parameters of the exciton creation operator. Interestingly, the spatial phase is then incorporated into the operators in the  $\mathbf{k}$ -basis representation (1.63), instead of its explicit appearance in the lattice site basis (1.47). For the sake of completeness, we also quote the quasispin  $X$  and  $Y$  operators in the  $\mathbf{k}$ -basis, which are immediately obtained using (1.8),

$$\hat{\Sigma}^x(\mathbf{k}) = \frac{1}{2} \sum_{\mathbf{p},s} \hat{a}_{\mathbf{p},s}^{\text{ex}\dagger} \hat{a}_{\mathbf{p}-\mathbf{k},s}^{\text{gr}} + \text{H.c.}, \quad (1.64)$$

$$\hat{\Sigma}^y(\mathbf{k}) = \frac{1}{2i} \sum_{\mathbf{p},s} (\hat{a}_{\mathbf{p},s}^{\text{ex}\dagger} \hat{a}_{\mathbf{p}-\mathbf{k},s}^{\text{gr}} - \text{H.c.}). \quad (1.65)$$

The total number of (ground-state or excited-state) atoms can be counted in the lattice site basis or in the momentum space  $\mathbf{k}$ -basis, i.e.,

$$\begin{aligned}\sum_{\mu,s} \hat{n}_{\mu,s}^\lambda &= \sum_{\mu,s} \hat{a}_{\mu,s}^{\lambda\dagger} \hat{a}_{\mu,s}^\lambda = \frac{1}{N} \sum_{\mu \mathbf{k} \mathbf{p},s} \hat{a}_{\mathbf{k},s}^{\lambda\dagger} \hat{a}_{\mathbf{p},s}^\lambda \exp\{i(\mathbf{p} - \mathbf{k}) \cdot \mathbf{r}_\mu\} \\ &= \sum_{\mathbf{k},s} \hat{a}_{\mathbf{k},s}^{\lambda\dagger} \hat{a}_{\mathbf{k},s}^\lambda = \sum_{\mathbf{k},s} \hat{n}_{\mathbf{k},s}^\lambda,\end{aligned}\quad (1.66)$$

where the summation relation (1.54) has been employed once more. We can then utilize (1.66) to easily transform the quasispin  $Z$  operator (1.50) to the  $\mathbf{k}$ -basis,

$$\hat{\Sigma}^z = \frac{1}{2} \sum_{\mathbf{k},s} (\hat{n}_{\mathbf{k},s}^{\text{ex}} - \hat{n}_{\mathbf{k},s}^{\text{gr}}). \quad (1.67)$$



In conclusion, the full Hamiltonian of the total system expressed in the momentum space  $\mathbf{k}$ -basis reads

$$\hat{H} = \hat{H}_{\text{lat}} + \omega \sum_{\mathbf{k},s} \hat{n}_{\mathbf{k},s}^{\text{ex}} + \int d^3k \omega_{\mathbf{k}} \hat{a}_{\mathbf{k}}^{\dagger} \hat{a}_{\mathbf{k}} + \hat{V}, \quad (1.68)$$

where  $\hat{H}_{\text{lat}}$  is inserted from (1.59) and (1.62) and the atom-field interaction Hamiltonian (1.45) incorporates the exciton creation operator in the  $\mathbf{k}$ -basis (1.63).

### Commutation and anticommutation relations in the $\mathbf{k}$ -basis

Finally, we can also deduce the (anti)commutation relations for bosonic or fermionic creation and annihilation operators in the momentum space  $\mathbf{k}$ -basis. Therefore, we apply the back transformation (1.53) together with the (anti)commutation relations in the lattice site basis (1.41) and employ the summation relation (1.54) once again,

$$\begin{aligned} \hat{a}_{\mathbf{k},s_1}^{\lambda} \hat{a}_{\mathbf{p},s_2}^{\lambda\dagger} \mp \hat{a}_{\mathbf{p},s_2}^{\lambda\dagger} \hat{a}_{\mathbf{k},s_1}^{\lambda} &= \frac{1}{N} \sum_{\mu\nu} \left( \hat{a}_{\mu,s_1}^{\lambda} \hat{a}_{\nu,s_2}^{\lambda\dagger} \mp \hat{a}_{\nu,s_2}^{\lambda\dagger} \hat{a}_{\mu,s_1}^{\lambda} \right) \exp\{-i\mathbf{k} \cdot \mathbf{r}_{\mu}\} \exp\{i\mathbf{p} \cdot \mathbf{r}_{\nu}\} \\ &= \delta_{\mathbf{k}\mathbf{p}} \delta_{s_1s_2}. \end{aligned} \quad (1.69)$$

As always, the upper written sign represents the bosonic case while the lower written sign describes the fermionic case. In the form of (anti)commutators, we have:

$$\left[ \hat{a}_{\mathbf{k},s_1}^{\lambda}, \hat{a}_{\mathbf{p},s_2}^{\lambda\dagger} \right] = \delta_{\mathbf{k}\mathbf{p}} \delta_{s_1s_2}, \quad \left[ \hat{a}_{\mathbf{k},s_1}^{\lambda}, \hat{a}_{\mathbf{p},s_2}^{\lambda} \right] = \left[ \hat{a}_{\mathbf{k},s_1}^{\lambda\dagger}, \hat{a}_{\mathbf{p},s_2}^{\lambda\dagger} \right] = 0, \quad (1.70)$$

$$\left\{ \hat{a}_{\mathbf{k},s_1}^{\lambda}, \hat{a}_{\mathbf{p},s_2}^{\lambda\dagger} \right\} = \delta_{\mathbf{k}\mathbf{p}} \delta_{s_1s_2}, \quad \left\{ \hat{a}_{\mathbf{k},s_1}^{\lambda}, \hat{a}_{\mathbf{p},s_2}^{\lambda} \right\} = \left\{ \hat{a}_{\mathbf{k},s_1}^{\lambda\dagger}, \hat{a}_{\mathbf{p},s_2}^{\lambda\dagger} \right\} = 0, \quad (1.71)$$

where the first row (1.70) applies to bosons and the second row (1.71) is valid for fermions of course.



## 2. Detection of stationary lattice states

*In the upcoming chapter, we will study the collective and coherent absorption and emission of photons by an ensemble of atoms in an optical lattice. We are interested in how the quantum state of the ensemble of atoms in the optical lattice may leave its footprint in the emission characteristics of the photon. To this end, we will make use of the properties of Dicke superradiance as introduced in section 1.2 and focus on the Bose-Hubbard model and Fermi-Hubbard model as introduced in section 1.3 to describe the evolution of the atom ensemble respectively. Please note that we will rely on the formalism introduced in the previous section 1.4.*

### 2.1. Single-photon probing scheme

#### 2.1.1. Initial state of the optical lattice

The initial state of the atom ensemble in the optical lattice can be a mixed state, represented by the density operator  $\hat{\rho}_{\text{in}}$ , or a pure state, represented by the state vector  $|\Psi_{\text{in}}\rangle$  respectively. In the following, we assume an arbitrary initial state, except that all the two-level atoms in the optical lattice should be in their internal ground state before the absorption of the probe photon. Technically, the initial state of the atom ensemble then does not contain any  $\hat{a}_{\mu,s}^{\text{ex}\dagger}$  excitations, i.e.,  $\hat{a}_{\mu,s}^{\text{ex}}|\Psi_{\text{in}}\rangle = 0$ , or rather  $\hat{a}_{\mu,s}^{\text{ex}}\hat{\rho}_{\text{in}} = 0$ , for all  $\mu, s$ . The upcoming calculations are exemplarily performed for a pure state  $|\Psi_{\text{in}}\rangle$ , for clarity. However, the derivation for a mixed state  $\hat{\rho}_{\text{in}}$  runs completely analogously, and the results will be stated for both cases.

Later, we will investigate specific examples. As there are no excited atoms initially, the spectrum of plausible initial states before the absorption of the probe photon is determined by the usual, single-species Bose-Hubbard model (1.32) or Fermi-Hubbard model (1.35), which are both special cases of the general lattice Hamiltonian (1.42). This can therefore range from a fully localized state (e.g., a Mott insulator) to a completely delocalized (e.g., superfluid or metallic) state, for example. In between these limiting cases for zero temperature, the initial state of the bosonic or fermionic optical lattice can also be given by a thermal state  $\hat{\rho}_{\text{in}} = \hat{\rho}_{\text{th}}$ .

### 2.1.2. Collective absorption of the probe photon

In a first step, we suppose that an incoming probe photon with wave vector  $\boldsymbol{\kappa}_{\text{in}}$  and frequency  $|\boldsymbol{\kappa}_{\text{in}}| = \omega_{\text{in}}$  (we set  $\hbar = c = 1$ ) is collectively absorbed by the atom ensemble in the optical lattice. Assuming that the coupling constant  $g_{\mathbf{k}}(t)$  is small, the resulting state can be calculated in first-order perturbation theory of the perturbation Hamiltonian (1.45) in the interaction picture,

$$\hat{V}_{\text{D}}(t) = e^{i\hat{H}_0 t} \hat{V} e^{-i\hat{H}_0 t} = \int d^3k g_{\mathbf{k}}(t) \hat{a}_{\mathbf{k}} e^{-i\omega_{\mathbf{k}} t} \hat{\Sigma}^+(\mathbf{k}, t) + \text{H.c.}, \quad (2.1)$$

where  $\hat{H}_0 = \hat{H} - \hat{V}$  represents the unperturbed Hamiltonian, given by the full system Hamiltonian (1.51) minus the perturbation Hamiltonian (1.45). In addition,  $\omega_{\mathbf{k}}$  denotes the frequency of a photon with wave vector  $\mathbf{k}$ , and

$$\hat{\Sigma}^+(\mathbf{k}, t) = e^{i\hat{H}_0 t} \hat{\Sigma}^+(\mathbf{k}) e^{-i\hat{H}_0 t} = e^{i\omega t} \sum_{\mu,s} \hat{a}_{\mu,s}^{\text{ex}\dagger}(t) \hat{a}_{\mu,s}^{\text{gr}}(t) \exp\{i\mathbf{k} \cdot \mathbf{r}_{\mu}\} \quad (2.2)$$

describes the exciton creation operator (1.47) in the interaction picture, where  $\omega$  is the energy difference between the two atomic levels. Here, the creation and annihilation operators carry the lattice dynamics (1.42), i.e.,  $\hat{a}_{\mu,s}^{\text{ex}\dagger}(t) = e^{i\hat{H}_{\text{lat}} t} \hat{a}_{\mu,s}^{\text{ex}\dagger} e^{-i\hat{H}_{\text{lat}} t}$  and  $\hat{a}_{\mu,s}^{\text{gr}}(t)$  analogously. The series expansion of the corresponding time evolution operator then reads

$$\hat{U}(\tau_A) = \mathcal{T} \exp \left\{ -i \int_0^{\tau_A} dt \hat{V}_{\text{D}}(t) \right\} = 1 - i \int_0^{\tau_A} dt_1 \hat{V}_{\text{D}}(t_1) + \mathcal{O}(g_{\mathbf{k}}^2(t)). \quad (2.3)$$

Using the commutation relation (1.46) for  $\hat{a}_{\mathbf{k}}$  and  $\hat{a}_{\boldsymbol{\kappa}_{\text{in}}}^{\dagger}$ , and projecting out the resulting vacuum of the photon field,  $\hat{a}_{\mathbf{k}}|0_{\text{ph}}\rangle = 0$ , the quantum state of the atom ensemble in the optical lattice after the absorption can be written as

$$\begin{aligned} |\Psi_{\text{abs}}\rangle &= -i \langle 0_{\text{ph}} | \int_0^{\tau_A} dt_1 \hat{V}_{\text{D}}(t_1) |\Psi_{\text{in}}\rangle \otimes \hat{a}_{\boldsymbol{\kappa}_{\text{in}}}^{\dagger} |0_{\text{ph}}\rangle \\ &= -i \int_0^{\tau_A} dt_1 g_{\boldsymbol{\kappa}_{\text{in}}}(t_1) e^{-i\omega_{\text{in}} t_1} \hat{\Sigma}^+(\boldsymbol{\kappa}_{\text{in}}, t_1) |\Psi_{\text{in}}\rangle. \end{aligned} \quad (2.4)$$

Of course, the Hermitian conjugate term vanishes in (2.4), as  $\hat{\Sigma}^-(\mathbf{k}, t) |\Psi_{\text{in}}\rangle = 0$  for all  $\mathbf{k}, t$ .

### 2.1.3. Collective re-emission of the probe photon

The subsequent collective and coherent re-emission of the probe photon is similarly calculated via first-order perturbation theory. Of course, we now start from the quantum state of the atom ensemble after the absorption (2.4), together with the vacuum state of the photon field. The resulting quantum state  $|\Psi_{\text{out}}\rangle$ , including the re-emitted photon, then reads

$$\begin{aligned} |\Psi_{\text{out}}\rangle &= -i \int_0^{\tau_E} dt_2 \hat{V}_D(t_2) |\Psi_{\text{abs}}\rangle \otimes |0_{\text{ph}}\rangle \\ &= -i \int_0^{\tau_E} dt_2 \int d^3q g_{\mathbf{q}}^*(t_2) \hat{a}_{\mathbf{q}}^\dagger e^{i\omega_{\mathbf{q}}t_2} \hat{\Sigma}^-(\mathbf{q}, t_2) |\Psi_{\text{abs}}\rangle \otimes |0_{\text{ph}}\rangle. \end{aligned} \quad (2.5)$$

After inserting (2.4), we obtain a combination of an exciton creation operator and an exciton annihilation operator with different wave vector parameters  $\boldsymbol{\kappa}_{\text{in}}$ ,  $\mathbf{q}$  and time parameters  $t_1$ ,  $t_2$  each,

$$\begin{aligned} |\Psi_{\text{out}}\rangle &= - \int_0^{\tau_E} dt_2 \int_0^{\tau_A} dt_1 \int d^3q g_{\mathbf{q}}^*(t_2) g_{\boldsymbol{\kappa}_{\text{in}}}(t_1) e^{i(\omega_{\mathbf{q}}t_2 - \omega_{\text{in}}t_1)} \\ &\quad \times \hat{\Sigma}^-(\mathbf{q}, t_2) \hat{\Sigma}^+(\boldsymbol{\kappa}_{\text{in}}, t_1) |\Psi_{\text{in}}\rangle \otimes \hat{a}_{\mathbf{q}}^\dagger |0_{\text{ph}}\rangle. \end{aligned} \quad (2.6)$$

### 2.1.4. Combined emission probability density

As a measurable quantity, we want to calculate the combined probability density that the probe photon with wave vector  $\boldsymbol{\kappa}_{\text{in}}$  is absorbed *and* subsequently re-emitted in a specified direction  $\boldsymbol{\kappa}_{\text{out}}$ . This probability density is obtained by projecting the outgoing quantum state (2.6) onto a state with a photon in the mode  $\boldsymbol{\kappa}_{\text{out}}$  and squaring the norm of the remaining atomic state vector,

$$P_{\boldsymbol{\kappa}_{\text{out}}} = \left\| \langle 0_{\text{ph}} | \hat{a}_{\boldsymbol{\kappa}_{\text{out}}} | \Psi_{\text{out}} \rangle \right\|^2. \quad (2.7)$$

Resolving the photonic part via its commutation relation (1.46), we obtain

$$P_{\boldsymbol{\kappa}_{\text{out}}} = \left\| \int_0^{\tau_E} dt_2 \int_0^{\tau_A} dt_1 g_{\boldsymbol{\kappa}_{\text{out}}}^*(t_2) g_{\boldsymbol{\kappa}_{\text{in}}}(t_1) e^{i(\omega_{\text{out}}t_2 - \omega_{\text{in}}t_1)} \hat{S}_{\boldsymbol{\kappa}_{\text{out}}}^{\boldsymbol{\kappa}_{\text{in}}}(t_1, t_2) |\Psi_{\text{in}}\rangle \right\|^2, \quad (2.8)$$

with the operatorial part

$$\hat{S}_{\boldsymbol{\kappa}_{\text{out}}}^{\boldsymbol{\kappa}_{\text{in}}}(t_1, t_2) = \hat{\Sigma}^-(\boldsymbol{\kappa}_{\text{out}}, t_2) \hat{\Sigma}^+(\boldsymbol{\kappa}_{\text{in}}, t_1), \quad (2.9)$$

consisting of an exciton creation operator with wave vector  $\boldsymbol{\kappa}_{\text{in}}$  at absorption time  $t_1$  and an exciton annihilation operator with wave vector  $\boldsymbol{\kappa}_{\text{out}}$  at emission time  $t_2$ . According to the definition (2.2), the operatorial part can be expanded as

$$\hat{S}_{\boldsymbol{\kappa}_{\text{out}}}^{\boldsymbol{\kappa}_{\text{in}}}(t_1, t_2) = e^{i\omega(t_1-t_2)} \sum_{\mu\nu, s_1 s_2} \hat{a}_{\mu, s_1}^{\text{gr}\dagger}(t_2) \hat{a}_{\mu, s_1}^{\text{ex}}(t_2) \hat{a}_{\nu, s_2}^{\text{ex}\dagger}(t_1) \hat{a}_{\nu, s_2}^{\text{gr}}(t_1) \times \exp\{-i(\boldsymbol{\kappa}_{\text{out}} \cdot \mathbf{r}_\mu - \boldsymbol{\kappa}_{\text{in}} \cdot \mathbf{r}_\nu)\}. \quad (2.10)$$

**Special case of a single atom** As a point of reference for later comparisons with collective emission probability densities, it is useful to consider the special case of a single atom absorbing and re-emitting the probe photon. Then, the initial lattice state simplifies to  $|\Psi_{\text{in}}\rangle = |\psi\rangle^{\text{gr}} \otimes |0\rangle^{\text{ex}}$  and the operatorial part (2.10) collapses to

$$\hat{S}_{\boldsymbol{\kappa}_{\text{out}}}^{\boldsymbol{\kappa}_{\text{in}}}(t_1, t_2) = e^{i\omega(t_1-t_2)} \sum_{s_1 s_2} \hat{a}_{s_1}^{\text{gr}\dagger} \hat{a}_{s_1}^{\text{ex}} \hat{a}_{s_2}^{\text{ex}\dagger} \hat{a}_{s_2}^{\text{gr}} \exp\{-i(\boldsymbol{\kappa}_{\text{out}} - \boldsymbol{\kappa}_{\text{in}}) \cdot \mathbf{r}\}, \quad (2.11)$$

as there is no lattice anymore, i.e.,  $\hat{H}_{\text{lat}} = 0$ , and thus the time-dependency of the creation and annihilation operators, e.g.,  $\hat{a}_{\mu, s}^{\lambda\dagger}(t) = e^{i\hat{H}_{\text{lat}}t} \hat{a}_{\mu, s}^{\lambda\dagger} e^{-i\hat{H}_{\text{lat}}t}$ , vanishes. Employing (anti)commutation relations (1.41), we can resolve the operators acting on excited atoms and  $|0\rangle^{\text{ex}}$ . The remaining operatorial part  $\sum_{s_1} \hat{n}_{s_1}^{\text{gr}} |\psi\rangle^{\text{gr}}$  simply counts the number of ground-state atoms, which should be one, i.e.,  $\|\sum_{s_1} \hat{n}_{s_1}^{\text{gr}} |\psi\rangle^{\text{gr}}\| = 1$ . Furthermore, we assume that the incoming probe photon is in resonance with the atomic transition,  $\omega_{\text{in}} = \omega$ . In summary, the combined probability density (2.8) then reduces to

$$P_{\boldsymbol{\kappa}_{\text{out}}}^{\text{single}} = \left| \int_0^{\tau_E} dt_2 \int_0^{\tau_A} dt_1 g_{\boldsymbol{\kappa}_{\text{out}}}^*(t_2) g_{\boldsymbol{\kappa}_{\text{in}}}(t_1) e^{i(\omega_{\text{out}} - \omega)t_2} \right|^2. \quad (2.12)$$

If it is supposed that the coupling constant  $g_{\boldsymbol{\kappa}_{\text{out}}}^*(t_2)$  does not depend on the orientation of the wave vector  $\boldsymbol{\kappa}_{\text{out}}$ , the emission in (2.12) is not directed, as expected in the case of a single atom [74]. Therefore, we may write  $P_{\text{single}} = P_{\boldsymbol{\kappa}_{\text{out}}}^{\text{single}}$  for the emission probability density in arbitrary direction  $\boldsymbol{\kappa}_{\text{out}}$ .

**General case** In the general case, the combined emission probability density (2.8) to absorb a photon with wave number  $\boldsymbol{\kappa}_{\text{in}}$  and (after a waiting time  $\Delta t$ , which will be detailed later) re-emit this photon with wave number  $\boldsymbol{\kappa}_{\text{out}}$  can be expanded via

its conjugate transpose as

$$P_{\boldsymbol{\kappa}_{\text{out}}} = \int_0^{\tau_E} dt_4 \int_0^{\tau_A} dt_3 \int_0^{\tau_E} dt_2 \int_0^{\tau_A} dt_1 g_{\boldsymbol{\kappa}_{\text{out}}}(t_4) g_{\boldsymbol{\kappa}_{\text{out}}}^*(t_2) g_{\boldsymbol{\kappa}_{\text{in}}}^*(t_3) g_{\boldsymbol{\kappa}_{\text{in}}}(t_1) \\ \times e^{-i(\omega_{\text{out}} - \omega)t_4} e^{i(\omega_{\text{out}} - \omega)t_2} \mathcal{D}_{\boldsymbol{\kappa}_{\text{out}}}^{\boldsymbol{\kappa}_{\text{in}}}(t_1, t_2, t_3, t_4), \quad (2.13)$$

where we have again assumed that the incoming probe photon is in resonance with the atomic transition,  $\omega_{\text{in}} = \omega$ . The expanded operatorial part  $\mathcal{D}_{\boldsymbol{\kappa}_{\text{out}}}^{\boldsymbol{\kappa}_{\text{in}}}(t_1, t_2, t_3, t_4)$  contains the lattice dynamics via the time dependence of the annihilation and creation operators, and the collective behavior of the absorption and emission process via the summation over the individual lattice sites and their spatial phases (see section 1.2.1). In general, this reads

$$\mathcal{D}_{\boldsymbol{\kappa}_{\text{out}}}^{\boldsymbol{\kappa}_{\text{in}}}(t_1, t_2, t_3, t_4) = \sum_{\mu\nu\rho\eta, s_1 s_2 s_3 s_4} \exp\{i(\boldsymbol{\kappa}_{\text{out}} \cdot \mathbf{r}_\rho - \boldsymbol{\kappa}_{\text{in}} \cdot \mathbf{r}_\eta)\} \exp\{-i(\boldsymbol{\kappa}_{\text{out}} \cdot \mathbf{r}_\mu - \boldsymbol{\kappa}_{\text{in}} \cdot \mathbf{r}_\nu)\} \\ \times \langle \Psi_{\text{in}} | \hat{a}_{\eta, s_4}^{\text{gr}\dagger}(t_3) \hat{a}_{\eta, s_4}^{\text{ex}}(t_3) \hat{a}_{\rho, s_3}^{\text{ex}\dagger}(t_4) \hat{a}_{\rho, s_3}^{\text{gr}}(t_4) \\ \times \hat{a}_{\mu, s_1}^{\text{gr}\dagger}(t_2) \hat{a}_{\mu, s_1}^{\text{ex}}(t_2) \hat{a}_{\nu, s_2}^{\text{ex}\dagger}(t_1) \hat{a}_{\nu, s_2}^{\text{gr}}(t_1) | \Psi_{\text{in}} \rangle. \quad (2.14)$$

As addressed in section 2.1.1, the combined emission probability density (2.13) can be derived for an arbitrary mixed initial state  $\hat{\rho}_{\text{in}}$  in complete analogy to the presented case of a pure initial state  $|\Psi_{\text{in}}\rangle$ . For a mixed initial state  $\hat{\rho}_{\text{in}}$ , the expanded operatorial part instead reads

$$\mathcal{D}_{\boldsymbol{\kappa}_{\text{out}}}^{\boldsymbol{\kappa}_{\text{in}}}(t_1, t_2, t_3, t_4) = \sum_{\mu\nu\rho\eta, s_1 s_2 s_3 s_4} \exp\{i(\boldsymbol{\kappa}_{\text{out}} \cdot \mathbf{r}_\rho - \boldsymbol{\kappa}_{\text{in}} \cdot \mathbf{r}_\eta)\} \exp\{-i(\boldsymbol{\kappa}_{\text{out}} \cdot \mathbf{r}_\mu - \boldsymbol{\kappa}_{\text{in}} \cdot \mathbf{r}_\nu)\} \\ \times \text{Tr}\{\hat{\rho}_{\text{in}} \hat{a}_{\eta, s_4}^{\text{gr}\dagger}(t_3) \hat{a}_{\eta, s_4}^{\text{ex}}(t_3) \hat{a}_{\rho, s_3}^{\text{ex}\dagger}(t_4) \hat{a}_{\rho, s_3}^{\text{gr}}(t_4) \\ \times \hat{a}_{\mu, s_1}^{\text{gr}\dagger}(t_2) \hat{a}_{\mu, s_1}^{\text{ex}}(t_2) \hat{a}_{\nu, s_2}^{\text{ex}\dagger}(t_1) \hat{a}_{\nu, s_2}^{\text{gr}}(t_1)\}. \quad (2.15)$$

In both cases, the four-times eight-point functions in (2.14, 2.15) contain not only information about the initial state of the optical lattice, but also about its time evolution. Unfortunately, though, they cannot be solved explicitly for the general lattice Hamiltonian (1.42) without further assumptions. Thus we will analyze two limiting cases in the upcoming sections, namely the case of separable states (i.e., small  $J$ ) in section 2.2 and the case of weak interactions (i.e.,  $J \gg U$ ) in section 2.3.

## 2.2. Detection in the separable state regime

First, we are going to study the combined emission probability density (2.8) in the separable state regime. The separable state regime is characterized by vanishingly small tunneling and negligible correlations between lattice sites, i.e.,  $J \ll U$ . As prototypical examples, one can think of the separable Mott insulator state (1.33) and Mott-Néel state (1.36), which exhibit no correlations between lattice sites (not to be confused with correlations between particles).

To this end, we employ the Gutzwiller ansatz [85, 86], that is, we assume that a pure initial state  $|\Psi_{\text{in}}\rangle$  resembles the Mott insulator state in the sense that it is a product of (bosonic or fermionic) normalized single-site states, i.e.,

$$|\Psi_{\text{in}}\rangle = \bigotimes_{\mu} |\Psi_{\mu}\rangle = \bigotimes_{\mu} (|\Psi_{\mu}\rangle^{\text{gr}} \otimes |0_{\mu}\rangle^{\text{ex}}), \quad (2.16)$$

with  $\langle \Psi_{\mu} | \Psi_{\mu} \rangle = 1$  for all  $\mu$  and thus  $\langle \Psi_{\text{in}} | \Psi_{\text{in}} \rangle = 1$ . Of course, the initial state still does not contain any  $\hat{a}_{\mu,s}^{\text{ex}\dagger}$  excitations, as introduced in section 2.1.1. In addition, we require that the time taken by the absorption or emission process itself is much shorter than the waiting time  $\Delta t = t' - t$  in between absorption and emission, such that it is justified to separate the operatorial part from the integration in (2.8). Prior to the separation, however, we make sure to extract the temporal phase  $e^{i\omega(t_1-t_2)}$ , which stems from the energy counting term for the excited-state atoms in the unperturbed Hamiltonian (1.51), i.e.,

$$P_{\kappa_{\text{out}}} = \left\| \int_0^{\tau_E} dt_2 \int_0^{\tau_A} dt_1 g_{\kappa_{\text{out}}}^*(t_2) g_{\kappa_{\text{in}}}(t_1) e^{i(\omega_{\text{out}} t_2 - \omega_{\text{in}} t_1)} e^{i\omega(t_1-t_2)} \right. \\ \left. \times e^{-i\omega(t_1-t_2)} \hat{S}_{\kappa_{\text{out}}}^{\kappa_{\text{in}}}(t_1, t_2) |\Psi_{\text{in}}\rangle \right\|^2. \quad (2.17)$$

In this way we make sure that the separated part (in the lower line) solely carries the lattice dynamics (1.42), while the remaining part with the integrations reduces to the emission probability density in the case of a single atom (2.12), assuming atomic resonance  $\omega_{\text{in}} = \omega$ . Summing up, the combined emission probability density (2.8) in this approximation becomes

$$P_{\kappa_{\text{out}}} = \left\| e^{-i\omega(t-t')} \hat{S}_{\kappa_{\text{out}}}^{\kappa_{\text{in}}}(t, t') |\Psi_{\text{in}}\rangle \right\|^2 P_{\text{single}}, \quad (2.18)$$

where we replaced  $t_1 = t$  and  $t_2 = t'$  with the (constant) absorption and emission



times respectively. After explicitly inserting the operatorial part (2.10) and the initial state (2.16), the temporal phase cancels out. In conclusion, the single-atom emission probability density is effectively enhanced by the factor

$$\begin{aligned} \tilde{\mathcal{D}}_{\mathbf{\kappa}_{\text{out}}}^{\mathbf{\kappa}_{\text{in}}}(t, t') = & \left\| \sum_{\mu\nu, s_1 s_2} \exp\{-i(\mathbf{\kappa}_{\text{out}} \cdot \mathbf{r}_\mu - \mathbf{\kappa}_{\text{in}} \cdot \mathbf{r}_\nu)\} \right. \\ & \left. \times \hat{a}_{\mu, s_1}^{\text{gr}\dagger}(t') \hat{a}_{\mu, s_1}^{\text{ex}}(t') \hat{a}_{\nu, s_2}^{\text{ex}\dagger}(t) \hat{a}_{\nu, s_2}^{\text{gr}}(t) \otimes_{\chi} |\Psi_\chi\rangle \right\|^2. \end{aligned} \quad (2.19)$$

As we are in the separable state regime ( $J \ll U$ ), we thereby require that the correlations between different lattice sites, which arise by way of the tunneling  $J$  during the waiting time  $\Delta t$ , remain negligible. In practice, we assume that a single-site state  $|\Psi_\mu\rangle$  is not affected by operators acting on a different lattice site  $\nu \neq \mu$ . For example, the  $|\Psi_\mu\rangle$  single-site state, which does not contain any  $\hat{a}_{\mu, s}^{\text{ex}\dagger}$  excitations, should be unaffected by the operators acting on the lattice site  $\nu \neq \mu$ , and thus the  $\hat{a}_{\mu, s_1}^{\text{ex}}(t')$  annihilation operator leads to a vanishing term  $\hat{a}_{\mu, s_1}^{\text{ex}}(t')|\Psi_\mu\rangle \approx 0$ . As a consequence, we omit all terms with  $\nu \neq \mu$  from (2.19), i.e.,

$$\begin{aligned} \tilde{\mathcal{D}}_{\mathbf{\kappa}_{\text{out}}}^{\mathbf{\kappa}_{\text{in}}}(t, t') = & \left\| \sum_{\mu, s_1 s_2} \exp\{-i(\mathbf{\kappa}_{\text{out}} - \mathbf{\kappa}_{\text{in}}) \cdot \mathbf{r}_\mu\} \right. \\ & \left. \times \hat{a}_{\mu, s_1}^{\text{gr}\dagger}(t') \hat{a}_{\mu, s_1}^{\text{ex}}(t') \hat{a}_{\mu, s_2}^{\text{ex}\dagger}(t) \hat{a}_{\mu, s_2}^{\text{gr}}(t) \otimes_{\chi} |\Psi_\chi\rangle \right\|^2. \end{aligned} \quad (2.20)$$

As a way to gain more insight into the structure of (2.20), it is possible to expand it via its conjugate transpose and then rearrange terms according to equal or distinct lattice site indices:

$$\begin{aligned} \tilde{\mathcal{D}}_{\mathbf{\kappa}_{\text{out}}}^{\mathbf{\kappa}_{\text{in}}}(t, t') = & \left| \sum_{\mu, s_1 s_2} \exp\{-i(\mathbf{\kappa}_{\text{out}} - \mathbf{\kappa}_{\text{in}}) \cdot \mathbf{r}_\mu\} \right. \\ & \left. \times \langle \Psi_\mu | \hat{a}_{\mu, s_1}^{\text{gr}\dagger}(t') \hat{a}_{\mu, s_1}^{\text{ex}}(t') \hat{a}_{\mu, s_2}^{\text{ex}\dagger}(t) \hat{a}_{\mu, s_2}^{\text{gr}}(t) | \Psi_\mu \rangle \right|^2 \\ & - \sum_{\mu} \left| \sum_{s_1 s_2} \langle \Psi_\mu | \hat{a}_{\mu, s_1}^{\text{gr}\dagger}(t') \hat{a}_{\mu, s_1}^{\text{ex}}(t') \hat{a}_{\mu, s_2}^{\text{ex}\dagger}(t) \hat{a}_{\mu, s_2}^{\text{gr}}(t) | \Psi_\mu \rangle \right|^2 \\ & + \sum_{\mu} \left\| \sum_{s_1 s_2} \hat{a}_{\mu, s_1}^{\text{gr}\dagger}(t') \hat{a}_{\mu, s_1}^{\text{ex}}(t') \hat{a}_{\mu, s_2}^{\text{ex}\dagger}(t) \hat{a}_{\mu, s_2}^{\text{gr}}(t) | \Psi_\mu \rangle \right\|^2. \end{aligned} \quad (2.21)$$

Importantly, the first term scales with  $\mathcal{O}(N^2)$ , as the sum over the  $N$  lattice sites  $\mu$  appears inside the absolute square, whereas the other two terms usually<sup>1</sup> only scale with  $\mathcal{O}(N)$ . Hence, the emission probability density is guided by the first term, which can be interpreted rather intuitively. The expectation value inside the spatial phase sum corresponds to the probability amplitude that the excited atom, which is created at lattice site  $\mu$  (and spin quantum number  $s_2$ ) via the  $\hat{a}_{\mu,s_2}^{\text{ex}\dagger}$  creation operator, is still at the same position  $\mu$  (with spin quantum number  $s_1$ ) after the waiting time  $\Delta t = t' - t$ .

If we give further consideration to the extreme case  $J = 0$ , where the atoms do not move at all, the time dependence of the creation and annihilation operators can be easily calculated according to the unperturbed Hamiltonian (1.51). Without tunneling, this only yields a global temporal phase, which can be omitted due to the absolute squares. After employing (anti)commutation relations  $\hat{a}_{\mu,s_1}^{\text{ex}} \hat{a}_{\mu,s_2}^{\text{ex}\dagger} = \delta_{s_1 s_2} \pm \hat{a}_{\mu,s_2}^{\text{ex}\dagger} \hat{a}_{\mu,s_1}^{\text{ex}}$  from (1.41) and considering that  $\hat{a}_{\mu,s_1}^{\text{ex}} |\Psi_\mu\rangle = 0$ , the operatorial part (2.21) then reduces to

$$\begin{aligned} \tilde{D}_{\boldsymbol{\kappa}_{\text{out}}}^{\boldsymbol{\kappa}_{\text{in}}}(t, t') &= \left| \sum_{\mu,s} \exp\{-i(\boldsymbol{\kappa}_{\text{out}} - \boldsymbol{\kappa}_{\text{in}}) \cdot \mathbf{r}_\mu\} \langle \Psi_\mu | \hat{n}_{\mu,s}^{\text{gr}} | \Psi_\mu \rangle \right|^2 \\ &\quad - \sum_{\mu} \left| \sum_s \langle \Psi_\mu | \hat{n}_{\mu,s}^{\text{gr}} | \Psi_\mu \rangle \right|^2 + \sum_{\mu} \left\| \sum_s \hat{n}_{\mu,s}^{\text{gr}} | \Psi_\mu \rangle \right\|^2. \end{aligned} \quad (2.22)$$

For states which satisfy  $\sum_s \hat{n}_{\mu,s}^{\text{gr}} | \Psi_\mu \rangle = n_\mu | \Psi_\mu \rangle$  for all  $\mu$ , where  $n_\mu$  is thus the total number of (ground-state) atoms at lattice site  $\mu$ , the last two terms cancel each other out and we get

$$\tilde{D}_{\boldsymbol{\kappa}_{\text{out}}}^{\boldsymbol{\kappa}_{\text{in}}}(t, t') = \left| \sum_{\mu} \exp\{-i(\boldsymbol{\kappa}_{\text{out}} - \boldsymbol{\kappa}_{\text{in}}) \cdot \mathbf{r}_\mu\} n_\mu \right|^2. \quad (2.23)$$

When the single-site states are not eigenstates<sup>2</sup> of the number operator sum  $\sum_s \hat{n}_{\mu,s}^{\text{gr}}$ , however, the result (2.23) is no longer accurate in all orders of  $N$ , but still valid to leading order  $\mathcal{O}(N^2)$  with  $n_\mu = \sum_s \langle \Psi_\mu | \hat{n}_{\mu,s}^{\text{gr}} | \Psi_\mu \rangle$ .

<sup>1</sup>Strictly speaking, the second and third term could also scale with  $\mathcal{O}(N^2)$  in the case of a state where all  $N$  atoms are concentrated on one or few lattice sites. In practice, however, this is not the case in the  $J \ll U$  (Mott) regime, where the atoms are more or less uniformly distributed over the lattice.

<sup>2</sup>Consider, for example, superposition single-site states  $|\Psi_\mu\rangle$  with non-integer expectation values, such as  $|\Psi_\mu\rangle = (|0\rangle + |1\rangle)/\sqrt{2}$  with  $n_\mu = 1/2$ .

Notably, the result (2.23) of the operatorial part for immovable atoms ( $J = 0$ ) can be understood as a discrete Fourier transform of the number distribution of the atoms in the optical lattice. The most straightforward example would be an initial state with exactly one atom per lattice site,  $n_\mu = 1$ . In this case we obtain (rigorously for a large number density),

$$\tilde{D}_{\kappa_{\text{out}}}^{\kappa_{\text{in}}}(t, t') = \left| \sum_{\mu} \exp\{-i(\kappa_{\text{out}} - \kappa_{\text{in}}) \cdot \mathbf{r}_{\mu}\} \right|^2 = N^2 \delta_{\kappa_{\text{in}} \kappa_{\text{out}}}, \quad (2.24)$$

i.e., a sharp peak, as expected from a Fourier transform.

In other words, when the atoms in the optical lattice are initially in the Mott insulator state (1.33) or in the Mott-Néel state (1.36), the combined probability density for the absorption of a probe photon  $\kappa_{\text{in}}$  and its subsequent re-emission in the same direction  $\kappa_{\text{out}} = \kappa_{\text{in}}$  is enhanced by a factor  $N^2$ ,

$$P_{\kappa_{\text{out}}} = N^2 \delta_{\kappa_{\text{in}} \kappa_{\text{out}}} P_{\text{single}}, \quad (2.25)$$

while it vanishes for all other emission angles. Naturally, this probability density does not depend on the waiting time  $\Delta t$ , as we have considered the limit of zero tunneling. The result (2.25) coincides with the well-known directed spontaneous superradiant emission for fixed atom ensembles [67, 68, 72]. Please note that only one factor of  $N$  corresponds to the (single-photon) superradiant enhancement, while another factor of  $N$  originates from the fact that  $N$  atoms absorb the incident probe photon  $N$  times more likely than one atom (see section 1.2).

Nevertheless, the separable state approximation (2.21) or (2.23) models accurately only for a narrow parameter range, and we will discover significant deviations in the limiting case of weak interactions ( $J \gg U$ ) discussed below.

### 2.3. Detection in the weak interactions regime

Let us now study the opposite limiting case  $J \gg U$ , i.e., the weak interactions regime, which typically features strong correlations between lattice sites. For example, the superfluid ground state (1.34) of the Bose-Hubbard model and the metallic ground state (1.37) of the Fermi-Hubbard model are exemplary for the weak interactions regime.

As the tunneling term dominates, the on-site repulsion term can be omitted from the general lattice Hamiltonian (1.42), i.e., we approximate  $U = 0$ . It is then convenient to carry out calculations in the momentum space  $\mathbf{k}$ -basis, as prepared in section 1.4.2, in which the tunneling term becomes diagonal (1.59). In contrast to the previous section, where we discussed the opposite (small  $J$ ) regime, the exciton creation operator (1.63) then picks up a vector-dependent phase from the tunneling term in the interaction picture,

$$\phi_{\mathbf{p}}^{\mathbf{k}}(t) = -J/Z(T_{\mathbf{p}} - T_{\mathbf{p}-\mathbf{k}})t, \quad (2.26)$$

in addition to the temporal phase from the excitation energy  $\omega$  in (1.68),

$$\hat{\Sigma}^+(\mathbf{k}, t) = e^{i\omega t} \sum_{\mathbf{p},s} \hat{a}_{\mathbf{p},s}^{\text{ex}\dagger} \hat{a}_{\mathbf{p}-\mathbf{k},s}^{\text{gr}} \exp\{i\phi_{\mathbf{p}}^{\mathbf{k}}(t)\}. \quad (2.27)$$

The tunneling phase (2.26) is proportional to the tunneling rate  $J$  and involves the lattice structure via  $T_{\mathbf{p}}$ , the Fourier transform (1.58) of the adjacency matrix  $T_{\mu\nu}$ , and the coordination number  $Z$ . As we will see below, it is responsible for a reduction in the spatial phase coherence due to the tunneling  $J$ . But first let us continue by expressing the operatorial part (2.9) in the  $\mathbf{k}$ -basis via (2.27)<sup>3</sup>,

$$\begin{aligned} \hat{S}_{\kappa_{\text{out}}}^{\kappa_{\text{in}}}(t_1, t_2) &= e^{i\omega(t_1-t_2)} \sum_{\mathbf{p}\mathbf{q},s_1s_2} \hat{a}_{\mathbf{p}-\kappa_{\text{out}},s_1}^{\text{gr}\dagger} \hat{a}_{\mathbf{p},s_1}^{\text{ex}} \hat{a}_{\mathbf{q},s_2}^{\text{ex}\dagger} \hat{a}_{\mathbf{q}-\kappa_{\text{in}},s_2}^{\text{gr}} \\ &\quad \times \exp\{i[\phi_{\mathbf{q}}^{\kappa_{\text{in}}}(t_1) - \phi_{\mathbf{p}}^{\kappa_{\text{out}}}(t_2)]\}, \end{aligned} \quad (2.28)$$

and inserting it into the combined emission probability density (2.8), where we as-

<sup>3</sup>As explained below (1.63), the wave vectors  $\kappa_{\text{in}}$  and  $\kappa_{\text{out}}$  have to match reciprocal lattice vectors in order to allow for this convenient representation. Throughout this Thesis, we thus assume that  $\kappa_{\text{in}}$  and  $\kappa_{\text{out}}$  are reciprocal lattice vectors. Otherwise, the calculations would become lengthy without providing more insight. In the experiment, however, the wave vector  $\kappa_{\text{in}}$  of the probe photon and the direction  $\kappa_{\text{out}}$  in which to detect the re-emission can be chosen to match reciprocal lattice vectors (chapter 5).

sume resonant absorption ( $\omega_{\text{in}} = \omega$ ),

$$P_{\kappa_{\text{out}}} = \left\| \int_0^{\tau_E} dt_2 \int_0^{\tau_A} dt_1 g_{\kappa_{\text{out}}}^*(t_2) g_{\kappa_{\text{in}}}(t_1) e^{i(\omega_{\text{out}} - \omega)t_2} \right. \\ \left. \times \sum_{pq, s_1 s_2} \hat{a}_{p-\kappa_{\text{out}}, s_1}^{\text{gr} \dagger} \hat{a}_{p, s_1}^{\text{ex}} \hat{a}_{q, s_2}^{\text{ex} \dagger} \hat{a}_{q-\kappa_{\text{in}}, s_2}^{\text{gr}} \exp \{i[\phi_q^{\kappa_{\text{in}}}(t_1) - \phi_p^{\kappa_{\text{out}}}(t_2)]\} |\Psi_{\text{in}}\rangle \right\|^2. \quad (2.29)$$

Of course, time-independent creation and annihilation operators corresponding to different species  $\lambda \in \{\text{gr}, \text{ex}\}$  of bosons or fermions always commute (see section 1.4.1). This is also intuitively clear, as ground-state atoms and excited-state atoms do not interfere with each other in the weak interactions limit ( $U = 0$ ). Hence we can employ (anti)commutation relations (1.69) on the operators of the excited-state atoms in order to reduce the expression via  $\hat{a}_{p, s_1}^{\text{ex}} \hat{a}_{q, s_2}^{\text{ex} \dagger} |\Psi_{\text{in}}\rangle = \delta_{pq} \delta_{s_1 s_2} |\Psi_{\text{in}}\rangle$ , where we considered that there were no excitations initially,  $\hat{a}_{\mu, s}^{\text{ex}} |\Psi_{\text{in}}\rangle = 0$ . In conclusion, we obtain

$$P_{\kappa_{\text{out}}} = \left\| \int_0^{\tau_E} dt_2 \int_0^{\tau_A} dt_1 g_{\kappa_{\text{out}}}^*(t_2) g_{\kappa_{\text{in}}}(t_1) e^{i(\omega_{\text{out}} - \omega)t_2} \right. \\ \left. \times \sum_{p, s} \hat{a}_{p-\kappa_{\text{out}}, s}^{\text{gr} \dagger} \hat{a}_{p-\kappa_{\text{in}}, s}^{\text{gr}} \exp \{i[\phi_p^{\kappa_{\text{in}}}(t_1) - \phi_p^{\kappa_{\text{out}}}(t_2)]\} |\Psi_{\text{in}}\rangle \right\|^2. \quad (2.30)$$

When we now expand the combined probability density (2.30) analogous to the general case in the lattice site basis (2.13), i.e., via its conjugate transpose, we get

$$P_{\kappa_{\text{out}}} = \int_0^{\tau_E} dt_4 \int_0^{\tau_A} dt_3 \int_0^{\tau_E} dt_2 \int_0^{\tau_A} dt_1 g_{\kappa_{\text{out}}}(t_4) g_{\kappa_{\text{out}}}^*(t_2) g_{\kappa_{\text{in}}}^*(t_3) g_{\kappa_{\text{in}}}(t_1) \\ \times e^{-i(\omega_{\text{out}} - \omega)t_4} e^{i(\omega_{\text{out}} - \omega)t_2} \mathcal{E}_{\kappa_{\text{out}}}^{\kappa_{\text{in}}}(t_1, t_2, t_3, t_4), \quad (2.31)$$

with an expanded operatorial part  $\mathcal{E}_{\kappa_{\text{out}}}^{\kappa_{\text{in}}}(t_1, t_2, t_3, t_4)$  in the  $\mathbf{k}$ -basis, which turns out to involve a four-point correlator instead of the eight-point correlator in the lattice site basis (2.14),

$$\mathcal{E}_{\kappa_{\text{out}}}^{\kappa_{\text{in}}}(t_1, t_2, t_3, t_4) = \sum_{pq} \exp \{i[\phi_q^{\kappa_{\text{out}}}(t_4) - \phi_q^{\kappa_{\text{in}}}(t_3) - \phi_p^{\kappa_{\text{out}}}(t_2) + \phi_p^{\kappa_{\text{in}}}(t_1)]\} \\ \times \sum_{s_1 s_2} \langle \Psi_{\text{in}} | \hat{a}_{q-\kappa_{\text{in}}, s_2}^{\text{gr} \dagger} \hat{a}_{q-\kappa_{\text{out}}, s_2}^{\text{gr}} \hat{a}_{p-\kappa_{\text{out}}, s_1}^{\text{gr} \dagger} \hat{a}_{p-\kappa_{\text{in}}, s_1}^{\text{gr}} | \Psi_{\text{in}} \rangle. \quad (2.32)$$

Analogously, the combined probability density (2.31) can be derived for an arbitrary

mixed initial state  $\hat{\rho}_{\text{in}}$  in place of a pure state  $|\Psi_{\text{in}}\rangle$ , see section 2.1.1. The expanded operatorial part (2.32) then reads,

$$\begin{aligned} \mathcal{E}_{\kappa_{\text{out}}}^{\kappa_{\text{in}}}(t_1, t_2, t_3, t_4) &= \sum_{pq} \exp\{i[\phi_q^{\kappa_{\text{out}}}(t_4) - \phi_q^{\kappa_{\text{in}}}(t_3) - \phi_p^{\kappa_{\text{out}}}(t_2) + \phi_p^{\kappa_{\text{in}}}(t_1)]\} \\ &\times \sum_{s_1 s_2} \text{Tr}\{\hat{\rho}_{\text{in}} \hat{a}_{q-\kappa_{\text{in}}, s_2}^{\text{gr} \dagger} \hat{a}_{q-\kappa_{\text{out}}, s_2}^{\text{gr}} \hat{a}_{p-\kappa_{\text{out}}, s_1}^{\text{gr} \dagger} \hat{a}_{p-\kappa_{\text{in}}, s_1}^{\text{gr}}\}. \end{aligned} \quad (2.33)$$

Once again, the four-point correlator in (2.32) or (2.33) contains the interesting physics. In particular, it includes the impact of the tunneling on the spatial phase coherence, which is essential for superradiant emission. In the following, we will analyze two general cases in which the four-point correlators in (2.32) or (2.33) can be explicitly calculated.

**Pure initial states** We start with the case of pure initial states  $|\Psi_{\text{in}}\rangle$ , which are eigenstates of the number operator in the  $\mathbf{k}$ -basis, i.e., states that satisfy the eigenvalue equation  $\hat{n}_{\mathbf{k}, s}^{\text{gr}} |\Psi_{\text{in}}\rangle = n_s(\mathbf{k}) |\Psi_{\text{in}}\rangle$  with a number distribution function  $n_s(\mathbf{k})$ . This applies to all bosonic or fermionic basis states of the momentum space  $\mathbf{k}$ -basis, which means all states of the shape

$$|\Psi_{\text{in}}\rangle = \prod_{\mathbf{k}, s} \frac{1}{\sqrt{n_s(\mathbf{k})!}} \left(\hat{a}_{\mathbf{k}, s}^{\text{gr} \dagger}\right)^{n_s(\mathbf{k})} |0\rangle, \quad (2.34)$$

and particularly to the superfluid ground state (1.34) and the metallic ground state (1.37). However, due to their fundamental (anti)commutation relations (1.69), we will obtain different results for the correlator (2.32) depending on whether we deal with bosonic or fermionic atoms in the optical lattice. Thus, we will analyze the two cases – which either correspond to the Bose-Hubbard model or to the Fermi-Hubbard model – separately in the two upcoming paragraphs:

**Bosonic four-point correlator** First, we calculate the four-point correlator (2.32) for an initial state (2.34) of two-level, bosonic atoms without additional degrees of freedom, i.e., with spin indices  $s_1, s_2$  omitted:

$$E_n^{\text{B}} = \langle \Psi_{\text{in}} | \hat{a}_{q-\kappa_{\text{in}}}^{\text{gr} \dagger} \hat{a}_{q-\kappa_{\text{out}}}^{\text{gr}} \hat{a}_{p-\kappa_{\text{out}}}^{\text{gr} \dagger} \hat{a}_{p-\kappa_{\text{in}}}^{\text{gr}} | \Psi_{\text{in}} \rangle. \quad (2.35)$$

Essentially there are two cases which can lead to a nonzero result – each annihilation operator either needs to be compensated by the creation operator to its left, i.e.,

$\boldsymbol{\kappa}_{\text{in}} = \boldsymbol{\kappa}_{\text{out}}$ , or by the opposite creation operator, i.e.,  $\boldsymbol{p} = \boldsymbol{q}$ . In addition, it is possible that all four  $\boldsymbol{k}$ -vectors are the same. Summing up, we expand (2.35) according to the possible nonzero cases,

$$E_n^B = \delta_{\boldsymbol{\kappa}_{\text{in}}\boldsymbol{\kappa}_{\text{out}}} \langle \Psi_{\text{in}} | \hat{n}_{\boldsymbol{q}-\boldsymbol{\kappa}_{\text{out}}}^{\text{gr}} \hat{n}_{\boldsymbol{p}-\boldsymbol{\kappa}_{\text{in}}}^{\text{gr}} | \Psi_{\text{in}} \rangle + \delta_{\boldsymbol{p}\boldsymbol{q}} \langle \Psi_{\text{in}} | \hat{a}_{\boldsymbol{q}-\boldsymbol{\kappa}_{\text{in}}}^{\text{gr}\dagger} \hat{a}_{\boldsymbol{q}-\boldsymbol{\kappa}_{\text{out}}}^{\text{gr}} \hat{a}_{\boldsymbol{p}-\boldsymbol{\kappa}_{\text{out}}}^{\text{gr}\dagger} \hat{a}_{\boldsymbol{p}-\boldsymbol{\kappa}_{\text{in}}}^{\text{gr}} | \Psi_{\text{in}} \rangle (1 - \delta_{\boldsymbol{\kappa}_{\text{in}}\boldsymbol{\kappa}_{\text{out}}}). \quad (2.36)$$

Note that the case in which all four  $\boldsymbol{k}$ -vectors are the same was subtracted from the second term, such that it was not included twice. Employing commutation relations (1.70), we can express everything in terms of number operators,

$$E_n^B = \delta_{\boldsymbol{\kappa}_{\text{in}}\boldsymbol{\kappa}_{\text{out}}} \langle \Psi_{\text{in}} | \hat{n}_{\boldsymbol{q}-\boldsymbol{\kappa}_{\text{out}}}^{\text{gr}} \hat{n}_{\boldsymbol{p}-\boldsymbol{\kappa}_{\text{in}}}^{\text{gr}} | \Psi_{\text{in}} \rangle + \delta_{\boldsymbol{p}\boldsymbol{q}} \langle \Psi_{\text{in}} | (\hat{n}_{\boldsymbol{q}-\boldsymbol{\kappa}_{\text{out}}}^{\text{gr}} + 1) \hat{n}_{\boldsymbol{p}-\boldsymbol{\kappa}_{\text{in}}}^{\text{gr}} | \Psi_{\text{in}} \rangle (1 - \delta_{\boldsymbol{\kappa}_{\text{in}}\boldsymbol{\kappa}_{\text{out}}}). \quad (2.37)$$

When  $|\Psi_{\text{in}}\rangle$  is a normalized eigenstate of the number operator, i.e.,  $\hat{n}_{\boldsymbol{k}}^{\text{gr}} |\Psi_{\text{in}}\rangle = n(\boldsymbol{k}) |\Psi_{\text{in}}\rangle$ , the result for the bosonic correlator (2.35) is then given by

$$E_n^B = n(\boldsymbol{p} - \boldsymbol{\kappa}_{\text{in}}) n(\boldsymbol{q} - \boldsymbol{\kappa}_{\text{out}}) (\delta_{\boldsymbol{\kappa}_{\text{in}}\boldsymbol{\kappa}_{\text{out}}} + \delta_{\boldsymbol{p}\boldsymbol{q}} - \delta_{\boldsymbol{p}\boldsymbol{q}} \delta_{\boldsymbol{\kappa}_{\text{in}}\boldsymbol{\kappa}_{\text{out}}}) + n(\boldsymbol{p} - \boldsymbol{\kappa}_{\text{in}}) (\delta_{\boldsymbol{p}\boldsymbol{q}} - \delta_{\boldsymbol{p}\boldsymbol{q}} \delta_{\boldsymbol{\kappa}_{\text{in}}\boldsymbol{\kappa}_{\text{out}}}). \quad (2.38)$$

**Fermionic four-point correlator** Let us now calculate the four-point correlator (2.32) for an initial state (2.34) of two-level, fermionic atoms with internal spin quantum numbers  $s_1, s_2 \in \{\uparrow, \downarrow\}$ :

$$E_n^F = \sum_{s_1 s_2} \langle \Psi_{\text{in}} | \hat{a}_{\boldsymbol{q}-\boldsymbol{\kappa}_{\text{in}}, s_2}^{\text{gr}\dagger} \hat{a}_{\boldsymbol{q}-\boldsymbol{\kappa}_{\text{out}}, s_2}^{\text{gr}} \hat{a}_{\boldsymbol{p}-\boldsymbol{\kappa}_{\text{out}}, s_1}^{\text{gr}\dagger} \hat{a}_{\boldsymbol{p}-\boldsymbol{\kappa}_{\text{in}}, s_1}^{\text{gr}} | \Psi_{\text{in}} \rangle. \quad (2.39)$$

Analogously to the bosonic case, we can expand the fermionic correlator (2.39) in terms of the relevant cases which can yield a nonzero result. However, while the spins can be arbitrary in the first case (first term), they have to be equal,  $s_1 = s_2$ , in the second case (second term),

$$E_n^F = \delta_{\boldsymbol{\kappa}_{\text{in}}\boldsymbol{\kappa}_{\text{out}}} \sum_{s_1 s_2} \langle \Psi_{\text{in}} | \hat{n}_{\boldsymbol{q}-\boldsymbol{\kappa}_{\text{out}}, s_2}^{\text{gr}} \hat{n}_{\boldsymbol{p}-\boldsymbol{\kappa}_{\text{in}}, s_1}^{\text{gr}} | \Psi_{\text{in}} \rangle + \delta_{\boldsymbol{p}\boldsymbol{q}} \sum_s \langle \Psi_{\text{in}} | \hat{a}_{\boldsymbol{q}-\boldsymbol{\kappa}_{\text{in}}, s}^{\text{gr}\dagger} \hat{a}_{\boldsymbol{q}-\boldsymbol{\kappa}_{\text{out}}, s}^{\text{gr}} \hat{a}_{\boldsymbol{p}-\boldsymbol{\kappa}_{\text{out}}, s}^{\text{gr}\dagger} \hat{a}_{\boldsymbol{p}-\boldsymbol{\kappa}_{\text{in}}, s}^{\text{gr}} | \Psi_{\text{in}} \rangle (1 - \delta_{\boldsymbol{\kappa}_{\text{in}}\boldsymbol{\kappa}_{\text{out}}}). \quad (2.40)$$

Again, the case that all  $\mathbf{k}$ -vectors and all spins are the same has been explicitly excluded from the second term, as it is already accounted for in the first term. Using anticommutation relations (1.71), further deviations from the bosonic case arise:

$$E_n^F = \delta_{\boldsymbol{\kappa}_{\text{in}}\boldsymbol{\kappa}_{\text{out}}} \sum_{s_1 s_2} \langle \Psi_{\text{in}} | \hat{n}_{\mathbf{q}-\boldsymbol{\kappa}_{\text{out}},s_2}^{\text{gr}} \hat{n}_{\mathbf{p}-\boldsymbol{\kappa}_{\text{in}},s_1}^{\text{gr}} | \Psi_{\text{in}} \rangle + \delta_{\mathbf{p}\mathbf{q}} \sum_s \langle \Psi_{\text{in}} | (1 - \hat{n}_{\mathbf{q}-\boldsymbol{\kappa}_{\text{out}},s}^{\text{gr}}) \hat{n}_{\mathbf{p}-\boldsymbol{\kappa}_{\text{in}},s}^{\text{gr}} | \Psi_{\text{in}} \rangle (1 - \delta_{\boldsymbol{\kappa}_{\text{in}}\boldsymbol{\kappa}_{\text{out}}}). \quad (2.41)$$

Due to the fermionic character, it is  $(\hat{n}_{\mathbf{p}-\boldsymbol{\kappa}_{\text{in}},s}^{\text{gr}})^2 = \hat{n}_{\mathbf{p}-\boldsymbol{\kappa}_{\text{in}},s}^{\text{gr}}$ , and thus the  $\delta_{\boldsymbol{\kappa}_{\text{in}}\boldsymbol{\kappa}_{\text{out}}}$  at the end of the second line can be left out, as the expectation value is zero anyway when  $\boldsymbol{\kappa}_{\text{in}} = \boldsymbol{\kappa}_{\text{out}}$  (and  $\mathbf{k} = \mathbf{q}$ ). Thus, the final result for the fermionic correlator (2.39) for an initial state  $|\Psi_{\text{in}}\rangle$  which is a normalized eigenstate of the number operator, i.e.,  $\hat{n}_{\mathbf{k},s}^{\text{gr}} |\Psi_{\text{in}}\rangle = n_s(\mathbf{k}) |\Psi_{\text{in}}\rangle$ , is given by

$$E_n^F = \delta_{\boldsymbol{\kappa}_{\text{in}}\boldsymbol{\kappa}_{\text{out}}} \sum_{s_1 s_2} n_{s_1}(\mathbf{p} - \boldsymbol{\kappa}_{\text{in}}) n_{s_2}(\mathbf{q} - \boldsymbol{\kappa}_{\text{out}}) + \delta_{\mathbf{p}\mathbf{q}} \sum_s n_s(\mathbf{p} - \boldsymbol{\kappa}_{\text{in}}) [1 - n_s(\mathbf{q} - \boldsymbol{\kappa}_{\text{out}})]. \quad (2.42)$$

**Wick's theorem** As another possibility, we can resort to Wick's theorem [87, 88] for Gaussian (mixed) initial states  $\hat{\rho}_{\text{in}} = \hat{\rho}_{\text{g}}$ . According to Wick's theorem, the four-point correlator in (2.33) can then be expanded as a sum of products of two-point correlators, given that the Hamiltonian is quadratic in the annihilation and creation operators. Note that this is obviously the case in the weak interactions regime ( $U = 0$ ), where the Hamiltonian only consists of the tunneling term (1.59). Starting from (the sum over) the four-point correlator in (2.33), we can thus separate it into:

$$E_{\text{Wick}}^{\text{B/F}} = \sum_{s_1 s_2} \text{Tr} \left\{ \hat{\rho}_{\text{g}} \hat{a}_{\mathbf{q}-\boldsymbol{\kappa}_{\text{in}},s_2}^{\text{gr}\dagger} \hat{a}_{\mathbf{q}-\boldsymbol{\kappa}_{\text{out}},s_2}^{\text{gr}} \hat{a}_{\mathbf{p}-\boldsymbol{\kappa}_{\text{out}},s_1}^{\text{gr}\dagger} \hat{a}_{\mathbf{p}-\boldsymbol{\kappa}_{\text{in}},s_1}^{\text{gr}} \right\} = \sum_{s_1 s_2} \left( \text{Tr} \left\{ \hat{\rho}_{\text{g}} \hat{a}_{\mathbf{q}-\boldsymbol{\kappa}_{\text{in}},s_2}^{\text{gr}\dagger} \hat{a}_{\mathbf{q}-\boldsymbol{\kappa}_{\text{out}},s_2}^{\text{gr}} \right\} \times \text{Tr} \left\{ \hat{\rho}_{\text{g}} \hat{a}_{\mathbf{p}-\boldsymbol{\kappa}_{\text{out}},s_1}^{\text{gr}\dagger} \hat{a}_{\mathbf{p}-\boldsymbol{\kappa}_{\text{in}},s_1}^{\text{gr}} \right\} + \text{Tr} \left\{ \hat{\rho}_{\text{g}} \hat{a}_{\mathbf{q}-\boldsymbol{\kappa}_{\text{in}},s_2}^{\text{gr}\dagger} \hat{a}_{\mathbf{p}-\boldsymbol{\kappa}_{\text{in}},s_1}^{\text{gr}} \right\} \times \text{Tr} \left\{ \hat{\rho}_{\text{g}} \hat{a}_{\mathbf{q}-\boldsymbol{\kappa}_{\text{out}},s_2}^{\text{gr}} \hat{a}_{\mathbf{p}-\boldsymbol{\kappa}_{\text{out}},s_1}^{\text{gr}\dagger} \right\} \right), \quad (2.43)$$

where the spin indices and their summation only apply in the fermionic case of course. Furthermore, if we assume that the Gaussian state  $\hat{\rho}_{\text{in}} = \hat{\rho}_{\text{g}}$  is diagonal in the  $\mathbf{k}$ -basis, we can simplify the two-point correlators in (2.43) to expectation values of number operators,  $n_s(\mathbf{k}) = \text{Tr} \{ \hat{\rho}_{\text{g}} \hat{n}_{\mathbf{k},s}^{\text{gr}} \}$ , analogous to the case of a pure



initial state (see above). In the bosonic case, the resulting expression then reads

$$E_{\text{Wick}}^{\text{B}} = n(\mathbf{p} - \boldsymbol{\kappa}_{\text{in}})n(\mathbf{q} - \boldsymbol{\kappa}_{\text{out}})(\delta_{\boldsymbol{\kappa}_{\text{in}}\boldsymbol{\kappa}_{\text{out}}} + \delta_{\mathbf{p}\mathbf{q}}) + n(\mathbf{p} - \boldsymbol{\kappa}_{\text{in}})\delta_{\mathbf{p}\mathbf{q}}, \quad (2.44)$$

where, in comparison with the bosonic four-point correlator for pure initial states (2.38), the terms corresponding to the situation where all four operators act on the same  $\mathbf{k}$ -mode are naturally missing. In the case of fermions, on the other hand, we obtain the same expression for Gaussian states from Wick's theorem as we obtained for pure initial states (2.42),

$$\begin{aligned} E_{\text{Wick}}^{\text{F}} &= \delta_{\boldsymbol{\kappa}_{\text{in}}\boldsymbol{\kappa}_{\text{out}}} \sum_{s_1 s_2} n_{s_1}(\mathbf{p} - \boldsymbol{\kappa}_{\text{in}})n_{s_2}(\mathbf{q} - \boldsymbol{\kappa}_{\text{out}}) \\ &+ \delta_{\mathbf{p}\mathbf{q}} \sum_s n_s(\mathbf{p} - \boldsymbol{\kappa}_{\text{in}})[1 - n_s(\mathbf{q} - \boldsymbol{\kappa}_{\text{out}})]. \end{aligned} \quad (2.45)$$

With these preparations, we are able to calculate the combined emission probability density (2.31) via the expanded operatorial parts (2.32, 2.33) in the weak interactions regime ( $J \gg U$ ) for a variety of initial lattice states  $|\Psi_{\text{in}}\rangle$  or  $\hat{\rho}_{\text{in}} = \hat{\rho}_{\text{g}}$ . On the one hand, we can evaluate this by inserting the number distribution (in reciprocal space)  $n_s(\mathbf{k})$  of a pure initial state into the bosonic (2.38) or fermionic (2.42) four-point correlator respectively. On the other hand, we may insert Gaussian initial states which are diagonal in the  $\mathbf{k}$ -basis, such as thermal states, into the corresponding expressions for bosons (2.44) or fermions (2.45). In the following sections, we will thus consider specific initial lattice states, such as the superfluid ground state (1.34) of the Bose-Hubbard model, the metallic ground state (1.37) of the Fermi-Hubbard model, or thermal states for both species.

### 2.3.1. Bose-Hubbard model

#### Superfluid ground state

The prime example of an initial lattice state in the superfluid regime of the Bose-Hubbard model is certainly the superfluid ground state, introduced in section 1.3.2,

$$|\Psi\rangle_{\text{sf}}^{U=0} = \frac{1}{\sqrt{N!}} (\hat{b}_{\mathbf{k}=\mathbf{0}}^\dagger)^N |0\rangle = \frac{1}{\sqrt{N!}} \left( \frac{1}{\sqrt{N}} \sum_{\mu=1}^N \hat{b}_\mu^\dagger \right)^N |0\rangle. \quad (2.46)$$

In the superfluid ground state, all  $N$  atoms are condensed in the  $\mathbf{k} = \mathbf{0}$  mode, and therefore its number distribution simply reads  $n^{\text{sf}}(\mathbf{k}) = N\delta_{\mathbf{k}\mathbf{0}}$ . Inserting this num-

ber distribution into the bosonic four-point correlator (2.38) yields

$$E_{n^{\text{sf}}}^{\text{B}} = N(N-1) \delta_{\mathbf{p}\mathbf{q}\boldsymbol{\kappa}_{\text{in}}\boldsymbol{\kappa}_{\text{out}}} + N \delta_{\mathbf{p}\mathbf{q}\boldsymbol{\kappa}_{\text{in}}}. \quad (2.47)$$

In the expanded operatorial part (2.32), we can then contract the sums and merge the phases as far as possible, leading to

$$\begin{aligned} \mathcal{E}_{\boldsymbol{\kappa}_{\text{out}}}^{\boldsymbol{\kappa}_{\text{in}}}(t_1, t_2, t_3, t_4) &= N(N-1) \delta_{\boldsymbol{\kappa}_{\text{in}}\boldsymbol{\kappa}_{\text{out}}} \exp\{i\phi_{\boldsymbol{\kappa}_{\text{in}}}^{\boldsymbol{\kappa}_{\text{in}}}(t_4 - t_3 - t_2 + t_1)\} \\ &+ N \exp\{i[\phi_{\boldsymbol{\kappa}_{\text{in}}}^{\boldsymbol{\kappa}_{\text{out}}}(t_4 - t_2) - \phi_{\boldsymbol{\kappa}_{\text{in}}}^{\boldsymbol{\kappa}_{\text{in}}}(t_3 - t_1)]\}. \end{aligned} \quad (2.48)$$

The crucial point here is that both the  $\mathbf{p}$  sum and  $\mathbf{q}$  sum were fixed, and thus only a global phase remains in each term. As the time taken by the absorption or emission process itself is usually much smaller than the waiting time  $\Delta t$  between absorption and emission, these global phases are to a good approximation constant during the integration period. Therefore, they can be neglected after insertion into the combined probability density (2.31), and we can write the result in terms of the single-atom emission probability density (2.12),

$$P_{\boldsymbol{\kappa}_{\text{out}}} = N(N-1) \delta_{\boldsymbol{\kappa}_{\text{in}}\boldsymbol{\kappa}_{\text{out}}} P_{\text{single}} + N P_{\text{single}}. \quad (2.49)$$

Summing up, we observe superradiant re-emission in the same direction in which the absorbed photon was incoming,  $\boldsymbol{\kappa}_{\text{out}} = \boldsymbol{\kappa}_{\text{in}}$ , if the lattice is in the superfluid ground state (2.46). To leading order, this outcome coincides with the result we obtained for the Mott insulator state and the Mott-Néel state (2.25) – notably it also does not depend on the waiting time  $\Delta t$ , which is due to the condensed nature of the superfluid ground state. While the incoherent emission in other directions  $\boldsymbol{\kappa}_{\text{out}} \neq \boldsymbol{\kappa}_{\text{in}}$  is completely suppressed for a Mott state (which is attributable to the uniformity of the “artificial crystal”), an incoherent contribution of the order  $\mathcal{O}(N)$  is present in the case of the superfluid ground state (2.49). In conclusion, the superfluid ground state cannot be distinguished from the Mott insulator state (1.33) or Mott-Néel state (1.36) by the pump-and-probe scheme that we suggest (section 1.1). Aside from that, a differentiation via the deviating incoherent emission probabilities should be possible, in principle. Such a detection method is comparable to instantaneous Bragg scattering [48–54].

### Partial condensation state

As a next example, we would like to study an initial state where not all  $N_\Psi$  but only  $N_1 \leq N_\Psi$  of the bosonic atoms are condensed in the  $\mathbf{k} = \mathbf{0}$  mode, while  $N_2$  other atoms should be equally distributed between all  $\mathbf{k}$ -modes, i.e.,

$$n^{\text{dt}}(\mathbf{k}) = N_1 \delta_{\mathbf{k}\mathbf{0}} + \frac{N_2}{N}. \quad (2.50)$$

Note that the number of bosonic atoms is denoted as  $N_\Psi = \sum_{\mathbf{k}} n^{\text{dt}}(\mathbf{k}) = N_1 + N_2$  on purpose, as here we are also considering optical lattices with a filling factor of  $N_\Psi/N$  greater than one (where  $N$  is the number of lattice sites). However, the number distribution (2.50) can of course also stem from a mixed state with  $N_\Psi = N$ . Physically, the partial condensation state (2.50) can serve as an insightful toy model for a more complex thermal state (which will also be discussed below). Inserting it into the bosonic four-point correlator (2.38) yields

$$\begin{aligned} E_{n^{\text{dt}}}^{\text{B}} &= N_1(N_1 - 1) \delta_{\mathbf{p}\mathbf{q}\boldsymbol{\kappa}_{\text{in}}\boldsymbol{\kappa}_{\text{out}}} + N_1 \delta_{\mathbf{p}\mathbf{q}\boldsymbol{\kappa}_{\text{in}}} \\ &+ \frac{N_1 N_2}{N} (\delta_{\mathbf{p}\boldsymbol{\kappa}_{\text{in}}\boldsymbol{\kappa}_{\text{out}}} + \delta_{\mathbf{q}\boldsymbol{\kappa}_{\text{in}}\boldsymbol{\kappa}_{\text{out}}} + \delta_{\mathbf{p}\mathbf{q}\boldsymbol{\kappa}_{\text{in}}} + \delta_{\mathbf{p}\mathbf{q}\boldsymbol{\kappa}_{\text{out}}} - 2\delta_{\mathbf{p}\mathbf{q}\boldsymbol{\kappa}_{\text{in}}\boldsymbol{\kappa}_{\text{out}}}) \\ &+ \frac{N_2^2}{N^2} (\delta_{\boldsymbol{\kappa}_{\text{in}}\boldsymbol{\kappa}_{\text{out}}} + \delta_{\mathbf{p}\mathbf{q}} - \delta_{\mathbf{p}\mathbf{q}} \delta_{\boldsymbol{\kappa}_{\text{in}}\boldsymbol{\kappa}_{\text{out}}}) + \frac{N_2}{N} (\delta_{\mathbf{p}\mathbf{q}} - \delta_{\mathbf{p}\mathbf{q}} \delta_{\boldsymbol{\kappa}_{\text{in}}\boldsymbol{\kappa}_{\text{out}}}), \end{aligned} \quad (2.51)$$

where the first line corresponds to the condensed part (2.47), the mixed terms are written in the second line and the distributed part is given in the last line. For the sake of simplicity, we assume that  $N_1$ ,  $N_2$  and  $N$  are all of the order  $\mathcal{O}(N) \gg 1$ , and only keep terms which scale with the highest order  $\mathcal{O}(N^2)$  in the operatorial part (2.32). Note that in this context it is important whether the summation indices  $\mathbf{p}$  and  $\mathbf{q}$  are fixed in (2.51), as the summations in (2.32) provide a factor  $N$  as well. In summary, the four-point correlator (2.51) reads to the highest order in  $N$ :

$$\tilde{E}_{n^{\text{dt}}}^{\text{B}} = \left( N_1^2 \delta_{\mathbf{p}\mathbf{q}\boldsymbol{\kappa}_{\text{in}}} + \frac{N_1 N_2}{N} (\delta_{\mathbf{p}\boldsymbol{\kappa}_{\text{in}}} + \delta_{\mathbf{q}\boldsymbol{\kappa}_{\text{in}}}) + \frac{N_2^2}{N^2} \right) \delta_{\boldsymbol{\kappa}_{\text{in}}\boldsymbol{\kappa}_{\text{out}}}, \quad (2.52)$$

where all remaining terms represent directed superradiant emission in the same direction  $\boldsymbol{\kappa}_{\text{out}} = \boldsymbol{\kappa}_{\text{in}}$  in which the absorbed photon was incoming. When we reduce the sums and combine the phase factors accordingly, the operatorial part (2.32) can

be evaluated to

$$\begin{aligned} \mathcal{E}_{\kappa_{\text{out}}}^{\kappa_{\text{in}}}(t_1, t_2, t_3, t_4) &= N_1^2 \delta_{\kappa_{\text{in}}\kappa_{\text{out}}} \exp \left\{ i\phi_{\kappa_{\text{in}}}^{\kappa_{\text{in}}}(t_4 - t_3 - t_2 + t_1) \right\} \\ &+ \frac{N_1 N_2}{N} \delta_{\kappa_{\text{in}}\kappa_{\text{out}}} \left( \sum_{\mathbf{q}} \exp \left\{ i[\phi_{\mathbf{q}}^{\kappa_{\text{in}}}(t_4 - t_3) - \phi_{\kappa_{\text{in}}}^{\kappa_{\text{in}}}(t_2 - t_1)] \right\} \right. \\ &\quad \left. + \sum_{\mathbf{p}} \exp \left\{ i[\phi_{\kappa_{\text{in}}}^{\kappa_{\text{in}}}(t_4 - t_3) - \phi_{\mathbf{p}}^{\kappa_{\text{in}}}(t_2 - t_1)] \right\} \right) \\ &+ \frac{N_2^2}{N^2} \delta_{\kappa_{\text{in}}\kappa_{\text{out}}} \sum_{\mathbf{p}\mathbf{q}} \exp \left\{ i[\phi_{\mathbf{q}}^{\kappa_{\text{in}}}(t_4 - t_3) - \phi_{\mathbf{p}}^{\kappa_{\text{in}}}(t_2 - t_1)] \right\}. \end{aligned} \quad (2.53)$$

Notably, the  $\mathbf{p}$  sums and  $\mathbf{q}$  sums separate both in the mixed term and in the last term, which motivates us to introduce the following abbreviation for sums over the vector-dependent phase (2.26),

$$\mathcal{J}_{\kappa}(\Delta t) = \frac{1}{N} \sum_{\mathbf{p}} \exp \left\{ -i\phi_{\mathbf{p}}^{\kappa}(\Delta t) \right\} = \frac{1}{N} \sum_{\mathbf{p}} \exp \left\{ iJ/Z(T_{\mathbf{p}} - T_{\mathbf{p}-\kappa})\Delta t \right\} \leq 1, \quad (2.54)$$

together with an abbreviation for the fixed phase (2.26) which appears,

$$\begin{aligned} \varphi(\Delta t) &= -\phi_{\kappa_{\text{in}}}^{\kappa_{\text{in}}}(\Delta t) = J/Z(T_{\kappa_{\text{in}}} - T_{\mathbf{0}})\Delta t \\ &= 2J/Z \left[ \cos(\kappa_{\text{in},x}\ell) + \cos(\kappa_{\text{in},y}\ell) - 2 \right] \Delta t. \end{aligned} \quad (2.55)$$

Using these abbreviations, we rearrange the operatorial part (2.53) in the shorter form

$$\begin{aligned} \mathcal{E}_{\kappa_{\text{out}}}^{\kappa_{\text{in}}}(t_1, t_2, t_3, t_4) &= \left[ N_1^2 \exp \left\{ i\varphi(t_3 - t_4) \right\} \exp \left\{ i\varphi(t_2 - t_1) \right\} \right. \\ &+ N_1 N_2 \left( \mathcal{J}_{\kappa_{\text{in}}}(t_3 - t_4) \exp \left\{ i\varphi(t_2 - t_1) \right\} + \mathcal{J}_{\kappa_{\text{in}}}(t_2 - t_1) \exp \left\{ i\varphi(t_3 - t_4) \right\} \right) \\ &\quad \left. + N_2^2 \mathcal{J}_{\kappa_{\text{in}}}(t_3 - t_4) \mathcal{J}_{\kappa_{\text{in}}}(t_2 - t_1) \right] \delta_{\kappa_{\text{in}}\kappa_{\text{out}}}, \end{aligned} \quad (2.56)$$

and reinsert it into the combined probability density (2.31), which then can be written via the absolute square

$$\begin{aligned} P_{\kappa_{\text{out}}} &= \left| \int_0^{\tau_E} dt_2 \int_0^{\tau_A} dt_1 g_{\kappa_{\text{out}}}^*(t_2) g_{\kappa_{\text{in}}}(t_1) e^{i(\omega_{\text{out}} - \omega)t_2} \right. \\ &\quad \left. \times \left[ N_1 \exp \left\{ i\varphi(t_2 - t_1) \right\} + N_2 \mathcal{J}_{\kappa_{\text{in}}}(t_2 - t_1) \right] \right|^2 \delta_{\kappa_{\text{in}}\kappa_{\text{out}}}. \end{aligned} \quad (2.57)$$

As in section 2.2, we assume that the waiting time  $\Delta t = t_2 - t_1$  is much larger than the integration periods for  $t_1$  and  $t_2$ , i.e., we regard  $\Delta t$  as constant over the integration periods. Then, we can again express the combined probability density (2.57) via the single-atom emission probability density (2.12), i.e.,

$$P_{\mathbf{\kappa}_{\text{out}}} = \left| N_1 \exp \{ i\varphi(\Delta t) \} + N_2 \mathcal{J}_{\mathbf{\kappa}_{\text{in}}}(\Delta t) \right|^2 \delta_{\mathbf{\kappa}_{\text{in}} \mathbf{\kappa}_{\text{out}}} P_{\text{single}}. \quad (2.58)$$

First, let us discuss the two extreme cases. For  $N_1 = N_\Psi$  and  $N_2 = 0$ , the result of the superfluid ground state (2.49) is reproduced to the highest order in  $N$ . The incoherent part of the probability density (2.49) is missing in (2.58), as we excluded it in (2.52), for simplicity. In the opposite case of all  $N_2 = N_\Psi$  atoms equally distributed between all  $\mathbf{k}$ -modes (and  $N_1 = 0$  condensed atoms), however, the combined emission probability density (2.58) gradually decays over the waiting time  $\Delta t$  due to the absolute square of the phase sum factor  $|\mathcal{J}_{\mathbf{\kappa}_{\text{in}}}(\Delta t)|^2$ . In between these two extreme cases, interference effects between the two terms are observable of course. The decay of the superradiant emission probability is depicted in Figure 2.1 for the two cases of  $N_2 = N_\Psi$  and  $N_2 = N_\Psi/2$  (dashed black lines).

**Phase sum** As it is responsible for the decay of the superradiant emission probability over the waiting time  $\Delta t$ , let us now study the phase sum (2.54),

$$\mathcal{J}_{\mathbf{\kappa}}(\Delta t) = \frac{1}{N} \sum_{\mathbf{p}} \exp \{ iJ/Z(T_{\mathbf{p}} - T_{\mathbf{p}-\mathbf{\kappa}})\Delta t \}, \quad (2.59)$$

and its dependence on the photon wave vector  $\mathbf{\kappa}$  in detail. First of all, the phase sum obviously yields  $\mathcal{J}_{\mathbf{0}}(\Delta t) = 1$  for  $\kappa_x = \kappa_y = 0$ , i.e., an orthogonally incoming photon. Going one step further, we can Taylor-expand the exponent for small photon wave vectors  $\mathbf{\kappa}$  as compared to the inverse of the lattice spacing  $\ell$ , i.e.,  $|\mathbf{\kappa}|\ell \ll 1$ ,

$$\begin{aligned} (T_{\mathbf{p}} - T_{\mathbf{p}-\mathbf{\kappa}}) &\approx \mathbf{\kappa} \cdot \nabla_{\mathbf{p}} T_{\mathbf{p}} \Big|_{\mathbf{p}} \\ &= -2\ell \left[ \kappa_x \sin(p_x \ell) + \kappa_y \sin(p_y \ell) \right], \end{aligned} \quad (2.60)$$

which enables to separate the phase sum (2.59) over the reciprocal lattice vectors  $\mathbf{p}$  into a product of one-dimensional sums over their components  $p_{x/y}$ , i.e.,

$$\mathcal{J}_{\mathbf{\kappa}}(\Delta t) = \mathcal{J}_{\mathbf{\kappa}}^x(\Delta t) \times \mathcal{J}_{\mathbf{\kappa}}^y(\Delta t). \quad (2.61)$$

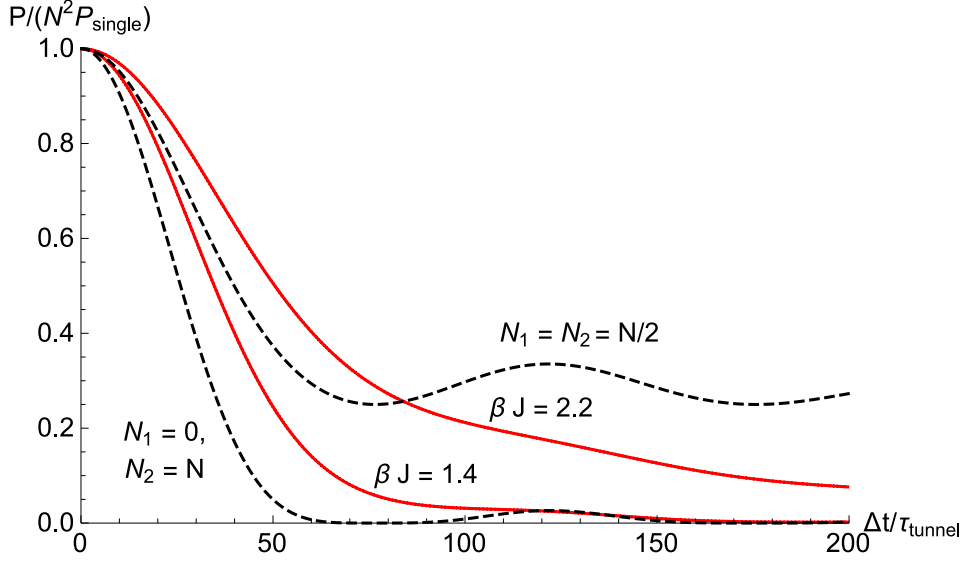


FIGURE 2.1. – The combined probability density  $P_{\kappa_{\text{out}}}$  in (2.31) for the absorption of a photon  $\kappa_{\text{in}}$  and subsequent re-emission in the same direction  $\kappa_{\text{out}} = \kappa_{\text{in}} = 2\pi/(L\ell) \cdot \{1, 1\}$ , normalized by  $N^2 P_{\text{single}}$ , is plotted against the waiting time  $\Delta t$  in units of the tunneling time  $\tau_{\text{tunnel}} = \hbar/J$ . The dashed black lines show numerical results for the partial condensation state (2.58), whereas the solid red lines represent numerical results for a thermal state, described by the Bose-Einstein distribution (2.68). For high temperatures,  $\beta J \ll 1$ , the thermal state behaves as the state where all momenta are equally populated (lower dashed line). The number of atoms (bosons) and lattice sites was set to  $N = L^2 = 100^2$  during the numerical evaluation.

The one-dimensional sums in the  $x$  and  $y$  part consist of  $L$  summands for the possible reciprocal lattice vector components  $p_x$  and  $p_y$  respectively,

$$\mathcal{J}_{\kappa}^{x/y}(\Delta t) := \frac{1}{L} \sum_{p_{x/y}} \exp \left\{ -i2\ell J/Z\kappa_{x/y} \sin(p_{x/y}\ell)\Delta t \right\}, \quad (2.62)$$

where  $L$  is the number of lattice sites in one dimension, i.e.,  $L^2 = N$ . As we generally assume a large lattice with  $L \gg 1$  lattice sites per dimension, it is acceptable to replace the sum over  $p_{x/y}$  with an integral, i.e.,

$$\mathcal{J}_{\kappa}^{x/y}(\Delta t) = \frac{1}{L} \sum_{n=-L/2+1}^{L/2} \exp \left\{ -i2\ell J/Z\kappa_{x/y} \sin(n2\pi/L)\Delta t \right\} \quad (2.63)$$

$$\approx \frac{1}{L} \int_{-L/2}^{L/2} d\lambda \exp \left\{ -i2\ell J/Z\kappa_{x/y} \sin(\lambda 2\pi/L)\Delta t \right\}. \quad (2.64)$$

By substituting  $z = \lambda 2\pi/L$ , we can finally identify [89] this integral as a (cylindrical) Bessel function  $J_0$ :

$$\begin{aligned} \mathcal{J}_{\kappa}^{x/y}(\Delta t) &\approx \frac{1}{2\pi} \int_{-\pi}^{\pi} dz \exp\{-i2\ell J/Z\kappa_{x/y} \sin(z)\Delta t\} \\ &= J_0\left(-2\frac{J\Delta t}{Z}\kappa_{x/y}\ell\right). \end{aligned} \quad (2.65)$$

Summing up, and considering that the Bessel functions  $J_0$  are even, the phase sum (2.59) can be approximated via the product of two Bessel functions, one for each dimension  $x$  and  $y$ ,

$$\mathcal{J}_{\kappa}(\Delta t) \approx J_0\left(2\frac{J\Delta t}{Z}\kappa_x\ell\right) J_0\left(2\frac{J\Delta t}{Z}\kappa_y\ell\right), \quad (2.66)$$

when the wave vector  $\kappa$  is small compared to the inverse lattice spacing  $1/\ell$ , and the number of lattice sites per dimension is large,  $L \gg 1$ .

Going back to the result of the combined probability density for the partial condensation state (2.58), we can thus now express the phase sum  $\mathcal{J}_{\kappa_{\text{in}}}(\Delta t)$  via the Bessel functions (2.66). Evidently, the reduction in superradiance is governed by the amount of tunneling  $J\Delta t$  which occurred during the waiting time  $\Delta t$ , on the one hand, and by the magnitude of the wave-vector components  $\kappa_{\text{in},x/y}$ , on the other.

In an intuitive picture, the decay of the superradiance peak (or, in other words, the decoherence of the collective excitation) is caused by the lattice dynamics during the waiting time  $\Delta t$ . The more pronounced the total amount of tunneling  $J\Delta t$  of the (excited) atoms, the more severe is the damage exerted on the spatial phase coherence of the Dicke state, which was created by the prior absorption of the probe photon  $\kappa_{\text{in}}$ . On the other hand, the wave-vector components  $\kappa_{\text{in},x/y}$  determine how much the spatial phases  $\exp\{i\kappa_{\text{in}} \cdot \mathbf{r}_{\mu}\}$  of the (adjacent) atoms differ. Naturally, the larger the difference of the spatial phases, the more damage is inflicted on the phase coherence of the overall state. For example, we find no reduction in the superradiance peak for an orthogonally incident probe photon,  $\kappa_{\text{in},x/y} = 0$ , as the spatial phases do not differ at all. On the contrary, the larger the wave-vector components  $\kappa_{\text{in},x/y}$  become, i.e., the more diagonal (as opposed to orthogonal) the probe photon is incident upon the optical lattice, the swifter the reduction in superradiance (2.66) takes place. Please note that a similar effect, the reduction of superradiance due to motional effects in a dense coherent medium, was very recently observed ex-

perimentally in [77] via collective emission from coherently driven ultracold  $^{88}\text{Sr}$  atoms.

After all, the result (2.66), with its explicit dependence on the wave vector  $\kappa_{\text{in}}$ , deviates significantly from the separable state approximation (2.21), which underlines the importance of the correlations (between lattice sites) which emerge because of the tunneling of the lattice atoms.

### Thermal state: Bose-Einstein distribution

In the last section, we considered the partial condensation state and observed a decay in the superradiance peak if not all atoms are condensed in the  $\mathbf{k} = \mathbf{0}$  mode. As in this case the combined emission probability density can be simplified to a short, analytic expression (2.58) via Bessel functions (2.66), the partial condensation state serves as an insightful toy model. In reality, however, the quantum state of the atoms in the optical lattice in thermal equilibrium is described by the density operator of the canonical ensemble [75],

$$\hat{\rho}_{\text{th}} = \frac{1}{\text{Tr}\{e^{-\beta\hat{H}}\}} e^{-\beta\hat{H}}, \quad (2.67)$$

where  $\beta = 1/(k_B T)$  with  $k_B$  the Boltzmann constant and  $T$  the absolute temperature. In the case of noninteracting bosons and thus a Hamiltonian which is diagonal in the  $\mathbf{k}$ -basis (1.59), its number distribution is (for  $N \gg 1$ ) given by the well-known Bose-Einstein distribution [90],

$$n^{\text{BE}}(\mathbf{k}) = \frac{1}{e^{\beta(E_{\mathbf{k}} - \mu)} - 1}, \quad (2.68)$$

where  $E_{\mathbf{k}} = -J/Z T_{\mathbf{k}}$  denotes the energy of a boson in mode  $\mathbf{k}$ , while  $\mu$  describes the chemical potential. Note that we principally assume a large but fixed number  $N$  of bosons (which equals the number of lattice sites) in the optical lattice, i.e., no exchange of particles with a reservoir. Therefore, the chemical potential is determined as a function of the absolute temperature  $T$  and the number of lattice sites  $N$ , in our case, via the condition

$$\sum_{\mathbf{k}} \frac{1}{e^{\beta(E_{\mathbf{k}} - \mu)} - 1} = N. \quad (2.69)$$



In Figure 2.2, we show density plots of the number distribution (2.68) in a two-dimensional reciprocal quadratic lattice for different temperatures  $\beta J$ :

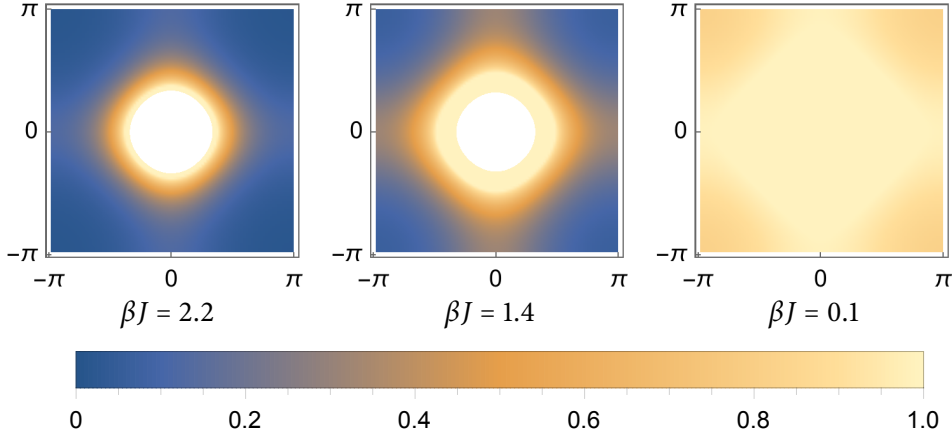


FIGURE 2.2. – Density plots of the Bose-Einstein distribution (2.68) for increasing temperatures  $\beta J = 2.2$ ,  $\beta J = 1.4$  and  $\beta J = 0.1$  (from left to right) in a two-dimensional reciprocal quadratic lattice. Plotted is the first Brillouin zone, i.e., the values for  $k_x \ell$  (x-axis) and  $k_y \ell$  (y-axis) range from  $-\pi$  to  $\pi$ . It can be observed that the number distribution broadens with increasing temperature. In the limit of high temperatures,  $\beta J \ll 1$ , all momenta are equally populated. Please note that the color scaling is capped at unity, i.e., all values greater than one, e.g. in the centers, appear in the same color.

Basically, we can now directly insert the Bose-Einstein distribution (2.68) into the bosonic four-point correlator for Gaussian initial states (2.44), and further into the expanded operatorial part (2.33) to analytically express the combined emission probability density (2.31). In practice, the resulting expression is quite lengthy, because the phase sums over  $\mathbf{p}$  and  $\mathbf{q}$  in the expanded operatorial part (2.33) cannot be reasonably simplified<sup>4</sup>, as in the case of the partial condensation state (2.56). Therefore, we plotted numerical results for the combined emission probability density (2.31) for a thermal state (2.68), together with the results of the partial condensation state, in Figure 2.1 (solid red lines). As a main result, we obtain a reduction

<sup>4</sup>In fact, under the assumption that we only consider the superradiant terms analog to (2.52) and apply the Bessel approximation (2.66), the results could in principle be analytically expressed via an infinite series of Bessel functions  $\sum_{n=0}^{\infty} c_n J_n(\Delta t \dots)$  using the Jacobi-Anger expansion [89]. The constant numbers  $c_n$  would then depend on the number distribution function  $n^{\text{BE}}(\mathbf{k})$ , i.e., on the temperature. However, as the physical insight added from this expansion is limited, we are focusing on numerical results instead. That way, the dashed black lines in Figure 2.1 originate from only  $J_0$ , while the solid red lines correspond to a mixture of Bessel functions given by the infinite series.

in the superradiance peak over the waiting time  $\Delta t$  similar to the case of the partial condensation state, but without the revivals that the partial condensation states show (dashed black lines). For very high temperatures, i.e.,  $\beta J \ll 1$ , the thermal state approaches the limit of a state where all momenta are equally populated, and thus shows the same decay as the partial condensation state (2.58) for  $N_1 = 0$  and  $N_2 = N_\Psi$ .

### 2.3.2. Fermi-Hubbard model

#### Metallic ground state

As a prototypical initial lattice state of the Fermi-Hubbard model in the weak interactions regime ( $J \gg U$ ), let us consider the metallic ground state (1.37), as introduced in section 1.3.3,

$$n_s^{\text{me}}(\mathbf{k}) = \frac{U=0}{\text{me}} \langle \Psi | \hat{n}_{\mathbf{k},s}^{\text{gr}} | \Psi \rangle_{\text{me}}^{U=0} = \begin{cases} 1, & \text{if } |k_x| + |k_y| < \pi/\ell, \\ 0, & \text{otherwise.} \end{cases} \quad (2.70)$$

The number distribution (2.70) describes the diamond-shaped Fermi surface in a two-dimensional (reciprocal) lattice [84]. As it is not spin-dependent (a specific  $\mathbf{k}$ -mode is either populated by two fermions of both spin states or by zero fermions), we can simplify the spin summations when we insert the number distribution (2.70) into the fermionic four-point correlator (2.42), leading to

$$E_{n^{\text{me}}}^{\text{F}} = 4n_s^{\text{me}}(\mathbf{p} - \boldsymbol{\kappa}_{\text{in}})n_s^{\text{me}}(\mathbf{q} - \boldsymbol{\kappa}_{\text{in}})\delta_{\boldsymbol{\kappa}_{\text{in}}\boldsymbol{\kappa}_{\text{out}}} + 2n_s^{\text{me}}(\mathbf{p} - \boldsymbol{\kappa}_{\text{in}})[1 - n_s^{\text{me}}(\mathbf{p} - \boldsymbol{\kappa}_{\text{out}})]\delta_{\mathbf{p}\mathbf{q}}. \quad (2.71)$$

Further inserting the four-point correlator (2.71) into the expanded operatorial part (2.32), we can simplify the summation of the second term and merge the phases as far as possible:

$$\begin{aligned} \mathcal{E}_{\boldsymbol{\kappa}_{\text{out}}}^{\boldsymbol{\kappa}_{\text{in}}}(t_1, t_2, t_3, t_4) &= 4\delta_{\boldsymbol{\kappa}_{\text{in}}\boldsymbol{\kappa}_{\text{out}}} \sum_{\mathbf{p}\mathbf{q}} n_s^{\text{me}}(\mathbf{p} - \boldsymbol{\kappa}_{\text{in}})n_s^{\text{me}}(\mathbf{q} - \boldsymbol{\kappa}_{\text{in}}) \\ &\quad \times \exp\{i[\phi_{\mathbf{q}}^{\boldsymbol{\kappa}_{\text{in}}}(t_4 - t_3) - \phi_{\mathbf{p}}^{\boldsymbol{\kappa}_{\text{in}}}(t_2 - t_1)]\} \\ &\quad + 2 \sum_{\mathbf{p}} n_s^{\text{me}}(\mathbf{p} - \boldsymbol{\kappa}_{\text{in}})[1 - n_s^{\text{me}}(\mathbf{p} - \boldsymbol{\kappa}_{\text{out}})] \\ &\quad \times \exp\{i[\phi_{\mathbf{p}}^{\boldsymbol{\kappa}_{\text{out}}}(t_4 - t_2) - \phi_{\mathbf{p}}^{\boldsymbol{\kappa}_{\text{in}}}(t_3 - t_1)]\}. \end{aligned} \quad (2.72)$$

Analogous to (2.52), we will only consider the coherent, directed ( $\boldsymbol{\kappa}_{\text{in}} = \boldsymbol{\kappa}_{\text{out}}$ ) superradiant emission which scales with  $\mathcal{O}(N^2)$ , as given by the first term. Thus, we neglect the second term, which corresponds to incoherent emission in arbitrary direction and only scales with  $\mathcal{O}(N)$ . In the first term we then apply index shifts  $\tilde{\boldsymbol{p}} = \boldsymbol{p} - \boldsymbol{\kappa}_{\text{in}}$  and  $\tilde{\boldsymbol{q}} = \boldsymbol{q} - \boldsymbol{\kappa}_{\text{in}}$ . According to the definition (2.70), the summand is nonzero only if the reciprocal lattice vectors  $\tilde{\boldsymbol{p}}$  or  $\tilde{\boldsymbol{q}}$  are located inside the diamond-shaped Fermi surface in (reciprocal)  $\boldsymbol{k}$ -space. Defining a set  $\mathcal{D}$ , which contains all reciprocal lattice vectors inside this diamond area, we can thus write

$$\begin{aligned} \mathcal{E}_{\boldsymbol{\kappa}_{\text{out}}}^{\boldsymbol{\kappa}_{\text{in}}}(t_1, t_2, t_3, t_4) &= 4\delta_{\boldsymbol{\kappa}_{\text{in}}\boldsymbol{\kappa}_{\text{out}}} \sum_{\tilde{\boldsymbol{p}} \in \mathcal{D}} \exp\left\{-i\phi_{\tilde{\boldsymbol{p}}+\boldsymbol{\kappa}_{\text{in}}}^{\boldsymbol{\kappa}_{\text{in}}}(t_2 - t_1)\right\} \\ &\quad \times \sum_{\tilde{\boldsymbol{q}} \in \mathcal{D}} \exp\left\{i\phi_{\tilde{\boldsymbol{q}}+\boldsymbol{\kappa}_{\text{in}}}^{\boldsymbol{\kappa}_{\text{in}}}(t_4 - t_3)\right\}. \end{aligned} \quad (2.73)$$

The individual sums already resemble the phase sum (2.59) which we approximated via Bessel functions in section 2.3.1. Indeed, we can perform the same steps, i.e., Taylor-expand the exponent for small photon wave vectors  $|\boldsymbol{\kappa}_{\text{in}}|\ell \ll 1$ . Analogous to (2.62), we then arrive at

$$\begin{aligned} \sum_{\tilde{\boldsymbol{p}} \in \mathcal{D}} \exp\left\{-i\phi_{\tilde{\boldsymbol{p}}+\boldsymbol{\kappa}_{\text{in}}}^{\boldsymbol{\kappa}_{\text{in}}}(\Delta t)\right\} &= \sum_{\tilde{\boldsymbol{p}} \in \mathcal{D}} \exp\left\{iJ/Z(T_{\tilde{\boldsymbol{p}}+\boldsymbol{\kappa}_{\text{in}}} - T_{\tilde{\boldsymbol{p}}})\Delta t\right\} \\ &\approx \sum_{\tilde{\boldsymbol{p}} \in \mathcal{D}} \exp\left\{-i2\ell J/Z\kappa_{\text{in},x} \sin(\tilde{p}_x\ell)\Delta t\right\} \\ &\quad \times \exp\left\{-i2\ell J/Z\kappa_{\text{in},y} \sin(\tilde{p}_y\ell)\Delta t\right\}, \end{aligned} \quad (2.74)$$

though, in contrast, we cannot easily separate the  $x$  and  $y$  part, as the summation runs only over the diamond area  $\mathcal{D}$ , instead of the whole first Brillouin zone. However, we can split the sum into two equal parts and apply another index shift  $\tilde{\boldsymbol{k}} = \tilde{\boldsymbol{p}} + \Delta\boldsymbol{k}$  with  $\Delta\boldsymbol{k} = \pi/\ell \cdot \{1, 1\}$  to one of the equal parts. The basic idea of this approach is to (mathematically) shift one part into the empty region of the first Brillouin zone, i.e., into the corners which are not populated in the metallic ground state (of course, one has to consider the  $2\pi$ -periodicity of  $\tilde{p}_{x/y}\ell$ ) – see Figure 2.3. When we define the set of all reciprocal lattice vectors which lie in these corners as

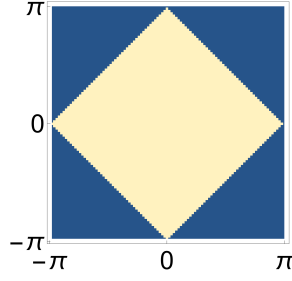


FIGURE 2.3. – Diamond-shaped Fermi surface of a half-filled two-dimensional quadratic lattice (see also Figure 1.8). Plotted is the first Brillouin zone, i.e., the values for  $k_x\ell$  (x-axis) and  $k_y\ell$  (y-axis) range from  $-\pi$  to  $\pi$ . The diamond area  $\mathcal{D}$  (yellow) can be shifted into the empty region of the first Brillouin zone, i.e., into the corners  $\mathcal{C}$  (blue) via an index shift  $\tilde{\mathbf{k}} = \tilde{\mathbf{p}} + \Delta\mathbf{k}$  with  $\Delta\mathbf{k} = \pi/\ell \cdot \{1, 1\}$ .

$\mathcal{C}$ , we arrive at:

$$\begin{aligned} \sum_{\tilde{\mathbf{p}} \in \mathcal{D}} \exp \left\{ -i\phi_{\tilde{\mathbf{p}} + \boldsymbol{\kappa}_{\text{in}}}^{\boldsymbol{\kappa}_{\text{in}}}(\Delta t) \right\} &\approx \frac{1}{2} \sum_{\tilde{\mathbf{p}} \in \mathcal{D}} \exp \left\{ -i2\ell J / Z\kappa_{\text{in},x} \sin(\tilde{p}_x\ell)\Delta t \right\} \\ &\quad \times \exp \left\{ -i2\ell J / Z\kappa_{\text{in},y} \sin(\tilde{p}_y\ell)\Delta t \right\} \\ &\quad + \frac{1}{2} \sum_{\tilde{\mathbf{k}} \in \mathcal{C}} \exp \left\{ i2\ell J / Z\kappa_{\text{in},x} \sin(\tilde{k}_x\ell)\Delta t \right\} \\ &\quad \times \exp \left\{ i2\ell J / Z\kappa_{\text{in},y} \sin(\tilde{k}_y\ell)\Delta t \right\}, \end{aligned} \quad (2.75)$$

where the sign of the sine functions has changed in the second term. However, in the symmetric summation  $\tilde{\mathbf{k}} \in \mathcal{C}$  we can simply exchange  $\tilde{\mathbf{k}} \leftrightarrow -\tilde{\mathbf{k}}$  and restore the original sign. Hence, we can then merge the summation over the diamond area  $\mathcal{D}$  and the corners  $\mathcal{C}$  into one summation over the complete first Brillouin zone, i.e.,

$$\begin{aligned} \sum_{\tilde{\mathbf{p}} \in \mathcal{D}} \exp \left\{ -i\phi_{\tilde{\mathbf{p}} + \boldsymbol{\kappa}_{\text{in}}}^{\boldsymbol{\kappa}_{\text{in}}}(\Delta t) \right\} &\approx \frac{1}{2} \sum_{\tilde{\mathbf{p}}} \exp \left\{ -i2\ell J / Z\kappa_{\text{in},x} \sin(\tilde{p}_x\ell)\Delta t \right\} \\ &\quad \times \exp \left\{ -i2\ell J / Z\kappa_{\text{in},y} \sin(\tilde{p}_y\ell)\Delta t \right\}. \end{aligned} \quad (2.76)$$

In conclusion, we obtain the same approximation via Bessel functions (2.66) as for the partial condensation state in section 2.3.1. All in all, we can finally write the expanded operatorial part (2.73) approximately (for small  $|\boldsymbol{\kappa}_{\text{in}}|\ell \ll 1$ ) in terms of the phase sum abbreviation (2.54), that is

$$\mathcal{E}_{\boldsymbol{\kappa}_{\text{out}}}^{\boldsymbol{\kappa}_{\text{in}}}(t_1, t_2, t_3, t_4) = N^2 \delta_{\boldsymbol{\kappa}_{\text{in}}\boldsymbol{\kappa}_{\text{out}}} \mathcal{J}_{\boldsymbol{\kappa}_{\text{in}}}(t_3 - t_4) \mathcal{J}_{\boldsymbol{\kappa}_{\text{in}}}(t_2 - t_1). \quad (2.77)$$

Analogously to steps (2.57) and (2.58), this extended operatorial part results in a combined emission probability density (2.31) of

$$P_{\kappa_{\text{out}}} = N^2 |\mathcal{J}_{\kappa_{\text{in}}}(\Delta t)|^2 \delta_{\kappa_{\text{in}}\kappa_{\text{out}}} P_{\text{single}}. \quad (2.78)$$

Interestingly, the emission probability density for the metallic ground state (1.37) reduces over the waiting time  $\Delta t$  similarly to the bosonic case where  $N$  atoms are distributed equally over all  $\mathbf{k}$ -modes (2.58 with  $N_1 = 0$  and  $N_2 = N$ ), which has already been plotted in Figure 2.1 (lower dashed line). Note that in both cases, many different momenta are populated and thus involved in the absorption and re-emission of the probe photon – as opposed to the bosonic superfluid ground state (1.34), where all atoms are condensed in the  $\mathbf{k} = \mathbf{0}$  mode. While in the bosonic case each  $\mathbf{k}$ -mode is occupied by exactly one boson, only half of the momenta (which are located inside the diamond area) are populated by two fermions each in the metallic ground state (1.37). As a rule of thumb, we may thus conclude that states where many  $\mathbf{k}$ -modes are populated show a decay in the superradiance peak, while condensed states are “invulnerable” to the lattice dynamics (cf. section 2.3.1). In Figure 2.4, numerical results for the combined emission probability density for the metallic ground state (2.78) are displayed again, together with an inset concerning thermal states.

### Thermal state: Fermi-Dirac distribution

Analogous to the bosonic case, we want to study the combined emission probability density (2.31) in the case of a fermionic lattice in thermal equilibrium. The quantum state of the atoms in the optical lattice is similarly described by the density operator of the canonical ensemble [75],

$$\hat{\rho}_{\text{th}} = \frac{1}{\text{Tr}\{e^{-\beta\hat{H}}\}} e^{-\beta\hat{H}}, \quad (2.79)$$

where again  $\beta = 1/(k_B T)$  with  $k_B$  the Boltzmann constant and  $T$  the absolute temperature, but the Hamiltonian (1.59) now describing noninteracting fermions in a corresponding lower-dimensional Hilbert space. Therefore, the number distribution of the fermions in the optical lattice in (reciprocal)  $\mathbf{k}$ -space is given by the

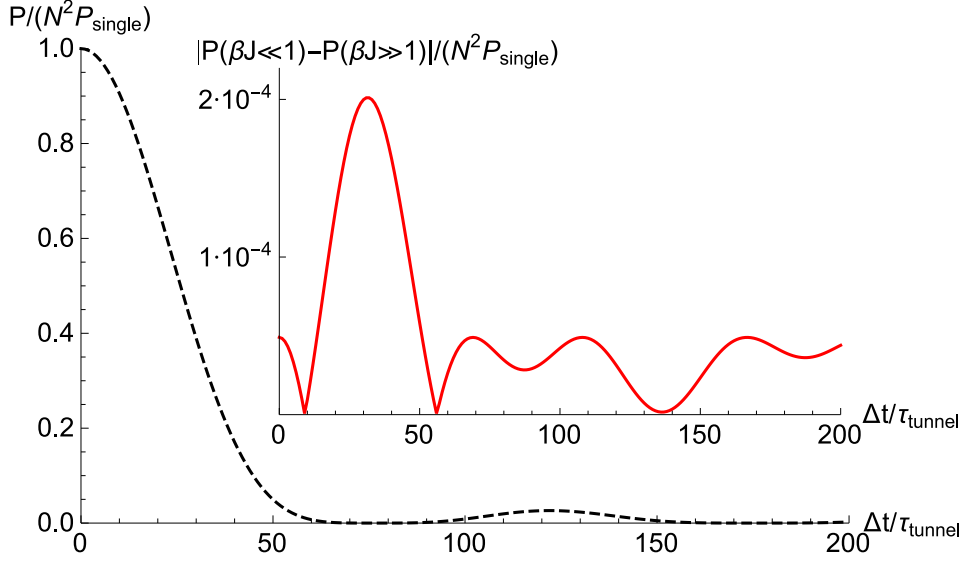


FIGURE 2.4. – The combined probability density  $P_{\kappa_{\text{out}}}$  in (2.31) for the absorption of a photon  $\kappa_{\text{in}}$  and subsequent re-emission in the same direction  $\kappa_{\text{out}} = \kappa_{\text{in}} = 2\pi/(L\ell) \cdot \{1, 1\}$ , normalized by  $N^2 P_{\text{single}}$ , is plotted against the waiting time  $\Delta t$  in units of the tunneling time  $\tau_{\text{tunnel}} = \hbar/J$ . The dashed black line shows numerical results for the metallic ground state (2.78). Note that for small  $|\kappa|\ell \ll 1$ , we obtained the same result for a bosonic state where all momenta are equally populated (lower dashed line in Figure 2.1) – which corresponds to a fermionic state with a very high temperature  $\beta J \ll 1$ . The minuscule deviations between a fermionic state with a very high ( $\beta J \ll 1$ ) and a very low ( $\beta J \gg 1$ ) temperature shown in the inset (solid red line) arise because of finite  $|\kappa|\ell = \mathcal{O}(10^{-1})$ . The number of atoms (fermions) and lattice sites was set to  $N = L^2 = 100^2$  during the numerical evaluation.

well-known Fermi-Dirac distribution [90],

$$n^{\text{FD}}(\mathbf{k}) = \frac{1}{e^{\beta(E_{\mathbf{k}} - \mu)} + 1}, \quad (2.80)$$

where, analogously,  $E_{\mathbf{k}} = -J/Z T_{\mathbf{k}}$  now describes the energy of a fermion in mode  $\mathbf{k}$ , and  $\mu$  denotes the chemical potential. Again, we fix the chemical potential via the normalization condition, i.e., it is chosen as a function of the absolute temperature  $T$  and the number of lattice sites and fermions  $N$  such that,

$$\sum_{\mathbf{k}} \frac{1}{e^{\beta(E_{\mathbf{k}} - \mu)} + 1} = N. \quad (2.81)$$

In Figure 2.5, we show density plots of the number distribution (2.80) in a two-dimensional reciprocal quadratic lattice for different temperatures  $\beta J$ :

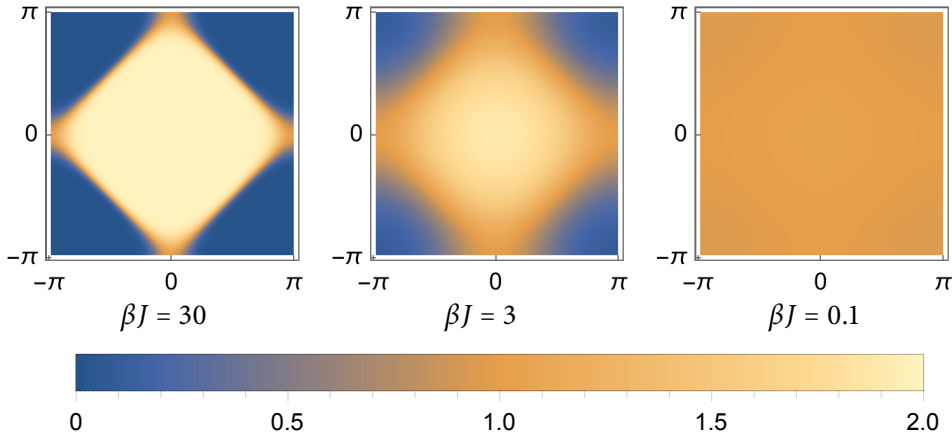


FIGURE 2.5. – Density plots of the Fermi-Dirac distribution (2.80) for increasing temperatures  $\beta J = 30$ ,  $\beta J = 3$  and  $\beta J = 0.1$  (from left to right) in a two-dimensional reciprocal quadratic lattice (sum of both spin orientations). Plotted is the first Brillouin zone, i.e., the values for  $k_x \ell$  (x-axis) and  $k_y \ell$  (y-axis) range from  $-\pi$  to  $\pi$ . The Fermi-Dirac distribution interpolates between the metallic ground state (very low temperature,  $\beta J \gg 1$ ) and a state where all momenta are equally populated (very high temperature,  $\beta J \ll 1$ ).

Similar to the bosonic case, one can insert the Fermi-Dirac distribution (2.80) into the fermionic four-point correlator for Gaussian states (2.45), and further into the expanded operatorial part (2.33) to obtain an analytic expression for the combined emission probability density (2.31). Although this results in a lengthy and complex expression for the emission probability density, the qualitative behavior is almost indistinguishable from the simple expression we obtained for the metallic ground state (2.78), which is independent of the temperature  $\beta J$ . This fact is demonstrated in the inset in Figure 2.4: the emission probability densities for very high temperatures  $\beta J \ll 1$  and very low temperatures  $\beta J \gg 1$  differ only marginally.

This outcome can be interpreted in the context of the previous results for the metallic ground state (2.78) and the bosonic state where all momenta are equally populated (2.58 with  $N_1 = 0$  and  $N_2 = N$ ). Starting with a very low temperature  $\beta J \gg 1$ , the fermions in the optical lattice are in the metallic ground state (1.37), where the superradiance peak decays according to (2.78), i.e., proportionally to  $|\mathcal{J}_{\kappa_{\text{in}}}(\Delta t)|^2$ . For very high temperatures  $\beta J \ll 1$ , on the other hand, the fermions in the optical lattice are about equally distributed among all  $\mathbf{k}$ -modes, such as in the bosonic state which shows an identical expression for the emission probability

density (2.58 with  $N_1 = 0$  and  $N_2 = N$ ). As the probability density is the same in the two extreme cases of the temperature spectrum (for small  $|\kappa_{\text{in}}|\ell \ll 1$ ), it is not surprising that it does not deviate much from this pattern in between, i.e., for arbitrary temperatures  $\beta J$ , where the Fermi-Dirac distribution only ranges between these two poles.

## 2.4. Summary of the detection of stationary lattice states

In this chapter we applied the single-photon pump-and-probe scheme depicted in Figure 1.3 to various initial quantum states of the atom ensemble in the optical lattice. As a key quantity, we calculated the combined emission probability density (2.7) for the collective absorption of a probe photon  $\kappa_{\text{in}}$  and its later coherent, superradiant re-emission in the same direction  $\kappa_{\text{out}} = \kappa_{\text{in}}$  after a waiting time  $\Delta t$ .

Regarding bosonic optical lattices, we found in section 2.2 on the separable state regime ( $J \ll U$ ) that the emission probability density (2.25) is enhanced by a factor  $N^2$  and does not decay over the waiting time  $\Delta t$  for the Mott insulator state (1.33). This result is not surprising, as it corresponds to the well-known directed spontaneous emission for fixed atom ensembles [67,68,72]. In the weak interactions regime ( $J \gg U$ ), however, we obtained the same result (2.49) for the superfluid ground state (1.34) in section 2.3. This interesting finding shows that the spatial phase coherence responsible for superradiance is “invulnerable”, as it were, to the extensive tunneling of the atoms in the case of a fully-condensed initial state. Furthermore, we studied the emission characteristics for a partial condensation state (2.50) and a thermal state, as given by the Bose-Einstein distribution (2.68). For these states, in contrast to the Mott insulator state and the superfluid ground state, the superradiant emission probability density (2.58) reduces over the waiting time  $\Delta t$  due to the lattice dynamics.

In conclusion, it can be stated that for a bosonic lattice the superfluid ground state (1.34) cannot<sup>5</sup> be distinguished from the Mott insulator state (1.33), but it can

<sup>5</sup>To be precise, it may be possible to distinguish the superfluid ground state from the Mott insulator state in analogy to [63,64], i.e., via the incoherent contribution  $\propto N$  which appears in the emission probability density for the superfluid ground state (2.49), but not for the Mott insulator state (2.25). In order to do so, one has to compare the emission characteristics specifically for incoherent, non-superradiant emission wave vectors  $\kappa_{\text{out}} \neq \kappa_{\text{in}}$ . This result also bears resemblance to the transverse (i.e., corresponding to a non-superradiant emission wave vector) light scattering into an optical cavity in [52, 54]. There, no photon is scattered for the Mott insulator state, while the photon number is proportional to the atom number  $N$  for the superfluid state. Throughout this Thesis, however, we focus on the clear signatures in the superradiance peak ( $\kappa_{\text{out}} = \kappa_{\text{in}}$ ) instead.



be differentiated from excited states such as the partial condensation state (2.50) and thermal states (2.68) by the pump-and-probe scheme we suggest. Regarding Figure 2.1, it may even be possible to perform thermometry with the proposed probe, as the swiftness of the decay in the probability density depends on the (inverse) temperature  $\beta J$ .

For fermionic optical lattices, we naturally obtained the same emission characteristics (2.25) for the Mott-Néel state (1.36) as for the Mott insulator state (1.33) in section 2.2, i.e., a superradiant enhancement by a factor  $N^2$  which is independent of the waiting time  $\Delta t$ . In the case of the metallic ground state (1.37) or a thermal state, as given by the Fermi-Dirac distribution (2.80), we found a reduction in superradiance (2.78) over the waiting time  $\Delta t$  in section 2.3, analogous to the bosonic case.

The conclusion for a fermionic lattice is that the metallic ground state (1.37) cannot be distinguished from excited states such as thermal states (2.80), but it can be differentiated from the Mott-Néel state (1.36) using the proposed probing scheme. This implies that in the case of a fermionic lattice, the current parameter regime can be detected: if there is no reduction in superradiance, the fermionic lattice is in the separable state regime ( $J \ll U$ ), while a decay of the superradiance peak is indicative of the weak interactions regime ( $J \gg U$ ).



## 3. Detection of quantum phase transitions

*In the previous chapter we studied how the proposed probing scheme can distinguish between different stationary states of the atoms in the optical lattice. In this chapter we want to discuss a slightly modified probing scheme which can be utilized to infer whether a quantum phase transition from the separable state regime ( $J \ll U$ ) to the weak interactions regime ( $J \gg U$ ) can be considered a sudden transition or an adiabatic transition within the meaning of the adiabatic theorem [75]. This modified probing sequence is similar to the one presented in Figure 1.3, with the addition of a phase transition which is (externally) induced immediately after the absorption of the probe photon in step one, but before the start of the waiting time  $\Delta t$  in step two, as depicted in Figure 3.1.*

### 3.1. Probing scheme to detect quantum phase transitions

For clarity, let us explicitly describe the modified probing sequence presented in Figure 3.1 again step-by-step. First, an incoming probe photon with wave vector  $\kappa_{\text{in}}$  is absorbed collectively by the atoms in the optical lattice, creating a coherent Dicke state (1.4) among them. In contrast to chapter 2, we consider a *specific* initial state of the atoms in the optical lattice. As we start in the separable state regime, we assume that the initial state of the optical lattice is either the Mott insulator state (1.33) in the case of bosons, or the Mott-Néel state (1.36) in the case of fermions. Immediately after absorption, the external lattice parameters are changed either abruptly (i.e., nonadiabatically) or slowly (adiabatically), transferring the optical lattice from the separable state regime ( $J \ll U$ ) to the weak interactions regime ( $J \gg U$ ). The resulting quantum state of the optical lattice then depends on the character of this quantum phase transition – in the adiabatic case, for example, the initial state can adapt to the new Hamiltonian, while it is unchanged in the case of a sudden transition. Now the sequence continues as described before (see Figure 1.3). In the second step, the atoms tunnel and interact according to the general lattice Hamiltonian (1.42). Note that intense tunneling is expected in the then prevailing weak interactions regime ( $J \gg U$ ). It depends on the quantum state of the optical lattice

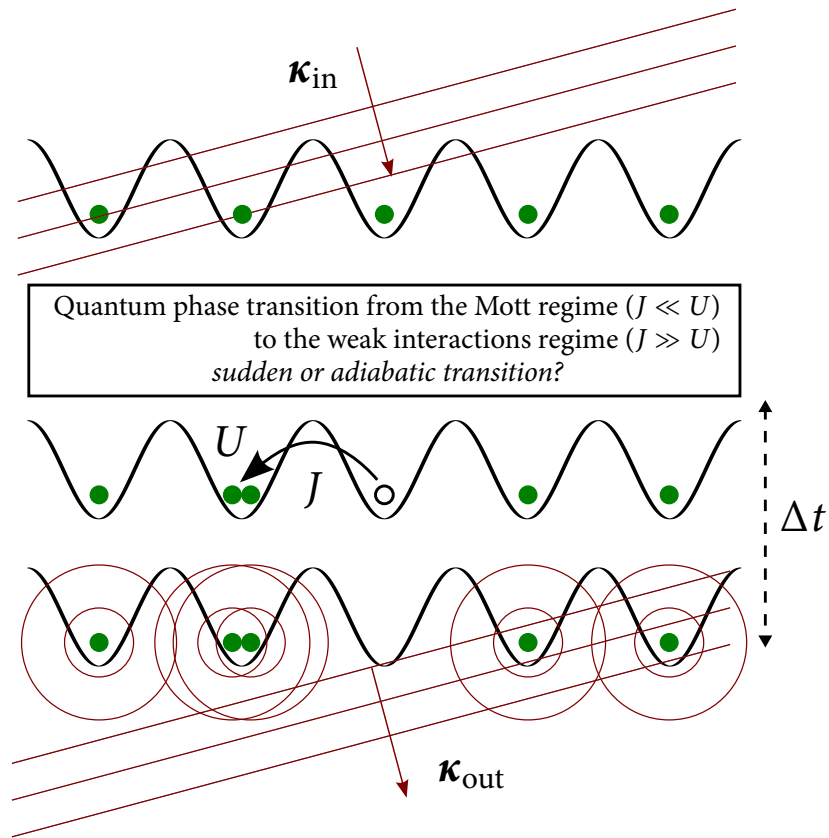


FIGURE 3.1. – Sketch of the modified probing sequence to detect quantum phase transitions (compare with Figure 1.3): An either abrupt or adiabatic phase transition is (externally) induced right after the absorption of the probe photon with wave vector  $\kappa_{in}$  in step one, but before the start of the waiting time  $\Delta t$  in step two. Apart from this, the sequence is unchanged. The atoms tunnel according to the general lattice Hamiltonian (1.42) during the waiting time  $\Delta t$ , and collectively re-emit the photon afterwards in the third step. However, depending on the specific quantum state immediately after the quantum phase transition (which depends on whether the transition can be considered abrupt or adiabatic), the tunneling of the atoms has a different effect on the spatial phase coherence, leading to a possible reduction in directed superradiant emission (i.e.,  $\kappa_{out} = \kappa_{in}$ ) in certain cases.

immediately after the quantum phase transition, and thus on the nature of the phase transition itself, to what extent the tunneling of the atoms corrupts the spatial phase coherence, which is responsible for directed superradiant emission. Thus, when the photon is finally collectively re-emitted by the atoms in the optical lattice, we may find a reduction in directed superradiant emission, depending on the nature of the quantum phase transition.

### 3.2. Absorption in the separable state regime

At the beginning, the optical lattice is in the separable state regime, where the tunneling rate  $J$  is small compared to the interaction energy  $U$ , i.e.,  $J \ll U$  (see above). Thus, we assume that the initial state of the atoms in the optical lattice is approximately given by the Mott insulator state (1.33) or the Mott-Néel state (1.36) in the case of bosons or fermions respectively. Analogous to section 2.1.2, we calculate the coherent excited state, which results from the collective absorption of the incoming probe photon with wave vector  $\boldsymbol{\kappa}_{\text{in}}$ , in first-order perturbation theory of the perturbation Hamiltonian (1.45). This then reads

$$|\Psi(\boldsymbol{\kappa}_{\text{in}})\rangle_{\text{ex}}^{\text{Mo/Né}} = -i \langle 0_{\text{ph}} | \int_0^{\tau_A} dt_1 \hat{V}_U(t_1) |\Psi\rangle_{\text{Mo/Né}}^{J=0} \otimes \hat{a}_{\boldsymbol{\kappa}_{\text{in}}}^\dagger |0_{\text{ph}}\rangle, \quad (3.1)$$

where the subscript index  $U$  of the perturbation Hamiltonian in the interaction picture (3.2) should remind us that we are deep in the separable state regime, i.e., the on-site repulsion energy  $U$  dominates over the tunneling rate  $J$ . Conversely, we will also write  $\hat{V}_J$  when we are deep in the weak interactions regime (i.e., after the quantum phase transition). These lattice parameters will be important when it comes to the interaction picture exciton creation operator  $\hat{\Sigma}_{U/J}^+(\mathbf{k}, t)$  in the various regimes,

$$\hat{V}_{U/J}(t) = \int d^3k g_{\mathbf{k}}(t) \hat{a}_{\mathbf{k}} e^{-i\omega_{\mathbf{k}}t} \hat{\Sigma}_{U/J}^+(\mathbf{k}, t) + \text{H.c.}, \quad (3.2)$$

which will be discussed below. Obviously, the coherent excited state (3.1) is still an eigenstate of the initial ( $J = 0$ ) Hamiltonian (1.42) in the separable state regime, as the absorption of the probe photon does not change the fact that there is a total of one atom per lattice site. Starting from this state, we are now going to calculate the emission characteristics in the two different cases of a sudden phase transition and an adiabatic phase transition.

### 3.3. Emission after a sudden phase transition

Analogous to section 2.1.4, we want to calculate the combined emission probability density for the absorption of a probe photon  $\boldsymbol{\kappa}_{\text{in}}$  and its collective re-emission in the direction  $\boldsymbol{\kappa}_{\text{out}}$  – but with the sudden transition in between in this case. By definition, the original excited state (3.1), an eigenstate of the initial ( $J = 0$ ) Hamiltonian (1.42) in the separable state regime, cannot adapt adiabatically in the case of a sudden transition. As a consequence, the unaltered excited state (3.1) is not an eigenstate of the “new” Hamiltonian in the weak interactions regime ( $J \gg U$ ). Therefore, we consider the collective emission of a photon from the unaltered state (3.1) via first-order perturbation theory in the “new” perturbation Hamiltonian  $\hat{V}_J$  in the weak interactions regime (3.2), as denoted by the subscript  $J$ . Afterwards, we project the resulting state onto a state with a photon in the mode  $\boldsymbol{\kappa}_{\text{out}}$  and square the norm of the remaining atomic state vector to obtain the relevant probability density:

$$P_{\boldsymbol{\kappa}_{\text{out}}} = \left\| \langle 0_{\text{ph}} | \hat{a}_{\boldsymbol{\kappa}_{\text{out}}} \int_0^{\tau_E} dt_2 \hat{V}_J(t_2) |\Psi(\boldsymbol{\kappa}_{\text{in}})\rangle_{\text{ex}}^{\text{Mo/Né}} \otimes |0_{\text{ph}}\rangle \right\|^2. \quad (3.3)$$

Resolving the photonic part similar to (2.8), we obtain

$$P_{\boldsymbol{\kappa}_{\text{out}}} = \left\| \int_0^{\tau_E} dt_2 \int_0^{\tau_A} dt_1 g_{\boldsymbol{\kappa}_{\text{out}}}^*(t_2) g_{\boldsymbol{\kappa}_{\text{in}}}(t_1) e^{i(\omega_{\text{out}} t_2 - \omega_{\text{in}} t_1)} \hat{\Sigma}_{\boldsymbol{\kappa}_{\text{out}}}^{\boldsymbol{\kappa}_{\text{in}}}(t_1, t_2) |\Psi\rangle_{\text{Mo/Né}}^{J=0} \right\|^2, \quad (3.4)$$

where, aside from the specific initial state (3.1), the difference lies in the operatorial part, which is now given as

$$\hat{\Sigma}_{\boldsymbol{\kappa}_{\text{out}}}^{\boldsymbol{\kappa}_{\text{in}}}(t_1, t_2) = \hat{\Sigma}_J^-(\boldsymbol{\kappa}_{\text{out}}, t_2) \hat{\Sigma}_U^+(\boldsymbol{\kappa}_{\text{in}}, t_1), \quad (3.5)$$

indicating that the exciton creation operator acts at the time  $t_1$  when the optical lattice is in the separable state regime ( $U$ ), while the exciton annihilation applies at the time  $t_2$  after the quantum phase transition, i.e., in the weak interactions regime ( $J$ ). It is helpful to write both operators in the momentum space  $\mathbf{k}$ -basis, i.e., as in section 2.3. For the exciton annihilation operator  $\hat{\Sigma}_J^-(\boldsymbol{\kappa}_{\text{out}}, t_2)$  we can directly insert (2.27) with the corresponding phase factor (2.26), which arises due to the tunneling in the weak interactions regime. This particular phase factor does not appear in the exciton creation operator  $\hat{\Sigma}_U^+(\boldsymbol{\kappa}_{\text{in}}, t_1)$ , as the tunneling is negligible ( $J = 0$ ) in the separable state regime ( $J \ll U$ ). Moreover, there is also no phase factor

arising from the on-site repulsion term in (1.42) in this case, as becomes evident when one considers the exciton creation operator in the lattice site basis (1.47). In conclusion, we obtain an expression similar to (2.28), but with only a single phase factor and the specific initial state (3.1),

$$\begin{aligned}
 \hat{S}_{\kappa_{\text{out}}}^{\kappa_{\text{in}}}(t_1, t_2) |\Psi\rangle_{\text{Mo/Né}}^{J=0} &= \hat{\Sigma}_J^-(\kappa_{\text{out}}, t_2) \hat{\Sigma}_U^+(\kappa_{\text{in}}, t_1) |\Psi\rangle_{\text{Mo/Né}}^{J=0} \\
 &= e^{i\omega(t_1-t_2)} \sum_{\mathbf{p}\mathbf{q}, s_1 s_2} \exp\{-i\phi_{\mathbf{p}}^{\kappa_{\text{out}}}(t_2)\} \hat{a}_{\mathbf{p}-\kappa_{\text{out}}, s_1}^{\text{gr}\dagger} \hat{a}_{\mathbf{p}, s_1}^{\text{ex}} \hat{a}_{\mathbf{q}, s_2}^{\text{ex}\dagger} \hat{a}_{\mathbf{q}-\kappa_{\text{in}}, s_2}^{\text{gr}} |\Psi\rangle_{\text{Mo/Né}}^{J=0} \\
 &= e^{i\omega(t_1-t_2)} \sum_{\mathbf{p}, s} \exp\{-i\phi_{\mathbf{p}}^{\kappa_{\text{out}}}(t_2)\} \hat{a}_{\mathbf{p}-\kappa_{\text{out}}, s}^{\text{gr}\dagger} \hat{a}_{\mathbf{p}-\kappa_{\text{in}}, s}^{\text{gr}} |\Psi\rangle_{\text{Mo/Né}}^{J=0}, \quad (3.6)
 \end{aligned}$$

where (anti)commutation relations (1.69) were used to dispose of the operators corresponding to excited-state atoms, as  $\hat{a}_{\mathbf{p}, s_1}^{\text{ex}} |\Psi\rangle_{\text{Mo/Né}}^{J=0} = 0$  for all  $\mathbf{p}, s_1$ . Analogous to (2.31) and (2.32), the combined probability density (3.4) can then be expanded via its conjugate transpose. The corresponding (bosonic or fermionic) four-point correlator, in contrast, now has to be calculated in the Mott insulator state (1.33) or the Mott-Néel state (1.36) respectively, i.e.,

$$E_{\text{Mo/Né}}^{\text{B/F}} = \sum_{s_1 s_2} \langle \Psi |_{\text{Mo/Né}}^{J=0} \hat{a}_{\mathbf{q}-\kappa_{\text{in}}, s_2}^{\text{gr}\dagger} \hat{a}_{\mathbf{q}-\kappa_{\text{out}}, s_2}^{\text{gr}} \hat{a}_{\mathbf{p}-\kappa_{\text{out}}, s_1}^{\text{gr}\dagger} \hat{a}_{\mathbf{p}-\kappa_{\text{in}}, s_1}^{\text{gr}} | \Psi \rangle_{\text{Mo/Né}}^{J=0}. \quad (3.7)$$

As the Mott insulator state and the Mott-Néel state are naturally given in the lattice site basis, we need to transform the creation and annihilation operators in (3.7) via back transformation (1.53). The resulting expression reads

$$\begin{aligned}
 E_{\text{Mo/Né}}^{\text{B/F}} &= \frac{1}{N^2} \sum_{\mu\nu\eta\rho, s_1 s_2} \langle \Psi |_{\text{Mo/Né}}^{J=0} \hat{a}_{\rho, s_2}^{\text{gr}\dagger} \hat{a}_{\eta, s_2}^{\text{gr}} \hat{a}_{\mu, s_1}^{\text{gr}\dagger} \hat{a}_{\nu, s_1}^{\text{gr}} | \Psi \rangle_{\text{Mo/Né}}^{J=0} \\
 &\quad \times \exp\{i(\mathbf{p}-\kappa_{\text{out}}) \cdot \mathbf{r}_{\mu}\} \exp\{-i(\mathbf{p}-\kappa_{\text{in}}) \cdot \mathbf{r}_{\nu}\} \\
 &\quad \times \exp\{-i(\mathbf{q}-\kappa_{\text{out}}) \cdot \mathbf{r}_{\eta}\} \exp\{i(\mathbf{q}-\kappa_{\text{in}}) \cdot \mathbf{r}_{\rho}\}. \quad (3.8)
 \end{aligned}$$

Now we can straightforwardly calculate the ensuing expectation value in the lattice site basis. For the bosonic (i.e., spin indices omitted) Mott insulator state (1.33) we find

$$\langle \Psi |_{\text{Mo}}^{J=0} \hat{b}_{\rho}^{\text{gr}\dagger} \hat{b}_{\eta}^{\text{gr}} \hat{b}_{\mu}^{\text{gr}\dagger} \hat{b}_{\nu}^{\text{gr}} | \Psi \rangle_{\text{Mo}}^{J=0} = \delta_{\mu\nu} \delta_{\eta\rho} + 2\delta_{\nu\rho} \delta_{\mu\eta} - 2\delta_{\mu\nu\eta\rho}, \quad (3.9)$$

where the first two terms correspond to the two possible cases of how the annihilation and creation operators can compensate for each other, and the third term

accounts for the case that all operators work on the same lattice site. For a more thorough explanation, please refer to Appendix A.3. Continuing, the bosonic four-point correlator (3.8) hence reduces to

$$\begin{aligned}
E_{\text{Mo}}^{\text{B}} &= \frac{1}{N^2} \sum_{\mu\eta} \exp \{ i(\boldsymbol{\kappa}_{\text{in}} - \boldsymbol{\kappa}_{\text{out}}) \cdot \mathbf{r}_{\mu} \} \exp \{ i(\boldsymbol{\kappa}_{\text{out}} - \boldsymbol{\kappa}_{\text{in}}) \cdot \mathbf{r}_{\eta} \} \\
&\quad + \frac{2}{N^2} \sum_{\mu\nu} \exp \{ i(\mathbf{p} - \mathbf{q}) \cdot \mathbf{r}_{\mu} \} \exp \{ i(\mathbf{q} - \mathbf{p}) \cdot \mathbf{r}_{\nu} \} - \frac{2}{N} \\
&= \delta_{\boldsymbol{\kappa}_{\text{in}}\boldsymbol{\kappa}_{\text{out}}} + 2\delta_{\mathbf{p}\mathbf{q}} - 2/N, \tag{3.10}
\end{aligned}$$

where we have used the summation relation (1.54) in the last step, valid for reciprocal lattice vectors  $\boldsymbol{\kappa}_{\text{in}} - \boldsymbol{\kappa}_{\text{out}}$  and  $\mathbf{p} - \mathbf{q}$ . For the fermionic case, on the other hand, we calculate the expectation value in the Mott-Néel state (1.36) analogously (for details, see Appendix A.3), leading to

$$\begin{aligned}
\langle \Psi_{\text{Né}}^{J=0} | c_{\rho,s_2}^{\text{gr}\dagger} c_{\eta,s_2}^{\text{gr}} c_{\mu,s_1}^{\text{gr}\dagger} c_{\nu,s_1}^{\text{gr}} | \Psi_{\text{Né}}^{J=0} \rangle &= \delta_{\mu\nu} \delta_{\eta\rho} \delta_{s_1 s_{\mu}} \delta_{s_2 s_{\eta}} + \delta_{\nu\rho} \delta_{\mu\eta} \delta_{s_1 s_2 s_{\nu}} \\
&\quad - \delta_{\nu\rho} \delta_{\mu\eta} \delta_{s_1 s_2 s_{\nu} s_{\mu}}, \tag{3.11}
\end{aligned}$$

where  $s_{\mu}$ ,  $s_{\eta}$  and  $s_{\nu}$  refer to the spin quantum number of the atoms at lattice sites  $\mu$ ,  $\eta$  and  $\nu$  in the Mott-Néel state respectively. After the insertion of (3.11) into the fermionic four-point correlator (3.8), the expression simplifies considerably. For example, all spin sums  $s_1$  and  $s_2$  are eliminated, i.e.,

$$\begin{aligned}
E_{\text{Né}}^{\text{F}} &= \frac{1}{N^2} \sum_{\mu\eta} \exp \{ i(\boldsymbol{\kappa}_{\text{in}} - \boldsymbol{\kappa}_{\text{out}}) \cdot \mathbf{r}_{\mu} \} \exp \{ i(\boldsymbol{\kappa}_{\text{out}} - \boldsymbol{\kappa}_{\text{in}}) \cdot \mathbf{r}_{\eta} \} \\
&\quad + \frac{1}{N^2} \sum_{\mu\nu} (1 - \delta_{s_{\nu} s_{\mu}}) \exp \{ i(\mathbf{p} - \mathbf{q}) \cdot \mathbf{r}_{\mu} \} \exp \{ i(\mathbf{q} - \mathbf{p}) \cdot \mathbf{r}_{\nu} \} \\
&= \delta_{\boldsymbol{\kappa}_{\text{in}}\boldsymbol{\kappa}_{\text{out}}} + \delta_{\mathbf{p}\mathbf{q}} - \frac{1}{N^2} \sum_{\mu\nu} \delta_{s_{\nu} s_{\mu}} \exp \{ i(\mathbf{p} - \mathbf{q}) \cdot \mathbf{r}_{\mu} \} \exp \{ i(\mathbf{q} - \mathbf{p}) \cdot \mathbf{r}_{\nu} \}. \tag{3.12}
\end{aligned}$$

To further simplify the third term, we need to split the sums over  $\mu$  and  $\nu$  according to the two sublattices  $\mathcal{A}$  and  $\mathcal{B}$ , which were established in the introduction of the Mott-Néel state (1.36). If we consider the Kronecker delta, only the terms in which



the lattice sites  $\mu$  and  $\nu$  belong to the same sublattice  $\mathcal{A}$  or  $\mathcal{B}$  remain,

$$\begin{aligned}
 & \sum_{\mu\nu} \delta_{s_\nu s_\mu} \exp\{i(\mathbf{p}-\mathbf{q})\cdot\mathbf{r}_\mu\} \exp\{i(\mathbf{q}-\mathbf{p})\cdot\mathbf{r}_\nu\} \\
 &= \left| \sum_{\mu\in\mathcal{A}} \exp\{i(\mathbf{p}-\mathbf{q})\cdot\mathbf{r}_\mu\} \right|^2 + \left| \sum_{\mu\in\mathcal{B}} \exp\{i(\mathbf{p}-\mathbf{q})\cdot\mathbf{r}_\mu\} \right|^2 \\
 &= \frac{N^2}{4} \delta_{\mathbf{p}\mathbf{q}} + \frac{N^2}{4} \delta_{\mathbf{p}\mathbf{q}} = \frac{N^2}{2} \delta_{\mathbf{p}\mathbf{q}}. \tag{3.13}
 \end{aligned}$$

Here we have used the fact that the summation relation (1.54) holds analogously if we sum over only every other lattice site – such as over sublattices  $\mathcal{A}$  or  $\mathcal{B}$ , which have  $N/2$  elements each. Summing up, the (spin sum over the) fermionic four-point correlator (3.8) finally reads

$$E_{N\dot{\epsilon}}^F = \delta_{\kappa_{\text{in}}\kappa_{\text{out}}} + \delta_{\mathbf{p}\mathbf{q}}/2. \tag{3.14}$$

Analogous to the approximation in (2.52) in section 2.3.1, we only keep the leading order term in  $N$ , which is represented by the Kronecker delta  $\delta_{\kappa_{\text{in}}\kappa_{\text{out}}}$  and stands for directed superradiant re-emission. Inserting the bosonic (3.10) or the fermionic (3.14) four-point correlator, we then obtain an identical result for the expanded operatorial part from (3.6) to leading order in  $N$ ,

$$\begin{aligned}
 & \langle \Psi |_{\text{Mo/N}\dot{\epsilon}}^{J=0} [\hat{S}_{\kappa_{\text{out}}}^{\kappa_{\text{in}}}(t_3, t_4)]^\dagger \hat{S}_{\kappa_{\text{out}}}^{\kappa_{\text{in}}}(t_1, t_2) | \Psi \rangle_{\text{Mo/N}\dot{\epsilon}}^{J=0} \times e^{-i\omega(t_1-t_2-t_3+t_4)} \\
 &= \delta_{\kappa_{\text{in}}\kappa_{\text{out}}} \sum_{\mathbf{p}\mathbf{q}} \exp\{i[\phi_{\mathbf{q}}^{\kappa_{\text{in}}}(t_4) - \phi_{\mathbf{p}}^{\kappa_{\text{in}}}(t_2)]\} = N^2 \delta_{\kappa_{\text{in}}\kappa_{\text{out}}} \mathcal{J}_{\kappa_{\text{in}}}(-t_4) \mathcal{J}_{\kappa_{\text{in}}}(t_2), \tag{3.15}
 \end{aligned}$$

with the already established phase sum abbreviation (2.54). The combined probability density (3.4) thus reads (assuming atomic resonance,  $\omega_{\text{in}} = \omega$ ):

$$P_{\kappa_{\text{out}}} = N^2 \delta_{\kappa_{\text{in}}\kappa_{\text{out}}} \left| \int_0^{\tau_E} dt_2 \int_0^{\tau_A} dt_1 g_{\kappa_{\text{out}}}^*(t_2) g_{\kappa_{\text{in}}}(t_1) e^{i(\omega_{\text{out}}-\omega)t_2} \mathcal{J}_{\kappa_{\text{in}}}(t_2) \right|^2. \tag{3.16}$$

Recalling the suggested probing sequence (see Figure 3.1), we so far have not considered the waiting time  $\Delta t$  in the derivation of (3.16). However, this can be easily modeled via the time-dependent coupling constant  $g_{\kappa_{\text{out}}}^*(t_2)$ . We assume that it is zero for a discretionary waiting time  $\Delta t$ , which starts immediately after the phase

transition, and takes its usual value for the atom-field coupling afterwards, i.e.,

$$g_{\kappa_{\text{out}}}^*(t_2) = \begin{cases} 0, & \text{if } t_2 < \Delta t, \\ g_{\kappa_{\text{out}}}^*, & \text{if } t_2 \geq \Delta t. \end{cases} \quad (3.17)$$

Experimentally, this either corresponds to an atomic transition lifetime which is long in comparison to the waiting time  $\Delta t$  or – probably more feasibly – to the deactivation of the emission process during a then adjustable waiting time  $\Delta t$ . There are several ways to achieve this deactivation, which will be detailed in chapter 5. In conclusion, the relevant time span in which the reduction in superradiance due to the lattice dynamics takes place is given by the waiting time  $\Delta t$ , i.e.,  $\mathcal{J}_{\kappa_{\text{in}}}(t_2) = \mathcal{J}_{\kappa_{\text{in}}}(\Delta t)$ , and we can simplify (3.16) to,

$$P_{\kappa_{\text{out}}} = N^2 |\mathcal{J}_{\kappa_{\text{in}}}(\Delta t)|^2 \delta_{\kappa_{\text{in}}\kappa_{\text{out}}} P_{\text{single}}. \quad (3.18)$$

Interestingly, the combined emission probability density after a sudden transition from the separable state regime ( $J \ll U$ ) to the weak interactions regime ( $J \gg U$ ) decays similarly to the bosonic state where all momenta are equally populated (2.58 with  $N_1 = 0$  and  $N_2 = N$ ) and the fermionic metallic ground state (2.78). This result can be understood intuitively: after a sudden switch to the weak interactions regime, the corresponding ( $U = 0$ ) Hamiltonian – which is then diagonal in the momentum space  $\mathbf{k}$ -basis – “recognizes” the Mott insulator (or Mott-Néel) state as a mixture in which the atoms are equally distributed between all  $\mathbf{k}$ -modes.

In conclusion, the combined emission probability density for directed (i.e.,  $\kappa_{\text{out}} = \kappa_{\text{in}}$ ) superradiant re-emission decays maximally both in the bosonic and in the fermionic case after a sudden phase transition to the weak interactions regime.

### 3.4. Emission after an adiabatic phase transition

Let us now discuss the opposite scenario, i.e., an adiabatic phase transition instead of a sudden phase transition. As the results differ substantially, we will treat the bosonic and fermionic cases separately:

#### 3.4.1. Emission after adiabatic transition in the bosonic case

Starting with the bosonic case, we can state the excited Mott insulator state (3.1) explicitly in the lattice site basis (1.47). Originating from the collective absorption of the incoming probe photon with wave vector  $\boldsymbol{\kappa}_{\text{in}}$ , it is proportional to a “timed Dicke state” (1.4) as introduced in section 1.2.1, i.e.,

$$\begin{aligned} |\Psi(\boldsymbol{\kappa}_{\text{in}})\rangle_{\text{ex}}^{\text{Mo}} &= c \sum_{\mu} \exp\{i\boldsymbol{\kappa}_{\text{in}} \cdot \mathbf{r}_{\mu}\} \hat{b}_{\mu}^{\text{ex}\dagger} \hat{b}_{\mu}^{\text{gr}} |\Psi\rangle_{\text{Mo}}^{J=0} \\ &= c \sum_{\mu} \exp\{i\boldsymbol{\kappa}_{\text{in}} \cdot \mathbf{r}_{\mu}\} \hat{b}_{\mu}^{\text{ex}\dagger} \prod_{\nu \neq \mu} \hat{b}_{\nu}^{\text{gr}\dagger} |0\rangle, \end{aligned} \quad (3.19)$$

where  $c \in \mathbb{C}$  is a constant stemming from the absorption process (3.1), i.e., the state is not normalized. When the entire Hilbert space consists of all possible lattice states (with an arbitrary number of excited-state atoms), state (3.19) evidently lives in a subspace which contains all states where one atom is excited and  $N - 1$  atoms are in the ground state. As the number of excited-state atoms can only be changed by the absorption or emission of photons, state (3.19) remains in this subspace during the quantum phase transition and the subsequent waiting time  $\Delta t$ , i.e., until the photon is collectively re-emitted in the last step (see Figure 3.1). In the limiting case of  $J = 0$ , the excited Mott insulator state (3.19) is also an exact ground state of the lattice Hamiltonian (1.43) in this subspace – regardless of the wave vector  $\boldsymbol{\kappa}_{\text{in}}$  – as the energy eigenvalue is zero for all contributions in the superposition<sup>1</sup>. Obviously, these ground states are highly degenerate. To be precise, any combination of the  $N$  basis vectors of the aforementioned subspace with arbitrary local phases possesses

<sup>1</sup>As we have witnessed via exact diagonalization of small systems with, e.g.,  $N = 3$  lattice sites and particles, this degeneracy is lifted for small but nonzero  $J \ll U$ . In this case, the tunneling term in (1.43) reduces the energy for superposition states which have an overlap with themselves after tunneling. Hence, the excited Mott insulator state (3.19) is a unique approximate ground state for  $\boldsymbol{\kappa}_{\text{in}} = \{0, 0, \kappa_z\}$  and an approximate excited eigenstate for reciprocal lattice vectors  $\boldsymbol{\kappa}_{\text{in}} = 2\pi/(L\ell) \cdot \{n, m\}$ . To be precise, the exact eigenstates for  $0 < J \ll U$  also contain small amplitudes of all other basis states, such as states with two or even more atoms per lattice site. These scale with (higher orders of)  $J/U$  and thus are negligible for  $J \ll U$ , i.e., deep in the separable state regime.

the same energy eigenvalue zero.

**Eigenstates of the translation operators** Therefore, as an additional tool to classify these ground states, we introduce the translation operators  $\hat{T}_{x/y}$  for the  $x$  and  $y$  direction in the two-dimensional lattice plane (we choose the coordinate system such that the lattice is contained in the  $z = 0$  plane). By definition, they shift the  $x/y$  indices of the bosonic operators  $\hat{b}_\mu^{\lambda(\dagger)} = \hat{b}_{\mu_x, \mu_y}^{\lambda(\dagger)}$  by one, i.e.,

$$\hat{T}_x \hat{b}_{\mu_x, \mu_y}^{\lambda(\dagger)} = \hat{b}_{\mu_x+1, \mu_y}^{\lambda(\dagger)} \hat{T}_x, \quad (3.20)$$

$$\hat{T}_y \hat{b}_{\mu_x, \mu_y}^{\lambda(\dagger)} = \hat{b}_{\mu_x, \mu_y+1}^{\lambda(\dagger)} \hat{T}_y, \quad (3.21)$$

and periodically, that is, from the last line/row index to the first line/row index. Assuming periodic boundary conditions, the translation operators  $\hat{T}_{x/y}$  then commute with the lattice Hamiltonian (1.43). Thus, we can now regard simultaneous eigenstates of the lattice Hamiltonian and the translation operators. Note that when  $L$  denotes the number of lattice sites per dimension, we return to the original situation by shifting  $L$  times, i.e.,  $\hat{T}_{x/y}^L = \mathbb{I}$ . Hence, the eigenvalues of the translation operators are given by the  $L$ -th roots of unity, that is,  $e^{i2\pi n/L}$  with  $n \in \{0, \dots, L-1\}$ .

Expressing the excited Mott insulator state (3.19) with separate indices  $\mu_{x/y}$  for the  $x$  and  $y$  direction instead of a single index  $\mu$ , this reads,

$$|\Psi(\boldsymbol{\kappa}_{\text{in}})\rangle_{\text{ex}}^{\text{Mo}} = c \sum_{\mu_x, \mu_y} \exp \left\{ i(\kappa_{\text{in},x} \mu_x \ell + \kappa_{\text{in},y} \mu_y \ell) \right\} \hat{b}_{\mu_x, \mu_y}^{\text{ex}\dagger} \hat{b}_{\mu_x, \mu_y}^{\text{gr}} |\Psi\rangle_{\text{Mo}}^{J=0}, \quad (3.22)$$

where, e.g.,  $\mu_{x/y} \in \{0, \dots, L-1\}$ , and  $\mathbf{r}_\mu = \{\mu_x \ell, \mu_y \ell, 0\}$  is the position vector of the lattice site  $\mu$ . Applying the translation operator (3.20) to the excited Mott insulator state (3.22), followed by an index shift  $\mu_x + 1 = \tilde{\mu}_x$ , yields

$$\begin{aligned} \hat{T}_x |\Psi(\boldsymbol{\kappa}_{\text{in}})\rangle_{\text{ex}}^{\text{Mo}} &= c \sum_{\tilde{\mu}_x, \mu_y} \exp \left\{ i(\kappa_{\text{in},x} [\tilde{\mu}_x - 1] \ell + \kappa_{\text{in},y} \mu_y \ell) \right\} \hat{b}_{\tilde{\mu}_x, \mu_y}^{\text{ex}\dagger} \hat{b}_{\tilde{\mu}_x, \mu_y}^{\text{gr}} |\Psi\rangle_{\text{Mo}}^{J=0} \\ &= \exp \left\{ -i \kappa_{\text{in},x} \ell \right\} c \sum_{\tilde{\mu}_x, \mu_y} \exp \left\{ i(\kappa_{\text{in},x} \tilde{\mu}_x \ell + \kappa_{\text{in},y} \mu_y \ell) \right\} \hat{b}_{\tilde{\mu}_x, \mu_y}^{\text{ex}\dagger} \hat{b}_{\tilde{\mu}_x, \mu_y}^{\text{gr}} |\Psi\rangle_{\text{Mo}}^{J=0}, \end{aligned} \quad (3.23)$$

where the translation operator logically does not affect a fully symmetric state such as the Mott insulator state, i.e.,  $\hat{T}_{x/y} |\Psi\rangle_{\text{Mo}}^{J=0} = |\Psi\rangle_{\text{Mo}}^{J=0}$ . If (and only if)  $\boldsymbol{\kappa}_{\text{in}}$  is a reciprocal lattice vector, that is  $\boldsymbol{\kappa}_{\text{in}} = 2\pi/(L\ell) \cdot \{n, m\}$  with  $n, m \in \{-L/2+1, \dots, L/2\}$ , is

the latter part identical to (3.22) again, and thus:

$$\hat{T}_x |\Psi(\boldsymbol{\kappa}_{\text{in}})\rangle_{\text{ex}}^{\text{Mo}} = \exp\{-i\boldsymbol{\kappa}_{\text{in},x}\ell\} |\Psi(\boldsymbol{\kappa}_{\text{in}})\rangle_{\text{ex}}^{\text{Mo}}. \quad (3.24)$$

Analogously, the excited Mott insulator state (3.22) is also an eigenstate of the translation operator for the  $y$  direction (3.21), i.e.,

$$\hat{T}_y |\Psi(\boldsymbol{\kappa}_{\text{in}})\rangle_{\text{ex}}^{\text{Mo}} = \exp\{-i\boldsymbol{\kappa}_{\text{in},y}\ell\} |\Psi(\boldsymbol{\kappa}_{\text{in}})\rangle_{\text{ex}}^{\text{Mo}}. \quad (3.25)$$

In other words, the collective absorption of an incoming photon with wave vector  $\boldsymbol{\kappa}_{\text{in}}$  prepares the atoms in the optical lattice in a simultaneous eigenstate (3.19) of the lattice Hamiltonian (1.43) and the translation operators (3.20) and (3.21) if  $\boldsymbol{\kappa}_{\text{in}}$  matches a reciprocal lattice vector (which we require throughout the whole Thesis, see, e.g., section 2.3).

**Adiabatic transition in the bosonic case** The adiabatic theorem [75] states that an initial eigenstate such as the excited Mott insulator state (3.19) adapts to a slowly changing Hamiltonian, so that it is altered to a corresponding eigenstate of the resulting Hamiltonian after adiabatic transition. In our case, the resulting Hamiltonian is the two-species Bose-Hubbard Hamiltonian (1.43) in the weak interactions regime ( $J \gg U$ ), also known as the superfluid regime in the bosonic case. The translation operators, on the other hand, do not change and commute with the slowly varying Hamiltonian at any instant of time. Therefore, the excited Mott insulator state (3.19), which is a ground state of the “old” ( $J = 0$ ) Hamiltonian in the aforementioned subspace, adiabatically evolves into a corresponding eigenstate of the “new” ( $U = 0$ ) Hamiltonian (in this subspace) – while the eigenvalues of the translation operators are also conserved. As the resulting ( $U = 0$ ) Hamiltonian is diagonal in the momentum space  $\mathbf{k}$ -basis (1.59), the eigenstates in the subspace with exactly one excited atom read

$$|\Psi(\boldsymbol{\kappa}_{\text{in}})\rangle_{\text{ex}}^{\text{sf}} \propto \hat{b}_{\mathbf{k}_N}^{\text{ex}\dagger} \prod_{i=1}^{N-1} \hat{b}_{\mathbf{k}_i}^{\text{gr}\dagger} |0\rangle, \quad (3.26)$$

where the  $\mathbf{k}_i$ ,  $i \in \{1, \dots, N\}$  denote arbitrary reciprocal lattice vectors. However, the eigenvalues of the translation operators (3.20,3.21) are conserved, on the one hand,

$$\hat{T}_{x/y} |\Psi(\boldsymbol{\kappa}_{\text{in}})\rangle_{\text{ex}}^{\text{sf}} = \exp\{-i\boldsymbol{\kappa}_{\text{in},x/y}\ell\} |\Psi(\boldsymbol{\kappa}_{\text{in}})\rangle_{\text{ex}}^{\text{sf}}, \quad (3.27)$$

which poses a constraint on the possible compositions of the  $\mathbf{k}_i$  vectors. Using back transformation (1.53), we can derive the effect of the translation operators (3.20, 3.21) on the bosonic creation and annihilation operators in the momentum space  $\mathbf{k}$ -basis in a manner analogous to (3.23):

$$\hat{T}_{x/y} \hat{b}_{\mathbf{k}}^{\lambda\dagger} = \hat{T}_{x/y} \frac{1}{\sqrt{N}} \sum_{\mu} \hat{b}_{\mu}^{\lambda\dagger} \exp\{i\mathbf{k} \cdot \mathbf{r}_{\mu}\} = \exp\{-ik_{x/y}\ell\} \hat{b}_{\mathbf{k}}^{\lambda\dagger} \hat{T}_{x/y}. \quad (3.28)$$

Therefore, on the other hand,

$$\hat{T}_{x/y} |\Psi(\boldsymbol{\kappa}_{\text{in}})\rangle_{\text{ex}}^{\text{sf}} = \exp\left\{-i\ell \sum_{i=1}^N k_{i,x/y}\right\} |\Psi(\boldsymbol{\kappa}_{\text{in}})\rangle_{\text{ex}}^{\text{sf}}, \quad (3.29)$$

where the translation operator naturally does not affect the vacuum state,  $\hat{T}_{x/y} |0\rangle = |0\rangle$ . If we compare (3.27) and (3.29), the  $\mathbf{k}_i$  vectors obviously need to fulfill the constraints  $\sum_{i=1}^N k_{i,x/y} = \kappa_{\text{in},x/y} + n2\pi/\ell$  with  $n \in \mathbb{Z}$ . In addition, remember that we started in the *ground* state of the “old” ( $J = 0$ ) Hamiltonian in the noted subspace. Thus, we are not searching for an arbitrary eigenstate of the “new” ( $U = 0$ ) Hamiltonian (1.59) in this subspace, but for the lowest energy eigenstate (generally not the ground state, as the degeneracy is lifted for  $J > 0$ ) of the form (3.26),

$$\langle \Psi(\boldsymbol{\kappa}_{\text{in}}) | \hat{H}_J | \Psi(\boldsymbol{\kappa}_{\text{in}}) \rangle_{\text{ex}}^{\text{sf}} = \sum_{i=1}^N E_{\mathbf{k}_i} = -\frac{J}{Z} \sum_{i=1}^N T_{\mathbf{k}_i}, \quad (3.30)$$

which satisfies the constraints above. As the Fourier transform of the adjacency matrix  $T_{\mathbf{k}} = 2[\cos(k_x\ell) + \cos(k_y\ell)]$  is maximum for  $\mathbf{k} = \mathbf{0}$ , this lowest energy eigenstate has as many atoms in the  $\mathbf{k} = \mathbf{0}$  mode as permitted by the constraint above – that is  $N - 1$  atoms in the  $\mathbf{k} = \mathbf{0}$  mode and one atom in the  $\mathbf{k} = \boldsymbol{\kappa}_{\text{in}}$  mode. This leaves us with two (assuming that  $\{\kappa_{\text{in},x}, \kappa_{\text{in},y}\} \neq \{0, 0\}$ , see below) possible states, which both have the same minimal energy eigenvalue as well as the same eigenvalues of the translation operators,

$$|\Psi_{\alpha}(\boldsymbol{\kappa}_{\text{in}})\rangle_{\text{ex}}^{\text{sf}} = \frac{c\sqrt{N}}{\sqrt{(N-2)!}} \hat{b}_{\boldsymbol{\kappa}_{\text{in}}}^{\text{gr}\dagger} (\hat{b}_{\mathbf{k}=\mathbf{0}}^{\text{gr}\dagger})^{N-2} \hat{b}_{\mathbf{k}=\mathbf{0}}^{\text{ex}\dagger} |0\rangle, \quad (3.31)$$

$$|\Psi_{\beta}(\boldsymbol{\kappa}_{\text{in}})\rangle_{\text{ex}}^{\text{sf}} = \frac{c\sqrt{N}}{\sqrt{(N-1)!}} (\hat{b}_{\mathbf{k}=\mathbf{0}}^{\text{gr}\dagger})^{N-1} \hat{b}_{\boldsymbol{\kappa}_{\text{in}}}^{\text{ex}\dagger} |0\rangle. \quad (3.32)$$

In other words, there is either an excited-state atom or a ground-state atom found in the mode  $\boldsymbol{\kappa}_{\text{in}}$  of the absorbed probe photon. To infer in which of these two states the atoms in the optical lattice are predominantly found after the adiabatic phase transition, we examine the situation for nonzero  $U$ . Therefore, we first calculate the matrix elements of the on-site repulsion term (1.62) for the two possible states (3.31) and (3.32), i.e.,

$$\begin{aligned} & \langle \Psi_{\alpha/\beta}(\boldsymbol{\kappa}_{\text{in}}) | \hat{H}_U | \Psi_{\alpha/\beta}(\boldsymbol{\kappa}_{\text{in}}) \rangle_{\text{ex}}^{\text{sf}} \\ &= \frac{U}{2N} \sum_{\mathbf{k}_2 \mathbf{k}_3 \mathbf{k}_4} \langle \Psi_{\alpha/\beta}(\boldsymbol{\kappa}_{\text{in}}) | \hat{b}_{\mathbf{k}_3+\mathbf{k}_4-\mathbf{k}_2}^{\text{gr}\dagger} \hat{b}_{\mathbf{k}_2}^{\text{gr}\dagger} \hat{b}_{\mathbf{k}_3}^{\text{gr}} \hat{b}_{\mathbf{k}_4}^{\text{gr}} | \Psi_{\alpha/\beta}(\boldsymbol{\kappa}_{\text{in}}) \rangle_{\text{ex}}^{\text{sf}} \\ &+ \frac{U}{N} \sum_{\mathbf{k}_2 \mathbf{k}_3 \mathbf{k}_4} \langle \Psi_{\alpha/\beta}(\boldsymbol{\kappa}_{\text{in}}) | \hat{b}_{\mathbf{k}_3+\mathbf{k}_4-\mathbf{k}_2}^{\text{gr}\dagger} \hat{b}_{\mathbf{k}_2}^{\text{ex}\dagger} \hat{b}_{\mathbf{k}_3}^{\text{ex}} \hat{b}_{\mathbf{k}_4}^{\text{gr}} | \Psi_{\alpha/\beta}(\boldsymbol{\kappa}_{\text{in}}) \rangle_{\text{ex}}^{\text{sf}}, \end{aligned} \quad (3.33)$$

where the  $\lambda = \text{ex}$ -term vanishes, as the state contains only one excited-state atom. To obtain a nonzero result, the two creation operators to the left evidently need to create (ground-state or excited-state) atoms in the same modes that were annihilated by the two annihilation operators on the right. A detailed discussion of the nonzero cases can be found in Appendix A.4. Here, we only state the results:

$$\langle \Psi_{\alpha}(\boldsymbol{\kappa}_{\text{in}}) | \hat{H}_U | \Psi_{\alpha}(\boldsymbol{\kappa}_{\text{in}}) \rangle_{\text{ex}}^{\text{sf}} = |c|^2 N \frac{U}{2N} (N^2 + N - 4), \quad (3.34)$$

$$\langle \Psi_{\beta}(\boldsymbol{\kappa}_{\text{in}}) | \hat{H}_U | \Psi_{\beta}(\boldsymbol{\kappa}_{\text{in}}) \rangle_{\text{ex}}^{\text{sf}} = |c|^2 N \frac{U}{2N} N(N - 1), \quad (3.35)$$

and

$$\begin{aligned} \langle \Psi_{\alpha}(\boldsymbol{\kappa}_{\text{in}}) | \hat{H}_U | \Psi_{\beta}(\boldsymbol{\kappa}_{\text{in}}) \rangle_{\text{ex}}^{\text{sf}} &= \langle \Psi_{\beta}(\boldsymbol{\kappa}_{\text{in}}) | \hat{H}_U | \Psi_{\alpha}(\boldsymbol{\kappa}_{\text{in}}) \rangle_{\text{ex}}^{\text{sf}} \\ &= |c|^2 N \frac{U}{N} \sqrt{N - 1}. \end{aligned} \quad (3.36)$$

Putting these matrix elements together, we can construct the  $2 \times 2$  matrix:

$$\begin{aligned} H_U^{(2 \times 2)} &= \begin{pmatrix} \langle \Psi_{\alpha}(\boldsymbol{\kappa}_{\text{in}}) | \hat{H}_U | \Psi_{\alpha}(\boldsymbol{\kappa}_{\text{in}}) \rangle_{\text{ex}}^{\text{sf}} & \langle \Psi_{\alpha}(\boldsymbol{\kappa}_{\text{in}}) | \hat{H}_U | \Psi_{\beta}(\boldsymbol{\kappa}_{\text{in}}) \rangle_{\text{ex}}^{\text{sf}} \\ \langle \Psi_{\beta}(\boldsymbol{\kappa}_{\text{in}}) | \hat{H}_U | \Psi_{\alpha}(\boldsymbol{\kappa}_{\text{in}}) \rangle_{\text{ex}}^{\text{sf}} & \langle \Psi_{\beta}(\boldsymbol{\kappa}_{\text{in}}) | \hat{H}_U | \Psi_{\beta}(\boldsymbol{\kappa}_{\text{in}}) \rangle_{\text{ex}}^{\text{sf}} \end{pmatrix} \\ &= |c|^2 \frac{U}{2} \begin{pmatrix} N^2 + N - 4 & 2\sqrt{N - 1} \\ 2\sqrt{N - 1} & N(N - 1) \end{pmatrix}, \end{aligned} \quad (3.37)$$

and solve for the superposition of (3.31) and (3.32) with the lowest energy expectation value for nonzero  $U$ , according to (3.37). As a result, we obtain

$$|\Psi(\boldsymbol{\kappa}_{\text{in}})\rangle_{\text{ex}}^{\text{sf}} = \frac{\sqrt{N-1}}{\sqrt{N}} |\Psi_{\beta}(\boldsymbol{\kappa}_{\text{in}})\rangle_{\text{ex}}^{\text{sf}} - \frac{1}{\sqrt{N}} |\Psi_{\alpha}(\boldsymbol{\kappa}_{\text{in}})\rangle_{\text{ex}}^{\text{sf}}, \quad (3.38)$$

i.e., for large  $N \gg 1$ , the atoms in the optical lattice are in the quantum state

$$|\Psi(\boldsymbol{\kappa}_{\text{in}})\rangle_{\text{ex}}^{\text{sf}} \approx |\Psi_{\beta}(\boldsymbol{\kappa}_{\text{in}})\rangle_{\text{ex}}^{\text{sf}} = \frac{c\sqrt{N}}{\sqrt{(N-1)!}} (\hat{b}_{\mathbf{k}=\mathbf{0}}^{\text{gr}\dagger})^{N-1} \hat{b}_{\boldsymbol{\kappa}_{\text{in}}}^{\text{ex}\dagger} |0\rangle, \quad (3.39)$$

after the adiabatic phase transition. Here, the excited-state atom is found in the mode  $\boldsymbol{\kappa}_{\text{in}}$  of the absorbed probe photon, while all  $N-1$  ground-state atoms are condensed in the  $\mathbf{k} = \mathbf{0}$  mode. Note that the special case of an orthogonally incoming probe photon,  $\kappa_{\text{in},x} = \kappa_{\text{in},y} = 0$ , needs to be treated separately but yields the same (indeed exact) result (3.39).

**Emission after adiabatic transition in the bosonic case** Now that we know the quantum state of the atoms in the optical lattice after adiabatic evolution (3.39), we can easily calculate the combined emission probability density analogous to (3.3), i.e., via first-order perturbation theory in the “new” perturbation Hamiltonian  $\hat{V}_J$  in the weak interactions regime (3.2). To take a shortcut, we may notice that the lattice state (3.39) after the adiabatic transition to the weak interactions (aka superfluid) regime can be expressed as exciton creation applied to the superfluid ground state (1.34), that is  $|\Psi(\boldsymbol{\kappa}_{\text{in}})\rangle_{\text{ex}}^{\text{sf}} \propto \hat{\Sigma}_U^+(\boldsymbol{\kappa}_{\text{in}}, t_1) |\Psi\rangle_{\text{sf}}^{U=0}$ . Exploiting this fact, we can consider an operatorial part analog to (3.6), which in simplified form reads

$$\begin{aligned} \hat{S}_{\boldsymbol{\kappa}_{\text{out}}}^{\boldsymbol{\kappa}_{\text{in}}}(t_1, t_2) |\Psi\rangle_{\text{sf}}^{U=0} &= \hat{\Sigma}_J^-(\boldsymbol{\kappa}_{\text{out}}, t_2) \hat{\Sigma}_U^+(\boldsymbol{\kappa}_{\text{in}}, t_1) |\Psi\rangle_{\text{sf}}^{U=0} \\ &= e^{i\omega(t_1-t_2)} \sum_{\mathbf{p}} \exp\{-i\phi_{\mathbf{p}}^{\boldsymbol{\kappa}_{\text{out}}}(t_2)\} \hat{b}_{\mathbf{p}-\boldsymbol{\kappa}_{\text{out}}}^{\text{gr}\dagger} \hat{b}_{\mathbf{p}-\boldsymbol{\kappa}_{\text{in}}}^{\text{gr}} |\Psi\rangle_{\text{sf}}^{U=0}. \end{aligned} \quad (3.40)$$

In the norm squared (3.4), the operatorial part traces back to the long-known four-point correlator of the superfluid ground state (2.47). Calculating the combined emission probability density from the state (3.39) of the atoms in the optical lattice after the adiabatic transition, we obtain to the leading order in  $N$ :

$$P_{\boldsymbol{\kappa}_{\text{out}}} = N^2 \delta_{\boldsymbol{\kappa}_{\text{in}}\boldsymbol{\kappa}_{\text{out}}} \left| \int_0^{\tau_E} dt_2 \int_0^{\tau_A} dt_1 g_{\boldsymbol{\kappa}_{\text{out}}}^*(t_2) g_{\boldsymbol{\kappa}_{\text{in}}}(t_1) e^{i(\omega_{\text{out}}-\omega)t_2} e^{i\phi(t_2)} \right|^2. \quad (3.41)$$



In contrast to the combined probability density after a sudden transition (3.16), no phase sum appears here, as the four-point correlator of the superfluid ground state (2.47) fixes these sums. Instead, we only find a time-dependent phase factor (2.55). However, the phase  $\varphi(t_2)$  is proportional to the tunneling rate  $J$ , which is much smaller than the optical energies in the temporal phase  $e^{i(\omega_{\text{out}} - \omega)t_2}$ . Hence, we neglect this phase factor and arrive at the result for usual, full superradiance,

$$P_{\kappa_{\text{out}}} = N^2 \delta_{\kappa_{\text{in}} \kappa_{\text{out}}} P_{\text{single}}. \quad (3.42)$$

Regarding the Mott-to-superfluid phase transition in a bosonic optical lattice, we first showed in section 3.3 that the superradiance peak decays as described by (3.18) in the case of a sudden transition. When the phase transition can be considered adiabatic, on the other hand, we derived in this section 3.4 that the superradiance peak remains intact (3.42), i.e., the combined emission probability density is independent of the waiting time  $\Delta t$ . In conclusion, the proposed probing scheme can distinguish between a sudden quantum phase transition and an adiabatic quantum phase transition via the different emission characteristics.

### 3.4.2. Emission after adiabatic transition in the fermionic case

After having studied the emission characteristics after an adiabatic Mott-to-superfluid phase transition in a bosonic lattice in the last section, we are now going to study it after an adiabatic Mott-to-metal transition in a fermionic lattice.

Technically, it is possible to perform the same steps as in the bosonic case, i.e., starting from (3.1) we can state the excited Mott-Néel state explicitly, analogous to (3.19). In the next step, we could employ the translation operators (3.20, 3.21) squared, i.e.,  $(\hat{T}_{x/y})^2$ , to shift the  $x/y$ -indices by two – such that the Mott-Néel state (checkerboard pattern) is invariant under the operation. We would then obtain the constraints  $2 \sum_{i=1}^N k_{i,x/y} = 2\kappa_{\text{in},x/y} + n2\pi/\ell$  with  $n \in \mathbb{Z}$ , similar to the bosonic case. Then, however, we still need to identify the lowest energy eigenstate of the “new” ( $U = 0$ ) Hamiltonian. In the bosonic case, it was clear that (3.30) is minimized when as many as possible atoms are condensed in the  $\mathbf{k} = \mathbf{0}$  mode, corresponding to the superfluid ground state. In the fermionic case, on the other hand, condensation is not possible because of the Pauli exclusion principle, and the energy is minimized in the metallic ground state (1.37). The lowest energy eigenstate, which is also a specified eigenstate of the squared translation operators, would thus correspond to a metallic state where one mode  $\mathbf{k}$  is transferred to a higher energy state,  $\mathbf{k} \rightarrow \mathbf{k} + \kappa_{\text{in}}$

(or even some superposition of such states). As opposed to the bosonic superfluid case – where there is only one possibility,  $\mathbf{k} = \mathbf{0}$  – we cannot say which mode  $\mathbf{k}$  is going to be transferred here (numerical investigations show that this particularly depends on  $\boldsymbol{\kappa}_{\text{in}}$  itself). In conclusion, we cannot unambiguously identify the resulting eigenstate in the weak interactions ( $U = 0$ ) regime after the adiabatic transition, which corresponds to the initial ground state in the separable state regime ( $J = 0$ ).

Therefore, as an approximation, we regard the situation for small wave vectors  $\boldsymbol{\kappa}_{\text{in}}$  of the probe photon. For this reason, we consider the time-dependent Hamiltonian  $\hat{H}_{\text{adiab}}(t)$ , which models the time evolution of the adiabatic transition from the separable state regime to the weak interactions (i.e., metallic) regime. This is essentially given by the general lattice Hamiltonian (1.42) with the time-dependent but slowly varying tunneling rate  $J(t)$  and interaction strength  $U(t)$ , i.e.,

$$\begin{aligned} \hat{H}_{\text{adiab}}(t) &= -\frac{J(t)}{Z} \sum_{\mu\nu, s, \lambda} T_{\mu\nu} \hat{c}_{\mu, s}^{\lambda \dagger} \hat{c}_{\nu, s}^{\lambda} + \frac{U(t)}{2} \sum_{\mu} \left( \sum_{s, \lambda} \hat{n}_{\mu, s}^{\lambda} \right) \left( \sum_{s, \lambda} \hat{n}_{\mu, s}^{\lambda} - 1 \right) \\ &= -\frac{J(t)}{Z} \sum_{\mathbf{k}, s, \lambda} T_{\mathbf{k}} \hat{n}_{\mathbf{k}, s}^{\lambda} + \frac{U(t)}{2} \sum_{\mu} \left( \sum_{s, \lambda} \hat{n}_{\mu, s}^{\lambda} \right) \left( \sum_{s, \lambda} \hat{n}_{\mu, s}^{\lambda} - 1 \right), \end{aligned} \quad (3.43)$$

where (only) the tunneling term has been written in the momentum space  $\mathbf{k}$ -basis in the second line in accordance with (1.59). Otherwise, as detailed in section 3.3, the exciton creation operator in the separable state regime reads

$$\hat{\Sigma}_U^+(\boldsymbol{\kappa}_{\text{in}}, t_1) = e^{i\omega t_1} \sum_{\mu, s} \hat{c}_{\mu, s}^{\text{ex} \dagger} \hat{c}_{\mu, s}^{\text{gr}} \exp\{i\boldsymbol{\kappa}_{\text{in}} \cdot \mathbf{r}_{\mu}\} = e^{i\omega t_1} \sum_{\mathbf{p}, s} \hat{c}_{\mathbf{p}, s}^{\text{ex} \dagger} \hat{c}_{\mathbf{p}-\boldsymbol{\kappa}_{\text{in}}, s}^{\text{gr}}, \quad (3.44)$$

in the lattice site basis and momentum space  $\mathbf{k}$ -basis respectively. Now we examine the commutator between the adiabatic Hamiltonian (3.43) and the exciton creation operator (3.44). As the number of atoms per lattice site is unchanged by the exciton creation operator, it can immediately be seen (in the lattice site basis) that it commutes with the on-site repulsion term in (3.43). Hence, the commutator reduces to

$$\begin{aligned} [\hat{H}_{\text{adiab}}(t), \hat{\Sigma}_U^+(\boldsymbol{\kappa}_{\text{in}}, t_1)] &= -\frac{J(t)}{Z} e^{i\omega t_1} \sum_{\mathbf{k}, \mathbf{p}, s_1, s_2, \lambda} T_{\mathbf{k}} [\hat{n}_{\mathbf{k}, s_1}^{\lambda}, \hat{c}_{\mathbf{p}, s_2}^{\text{ex} \dagger} \hat{c}_{\mathbf{p}-\boldsymbol{\kappa}_{\text{in}}, s_2}^{\text{gr}}] \\ &= -\frac{J(t)}{Z} e^{i\omega t_1} \sum_{\mathbf{p}, s} \hat{c}_{\mathbf{p}, s}^{\text{ex} \dagger} \hat{c}_{\mathbf{p}-\boldsymbol{\kappa}_{\text{in}}, s}^{\text{gr}} (T_{\mathbf{p}} - T_{\mathbf{p}-\boldsymbol{\kappa}_{\text{in}}}), \end{aligned} \quad (3.45)$$

where, according to fundamental anticommutation relations (1.71), we calculated

$$\begin{aligned} \sum_{\lambda} [\hat{n}_{\mathbf{k},s_1}^{\lambda}, \hat{c}_{\mathbf{p},s_2}^{\text{ex}\dagger} \hat{c}_{\mathbf{p}-\boldsymbol{\kappa}_{\text{in}},s_2}^{\text{gr}}] &= \hat{c}_{\mathbf{p},s_2}^{\text{ex}\dagger} [\hat{n}_{\mathbf{k},s_1}^{\text{gr}}, \hat{c}_{\mathbf{p}-\boldsymbol{\kappa}_{\text{in}},s_2}^{\text{gr}}] + [\hat{n}_{\mathbf{k},s_1}^{\text{ex}}, \hat{c}_{\mathbf{p},s_2}^{\text{ex}\dagger}] \hat{c}_{\mathbf{p}-\boldsymbol{\kappa}_{\text{in}},s_2}^{\text{gr}} \\ &= \hat{c}_{\mathbf{p},s_2}^{\text{ex}\dagger} \hat{c}_{\mathbf{p}-\boldsymbol{\kappa}_{\text{in}},s_2}^{\text{gr}} (\delta_{\mathbf{k},\mathbf{p}} - \delta_{\mathbf{k},\mathbf{p}-\boldsymbol{\kappa}_{\text{in}}}) \delta_{s_1 s_2}. \end{aligned} \quad (3.46)$$

Recalling the approximation for small wave vectors  $|\boldsymbol{\kappa}_{\text{in}}|\ell \ll 1$  from (2.60),

$$(T_{\mathbf{p}} - T_{\mathbf{p}-\boldsymbol{\kappa}_{\text{in}}}) \approx -2\ell [\kappa_{\text{in},x} \sin(p_x \ell) + \kappa_{\text{in},y} \sin(p_y \ell)], \quad (3.47)$$

we observe that the commutator scales linearly in  $\kappa_{\text{in},x/y}$ . In a zeroth-order approximation, we can thus neglect the commutator, which means that we can apply the exciton creation operator after the adiabatic evolution  $\hat{U}_{\text{adiab}}(t) |\Psi\rangle_{\text{Né}}^{J=0} = |\Psi\rangle_{\text{me}}^{U=0}$  instead of beforehand. As a consequence, the combined emission probability density (3.4) can be then calculated according to

$$\begin{aligned} \hat{S}_{\boldsymbol{\kappa}_{\text{out}}}^{\boldsymbol{\kappa}_{\text{in}}}(t_1, t_2) |\Psi\rangle_{\text{me}}^{U=0} &= \hat{\Sigma}_J^-(\boldsymbol{\kappa}_{\text{out}}, t_2) \hat{\Sigma}_J^+(\boldsymbol{\kappa}_{\text{in}}, t_1) |\Psi\rangle_{\text{me}}^{U=0} \\ &= e^{i\omega(t_1-t_2)} \sum_{\mathbf{p},s} \exp\{-i\phi_{\mathbf{p}}^{\boldsymbol{\kappa}_{\text{out}}}(t_2)\} \hat{c}_{\mathbf{p}-\boldsymbol{\kappa}_{\text{out}},s}^{\text{gr}\dagger} \hat{c}_{\mathbf{p}-\boldsymbol{\kappa}_{\text{in}},s}^{\text{gr}} |\Psi\rangle_{\text{me}}^{U=0}, \end{aligned}$$

which leads back to the four-point correlator of the metallic ground state (2.71), which was already shown in section 2.3.2 to cause a decay of the superradiance peak according to (2.78), i.e.,

$$P_{\boldsymbol{\kappa}_{\text{out}}} = N^2 |\mathcal{J}_{\boldsymbol{\kappa}_{\text{in}}}(\Delta t)|^2 \delta_{\boldsymbol{\kappa}_{\text{in}} \boldsymbol{\kappa}_{\text{out}}} P_{\text{single}}. \quad (3.48)$$

Note that the zeroth-order approximation presented here for the fermionic case also works in the bosonic case, where it yields the correct result (3.39). In the general case of larger wave vectors  $\boldsymbol{\kappa}_{\text{in}}$  of the probe photon, the zeroth-order approximation is probably not accurate though. But even when the adiabatic evolution does not commute with the exciton creation, the quantum state after the adiabatic evolution will still be similar to the metallic ground state in the sense that the atoms are distributed over many  $\mathbf{k}$ -modes. For these states, we generally expect a decay of the superradiance peak over the waiting time  $\Delta t$ , as described in section 2.3.2 and also for the bosonic distributed case (2.58 with  $N_1 = 0$  and  $N_2 = N$ ), and as can be seen in Figure 2.4.

To sum up the results of the Mott-to-metal transition in a fermionic lattice, we found that the superradiance peak decays after a sudden transition (3.18), as well as

after an adiabatic transition (3.48). As opposed to the situation for a bosonic lattice, the proposed probing scheme is thus unfortunately not able to distinguish a sudden Mott-to-metal transition from an adiabatic transition in a fermionic lattice.

### 3.5. Summary of the detection of phase transitions

In this chapter we employed a single-photon pump-and-probe scheme (see Figure 3.1) to explore ultracold atoms in an optical lattice undergoing a structural quantum phase transition from the separable state regime ( $J \ll U$ ) to the weak interactions regime ( $J \gg U$ ). Both for bosonic and fermionic atoms in the optical lattice, we calculated the combined emission probability density for the absorption of a probe photon  $\kappa_{\text{in}}$  and its directed superradiant re-emission into the same mode  $\kappa_{\text{out}} = \kappa_{\text{in}}$ , with the phase transition and a subsequent waiting time  $\Delta t$  between absorption and re-emission (Figure 3.1).

Regarding the Mott-to-superfluid transition in the case of bosonic atoms, on the one hand, we found that the superradiant emission probability density reduces over the waiting time  $\Delta t$  after a sudden transition (3.18), while it does not decay in the case of an adiabatic transition (3.42). Comparing the two cases, a sudden transition (section 3.3) can thus be distinguished from an adiabatic transition (section 3.4.1) in a bosonic optical lattice using the suggested pump-and-probe scheme.

For the fermionic Mott-to-metal transition, on the other hand, the superradiant emission probability density decays over the waiting time  $\Delta t$  similarly, both in the case of a sudden transition (3.18) and in the case of an adiabatic transition (3.48). As opposed to the case of bosons, the proposed pump-and-probe scheme can therefore not be used to infer whether a transition can be considered sudden (section 3.3) or adiabatic (section 3.4.2) in a fermionic optical lattice.

## 4. Detection via classical laser fields

*In the two preceding chapters we have discussed the single-photon pump-and-probe scheme (see Figure 1.3) extensively both to detect stationary lattice states (chapter 2) and quantum phase transitions (chapter 3). Below, we want to study an alternative probing scheme, for which single-photon absorption and emission is replaced by the interaction with classical laser fields. Although the superradiant excitation and de-excitation dynamics differ substantially from the single-photon case, we show that comparable information on the atoms in the optical lattice can be obtained. In short, the alternative probing scheme presented in this chapter may facilitate experimental implementation, while it preserves the important features of the single-photon probing scheme.*

### 4.1. Probing scheme employing classical laser fields

In principle, we consider the same pump-and-probe scheme as depicted in Figure 1.3, which has already been investigated in chapter 2, and, in a slightly modified form, in chapter 3. However, instead of the absorption of a single probe photon in the first step, we suggest excitation via two counter-propagating laser beams which are switched on for a short period of time. Equivalently, we consider de-excitation via the (same) laser beams in the third step, i.e., in place of the spontaneous directed emission of a single photon. By using two counter-propagating laser beams, it is possible to transfer the internal state of the atoms in the optical lattice from the ground state to a metastable state via a detuned two-photon Raman transition, as sketched in Figure 4.1. The main advantage of this approach is evident: by exciting the atoms in the optical lattice from the ground state to a *metastable* state (which is not possible via a single photon), the atomic excitation does not decay via spontaneous emission in the absence of the laser fields. The waiting time  $\Delta t$  then simply corresponds to the time interval between excitation and de-excitation, in which the lasers are switched off – and thus can be freely chosen.

Before we start with the calculations in the next section, let us briefly summarize the complete probing sequence employing classical laser fields (cf. Figure 1.3): At the beginning, the atom ensemble in the optical lattice is in a certain initial state as described in section 2.1.1, i.e., with all atoms in their internal ground state. Then,

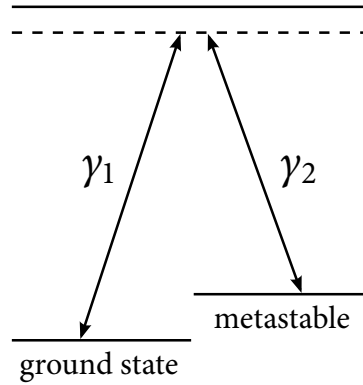


FIGURE 4.1. – A detuned two-photon Raman transition from the ground state to a metastable state. We propose excitation and de-excitation via two counter-propagating laser fields  $\gamma_1$  and  $\gamma_2$ . Between the excitation and de-excitation periods, the laser fields are switched off, such that the internal state of the atoms in the optical lattice is preserved, i.e., they stay in the ground state or in the metastable state respectively. As a consequence, the waiting time  $\Delta t$  can be chosen freely by the experimentalist. Please note that possible atomic level schemes are further discussed in chapter 5.

in a *first step*, the two counter-propagating laser beams  $\gamma_1$  and  $\gamma_2$  are switched on for a short period  $\tau_A$ , in which they coherently excite one (or a few) atoms from the ground state to a metastable state, as depicted in Figure 4.1. The joint laser wave vector  $\kappa_{\text{in}} = \mathbf{k}_1 - \mathbf{k}_2$  of the two counter-propagating laser beams is thereby imprinted on the coherent excited state, analogous (but not equal) to the Dicke state in section 1.2.1. After the excitation period, the lasers are switched off for a waiting time  $\Delta t$  in the *second step*. During this waiting time, the atoms tunnel and interact as modeled by the general lattice Hamiltonian (1.42). When the two counter-propagating laser beams are switched on again for a second period  $\tau_E$  in the *third step*, the atoms can finally decay from the metastable state back to the ground state. Choosing the same joint laser wave vectors  $\kappa_{\text{out}} = \kappa_{\text{in}} = \mathbf{k}_1 - \mathbf{k}_2$  and identical time periods  $\tau_E = \tau_A$ , but the opposite sign for the effective classical field for the excitation and de-excitation process, one would expect the coherent excitation to reverse perfectly, i.e., for all atoms to be in the ground state again after the completed sequence. However, if the lattice dynamics between the excitation and de-excitation period have reduced the spatial phase coherence, the de-excitation process is impaired, and a certain number of atoms remains in the metastable state after the full sequence. Measuring this number of remaining atoms, we can obtain comparable information about stationary lattice states (chapter 2) or about quantum phase transitions (chapter 3) to the information obtained by measuring the superradiance

peak in the case of the single-photon probing scheme.

In the next sections we are therefore going to calculate the number of atoms which are still in the metastable state after the full sequence in various situations. To this end, we will first introduce a perturbation Hamiltonian for the on-site atom-field coupling in the case of classical laser fields, analogous to (1.45) in the (full quantum-mechanical) case of single-photon absorption and emission.

## 4.2. Hamiltonian and excitation process

In the single-photon approach, we employed the perturbation Hamiltonian (1.45) to couple the internal states of the atoms to the free-space electromagnetic field (see section 1.4),

$$\hat{V} = \int d^3k g_k(t) \hat{a}_k \hat{\Sigma}^+(\mathbf{k}) + \text{H.c.}, \quad (4.1)$$

which integrates over all possible modes  $\mathbf{k}$  for the coupling constant  $g_k(t)$ , the annihilation operator  $\hat{a}_k$  of a single photon in mode  $\mathbf{k}$  and the spatial phases in the exciton creation operator  $\hat{\Sigma}^+(\mathbf{k})$ . In this chapter, in contrast, the electromagnetic field should be treated classically, and we consider the interaction of the atoms in the optical lattice with the two counter-propagating lasers via one effective joint laser mode  $\mathbf{k} = \mathbf{k}_1 - \mathbf{k}_2$ ,

$$\hat{V}_k(t) = g A_{\text{eff}}(t) \hat{\Sigma}^+(\mathbf{k}) + \text{H.c.}, \quad (4.2)$$

where  $A_{\text{eff}}(t)$  denotes the effective classical field of the two counter-propagating lasers combined, and  $g$  describes an effective coupling constant. In general, the coupling constant  $g$  is determined by atomic properties. When we assume that it is real, we can express the perturbation Hamiltonian (4.2) in a convenient form via the quasispin  $X$  operator (1.48,1.64),

$$\hat{V}_k(t) = g A_{\text{eff}}(t) [\hat{\Sigma}^+(\mathbf{k}) + \text{H.c.}] = 2g A_{\text{eff}}(t) \hat{\Sigma}^x(\mathbf{k}). \quad (4.3)$$

Let us now regard the excitation process, in which the two counter-propagating laser beams are switched on for a short period  $\tau_A$  to generate a coherent excited

state. The corresponding time evolution operator is then given by

$$\hat{U}_{\mathbf{k}}(\tau_A) = \exp \left\{ -i \int_0^{\tau_A} dt 2g A_{\text{eff}}(t) \hat{\Sigma}^x(\mathbf{k}) \right\}. \quad (4.4)$$

Motivated by the fact that the quasispin  $X$  operator can be interpreted as the generator of rotations of the quasispin (see section 1.2.2) about the  $x$ -axis, we condense the prefactor into an angle,

$$\alpha = 2g \int_0^{\tau_A} dt A_{\text{eff}}(t), \quad (4.5)$$

which reflects the magnitude of the overall quasispin rotation, which is guided by the effective classical field  $A_{\text{eff}}(t)$  during the excitation period  $\tau_A$ . In short, the time evolution operator then reads

$$\hat{U}_{\mathbf{k}}(\alpha) = \exp \left\{ -i\alpha \hat{\Sigma}^x(\mathbf{k}) \right\}. \quad (4.6)$$

In the sense of the Heisenberg picture, this time evolution can then be applied to the quasispin  $Z$  operator (1.50,1.67) using the Baker-Hausdorff lemma (sometimes also referred to as Lie's expansion formula, see for example [75]),

$$\begin{aligned} \hat{\Sigma}_{\alpha}^z &= \hat{U}_{\kappa_{\text{in}}}^{\dagger}(\alpha) \hat{\Sigma}^z \hat{U}_{\kappa_{\text{in}}}(\alpha) = \exp \left\{ i\alpha \hat{\Sigma}^x(\kappa_{\text{in}}) \right\} \hat{\Sigma}^z \exp \left\{ -i\alpha \hat{\Sigma}^x(\kappa_{\text{in}}) \right\} \\ &= \sum_{m=0}^{\infty} \frac{1}{m!} \left[ i\alpha \hat{\Sigma}^x(\kappa_{\text{in}}), \hat{\Sigma}^z \right]_m, \end{aligned} \quad (4.7)$$

where  $[\hat{A}, \hat{B}]_m$  stands for the  $m$ -th commutator, i.e.,  $[\hat{A}, \hat{B}]_m = [\hat{A}, [\hat{A}, \hat{B}]_{m-1}]$  with the starting point  $[\hat{A}, \hat{B}]_0 = \hat{B}$ . Calculating these iterated commutators is straightforward, as the quasispin operators stay in their  $SU(2)$  algebra (see section 1.2.2). Thus we obtain

$$\hat{\Sigma}_{\alpha}^z = \hat{U}_{\kappa_{\text{in}}}^{\dagger}(\alpha) \hat{\Sigma}^z \hat{U}_{\kappa_{\text{in}}}(\alpha) = \cos(\alpha) \hat{\Sigma}^z + \sin(\alpha) \hat{\Sigma}^y(\kappa_{\text{in}}), \quad (4.8)$$

i.e., a simple rotation by an angle  $\alpha$  about the  $x$ -axis, as expected. Note that we are employing the Heisenberg picture because writing out the resulting coherent states is much more complex. As opposed to Dicke states (1.4), they do not exhibit a well-defined number of excitations.



### 4.3. De-excitation process with arbitrary wave vector

#### 4.3.1. De-excitation dynamics applied to the $\hat{\Sigma}_\alpha^z$ operator

Before we also include the lattice dynamics in section 4.4, let us first rediscover the directed superradiant emission for the case of classical laser fields. To this end, we are going to reverse the quasispin rotation (4.8) by applying the time evolution of the second (de-exciting) laser period with an arbitrary joint laser wave vector  $\boldsymbol{\kappa}_{\text{out}}$  directly after the first (exciting) laser period, i.e.,

$$\hat{\Sigma}_{\alpha,\beta}^z = \hat{U}_{\boldsymbol{\kappa}_{\text{out}}}^\dagger(\beta) \hat{U}_{\boldsymbol{\kappa}_{\text{in}}}^\dagger(\alpha) \hat{\Sigma}^z \hat{U}_{\boldsymbol{\kappa}_{\text{in}}}(\alpha) \hat{U}_{\boldsymbol{\kappa}_{\text{out}}}(\beta) = \hat{U}_{\boldsymbol{\kappa}_{\text{out}}}^\dagger(\beta) \hat{\Sigma}_\alpha^z \hat{U}_{\boldsymbol{\kappa}_{\text{out}}}(\beta). \quad (4.9)$$

Analogous to the angle  $\alpha$  for the first (exciting) laser period (4.5), the quasispin-rotation angle  $\beta$  is given by  $\beta = 2g \int_0^{\tau_E} dt A_{\text{eff}}(t)$ , with  $\tau_E$  the duration of the second (de-exciting) laser period. Inserting the result after the first (exciting) laser period (4.8), we find

$$\hat{\Sigma}_{\alpha,\beta}^z = \cos(\alpha) \hat{U}_{\boldsymbol{\kappa}_{\text{out}}}^\dagger(\beta) \hat{\Sigma}^z \hat{U}_{\boldsymbol{\kappa}_{\text{out}}}(\beta) + \sin(\alpha) \hat{U}_{\boldsymbol{\kappa}_{\text{out}}}^\dagger(\beta) \hat{\Sigma}^y(\boldsymbol{\kappa}_{\text{in}}) \hat{U}_{\boldsymbol{\kappa}_{\text{out}}}(\beta), \quad (4.10)$$

where, using again the result (4.8), the first term can immediately be evaluated to

$$\begin{aligned} \cos(\alpha) \hat{U}_{\boldsymbol{\kappa}_{\text{out}}}^\dagger(\beta) \hat{\Sigma}^z \hat{U}_{\boldsymbol{\kappa}_{\text{out}}}(\beta) &= \cos(\alpha) \cos(\beta) \hat{\Sigma}^z \\ &+ \cos(\alpha) \sin(\beta) \hat{\Sigma}^y(\boldsymbol{\kappa}_{\text{out}}). \end{aligned} \quad (4.11)$$

For the second term, we have to assess the expression

$$\begin{aligned} \hat{U}_{\boldsymbol{\kappa}_{\text{out}}}^\dagger(\beta) \hat{\Sigma}^y(\boldsymbol{\kappa}_{\text{in}}) \hat{U}_{\boldsymbol{\kappa}_{\text{out}}}(\beta) &= \exp\{i\beta \hat{\Sigma}^x(\boldsymbol{\kappa}_{\text{out}})\} \hat{\Sigma}^y(\boldsymbol{\kappa}_{\text{in}}) \exp\{-i\beta \hat{\Sigma}^x(\boldsymbol{\kappa}_{\text{out}})\} \\ &= \sum_{m=0}^{\infty} \frac{1}{m!} [i\beta \hat{\Sigma}^x(\boldsymbol{\kappa}_{\text{out}}), \hat{\Sigma}^y(\boldsymbol{\kappa}_{\text{in}})]_m, \end{aligned} \quad (4.12)$$

i.e., the  $m$ -th commutator between  $\hat{\Sigma}^x(\boldsymbol{\kappa}_{\text{out}})$  and  $\hat{\Sigma}^y(\boldsymbol{\kappa}_{\text{in}})$ . Please note that  $\hat{\Sigma}^x(\boldsymbol{\kappa}_{\text{out}})$ ,  $\hat{\Sigma}^y(\boldsymbol{\kappa}_{\text{in}})$  and  $\hat{\Sigma}^z$  only form an  $SU(2)$  algebra in the trivial case  $\boldsymbol{\kappa}_{\text{out}} = \boldsymbol{\kappa}_{\text{in}}$ . As we want to study the general case of two differing wave vectors  $\boldsymbol{\kappa}_{\text{out}} \neq \boldsymbol{\kappa}_{\text{in}}$  here, the result of the first commutator reads (for a detailed calculation, see Appendix A.5)

$$[\hat{\Sigma}^x(\boldsymbol{\kappa}_{\text{out}}), \hat{\Sigma}^y(\boldsymbol{\kappa}_{\text{in}})] = i \hat{\Sigma}_D^z(\boldsymbol{\kappa}_{\text{out}}, \boldsymbol{\kappa}_{\text{in}}), \quad (4.13)$$

where we have introduced a generalized quasispin  $Z$  operator

$$\begin{aligned}\hat{\Sigma}_D^z(\boldsymbol{\kappa}_{\text{out}}, \boldsymbol{\kappa}_{\text{in}}) &:= \frac{1}{4} \sum_{\boldsymbol{p}, s} \left( \hat{a}_{\boldsymbol{p}-\boldsymbol{\kappa}_{\text{out}}, s}^{\text{ex} \dagger} \hat{a}_{\boldsymbol{p}-\boldsymbol{\kappa}_{\text{in}}, s}^{\text{ex}} - \hat{a}_{\boldsymbol{p}-\boldsymbol{\kappa}_{\text{out}}, s}^{\text{gr} \dagger} \hat{a}_{\boldsymbol{p}-\boldsymbol{\kappa}_{\text{in}}, s}^{\text{gr}} + \text{H.c.} \right) \\ &= \frac{1}{2} \sum_{\mu, s} \left( \hat{n}_{\mu, s}^{\text{ex}} - \hat{n}_{\mu, s}^{\text{gr}} \right) \cos \left[ (\boldsymbol{\kappa}_{\text{in}} - \boldsymbol{\kappa}_{\text{out}}) \cdot \boldsymbol{r}_{\mu} \right],\end{aligned}\quad (4.14)$$

which resembles the usual quasispin  $Z$  operator (1.50,1.67), with (in the lattice site basis) the sole difference being the lattice site-dependent cosine factor. Hence, the usual quasispin  $Z$  operator is reproduced for the special case  $\boldsymbol{\kappa}_{\text{out}} = \boldsymbol{\kappa}_{\text{in}}$ , i.e.,  $\hat{\Sigma}_D^z(\boldsymbol{\kappa}_{\text{out}}, \boldsymbol{\kappa}_{\text{out}}) = \hat{\Sigma}^z$ , satisfying the  $SU(2)$  algebra property. For the second ( $m = 2$ ) commutator in (4.12) it is necessary to calculate the commutator of  $\hat{\Sigma}^x(\boldsymbol{\kappa}_{\text{out}})$  with the result of the first ( $m = 1$ ) commutator (4.13),

$$\left[ \hat{\Sigma}^x(\boldsymbol{\kappa}_{\text{out}}), \hat{\Sigma}_D^z(\boldsymbol{\kappa}_{\text{out}}, \boldsymbol{\kappa}_{\text{in}}) \right] = -i \hat{\Sigma}_D^y(\boldsymbol{\kappa}_{\text{out}}, \boldsymbol{\kappa}_{\text{in}}), \quad (4.15)$$

where we obtain (see Appendix A.5) a generalized version of the  $\hat{\Sigma}^y(\boldsymbol{\kappa}_{\text{out}})$  quasispin operator,

$$\begin{aligned}\hat{\Sigma}_D^y(\boldsymbol{\kappa}_{\text{out}}, \boldsymbol{\kappa}_{\text{in}}) &:= \frac{1}{2} \left[ \hat{\Sigma}^y(\boldsymbol{\kappa}_{\text{in}}) + \hat{\Sigma}^y(2\boldsymbol{\kappa}_{\text{out}} - \boldsymbol{\kappa}_{\text{in}}) \right] \\ &= \frac{1}{4i} \sum_{\boldsymbol{p}, s} \left( \hat{a}_{\boldsymbol{p}, s}^{\text{ex} \dagger} \hat{a}_{\boldsymbol{p}-\boldsymbol{\kappa}_{\text{in}}, s}^{\text{gr}} + \hat{a}_{\boldsymbol{p}, s}^{\text{ex} \dagger} \hat{a}_{\boldsymbol{p}-2\boldsymbol{\kappa}_{\text{out}}+\boldsymbol{\kappa}_{\text{in}}, s}^{\text{gr}} - \text{H.c.} \right) \\ &= \frac{1}{2i} \sum_{\mu, s} \left( \hat{a}_{\mu, s}^{\text{ex} \dagger} \hat{a}_{\mu, s}^{\text{gr}} \exp \{ i \boldsymbol{\kappa}_{\text{out}} \cdot \boldsymbol{r}_{\mu} \} - \text{H.c.} \right) \cos \left[ (\boldsymbol{\kappa}_{\text{in}} - \boldsymbol{\kappa}_{\text{out}}) \cdot \boldsymbol{r}_{\mu} \right].\end{aligned}\quad (4.16)$$

Compared to (4.14), the difference to the usual quasispin  $Y$  operator (1.49,1.65) is given by the same lattice site-dependent cosine factor. Accordingly, the usual quasispin  $Y$  operator is retrieved for  $\boldsymbol{\kappa}_{\text{out}} = \boldsymbol{\kappa}_{\text{in}}$ , i.e.,  $\hat{\Sigma}_D^y(\boldsymbol{\kappa}_{\text{out}}, \boldsymbol{\kappa}_{\text{out}}) = \hat{\Sigma}^y(\boldsymbol{\kappa}_{\text{out}})$ . The third ( $m = 3$ ) commutator for (4.12) fortunately yields the same result as the first ( $m = 1$ ) commutator, that is (see Appendix A.5),

$$\left[ \hat{\Sigma}^x(\boldsymbol{\kappa}_{\text{out}}), \hat{\Sigma}_D^y(\boldsymbol{\kappa}_{\text{out}}, \boldsymbol{\kappa}_{\text{in}}) \right] = i \hat{\Sigma}_D^z(\boldsymbol{\kappa}_{\text{out}}, \boldsymbol{\kappa}_{\text{in}}). \quad (4.17)$$

Thus, the result of the  $m$ -th commutator is known for all  $m \geq 1$ ,

$$\left[ \hat{\Sigma}^x(\boldsymbol{\kappa}_{\text{out}}), \hat{\Sigma}^y(\boldsymbol{\kappa}_{\text{in}}) \right]_m = \begin{cases} \hat{\Sigma}_D^y(\boldsymbol{\kappa}_{\text{out}}, \boldsymbol{\kappa}_{\text{in}}), & \text{if } m \text{ is even,} \\ i \hat{\Sigma}_D^z(\boldsymbol{\kappa}_{\text{out}}, \boldsymbol{\kappa}_{\text{in}}), & \text{if } m \text{ is odd,} \end{cases} \quad (4.18)$$

and by definition,  $[\hat{\Sigma}^x(\boldsymbol{\kappa}_{\text{out}}), \hat{\Sigma}^y(\boldsymbol{\kappa}_{\text{in}})]_0 = \hat{\Sigma}^y(\boldsymbol{\kappa}_{\text{in}})$  for  $m = 0$ . Going back to (4.12), we can now split the infinite (exponential-like) series into a sine series and a cosine series, where the  $m = 0$  term requires additional attention, i.e.,

$$\begin{aligned} \hat{U}_{\boldsymbol{\kappa}_{\text{out}}}^\dagger(\beta) \hat{\Sigma}^y(\boldsymbol{\kappa}_{\text{in}}) \hat{U}_{\boldsymbol{\kappa}_{\text{out}}}(\beta) &= \sum_{m=0}^{\infty} \frac{(i\beta)^m}{m!} [\hat{\Sigma}^x(\boldsymbol{\kappa}_{\text{out}}), \hat{\Sigma}^y(\boldsymbol{\kappa}_{\text{in}})]_m \\ &= \sum_{m=0}^{\infty} \frac{(i\beta)^{2m}}{(2m)!} [\hat{\Sigma}^x(\boldsymbol{\kappa}_{\text{out}}), \hat{\Sigma}^y(\boldsymbol{\kappa}_{\text{in}})]_{2m} + \sum_{m=0}^{\infty} \frac{(i\beta)^{2m+1}}{(2m+1)!} [\hat{\Sigma}^x(\boldsymbol{\kappa}_{\text{out}}), \hat{\Sigma}^y(\boldsymbol{\kappa}_{\text{in}})]_{2m+1} \\ &= \hat{\Sigma}^y(\boldsymbol{\kappa}_{\text{in}}) + \hat{\Sigma}_D^y(\boldsymbol{\kappa}_{\text{out}}, \boldsymbol{\kappa}_{\text{in}}) [\cos(\beta) - 1] - \hat{\Sigma}_D^z(\boldsymbol{\kappa}_{\text{out}}, \boldsymbol{\kappa}_{\text{in}}) \sin(\beta). \end{aligned} \quad (4.19)$$

Putting the pieces (4.11) and (4.19) together, the result for the quasispin  $Z$  operator after the time evolution of both (exciting and de-exciting) laser periods (4.10) is given by

$$\begin{aligned} \hat{\Sigma}_{\alpha,\beta}^z &= \cos(\alpha) \cos(\beta) \hat{\Sigma}^z - \sin(\alpha) \sin(\beta) \hat{\Sigma}_D^z(\boldsymbol{\kappa}_{\text{out}}, \boldsymbol{\kappa}_{\text{in}}) + \sin(\alpha) \hat{\Sigma}^y(\boldsymbol{\kappa}_{\text{in}}) \\ &\quad + \cos(\alpha) \sin(\beta) \hat{\Sigma}^y(\boldsymbol{\kappa}_{\text{out}}) + \sin(\alpha) [\cos(\beta) - 1] \hat{\Sigma}_D^y(\boldsymbol{\kappa}_{\text{out}}, \boldsymbol{\kappa}_{\text{in}}), \end{aligned} \quad (4.20)$$

which is, at first sight, a rather complex expression. Therefore, we are going to examine it in detail in the next section.

### 4.3.2. Interpretation and expectation values

To obtain more intuitive results, it is useful to consider specific expectation values taken in various initial lattice states. Beforehand, note that for the coherent case of  $\boldsymbol{\kappa}_{\text{out}} = \boldsymbol{\kappa}_{\text{in}}$ , the result (4.20) can be simplified to

$$\hat{\Sigma}_{\alpha,\beta}^z = \cos(\alpha + \beta) \hat{\Sigma}^z + \sin(\alpha + \beta) \hat{\Sigma}^y(\boldsymbol{\kappa}_{\text{in}}), \quad (4.21)$$

using trigonometric identities. Considering, e.g., a rotation back and forth about the same angle  $\alpha = -\beta$  (i.e., for the same duration but with opposite sign) with the same joint laser wave vector  $\boldsymbol{\kappa}_{\text{out}} = \boldsymbol{\kappa}_{\text{in}}$ , we reasonably reproduce the initial situation  $\hat{\Sigma}_{\alpha,-\alpha}^z = \hat{\Sigma}^z$ . Note that the phase-matched case  $\boldsymbol{\kappa}_{\text{out}} = \boldsymbol{\kappa}_{\text{in}}$  directly corresponds to the superradiant case in the single-photon approach. In the latter, the spatial phase coherence leads to the directed spontaneous, superradiant emission. Here, the spatial phase coherence assures complete de-excitation in the case of  $\boldsymbol{\kappa}_{\text{out}} = \boldsymbol{\kappa}_{\text{in}}$  – or, in the quasispin picture, rotation back to the exact initial state of the quasispin  $Z$  operator,  $\hat{\Sigma}^z$ .

Let us now narrow down the analysis of the time-evolved  $\hat{\Sigma}_{\alpha,\beta}^z$  quasispin operator in (4.20) to the expectation values taken in the initial state  $\hat{\rho}_{\text{in}}$  or  $|\Psi_{\text{in}}\rangle$  of the optical lattice, as introduced in section 2.1.1. Then, as both involved quasispin  $Y$  operators (1.65) and (4.16) always create or annihilate excited-state atoms (which are not present in the initial state), the expectation values of all quasispin  $Y$  terms vanish, i.e.,

$$\begin{aligned} \langle \hat{\Sigma}_{\alpha,\beta}^z \rangle_{\text{in}} &= \cos(\alpha) \cos(\beta) \langle \hat{\Sigma}^z \rangle_{\text{in}} - \sin(\alpha) \sin(\beta) \langle \hat{\Sigma}_D^z(\boldsymbol{\kappa}_{\text{out}}, \boldsymbol{\kappa}_{\text{in}}) \rangle_{\text{in}} \\ &= \cos(\alpha + \beta) \langle \hat{\Sigma}^z \rangle_{\text{in}} - \sin(\alpha) \sin(\beta) \left[ \langle \hat{\Sigma}_D^z(\boldsymbol{\kappa}_{\text{out}}, \boldsymbol{\kappa}_{\text{in}}) \rangle_{\text{in}} - \langle \hat{\Sigma}^z \rangle_{\text{in}} \right]. \end{aligned} \quad (4.22)$$

Furthermore, the expectation value of the usual quasispin  $Z$  operator is given by  $\langle \hat{\Sigma}^z \rangle_{\text{in}} = -N/2$  for the same reason, i.e., because all  $N$  atoms are in their internal ground state initially. Conversely, we obtain the expectation value for the number of atoms which are left in the excited state after the full (exciting and de-exciting) laser sequence directly by adding  $N/2$  to the expectation value (4.22):

$$\begin{aligned} \langle \hat{N}_{\text{total}}^{\text{ex}} \rangle_{\text{in}} &= \langle \hat{\Sigma}_{\alpha,\beta}^z \rangle_{\text{in}} + \frac{N}{2} \\ &= -\frac{N}{2} \left\{ \cos(\alpha + \beta) - \sin(\alpha) \sin(\beta) \left[ -\frac{2}{N} \langle \hat{\Sigma}_D^z(\boldsymbol{\kappa}_{\text{out}}, \boldsymbol{\kappa}_{\text{in}}) \rangle_{\text{in}} - 1 \right] - 1 \right\}. \end{aligned} \quad (4.23)$$

Considering excitation and de-excitation with the same joint laser wave vector  $\boldsymbol{\kappa}_{\text{out}} = \boldsymbol{\kappa}_{\text{in}}$ , the second term vanishes from (4.23). Thus, the remaining terms represent the coherent part of the de-excitation process, which is complete for  $\alpha = -\beta$ . On the other hand, the second term increases (if  $\alpha$  and  $\beta$  have a different sign, which we require for small rotation back and forth) the number of atoms still in the excited (metastable) state after the full sequence in the incoherent case of  $\boldsymbol{\kappa}_{\text{out}} \neq \boldsymbol{\kappa}_{\text{in}}$ .

As a side note, when we have full rotation upwards instead of small rotation, i.e.,  $\alpha = \pi$ , the second (incoherent) term also vanishes. In this special case, the quasispin  $Z$  vector is rotated all the way from  $-N/2$  (all atoms in the ground state) to  $+N/2$  (all atoms in the excited state). In both extreme cases there is no spatial phase coherence, as they are represented by basis states. Thus, the de-excitation wave vector  $\boldsymbol{\kappa}_{\text{out}}$  can be arbitrary in this case, as it does not need to match certain spatial phases.

Inserting specific initial states for the expectation value of the  $\hat{\Sigma}_D^z(\boldsymbol{\kappa}_{\text{out}}, \boldsymbol{\kappa}_{\text{in}})$  quasi-

spin operator (4.14), one finds

$$\begin{aligned} {}_{\text{Mo/Né}}^{J=0}\langle\Psi|\hat{\Sigma}_D^z(\boldsymbol{\kappa}_{\text{out}}, \boldsymbol{\kappa}_{\text{in}})|\Psi\rangle_{\text{Mo/Né}}^{J=0} &= -\frac{1}{2}\sum_{\mu}\cos[(\boldsymbol{\kappa}_{\text{in}}-\boldsymbol{\kappa}_{\text{out}})\cdot\mathbf{r}_{\mu}] \\ &= -\frac{N}{2}\delta_{\boldsymbol{\kappa}_{\text{in}}\boldsymbol{\kappa}_{\text{out}}}, \end{aligned} \quad (4.24)$$

for the Mott insulator state (1.33) and the Mott-Néel state (1.36), and

$${}_{\text{sf/me}}^{U=0}\langle\Psi|\hat{\Sigma}_D^z(\boldsymbol{\kappa}_{\text{out}}, \boldsymbol{\kappa}_{\text{in}})|\Psi\rangle_{\text{sf/me}}^{U=0} = -\frac{N}{2}\delta_{\boldsymbol{\kappa}_{\text{in}}\boldsymbol{\kappa}_{\text{out}}}, \quad (4.25)$$

for the superfluid ground state (1.34) and the metallic ground state (1.37) as well. Note that to obtain these results, the fact that  $\boldsymbol{\kappa}_{\text{in}}$  and  $\boldsymbol{\kappa}_{\text{out}}$  are both reciprocal lattice vectors was used. For the case that  $\boldsymbol{\kappa}_{\text{out}} \neq \boldsymbol{\kappa}_{\text{in}}$ , the expectation value in (4.23) thus becomes zero, and we find that the number of atoms still in the excited (metastable) state after the full laser sequence is given by

$$\left\langle\hat{N}_{\text{total}}^{\text{ex}}\right\rangle_{\text{in}} = -\frac{N}{2}\{\cos(\alpha)\cos(\beta)-1\}. \quad (4.26)$$

The conclusion for an incoherent de-excitation process,  $\boldsymbol{\kappa}_{\text{out}} \neq \boldsymbol{\kappa}_{\text{in}}$ , is therefore that it is impossible to have all atoms in the ground state again at the end (except for the trivial case that  $\alpha = \beta = \pi$ ). In the next section, where we also include the lattice dynamics between the excitation and de-excitation process, we will thus restrict ourselves to the case of coherent de-excitation,  $\boldsymbol{\kappa}_{\text{out}} = \boldsymbol{\kappa}_{\text{in}}$ .

## 4.4. De-excitation process after tunneling dynamics

### 4.4.1. Tunneling dynamics applied to the $\hat{\Sigma}_{\alpha}^z$ operator

After having discussed the concept of directed superradiant emission in the context of classical laser fields in the previous section, let us now calculate the complete time evolution of the suggested laser probing sequence, including the tunneling dynamics in the weak interactions regime ( $J \gg U$ ). The proposed probing sequence was described in section 4.1: after the first (exciting) laser period (section 4.2), the atoms in the optical lattice tunnel and interact according to the general lattice Hamiltonian (1.42). For weak interactions ( $U = 0$ ) this reduces to the tunneling term (1.59), diagonal in the momentum space  $\mathbf{k}$ -basis, which we have already employed in the single-photon approach in section 2.3. Now we want to apply the time evolution

stemming from the tunneling term (1.59) over the waiting time  $\Delta t$ ,

$$\hat{U}_j(\Delta t) = \exp \left\{ i \frac{J\Delta t}{Z} \sum_{\mathbf{k},s,\lambda} T_{\mathbf{k}} \hat{n}_{\mathbf{k},s}^\lambda \right\}, \quad (4.27)$$

after the first (exciting) laser period, i.e. to the (up)rotated quasispin  $Z$  operator as given in (4.8), i.e.,

$$\hat{\Sigma}_{\alpha,\Delta t}^z = \hat{U}_j^\dagger(\Delta t) \hat{U}_{\kappa_{\text{in}}}^\dagger(\alpha) \hat{\Sigma}^z \hat{U}_{\kappa_{\text{in}}}(\alpha) \hat{U}_j(\Delta t) = \hat{U}_j^\dagger(\Delta t) \hat{\Sigma}_\alpha^z \hat{U}_j(\Delta t). \quad (4.28)$$

Inserting the result after the excitation period (4.8), we find that the first term is unchanged by the tunneling dynamics, as the number operators in  $\hat{U}_j(\Delta t)$  and  $\hat{\Sigma}^z$  in (1.67) obviously commute:

$$\begin{aligned} \hat{\Sigma}_{\alpha,\Delta t}^z &= \cos(\alpha) \hat{U}_j^\dagger(\Delta t) \hat{\Sigma}^z \hat{U}_j(\Delta t) + \sin(\alpha) \hat{U}_j^\dagger(\Delta t) \hat{\Sigma}^y(\kappa_{\text{in}}) \hat{U}_j(\Delta t) \\ &= \cos(\alpha) \hat{\Sigma}^z + \sin(\alpha) \hat{\Sigma}_j^y(\kappa_{\text{in}}). \end{aligned} \quad (4.29)$$

For the second term, the tunneling-evolved quasispin  $Y$  operator  $\hat{\Sigma}_j^y(\kappa_{\text{in}})$  has been introduced. It can be easily shown that the usual  $\hat{\Sigma}^y(\kappa_{\text{in}})$  quasispin operator (1.65) picks up local, vector-dependent phase factors (2.26), analogous to the single-photon considerations (2.27) above, i.e.,

$$\begin{aligned} \hat{\Sigma}_j^y(\kappa_{\text{in}}) &:= \hat{U}_j^\dagger(\Delta t) \hat{\Sigma}^y(\kappa_{\text{in}}) \hat{U}_j(\Delta t) \\ &= \frac{1}{2i} \left( \sum_{\mathbf{p},s} \hat{a}_{\mathbf{p},s}^{\text{ex}\dagger} \hat{a}_{\mathbf{p}-\kappa_{\text{in}},s}^{\text{gr}} \exp \{ i\phi_{\mathbf{p}}^{\kappa_{\text{in}}}(\Delta t) \} - \text{H.c.} \right). \end{aligned} \quad (4.30)$$

Of course, the exponential phase factors are unity for  $J = 0$ , and the tunneling-evolved  $\hat{\Sigma}_j^y(\kappa_{\text{in}})$  quasispin operator then reduces to the usual  $\hat{\Sigma}^y(\kappa_{\text{in}})$  quasispin operator (1.65) again.

#### 4.4.2. De-excitation dynamics applied after tunneling

As the third step after the first (exciting) laser period (section 4.2) and the subsequent waiting time  $\Delta t$  featuring the tunneling dynamics (section 4.4.1), we want to apply the time evolution of the second (de-exciting) laser period, which allows the atoms to decay back to the ground state. In contrast to section 4.3, we will restrict ourselves to the coherent case of the same joint laser wave vectors  $\kappa_{\text{out}} = \kappa_{\text{in}}$  for the first (exciting,  $\kappa_{\text{in}}$ ) and second (de-exciting,  $\kappa_{\text{out}}$ ) laser period. The com-

pletely time-evolved quasispin  $Z$  operator after the full suggested probing sequence (see section 4.1) then reads

$$\begin{aligned}\hat{\Sigma}_{\alpha,\Delta t,\beta}^z &= \hat{U}_{\kappa_{\text{in}}}^\dagger(\beta) \hat{U}_J^\dagger(\Delta t) \hat{U}_{\kappa_{\text{in}}}^\dagger(\alpha) \hat{\Sigma}_{\kappa_{\text{in}}}^z \hat{U}_{\kappa_{\text{in}}}(\alpha) \hat{U}_J(\Delta t) \hat{U}_{\kappa_{\text{in}}}(\beta) \\ &= \hat{U}_{\kappa_{\text{in}}}^\dagger(\beta) \hat{\Sigma}_{\alpha,\Delta t}^z \hat{U}_{\kappa_{\text{in}}}(\beta).\end{aligned}\quad (4.31)$$

Inserting the result (4.29) after the excitation period and subsequent tunneling from the previous section 4.4.1, we obtain

$$\hat{\Sigma}_{\alpha,\Delta t,\beta}^z = \cos(\alpha) \hat{U}_{\kappa_{\text{in}}}^\dagger(\beta) \hat{\Sigma}_{\kappa_{\text{in}}}^z \hat{U}_{\kappa_{\text{in}}}(\beta) + \sin(\alpha) \hat{U}_{\kappa_{\text{in}}}^\dagger(\beta) \hat{\Sigma}_J^y(\kappa_{\text{in}}) \hat{U}_{\kappa_{\text{in}}}(\beta). \quad (4.32)$$

Fortunately, the first term (4.11) has already been calculated for the case without lattice dynamics in section 4.3.1. Regarding the second term in (4.32), we have to assess an expression resembling (4.12),

$$\begin{aligned}\hat{U}_{\kappa_{\text{in}}}^\dagger(\beta) \hat{\Sigma}_J^y(\kappa_{\text{in}}) \hat{U}_{\kappa_{\text{in}}}(\beta) &= \exp\{i\beta \hat{\Sigma}^x(\kappa_{\text{in}})\} \hat{\Sigma}_J^y(\kappa_{\text{in}}) \exp\{-i\beta \hat{\Sigma}^x(\kappa_{\text{in}})\} \\ &= \sum_{m=0}^{\infty} \frac{1}{m!} [i\beta \hat{\Sigma}^x(\kappa_{\text{in}}), \hat{\Sigma}_J^y(\kappa_{\text{in}})]_m,\end{aligned}\quad (4.33)$$

i.e., the  $m$ -th commutator between  $\hat{\Sigma}^x(\kappa_{\text{in}})$  and  $\hat{\Sigma}_J^y(\kappa_{\text{in}})$ . As in the previous section 4.3.1, a recurrence appears, such that we only have to calculate three commutators explicitly. Details on the calculation are given in Appendix A.6. The results for the three relevant commutators read:

$$[\hat{\Sigma}^x(\kappa_{\text{in}}), \hat{\Sigma}_J^y(\kappa_{\text{in}})] = i\hat{\Sigma}_C^z(\kappa_{\text{in}}), \quad (4.34)$$

$$[\hat{\Sigma}^x(\kappa_{\text{in}}), \hat{\Sigma}_C^z(\kappa_{\text{in}})] = -i\hat{\Sigma}_C^y(\kappa_{\text{in}}), \quad (4.35)$$

$$[\hat{\Sigma}^x(\kappa_{\text{in}}), \hat{\Sigma}_C^y(\kappa_{\text{in}})] = i\hat{\Sigma}_C^z(\kappa_{\text{in}}), \quad (4.36)$$

where the newly introduced  $\hat{\Sigma}_C^{y/z}(\kappa_{\text{in}})$  quasispin operators carry a cosine factor, unlike the usual quasispin  $Y/Z$  operators (1.65,1.67), i.e.,

$$\hat{\Sigma}_C^z(\kappa_{\text{in}}) := \frac{1}{2} \sum_{\mathbf{p},s} (\hat{n}_{\mathbf{p},s}^{\text{ex}} - \hat{n}_{\mathbf{p}-\kappa_{\text{in}},s}^{\text{gr}}) \cos\{\phi_{\mathbf{p}}^{\kappa_{\text{in}}}(\Delta t)\}, \quad (4.37)$$

$$\hat{\Sigma}_C^y(\kappa_{\text{in}}) := \frac{1}{2i} \sum_{\mathbf{p},s} (\hat{a}_{\mathbf{p},s}^{\text{ex}\dagger} \hat{a}_{\mathbf{p}-\kappa_{\text{in}},s}^{\text{gr}} - \text{H.c.}) \cos\{\phi_{\mathbf{p}}^{\kappa_{\text{in}}}(\Delta t)\}. \quad (4.38)$$

Conversely, the  $\hat{\Sigma}_C^{y/z}(\boldsymbol{\kappa}_{\text{in}})$  quasispin operators clearly reduce to the usual  $\hat{\Sigma}^{y/z}(\boldsymbol{\kappa}_{\text{in}})$  quasispin operators (1.65,1.67) again for  $J = 0$  (for the  $\hat{\Sigma}_C^z(\boldsymbol{\kappa}_{\text{in}})$  operator, an index shift has to be applied to the second term). Ultimately, the result of the  $m$ -th commutator in (4.33) is known for all  $m \geq 1$ :

$$[\hat{\Sigma}^x(\boldsymbol{\kappa}_{\text{in}}), \hat{\Sigma}_J^y(\boldsymbol{\kappa}_{\text{in}})]_m = \begin{cases} \hat{\Sigma}_C^y(\boldsymbol{\kappa}_{\text{in}}), & \text{if } m \text{ is even,} \\ i\hat{\Sigma}_C^z(\boldsymbol{\kappa}_{\text{in}}), & \text{if } m \text{ is odd.} \end{cases} \quad (4.39)$$

Analogous to (4.19), we can then split the infinite series in (4.33) into a sine series and a cosine series, with additional attention to the  $m = 0$ -term, i.e.,

$$\hat{U}_{\boldsymbol{\kappa}_{\text{in}}}^\dagger(\beta) \hat{\Sigma}_J^y(\boldsymbol{\kappa}_{\text{in}}) \hat{U}_{\boldsymbol{\kappa}_{\text{in}}}(\beta) = \hat{\Sigma}_J^y(\boldsymbol{\kappa}_{\text{in}}) + \hat{\Sigma}_C^y(\boldsymbol{\kappa}_{\text{in}}) [\cos(\beta) - 1] - \hat{\Sigma}_C^z(\boldsymbol{\kappa}_{\text{in}}) \sin(\beta). \quad (4.40)$$

Combining the first term (4.11) and the second term (4.40), we can finally state the result for the quasispin  $Z$  operator (4.32) after the full probing sequence,

$$\begin{aligned} \hat{\Sigma}_{\alpha, \Delta t, \beta}^z &= \cos(\alpha) \cos(\beta) \hat{\Sigma}^z - \sin(\alpha) \sin(\beta) \hat{\Sigma}_C^z(\boldsymbol{\kappa}_{\text{in}}) + \sin(\alpha) \hat{\Sigma}_J^y(\boldsymbol{\kappa}_{\text{in}}) \\ &\quad + \cos(\alpha) \sin(\beta) \hat{\Sigma}_J^y(\boldsymbol{\kappa}_{\text{in}}) + \sin(\alpha) [\cos(\beta) - 1] \hat{\Sigma}_C^y(\boldsymbol{\kappa}_{\text{in}}). \end{aligned} \quad (4.41)$$

Again, we will discuss this result in detail in the upcoming section.

### 4.4.3. Interpretation and expectation values

For the trivial case without tunneling, i.e.,  $J = 0$ , all operators reduce to the usual quasispin  $Y/Z$  operators and the result (4.41) simplifies to

$$\hat{\Sigma}_{\alpha, \Delta t, \beta}^z = \cos(\alpha + \beta) \hat{\Sigma}^z + \sin(\alpha + \beta) \hat{\Sigma}^y(\boldsymbol{\kappa}_{\text{in}}), \quad (4.42)$$

which has already been discussed in section 4.3.2. Analogously to this previous section, we discuss the general ( $J \neq 0$ ) case by considering the expectation values of (4.41) taken in possible initial states  $\hat{\rho}_{\text{in}}$  or  $|\Psi_{\text{in}}\rangle$  of the optical lattice. As the expectation values of the various quasispin  $Y$  terms then vanish and the expectation



value of the quasispin  $Z$  operator is given<sup>1</sup> by  $\langle \hat{\Sigma}^z \rangle_{\text{in}} = -N_\Psi/2$ , we obtain

$$\begin{aligned} \langle \hat{N}_{\text{total}}^{\text{ex}} \rangle_{\text{in}} &= \langle \hat{\Sigma}_{\alpha, \Delta t, \beta}^z \rangle_{\text{in}} + \frac{N_\Psi}{2} \\ &= -\frac{N_\Psi}{2} \left\{ \cos(\alpha + \beta) - \sin(\alpha) \sin(\beta) \left[ -\frac{2}{N_\Psi} \langle \hat{\Sigma}_C^z(\boldsymbol{\kappa}_{\text{in}}) \rangle_{\text{in}} - 1 \right] - 1 \right\}, \end{aligned} \quad (4.43)$$

as the expectation value for the number of atoms which are left in the excited (metastable) state after the full laser sequence, analogous to (4.23). In the case of zero tunneling, the second term vanishes – this corresponds to a situation where quasispin rotation  $\alpha$  about the  $x$ -axis (4.8) would be perfectly reversed via back rotation  $\beta = -\alpha$ , finally resulting in zero excited-state atoms. Conversely, nonzero tunneling causes the expectation value of the  $\hat{\Sigma}_C^z(\boldsymbol{\kappa}_{\text{in}})$  quasispin operator (4.37) to assume values greater than  $-N_\Psi/2$ , leading to a finite probability of atoms still in the excited (metastable) state after the full laser sequence. The remaining task is to calculate this expectation value for specific initial states, i.e.,

$$\langle \hat{\Sigma}_C^z(\boldsymbol{\kappa}_{\text{in}}) \rangle_{\text{in}} = -\frac{1}{2} \sum_{\mathbf{p}, s} \langle \hat{n}_{\mathbf{p}-\boldsymbol{\kappa}_{\text{in}}, s}^{\text{gr}} \rangle_{\text{in}} \cos \{ \phi_{\mathbf{p}}^{\boldsymbol{\kappa}_{\text{in}}}(\Delta t) \}. \quad (4.44)$$

Of course, we can identify  $n_s(\mathbf{p} - \boldsymbol{\kappa}_{\text{in}}) = \langle \hat{n}_{\mathbf{p}-\boldsymbol{\kappa}_{\text{in}}, s}^{\text{gr}} \rangle_{\text{in}}$  with the same number distribution functions  $n_s(\mathbf{k})$  as introduced for specific initial lattice states in section 2.3.

### Short laser pulses: perturbation theory

To compare the (classical) laser probing scheme with the single-photon probing scheme in section 2.3, let us investigate very short laser pulses  $\alpha \ll 1$  and  $\beta = -\alpha$ . We can then use second-order perturbation theory in the quasispin-rotation angles  $\alpha$  and  $\beta$ . For example, using (4.8) we conclude that the average number of excited-state (metastable-state) atoms immediately after the first laser sequence is given by

$$\bar{n} = \langle \hat{\Sigma}_\alpha^z \rangle_{\text{in}} + \frac{N_\Psi}{2} = \cos(\alpha) \langle \hat{\Sigma}^z \rangle_{\text{in}} + \frac{N_\Psi}{2} \approx \alpha^2 N_\Psi / 4. \quad (4.45)$$

We envisage that  $\bar{n}$  is about unity (or even smaller), i.e., the length of the (short) laser pulses  $\alpha$  and  $\beta$  should be chosen accordingly. Note that when  $\bar{n}$  is smaller than unity, one can think of the resulting coherent state as a coherent superposition

<sup>1</sup>In section 4.3.2 we only considered initial states where the number of atoms matches the number of lattice sites  $N$ . Here, we are more generally considering states with  $N_\Psi$  atoms, i.e., with a filling factor of  $N_\Psi/N$  possibly greater than one.

of the ground state  $|\sigma = 0\rangle$  and the first excited Dicke state  $|\sigma = 1\rangle$ , as introduced in section 1.2.2. The number of atoms remaining in the excited (metastable) state after the full laser sequence (4.43), in the case of short laser pulses, is then given by

$$\left\langle \hat{N}_{\text{total}}^{\text{ex}} \right\rangle_{\text{in}} = \left\langle \hat{\Sigma}_{\alpha, \Delta t, \beta}^z \right\rangle_{\text{in}} + \frac{N_{\Psi}}{2} = 2\bar{n} \left[ \frac{2}{N_{\Psi}} \left\langle \hat{\Sigma}_C^z(\boldsymbol{\kappa}_{\text{in}}) \right\rangle_{\text{in}} + 1 \right]. \quad (4.46)$$

In analogy to section 2.3.1 and section 2.3.2, we will now examine the situation for exemplary initial states of the atoms in the optical lattice in the weak interactions regime ( $J \gg U$ ):

**Superfluid ground state** For the bosonic superfluid ground state (1.34) with  $N_{\Psi} = N$  and the number distribution function  $n^{\text{sf}}(\mathbf{k}) = N\delta_{\mathbf{k}\mathbf{0}}$ , the expectation value (4.44) reads

$${}_{\text{sf}}^{U=0} \langle \Psi | \hat{\Sigma}_C^z(\boldsymbol{\kappa}_{\text{in}}) | \Psi \rangle_{\text{sf}}^{U=0} = -\frac{N}{2} \cos \{ \phi_{\boldsymbol{\kappa}_{\text{in}}}^{\boldsymbol{\kappa}_{\text{in}}}(\Delta t) \} = -\frac{N}{2} \cos \{ \varphi(\Delta t) \}. \quad (4.47)$$

Interestingly, the expectation value oscillates with the exact same phase that we have already encountered in the single-photon approach (2.55). This oscillation is a consequence of the fact that the coherent state, which is created by the classical laser fields, is not an exact eigenstate of the system, but rather a coherent superposition of excited states with different energies. In the quasispin picture, the oscillation can thus be interpreted as a Larmor precession of the quasispin vector about the  $z$ -axis during the waiting time  $\Delta t$ . Obviously, the spatial phase coherence is not (permanently) impaired due to the tunneling in the case of the superfluid ground state (4.47), as the final number of excited-state atoms (4.46) repeatedly reverts to zero, even for arbitrarily long waiting times  $\Delta t$ .

**Partial condensation state** Proceeding with the partial condensation state (2.50), in which  $N_1$  atoms are condensed in the  $\mathbf{k} = \mathbf{0}$  mode, while  $N_2$  other atoms are equally distributed over all  $\mathbf{k}$ -modes,

$$n^{\text{dt}}(\mathbf{k}) = N_1 \delta_{\mathbf{k}\mathbf{0}} + \frac{N_2}{N}, \quad N_{\Psi} = \sum_{\mathbf{k}} n^{\text{dt}}(\mathbf{k}) = N_1 + N_2, \quad (4.48)$$

we can calculate the expectation value (4.44) to

$$\begin{aligned}
 \langle \hat{\Sigma}_C^z(\boldsymbol{\kappa}_{\text{in}}) \rangle_{\text{dt}}^{U=0} &= -\frac{1}{2} \sum_{\mathbf{p}} n^{\text{dt}}(\mathbf{p} - \boldsymbol{\kappa}_{\text{in}}) \cos \{ \phi_{\mathbf{p}}^{\boldsymbol{\kappa}_{\text{in}}}(\Delta t) \} \\
 &= -\frac{N_1}{2} \cos \{ \phi_{\boldsymbol{\kappa}_{\text{in}}}(\Delta t) \} - \frac{1}{2} \frac{N_2}{N} \sum_{\mathbf{p}} \cos \{ \phi_{\mathbf{p}}^{\boldsymbol{\kappa}_{\text{in}}}(\Delta t) \} \\
 &= -\frac{N_1}{2} \cos \{ \varphi(\Delta t) \} - \frac{N_2}{2} \mathcal{J}_{\boldsymbol{\kappa}_{\text{in}}}(\Delta t), \tag{4.49}
 \end{aligned}$$

where, in addition to the oscillating term, the sum over cosine was identified as the same phase sum (2.54) as in the single-photon approach (2.58). For details on the phase sum and its real and imaginary part, see Appendix A.7. The number of atoms remaining in the excited state after the full sequence (4.46) is thus given by

$$\langle \hat{N}_{\text{total}}^{\text{ex}} \rangle_{\text{in}} = 2\bar{n} \left[ 1 - \frac{N_1}{N_{\Psi}} \cos \{ \varphi(\Delta t) \} - \frac{N_2}{N_{\Psi}} \mathcal{J}_{\boldsymbol{\kappa}_{\text{in}}}(\Delta t) \right], \tag{4.50}$$

for the partial condensation state as the initial state. Due to the second term involving the phase sum (2.54), the final number of excited-state atoms (4.50) increases over the waiting time  $\Delta t$ , and does not revert to zero, as opposed to the superfluid ground state. Measuring (4.50) as a function of the waiting time  $\Delta t$ , we can thus infer the number  $N_1$  of condensed atoms. Physically, the term  $N_2 \mathcal{J}_{\boldsymbol{\kappa}_{\text{in}}}(\Delta t)$  corresponds to the deterioration of the spatial phase coherence caused by the tunneling of the atoms, similar to the single-photon approach in section 2.3.1.

**Metallic ground state** Let us now consider the expectation value (4.44) in the fermionic metallic ground state (1.37), i.e.,

$$n_s^{\text{me}}(\mathbf{k}) = \begin{cases} 1, & \text{if } |k_x| + |k_y| < \pi/\ell, \\ 0, & \text{otherwise.} \end{cases} \tag{4.51}$$

After a shift  $\tilde{\mathbf{p}} = \mathbf{p} - \boldsymbol{\kappa}_{\text{in}}$ , and according to the definition in (4.51), the summation runs over all reciprocal lattice vectors  $\tilde{\mathbf{p}}$  in diamond area  $\mathcal{D}$  – see section 2.3.2. Thus,

we may write

$$\begin{aligned} \langle \Psi | \hat{\Sigma}_C^z(\boldsymbol{\kappa}_{\text{in}}) | \Psi \rangle_{\text{me}}^{U=0} &= -\frac{1}{2} \sum_{\boldsymbol{p}, s} n_s^{\text{me}}(\boldsymbol{p} - \boldsymbol{\kappa}_{\text{in}}) \cos \{ \phi_{\boldsymbol{p}}^{\boldsymbol{\kappa}_{\text{in}}}(\Delta t) \} \\ &= -\sum_{\tilde{\boldsymbol{p}} \in \mathcal{D}} \cos \{ \phi_{\tilde{\boldsymbol{p}} + \boldsymbol{\kappa}_{\text{in}}}^{\boldsymbol{\kappa}_{\text{in}}}(\Delta t) \}. \end{aligned} \quad (4.52)$$

We can then split the sum into two equal parts and apply another index shift  $\tilde{\boldsymbol{q}} = \tilde{\boldsymbol{p}} + \Delta \boldsymbol{k}$  with  $\Delta \boldsymbol{k} = \pi/\ell \cdot \{1, 1\}$  to the second part. Considering the  $2\pi$ -periodicity of the summand in  $\tilde{p}_{x/y}\ell$ , the resulting shifted summation runs over all reciprocal lattice vectors  $\tilde{\boldsymbol{q}}$  in the corners  $\mathcal{C}$  of the first Brillouin zone (see Figure 2.3 above),

$$\sum_{\tilde{\boldsymbol{p}} \in \mathcal{D}} \cos \{ \phi_{\tilde{\boldsymbol{p}} + \boldsymbol{\kappa}_{\text{in}}}^{\boldsymbol{\kappa}_{\text{in}}}(\Delta t) \} = \frac{1}{2} \sum_{\tilde{\boldsymbol{p}} \in \mathcal{D}} \cos \{ \phi_{\tilde{\boldsymbol{p}} + \boldsymbol{\kappa}_{\text{in}}}^{\boldsymbol{\kappa}_{\text{in}}}(\Delta t) \} + \frac{1}{2} \sum_{\tilde{\boldsymbol{q}} \in \mathcal{C}} \cos \{ \phi_{\tilde{\boldsymbol{q}} + \boldsymbol{\kappa}_{\text{in}} - \Delta \boldsymbol{k}}^{\boldsymbol{\kappa}_{\text{in}}}(\Delta t) \}. \quad (4.53)$$

Note that the Fourier transform of the adjacency matrix (1.58) changes its sign when shifted by  $\Delta \boldsymbol{k}$ , i.e.,  $T_{\boldsymbol{p} \pm \Delta \boldsymbol{k}} = -T_{\boldsymbol{p}}$ . Hence, the spatial phase (2.26) also changes sign, i.e.,  $\phi_{\boldsymbol{p} \pm \Delta \boldsymbol{k}}^{\boldsymbol{k}}(t) = -\phi_{\boldsymbol{p}}^{\boldsymbol{k}}(t)$ , which does not matter as it appears in a cosine. In conclusion, we can merge the two summations into one sum over the whole first Brillouin zone, which (after reversing the shift  $\tilde{\boldsymbol{p}} = \boldsymbol{p} - \boldsymbol{\kappa}_{\text{in}}$ ) can be expressed via the phase sum (2.54), that is,

$$\sum_{\tilde{\boldsymbol{p}} \in \mathcal{D}} \cos \{ \phi_{\tilde{\boldsymbol{p}} + \boldsymbol{\kappa}_{\text{in}}}^{\boldsymbol{\kappa}_{\text{in}}}(\Delta t) \} = \frac{1}{2} \sum_{\tilde{\boldsymbol{p}}} \cos \{ \phi_{\tilde{\boldsymbol{p}} + \boldsymbol{\kappa}_{\text{in}}}^{\boldsymbol{\kappa}_{\text{in}}}(\Delta t) \} = \frac{N}{2} \mathcal{J}_{\boldsymbol{\kappa}_{\text{in}}}(\Delta t). \quad (4.54)$$

Thus, the expectation value (4.44) in the metallic ground state (1.37) is given by

$$\langle \Psi | \hat{\Sigma}_C^z(\boldsymbol{\kappa}_{\text{in}}) | \Psi \rangle_{\text{me}}^{U=0} = -\frac{N}{2} \mathcal{J}_{\boldsymbol{\kappa}_{\text{in}}}(\Delta t), \quad (4.55)$$

which is the same result as for the partial condensation state (4.49) when  $N_1 = 0$  and  $N_2 = N = N_{\Psi}$ , i.e.,

$$\langle \hat{N}_{\text{total}}^{\text{ex}} \rangle_{\text{in}} = 2\bar{n} [1 - \mathcal{J}_{\boldsymbol{\kappa}_{\text{in}}}(\Delta t)]. \quad (4.56)$$

In the following, we are going to compare the results obtained here for the probing scheme employing classical laser fields with the results of the single-photon probing scheme detailed in section 2.3.

## 4.5. Summary of the detection via classical laser fields

In the single-photon probing scheme (chapter 2), a deterioration in the spatial phase coherence was generally detected via a reduction in the superradiant emission probability, for example in (2.58). Regarding the probing scheme employing classical laser fields, the same deterioration in spatial phase coherence manifests itself in a finite number of excited-state (metastable-state) atoms remaining after the full laser probing sequence. Furthermore, the similarity of the two approaches is underlined by the fact that the exact same expressions  $\varphi(\Delta t)$  and  $\mathcal{J}_{\kappa_{\text{in}}}(\Delta t)$  emerge in (4.50), although the derivations have not much in common (quantum-mechanical, time-dependent, first-order perturbation theory vs. full evolution in the Heisenberg picture for classical laser fields).

One main result of the single-photon probing scheme for bosonic optical lattices was the possibility of distinguishing (partially) excited states from condensed states via the modified superradiant emission characteristics (section 2.4). Evidently, the same is possible using the laser probing scheme by counting the final number of excited-state (metastable-state) atoms as a function of the waiting time  $\Delta t$ . The ongoing increase in this number in a partially excited state (4.50) should be easily distinguishable from the oscillation in a condensed state (4.47).

Considering the laser probing sequence for a fermionic optical lattice, we found that the final number of excited-state atoms increases over the waiting time  $\Delta t$  in the metallic ground state (4.56). In the Mott-Néel state in the separable state regime, on the other hand, this would not be the case, as there is no tunneling involved which could scramble the spatial phases. Thus, analogously to the single-photon probing scheme, it is possible to detect the current parameter regime of a fermionic optical lattice using the proposed laser probing sequence.

Regarding the detection of quantum phase transitions (chapter 3), it is not possible to explicitly calculate the de-excitation dynamics of the laser probing sequence, because we worked in the Heisenberg picture and did not specifically indicate the coherent excited state, nor how it could adiabatically evolve. However, note that the Mott insulator state would be analogously recognized as a state where all momenta are equally populated by the “new” ( $U = 0$ ) Hamiltonian after a sudden switch to the weak interactions regime (cf. section 3.3). Hence, we would expect the final number of excited-state (metastable-state) atoms to increase according to (4.50) with  $N_1 = 0$  and  $N_2 = N = N_{\Psi}$  over the waiting time  $\Delta t$ . This indicates that it should also be possible to differentiate between an adiabatic transition and a sudden transition via

the laser probing sequence, as in the single-photon approach (section 3.5).

In conclusion, we have shown that the probing scheme employing classical laser fields preserves the important features of the single-photon probing scheme. In addition, it may facilitate experimental realization, as discussed in section 4.1 and in the upcoming chapter 5.

## 5. Experimental realization

In the preceding chapters we have developed the theoretical framework for a non-destructive probing scheme for optical lattices, relying either on single-photon superradiance (chapter 2, 3) or on superradiance in the context of classical laser fields (chapter 4). Following this theoretical study, we want to make concrete suggestions for experimental implementation. Therefore, we are going to discuss example values for the important quantities and possible atomic level schemes.

We have already argued in section 1.2.3 that the probe-photon (or laser-field) wavelength  $\lambda_{\text{probe}}$  needs to be large in comparison to the lattice spacing  $\ell$  so that the time scale of coherent superradiant emission  $\tau_{\text{sp}}$  is much smaller than the time scale of incoherent spontaneous emission  $\tau_{\text{single}}$ , i.e.,  $\tau_{\text{sp}} \ll \tau_{\text{single}}$ . Considering again the *qualitative* superradiance condition from reference [3],

$$\frac{\tau_{\text{sp}}}{\tau_{\text{single}}} = \left( 8\pi \frac{\ell}{\lambda_{\text{probe}}} \right)^2 \ll 1, \quad (5.1)$$

we suggest a probe-photon (or laser-field) wavelength of  $\lambda_{\text{probe}} = 2\pi/|\kappa_{\text{in}}| = 10.6 \mu\text{m}$ , i.e., infrared light as, for example, produced by CO<sub>2</sub> lasers [91]. The lattice spacing  $\ell$  of the optical lattice is determined by the wavelength of the counter-propagating laser beams which create the lattice potential (section 1.3.1). Considering a lattice created by green (e.g., argon-ion [92]) lasers with  $\lambda_{\text{lat}} = 514 \text{ nm}$ , we obtain a comparatively small lattice spacing of  $\ell = \lambda_{\text{lat}}/2 = 257 \text{ nm}$  [11, 12, 93]. Together, this leads to a ratio of  $\tau_{\text{sp}}/\tau_{\text{single}} = 0.37$ , which assures that collective, coherent emission (i.e., Dicke superradiance) is indeed the dominant decay channel. Note that condition (5.1) only provides a conservative estimate (see section 1.2.3 and the paragraph below), i.e., the suggested parameters involve a sizeable margin of safety. Furthermore, considering  $L = 100$  lattice sites per dimension, for example, the lattice has a side length of  $L\ell = 25.7 \mu\text{m}$ , which is large compared to the radiation wavelength  $\lambda_{\text{probe}} = 10.6 \mu\text{m}$ . This ensures that we are in the “large system” limit of Dicke superradiance [65, 66], where the local spatial phases are not negligible (see footnote 2 on page 24). In addition, we can readily calculate that the recoil energy  $E_R^{\text{probe}}$  of the infrared probe photon is a factor  $E_R^{\text{lat}}/E_R^{\text{probe}} = 4 \cdot 10^2$  smaller than the recoil energy  $E_R^{\text{lat}}$  associated with an optical lattice photon, demonstrating that the requirement of negligible atomic recoil is also fulfilled (see section 1.2.3).

If these proposed parameters, which require atoms (or molecules) that provide a far-infrared transition while allowing to be trapped in a green lattice, pose too hard a challenge experimentally, recent results [76,77] suggest that they can be somewhat mitigated. Following these studies, cooperative effects such as Dicke superradiance already dominate for lattice spacings  $\ell$  which are of the same order (e.g., slightly smaller) than the probe-photon wavelength  $\lambda_{\text{probe}}$ . Therefore, larger optical lattice wavelengths in the range of  $\lambda_{\text{lat}} = 500 - 1000$  nm, as commonly realized [25, 32, 34, 94–96], or smaller probe-photon wavelengths, e.g., ranging from the near-infrared to the far-infrared,  $\lambda_{\text{probe}} = 1 - 10$   $\mu\text{m}$ , should also be feasible. This latitude in the two most important experimental parameters should facilitate the search for an atom (or molecule) with a corresponding level scheme, which supports both the transition wavelength  $\lambda_{\text{probe}}$  (although we discuss other options below) and an optical lattice wavelength  $\lambda_{\text{lat}}$ .

Regarding the number of atoms and lattice sites in the optical lattice, we envisage this to be in the range of  $N = 10^2 - 10^4$ , which is routinely realized in two-dimensional optical lattice experiments [27, 35, 40, 42, 43]. Note that the utilized effect of single-photon superradiance becomes more pronounced with increasing atom number in the optical lattice (see, e.g., 2.25). Therefore, a higher number of atoms leads in principle to the improved efficiency of the proposed probe. However, keep in mind that we have assumed equal coupling of all atoms to the photon field (1.45), which becomes more difficult to achieve for a larger number of atoms.

In the four paragraphs and in Figure 5.1 below we further suggest possible level schemes and techniques for experimental realization:

**Direct implementation using two-level atoms** To enable the probing sequence depicted in Figure 1.3 we first require atoms which feature an infrared transition via their level scheme, such that they are able to resonantly absorb and re-emit the infrared probe photon. Secondly, the proposed probing scheme presumes that significant tunneling takes place in the waiting time  $\Delta t$  between the absorption and re-emission of the probe photon. Thus, it is crucial that the lifetime of the infrared transition is large compared to the typical tunneling time of, e.g.,  $\tau_{\text{tunnel}} = \hbar/J = 5 \cdot 10^{-5}$  s. Thirdly, the atoms should be trapped in an optical lattice with preferably small spacing (e.g., a green lattice), which poses an additional requirement for their level scheme. Regarding the atomic species which are popular in optical lattice experiments, such as Rb, Na and Li, these requirements are probably hard to fulfill at the same time. However, other appropriate elements may be found.



If it proves challenging to find atomic species which feature a long-lived infrared transition while being able to be trapped in an optical lattice, molecules [95, 96] may provide an interesting alternative. It has recently been shown that optical lattices trapping, e.g.,  $\text{Rb}_2$  [95] or potassium-rubidium (KRb) molecules [96] can be created using magnetoassociation. These molecules may provide different (e.g., microwave) transitions with longer lifetimes. In summary, direct implementation may be possible employing two-level atoms or molecules in an optical lattice which offer the required infrared transition.

**Laser-assisted multiphoton transition** Instead of being reliant on the transition lifetimes which certain atoms or molecules may (or may not) provide in single-photon transitions, we can turn the tables by employing a laser-assisted multiphoton transition between the ground state and a metastable state of the atoms. The basic idea here is to provide additional laser fields during absorption and re-emission, which *only then* enable the required infrared transition. During the first step of the probing sequence (depicted in Figure 1.3), the assisting lasers should be switched on, such that the infrared probe photon can be collectively absorbed by the atoms in the optical lattice. Then, however, the assisting lasers are switched off during the waiting time  $\Delta t$  in the second step. As the individual atoms are either in the ground state or in the metastable state after absorption, the light-matter coupling (1.45) now is essentially (barring other, nondominant decay channels) disabled. After a waiting time  $\Delta t$  – which in this scenario can be chosen freely by the experimentalist – the lasers are switched on for a second time to allow the atoms to decay back to their ground state via collective re-emission of the infrared probe photon.

In this way, comparably long waiting times of, e.g.,  $\Delta t = \mathcal{O}(10^2) \cdot \tau_{\text{tunnel}}$  are viable, allowing to probe quantum states or phase transitions with high efficiency<sup>1</sup>. As an example, we can think of a detuned four-photon transition, as illustrated in Figure 5.1(a). Here, the absorption or re-emission of the probe photon  $\gamma_{\text{IR}}$  is only possible when three assisting fields  $\gamma_1$ ,  $\gamma_2$ , and  $\gamma_4$  are present, i.e., if the corresponding assisting external lasers are switched on. However, apart from supporting a multiphoton transition from the ground state to a metastable state, the atomic level

---

<sup>1</sup>As shown in Figure 2.1 and, e.g., (2.66), the superradiant emission probability decreases with increasing waiting time  $\Delta t$  for certain lattice states or after a sudden Mott-to-superfluid transition. In other cases (e.g., the Mott insulator state or an adiabatic Mott-to-superfluid transition), the superradiant emission probability remains constant during the waiting time  $\Delta t$ . Evidently, the two cases can be distinguished all the better, the greater the difference in the emission probability is, i.e., the longer the waiting time  $\Delta t$  was.

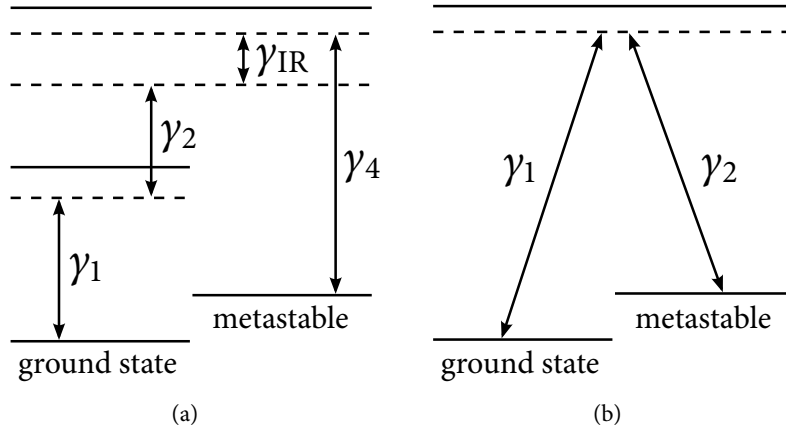


FIGURE 5.1. – Examples of two level schemes suggested for experimental realization. (a) A laser-assisted multiphoton transition, where the infrared probe photon  $\gamma_{\text{IR}}$  can only be absorbed or re-emitted when the assisting external laser fields  $\gamma_1$ ,  $\gamma_2$ , and  $\gamma_4$  are present. (b) A detuned two-photon transition. An incident (single) photon  $\gamma_1$  can excite the metastable state via spontaneous Raman scattering of a Stokes photon  $\gamma_2$ . The emission process would then be initiated by a  $\pi$ -pulse on demand. Alternatively, we can employ two counter-propagating, classical laser fields  $\gamma_1$  and  $\gamma_2$  for the excitation and de-excitation process.

scheme can be arbitrary in this scenario. The assisting lasers (not necessarily four) should then be chosen in accordance with the specific level scheme. Note that a comparable pump-and-probe detection scheme with variable storage (waiting) time  $\Delta t$  was proposed recently [61].

**Two-photon double-Raman process** Another possibility is to employ a spontaneous Raman process for the collective excitation from the ground state to a metastable state, and a subsequent  $\pi$ -pulse to initiate the de-excitation back to the ground state [67, 68]. More specifically, consider an incoming probe photon  $\gamma_1$  with wave vector  $\mathbf{k}_1$  in the level scheme depicted in Figure 5.1(b). In a spontaneous Raman process, the incident photon  $\mathbf{k}_1$  is inelastically scattered from the atom ensemble in the optical lattice, where a Stokes photon  $\mathbf{k}_2$  is emitted. This procedure creates a Dicke state among the lattice atoms, whose excitation wave vector  $\boldsymbol{\kappa}_{\text{in}}$ , encoded in the spatial phases, is given by the difference between the wave vectors involved,  $\boldsymbol{\kappa}_{\text{in}} = \mathbf{k}_1 - \mathbf{k}_2$  (i.e., the scattered Stokes photon  $\mathbf{k}_2$  needs to be detected to infer  $\boldsymbol{\kappa}_{\text{in}}$ ). Note that the incident photon  $\gamma_1$  does not have to be in the infrared regime, nor does the level scheme have to support a direct infrared transition. Only

the excitation wave vector  $\kappa_{\text{in}}$  of the Dicke state should be in the infrared region. Then, after a (self-chosen) waiting time  $\Delta t$ , a  $\pi$ -pulse with wave vector  $\mathbf{k}_3$  can be applied to the atom ensemble, which enables a second Raman transition from the metastable state back to the ground state, emitting an anti-Stokes photon with wave vector  $\mathbf{k}_4$ . The superradiance peak would then appear for an emission wave vector  $\mathbf{k}_4 = \kappa_{\text{in}} + \mathbf{k}_3$  due to the phase-matching condition.

**Implementation employing classical laser fields** The fourth option has already been presented in chapter 4. In short, we can alter the single-photon probing scheme into a probing scheme employing only classical laser fields. Although the excitation and de-excitation dynamics differ substantially compared to the single-photon probing scheme (for details please refer back to chapter 4), the main features of the probe are retained. As in the previous paragraph, we assume a level scheme as depicted in Figure 5.1(b). To drive the excitation from the ground state to the metastable state, we envisage two counter-propagating lasers  $\gamma_1$  and  $\gamma_2$ . At the beginning, all of the atoms in the optical lattice are in the ground state, which means that switching on the two lasers for a short period excites a few atoms to the metastable state. The lasers are then switched off during the waiting time  $\Delta t$ , which again can be chosen freely [61]. Assuming zero tunneling, switching on the lasers for a second identical period (but with an opposite sign of the effective vector potential) leads to perfect de-excitation, i.e., all atoms are in the ground state again. For nonzero tunneling, however, the spatial phases deteriorate in a similar manner to the single-photon case, leading to an imperfect de-excitation process. In conclusion, some atoms remain in the metastable state after the full sequence.

As we have already shown in chapter 4, measuring the number of atoms which are still in the metastable state after the full sequence then allows us to extract similar information as when observing the decay of the superradiance peak in the single-photon probing scheme (chapter 2,3).



## 6. Conclusions

The nondestructive probing of ultracold atoms in optical lattices, in particular the observation of nonequilibrium phenomena, would provide a groundbreaking tool to explore fundamental many-body quantum physics with unprecedented clarity. To this end, we have developed a comprehensive proposal for a nondestructive probing scheme, utilizing the unique features of Dicke superradiance, in this dissertation.

In short, the probing scheme is based on the idea that the phase coherence of an excited Dicke state after the collective absorption of a probe photon is altered due to the subsequent lattice dynamics (e.g., tunneling of atoms). The impaired phase coherence then leads to modified superradiant emission characteristics, which can be employed to obtain information about the underlying quantum state (or its evolution) of the optical lattice.

Starting from the single-photon pump-and-probe scheme sketched in Figure 1.3, we studied the superradiant emission characteristics as a function of the initial quantum state of the atom ensemble in the optical lattice in chapter 2: for bosonic atoms in an optical lattice, as described by the Bose-Hubbard model, we recognized the possibility of differentiating between (partially) excited states, such as thermal states, and the superfluid ground state in the case of weak interactions. Interestingly, it is not possible to distinguish the superfluid ground state from the Mott insulator state, as these ground states of the two opposing parameter regimes show the same unmodified superradiant emission characteristics (to the leading order). Considering fermionic atoms in an optical lattice, as covered by the Fermi-Hubbard model, we found that the proposed probe is able to differentiate between the Mott insulator phase and the metallic phase, which enables to determine the current parameter regime of the optical lattice. On the downside, a distinction between the (metallic) ground state and a thermal state within the weak interactions regime is not possible in the fermionic case, as opposed to the bosonic case (section 2.4).

It is important to note that the pump-probe characteristic (analogous to pump-probe spectroscopy in solid-state physics) of the suggested probing scheme allows to obtain information about nonequilibrium phenomena, as it accesses time-resolved correlation functions. This stands in opposition to a plethora of previous approaches, e.g., Bragg scattering, which are only sensitive to single-particle equal-time correl-

ators.

Emphasizing this advantage of our proposal, we further investigated the non-destructive measurement of nonequilibrium phenomena by taking the example of a phase transition from the Mott insulator phase to the superfluid or metallic phase, respectively, in chapter 3. We discovered that a sudden phase transition can be distinguished from an adiabatic phase transition via the temporal behavior of the emission probability in the case of a bosonic optical lattice. For a fermionic optical lattice, on the other hand, such a differentiation is unfortunately not possible (section 3.5).

Refining the single-photon probing scheme, we also examined the coherent excitation and de-excitation of the atoms in the optical lattice via classical laser fields in chapter 4. While the excitation and de-excitation dynamics differ substantially compared to single-photon absorption and emission, similar information about the optical lattice can be obtained. Notably, the application of two counter-propagating lasers allows arbitrary waiting times between the pump and probe (section 4.5).

Finally, we also discussed typical experimental parameters and explored various options for atomic level schemes which may facilitate the experimental realization of the suggested pump-and-probe sequence in chapter 5.

The proposed probing scheme may also potentially serve as a tool for detecting the number of condensed atoms or inferring the absolute temperature of an ensemble of bosons in an optical lattice, as explained in section 2.4. Of course, the suggested pump-and-probe scheme is not restricted to the well-known Mott-to-superfluid and Mott-to-metal transitions in optical lattices. In principle, our method applies to all nonequilibrium phenomena and complex quantum phases which show signatures in time-resolved correlation (Green) functions [97]. For example, we may thus distinguish even and odd-frequency correlators [98]. As another promising direction for future research, one might explore whether superconducting phases can also be detected using the proposed probing scheme.

In conclusion, the realization of a versatile method for nondestructive measurements in clean model systems (such as optical lattices) would significantly advance our understanding of fundamental many-body quantum physics.

For a brief overview, the main results are also summarized in Table 6.1 below.

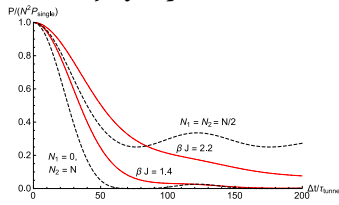
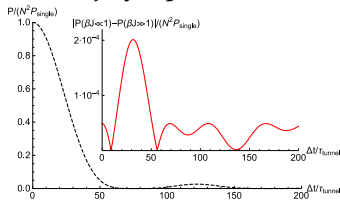
Detection of stationary lattice states (chapter 2)				
Parameters	Bose-Hubbard model		Fermi-Hubbard model	
$U \gg J$ (sect. 2.2)	<b>Mott insulator state</b> <i>Usual superradiance:</i> $P_{\kappa_{out}} = N^2 \delta_{\kappa_{in} \kappa_{out}} P_{single}$ (2.25)		<b>Mott-Néel state</b> <i>Usual superradiance:</i> $P_{\kappa_{out}} = N^2 \delta_{\kappa_{in} \kappa_{out}} P_{single}$ (2.25)	
$J \gg U$ ( $T = 0$ ) (sect. 2.3)	<b>Superfluid ground state</b> <i>Usual superradiance (to the leading order):</i> $P_{\kappa_{out}} = N(N-1) \delta_{\kappa_{in} \kappa_{out}} P_{single} + N P_{single}$ (2.49)		<b>Metallic ground state</b> <i>Decay of superradiance:</i> $P_{\kappa_{out}} = N^2  \mathcal{J}_{\kappa_{in}}(\Delta t) ^2 \delta_{\kappa_{in} \kappa_{out}} P_{single}$ (2.78)	
$J \gg U$ (toy model) (sect. 2.3)	<b>Partial condensation state</b> <i>Decay of superradiance:</i> $P_{\kappa_{out}} =  N_1 \exp\{i\varphi(\Delta t)\} + N_2 \mathcal{J}_{\kappa_{in}}(\Delta t) ^2 \times \delta_{\kappa_{in} \kappa_{out}} P_{single}$ (2.58)			
$J \gg U$ ( $T > 0$ )  (sect. 2.3)	<b>Bose-Einstein thermal state</b> <i>Decay of superradiance:</i>  (Figure 2.1)		<b>Fermi-Dirac thermal state</b> <i>Decay of superradiance:</i>  (Figure 2.4)	
Detection of quantum phase transitions (chapter 3)				
Parameters	Bose-Hubbard model		Fermi-Hubbard model	
$U \gg J$	<b>Mott insulator state</b> adiabatic (sect. 3.4.1) sudden (sect. 3.3)		<b>Mott-Néel state</b> adiabatic (sect. 3.4.2) sudden (sect. 3.3)	
$J \gg U$	<i>Usual superradiance:</i> $P_{\kappa_{out}} = N^2 \delta_{\kappa_{in} \kappa_{out}} P_{single}$ (3.42)		<i>Decay of superradiance:</i> $P_{\kappa_{out}} = N^2  \mathcal{J}_{\kappa_{in}}(\Delta t) ^2 \delta_{\kappa_{in} \kappa_{out}} P_{single}$ (3.18)	

TABLE 6.1. – Main results summarized in tabular form.





# A. Appendix

## A.1. $SU(2)$ algebra property of the quasispin operators

We prove the  $SU(2)$  algebra property (1.10) of the quasispin  $X$ ,  $Y$  and  $Z$  operators  $\hat{\Sigma}^x(\mathbf{k})$ ,  $\hat{\Sigma}^y(\mathbf{k})$  and  $\hat{\Sigma}^z$ , that is

$$[\hat{\Sigma}^\ell, \hat{\Sigma}^m] = \sum_n i\varepsilon_{\ell mn} \hat{\Sigma}^n. \quad (\text{A.1})$$

According to definitions (1.6), (1.8) and (1.9), the quasispin  $X$ ,  $Y$  and  $Z$  operators are given by

$$\hat{\Sigma}^x(\mathbf{k}) = \frac{1}{2} \sum_{\mu=1}^S (\hat{\sigma}_\mu^+ \exp\{i\mathbf{k} \cdot \mathbf{r}_\mu\} + \hat{\sigma}_\mu^- \exp\{-i\mathbf{k} \cdot \mathbf{r}_\mu\}), \quad (\text{A.2})$$

$$\hat{\Sigma}^y(\mathbf{k}) = \frac{1}{2i} \sum_{\mu=1}^S (\hat{\sigma}_\mu^+ \exp\{i\mathbf{k} \cdot \mathbf{r}_\mu\} - \hat{\sigma}_\mu^- \exp\{-i\mathbf{k} \cdot \mathbf{r}_\mu\}), \quad (\text{A.3})$$

and  $\hat{\Sigma}^z = \frac{1}{2} \sum_{\mu=1}^S \hat{\sigma}_\mu^z$ . As another preparation, we can infer the following commutator relations for the ladder operators from the angular momentum algebra of the Pauli matrices (1.7),

$$[\hat{\sigma}_\mu^+, \hat{\sigma}_\nu^z] = -2\hat{\sigma}_\mu^+ \delta_{\mu\nu}, \quad [\hat{\sigma}_\mu^-, \hat{\sigma}_\nu^z] = +2\hat{\sigma}_\mu^- \delta_{\mu\nu}, \quad [\hat{\sigma}_\mu^+, \hat{\sigma}_\nu^-] = +\hat{\sigma}_\mu^z \delta_{\mu\nu}. \quad (\text{A.4})$$

Resorting to these findings, the calculation of the three commutators necessary to prove the  $SU(2)$  algebra property is straightforward:

$$\begin{aligned} [\hat{\Sigma}^x(\mathbf{k}), \hat{\Sigma}^z] &= \left[ \frac{1}{2} \sum_{\mu=1}^S (\hat{\sigma}_\mu^+ \exp\{i\mathbf{k} \cdot \mathbf{r}_\mu\} + \hat{\sigma}_\mu^- \exp\{-i\mathbf{k} \cdot \mathbf{r}_\mu\}), \frac{1}{2} \sum_{\nu=1}^S \hat{\sigma}_\nu^z \right] \\ &= \frac{1}{4} \sum_{\mu, \nu=1}^S (\exp\{i\mathbf{k} \cdot \mathbf{r}_\mu\} [\hat{\sigma}_\mu^+, \hat{\sigma}_\nu^z] + \exp\{-i\mathbf{k} \cdot \mathbf{r}_\mu\} [\hat{\sigma}_\mu^-, \hat{\sigma}_\nu^z]) \\ &= \frac{1}{2} \sum_{\mu=1}^S (\hat{\sigma}_\mu^- \exp\{-i\mathbf{k} \cdot \mathbf{r}_\mu\} - \hat{\sigma}_\mu^+ \exp\{i\mathbf{k} \cdot \mathbf{r}_\mu\}) \\ &= \frac{1}{2} (\hat{\Sigma}^-(\mathbf{k}) - \hat{\Sigma}^+(\mathbf{k})) = -i\hat{\Sigma}^y(\mathbf{k}), \end{aligned} \quad (\text{A.5})$$

$$\begin{aligned}
[\hat{\Sigma}^y(\mathbf{k}), \hat{\Sigma}^z] &= \left[ \frac{1}{2i} \sum_{\mu=1}^S (\hat{\sigma}_\mu^+ \exp\{i\mathbf{k} \cdot \mathbf{r}_\mu\} - \hat{\sigma}_\mu^- \exp\{-i\mathbf{k} \cdot \mathbf{r}_\mu\}), \frac{1}{2} \sum_{v=1}^S \hat{\sigma}_v^z \right] \\
&= \frac{1}{4i} \sum_{\mu,v=1}^S (\exp\{i\mathbf{k} \cdot \mathbf{r}_\mu\} [\hat{\sigma}_\mu^+, \hat{\sigma}_v^z] - \exp\{-i\mathbf{k} \cdot \mathbf{r}_\mu\} [\hat{\sigma}_\mu^-, \hat{\sigma}_v^z]) \\
&= -\frac{1}{2i} \sum_{\mu=1}^S (\hat{\sigma}_\mu^+ \exp\{i\mathbf{k} \cdot \mathbf{r}_\mu\} + \hat{\sigma}_\mu^- \exp\{-i\mathbf{k} \cdot \mathbf{r}_\mu\}) \\
&= i \frac{1}{2} (\hat{\Sigma}^+(\mathbf{k}) + \hat{\Sigma}^-(\mathbf{k})) = i \hat{\Sigma}^x(\mathbf{k}), \tag{A.6}
\end{aligned}$$

and finally

$$\begin{aligned}
[\hat{\Sigma}^x(\mathbf{k}), \hat{\Sigma}^y(\mathbf{k})] &= \frac{1}{4i} [\hat{\Sigma}^+(\mathbf{k}) + \hat{\Sigma}^-(\mathbf{k}), \hat{\Sigma}^+(\mathbf{k}) - \hat{\Sigma}^-(\mathbf{k})] = -\frac{1}{2i} [\hat{\Sigma}^+(\mathbf{k}), \hat{\Sigma}^-(\mathbf{k})] \\
&= -\frac{1}{2i} \sum_{\mu,v=1}^S \exp\{i\mathbf{k} \cdot (\mathbf{r}_\mu - \mathbf{r}_v)\} [\hat{\sigma}_\mu^+, \hat{\sigma}_v^-] = i \frac{1}{2} \sum_{\mu=1}^S \hat{\sigma}_\mu^z = i \hat{\Sigma}^z. \tag{A.7}
\end{aligned}$$

## A.2. Angular momentum algebra of the Pauli operators

Here we want to prove that the wiggled Pauli operators  $\hat{\sigma}_\mu^x = \hat{\sigma}_\mu^+ + \hat{\sigma}_\mu^-$ ,  $\hat{\sigma}_\mu^y = -i(\hat{\sigma}_\mu^+ - \hat{\sigma}_\mu^-)$  and  $\hat{\sigma}_\mu^z = \sum_s (\hat{n}_{\mu,s}^{\text{ex}} - \hat{n}_{\mu,s}^{\text{gr}})$ , defined in the context of the exciton creation and annihilation operators (1.47) in section 1.4.1 via  $\hat{\sigma}_\mu^+ := \sum_s \hat{a}_{\mu,s}^{\text{ex}\dagger} \hat{a}_{\mu,s}^{\text{gr}}$  and  $\hat{\sigma}_\mu^- := [\hat{\sigma}_\mu^+]^\dagger$ , satisfy the same angular momentum algebra property as the usual Pauli matrices (1.7), that is,

$$[\hat{\sigma}_\mu^\ell, \hat{\sigma}_\nu^m] = \sum_n 2i\epsilon_{lmn} \hat{\sigma}_\mu^n \delta_{\mu\nu}. \tag{A.8}$$

Therefore, we start with the commutator between  $\hat{\sigma}_\mu^x$  and  $\hat{\sigma}_\nu^y$ , i.e.,

$$\begin{aligned}
[\hat{\sigma}_\mu^x, \hat{\sigma}_\nu^y] &= -i [\hat{\sigma}_\mu^+ + \hat{\sigma}_\mu^-, \hat{\sigma}_\nu^+ - \hat{\sigma}_\nu^-] = -i ([\hat{\sigma}_\mu^-, \hat{\sigma}_\nu^+] + \text{H.c.}) \\
&= -i \sum_{s_1 s_2} \left( [\hat{a}_{\mu,s_1}^{\text{gr}\dagger} \hat{a}_{\mu,s_1}^{\text{ex}}, \hat{a}_{\nu,s_2}^{\text{ex}\dagger} \hat{a}_{\nu,s_2}^{\text{gr}}] + \text{H.c.} \right) \\
&= 2i \sum_s (\hat{n}_{\mu,s}^{\text{ex}} - \hat{n}_{\mu,s}^{\text{gr}}) \delta_{\mu\nu} = 2i \hat{\sigma}_\mu^z \delta_{\mu\nu}, \tag{A.9}
\end{aligned}$$

where in the first line that we used  $[\hat{\sigma}_\mu^+, \hat{\sigma}_\nu^+] = \sum_{s_1 s_2} [\hat{a}_{\mu,s_1}^{\text{ex}\dagger} \hat{a}_{\mu,s_1}^{\text{gr}}, \hat{a}_{\nu,s_2}^{\text{ex}\dagger} \hat{a}_{\nu,s_2}^{\text{gr}}] = 0$ , and thus also  $[\hat{\sigma}_\mu^-, \hat{\sigma}_\nu^-] = 0$ , in the bosonic as well as in the fermionic case. In the second

line we encountered the commutator

$$\begin{aligned}
\left[ \hat{a}_{\mu,s_1}^{\text{gr}\dagger} \hat{a}_{\mu,s_1}^{\text{ex}}, \hat{a}_{\nu,s_2}^{\text{ex}\dagger} \hat{a}_{\nu,s_2}^{\text{gr}} \right] &= \hat{a}_{\mu,s_1}^{\text{gr}\dagger} \hat{a}_{\mu,s_1}^{\text{ex}} \hat{a}_{\nu,s_2}^{\text{ex}\dagger} \hat{a}_{\nu,s_2}^{\text{gr}} - \hat{a}_{\nu,s_2}^{\text{ex}\dagger} \hat{a}_{\nu,s_2}^{\text{gr}} \hat{a}_{\mu,s_1}^{\text{gr}\dagger} \hat{a}_{\mu,s_1}^{\text{ex}} \\
&= \hat{a}_{\mu,s_1}^{\text{gr}\dagger} \hat{a}_{\mu,s_1}^{\text{ex}} \hat{a}_{\nu,s_2}^{\text{ex}\dagger} \hat{a}_{\nu,s_2}^{\text{gr}} - (\mp \delta_{\mu\nu} \delta_{s_1 s_2} \pm \hat{a}_{\mu,s_1}^{\text{ex}} \hat{a}_{\nu,s_2}^{\text{ex}\dagger}) (\pm \delta_{\mu\nu} \delta_{s_1 s_2} \pm \hat{a}_{\mu,s_1}^{\text{gr}\dagger} \hat{a}_{\nu,s_2}^{\text{gr}}) \\
&= \delta_{\mu\nu} \delta_{s_1 s_2} \left( \hat{a}_{\mu,s_1}^{\text{gr}\dagger} \hat{a}_{\nu,s_2}^{\text{gr}} \mp \hat{a}_{\mu,s_1}^{\text{ex}} \hat{a}_{\nu,s_2}^{\text{ex}\dagger} \pm 1 \right) = \delta_{\mu\nu} \delta_{s_1 s_2} \left( \hat{n}_{\mu,s_1}^{\text{gr}} - \hat{n}_{\mu,s_1}^{\text{ex}} \right), \quad (\text{A.10})
\end{aligned}$$

which also yields the same result for bosons (upper written sign) and fermions (lower written sign). Using the fact that the number operators are self-adjoint, the commutator between  $\hat{\sigma}_\mu^z$  and  $\hat{\sigma}_\nu^x$  can be written as

$$\begin{aligned}
\left[ \hat{\sigma}_\mu^z, \hat{\sigma}_\nu^x \right] &= \sum_{s_1 s_2} \left( \left[ \hat{n}_{\mu,s_1}^{\text{ex}} - \hat{n}_{\mu,s_1}^{\text{gr}}, \hat{a}_{\nu,s_2}^{\text{ex}\dagger} \hat{a}_{\nu,s_2}^{\text{gr}} \right] - \text{H.c.} \right) \\
&= 2 \sum_s \left( \hat{a}_{\mu,s}^{\text{ex}\dagger} \hat{a}_{\mu,s}^{\text{gr}} - \text{H.c.} \right) \delta_{\mu\nu} = 2 \left( \hat{\sigma}_\mu^+ - \hat{\sigma}_\mu^- \right) \delta_{\mu\nu} = 2i \hat{\sigma}_\mu^y \delta_{\mu\nu}, \quad (\text{A.11})
\end{aligned}$$

where we come across the commutator

$$\begin{aligned}
\left[ \hat{n}_{\mu,s_1}^{\text{ex}} - \hat{n}_{\mu,s_1}^{\text{gr}}, \hat{a}_{\nu,s_2}^{\text{ex}\dagger} \hat{a}_{\nu,s_2}^{\text{gr}} \right] &= \left[ \hat{n}_{\mu,s_1}^{\text{ex}}, \hat{a}_{\nu,s_2}^{\text{ex}\dagger} \right] \hat{a}_{\nu,s_2}^{\text{gr}} - \hat{a}_{\nu,s_2}^{\text{ex}\dagger} \left[ \hat{n}_{\mu,s_1}^{\text{gr}}, \hat{a}_{\nu,s_2}^{\text{gr}} \right] \\
&= 2 \delta_{\mu\nu} \delta_{s_1 s_2} \hat{a}_{\mu,s_1}^{\text{ex}\dagger} \hat{a}_{\mu,s_1}^{\text{gr}}, \quad (\text{A.12})
\end{aligned}$$

with

$$\begin{aligned}
\left[ \hat{n}_{\mu,s_1}^{\text{ex}}, \hat{a}_{\nu,s_2}^{\text{ex}\dagger} \right] &= \hat{a}_{\mu,s_1}^{\text{ex}\dagger} \hat{a}_{\mu,s_1}^{\text{ex}} \hat{a}_{\nu,s_2}^{\text{ex}\dagger} - \hat{a}_{\nu,s_2}^{\text{ex}\dagger} \hat{a}_{\mu,s_1}^{\text{ex}\dagger} \hat{a}_{\mu,s_1}^{\text{ex}} \\
&= \hat{a}_{\mu,s_1}^{\text{ex}\dagger} \hat{a}_{\mu,s_1}^{\text{ex}} \hat{a}_{\nu,s_2}^{\text{ex}\dagger} \mp \hat{a}_{\nu,s_2}^{\text{ex}\dagger} \left( \mp \delta_{\mu\nu} \delta_{s_1 s_2} \pm \hat{a}_{\mu,s_1}^{\text{ex}} \hat{a}_{\nu,s_2}^{\text{ex}\dagger} \right) \\
&= \delta_{\mu\nu} \delta_{s_1 s_2} \hat{a}_{\mu,s_1}^{\text{ex}\dagger}, \quad (\text{A.13})
\end{aligned}$$

and  $\left[ \hat{n}_{\mu,s_1}^{\text{gr}}, \hat{a}_{\nu,s_2}^{\text{gr}} \right] = -\delta_{\mu\nu} \delta_{s_1 s_2} \hat{a}_{\mu,s_1}^{\text{gr}}$ , analogously. The last missing commutator is the one between  $\hat{\sigma}_\mu^y$  and  $\hat{\sigma}_\nu^z$ , i.e.,

$$\begin{aligned}
\left[ \hat{\sigma}_\mu^y, \hat{\sigma}_\nu^z \right] &= -i \sum_{s_1 s_2} \left( \left[ \hat{a}_{\mu,s_1}^{\text{ex}\dagger} \hat{a}_{\mu,s_1}^{\text{gr}}, \hat{n}_{\nu,s_2}^{\text{ex}} - \hat{n}_{\nu,s_2}^{\text{gr}} \right] + \text{H.c.} \right) \\
&= 2i \sum_s \left( \hat{a}_{\mu,s}^{\text{ex}\dagger} \hat{a}_{\mu,s}^{\text{gr}} + \text{H.c.} \right) \delta_{\mu\nu} = 2i \left( \hat{\sigma}_\mu^+ + \hat{\sigma}_\mu^- \right) \delta_{\mu\nu} = 2i \hat{\sigma}_\mu^x \delta_{\mu\nu}, \quad (\text{A.14})
\end{aligned}$$

where (A.12) is used again, but with switched indices and sign. To sum up, we have provided proof of the angular momentum algebra property (A.8).

### A.3. Four-point correlator in the lattice site basis

#### A.3.1. Expectation value in the Mott insulator state

The calculation of the expectation value (3.9) in the bosonic Mott insulator state (1.33) is straightforward. For example, we can use the bosonic commutation relation (1.39) to obtain

$$\begin{aligned} \langle \Psi | \hat{b}_\rho^{\text{gr}\dagger} \hat{b}_\eta^{\text{gr}} \hat{b}_\mu^{\text{gr}\dagger} \hat{b}_\nu^{\text{gr}} | \Psi \rangle_{\text{Mo}}^{J=0} &= \langle \Psi | \hat{b}_\rho^{\text{gr}\dagger} \hat{b}_\mu^{\text{gr}\dagger} \hat{b}_\eta^{\text{gr}} \hat{b}_\nu^{\text{gr}} | \Psi \rangle_{\text{Mo}}^{J=0} \\ &+ \delta_{\mu\eta} \langle \Psi | \hat{b}_\rho^{\text{gr}\dagger} \hat{b}_\nu^{\text{gr}} | \Psi \rangle_{\text{Mo}}^{J=0}. \end{aligned} \quad (\text{A.15})$$

Because the Mott insulator state (1.33) is a basis state with one atom per lattice site, it is clear that the second term is nonzero only for  $\nu = \rho$ . By the same reasoning, the first term can only be nonzero for  $\nu \neq \eta$ . Then there are two possible cases, either  $\mu = \nu$  and  $\eta = \rho$  or  $\nu = \rho$  and  $\mu = \eta$  respectively. In summary, we arrive at

$$\begin{aligned} \langle \Psi | \hat{b}_\rho^{\text{gr}\dagger} \hat{b}_\eta^{\text{gr}} \hat{b}_\mu^{\text{gr}\dagger} \hat{b}_\nu^{\text{gr}} | \Psi \rangle_{\text{Mo}}^{J=0} &= (1 - \delta_{\nu\eta}) (\delta_{\mu\nu} \delta_{\eta\rho} + \delta_{\nu\rho} \delta_{\mu\eta}) + \delta_{\nu\rho} \delta_{\mu\eta} \\ &= \delta_{\mu\nu} \delta_{\eta\rho} + 2\delta_{\nu\rho} \delta_{\mu\eta} - 2\delta_{\mu\nu\eta\rho}, \end{aligned} \quad (\text{A.16})$$

i.e., the result in (3.9).

#### A.3.2. Expectation value in the Mott-Néel state

To calculate the expectation value (3.11) in the fermionic Mott-Néel state (1.36), we first employ fermionic anticommutation relations (1.40) such that

$$\begin{aligned} \langle \Psi | \hat{c}_{\rho,s_2}^{\text{gr}\dagger} \hat{c}_{\eta,s_2}^{\text{gr}} \hat{c}_{\mu,s_1}^{\text{gr}\dagger} \hat{c}_{\nu,s_1}^{\text{gr}} | \Psi \rangle_{\text{Né}}^{J=0} &= - \langle \Psi | \hat{c}_{\rho,s_2}^{\text{gr}\dagger} \hat{c}_{\mu,s_1}^{\text{gr}\dagger} \hat{c}_{\eta,s_2}^{\text{gr}} \hat{c}_{\nu,s_1}^{\text{gr}} | \Psi \rangle_{\text{Né}}^{J=0} \\ &+ \delta_{\mu\eta} \delta_{s_1 s_2} \langle \Psi | \hat{c}_{\rho,s_2}^{\text{gr}\dagger} \hat{c}_{\nu,s_1}^{\text{gr}} | \Psi \rangle_{\text{Né}}^{J=0}. \end{aligned} \quad (\text{A.17})$$

The Mott-Néel state (1.36) is a basis state with one atom per lattice site, which has either spin up or spin down. Thus, the second term is nonzero only if  $\nu = \rho$  and  $s_1 = s_2 = s_\nu$ , where  $s_\nu$  denotes the spin quantum number of the atom at lattice site  $\nu$  in the Mott-Néel state. The first term can only be nonzero for  $\nu \neq \eta$ , as there is only one atom per lattice site which can be annihilated. Furthermore, the spin quantum numbers have to match, which yields the conditions  $s_1 = s_\nu$  and  $s_2 = s_\eta$ . Then there are two possible cases: either  $\mu = \nu$  and  $\eta = \rho$ , where  $s_1$  and  $s_2$  can be distinct, or  $\nu = \rho$  and  $\mu = \eta$ , where  $s_1 = s_2$ . In addition, we need to consider that we are dealing with *fermionic* creation and annihilation operators. Therefore, we have

to commute the middle two operators to ultimately obtain number operators in the first case, while we have to perform *two* commutations in the second case. Due to the anticommutation property, the first case thus collects a minus sign, while the second term stays positive. In summary, we arrive at

$$\begin{aligned} \frac{J=0}{N\dot{\epsilon}} \langle \Psi | \hat{c}_{\rho,s_2}^{\text{gr}\dagger} \hat{c}_{\eta,s_2}^{\text{gr}} \hat{c}_{\mu,s_1}^{\text{gr}\dagger} \hat{c}_{\nu,s_1}^{\text{gr}} | \Psi \rangle_{N\dot{\epsilon}}^{J=0} = & - (1 - \delta_{\nu\eta}) \delta_{s_1 s_\nu} \delta_{s_2 s_\eta} \left( - \delta_{\mu\nu} \delta_{\eta\rho} + \delta_{\nu\rho} \delta_{\mu\eta} \delta_{s_1 s_2} \right) \\ & + \delta_{\nu\rho} \delta_{\mu\eta} \delta_{s_1 s_2 s_\nu}, \quad (\text{A.18}) \end{aligned}$$

where the term proportional to  $\delta_{\nu\eta}$  vanishes because  $\nu = \eta$  implies  $s_1 = s_2$ , and the two terms in the second brackets then cancel each other out. After some rearrangements, we obtain the result (3.11):

$$\begin{aligned} \frac{J=0}{N\dot{\epsilon}} \langle \Psi | \hat{c}_{\rho,s_2}^{\text{gr}\dagger} \hat{c}_{\eta,s_2}^{\text{gr}} \hat{c}_{\mu,s_1}^{\text{gr}\dagger} \hat{c}_{\nu,s_1}^{\text{gr}} | \Psi \rangle_{N\dot{\epsilon}}^{J=0} = & \delta_{\mu\nu} \delta_{\eta\rho} \delta_{s_1 s_\mu} \delta_{s_2 s_\eta} + \delta_{\nu\rho} \delta_{\mu\eta} \delta_{s_1 s_2 s_\nu} \\ & - \delta_{\nu\rho} \delta_{\mu\eta} \delta_{s_1 s_2 s_\nu s_\mu}. \quad (\text{A.19}) \end{aligned}$$

## A.4. Matrix elements of the on-site repulsion term

### A.4.1. Diagonal matrix elements of the on-site repulsion term

Starting with the first state (3.31), let us examine the possible nonzero contributions for the first term of (3.33). First, if  $\mathbf{k}_3 = \mathbf{k}_4 = \mathbf{0}$ , then also  $\mathbf{k}_2 = \mathbf{0}$  and this case yields a bosonic factor of  $(N-2)(N-3)$ . The other possible cases are  $\mathbf{k}_4 = \boldsymbol{\kappa}_{\text{in}}$  and  $\mathbf{k}_3 = \mathbf{0}$  or vice versa, i.e.,  $\mathbf{k}_4 = \mathbf{0}$  and  $\mathbf{k}_3 = \boldsymbol{\kappa}_{\text{in}}$ . For both cases, there are again two possible values of  $\mathbf{k}_2 = \mathbf{0}$  or  $\mathbf{k}_2 = \boldsymbol{\kappa}_{\text{in}}$ , which each yield the bosonic factor  $(N-2)$ . Adding up all contributions yields:

$$\begin{aligned} \sum_{\mathbf{k}_2 \mathbf{k}_3 \mathbf{k}_4} \text{sf}_{\text{ex}} \langle \Psi_\alpha(\boldsymbol{\kappa}_{\text{in}}) | \hat{b}_{\mathbf{k}_3 + \mathbf{k}_4 - \mathbf{k}_2}^{\text{gr}\dagger} \hat{b}_{\mathbf{k}_2}^{\text{gr}\dagger} \hat{b}_{\mathbf{k}_3}^{\text{gr}} \hat{b}_{\mathbf{k}_4}^{\text{gr}} | \Psi_\alpha(\boldsymbol{\kappa}_{\text{in}}) \rangle_{\text{ex}}^{\text{sf}} \\ = |c|^2 N [(N-2)(N-3) + 4(N-2)] = |c|^2 N(N+1)(N-2). \quad (\text{A.20}) \end{aligned}$$

Regarding the second term of (3.33), there are only two nonzero cases: one where  $\mathbf{k}_3 = \mathbf{k}_4 = \mathbf{0}$  and thus  $\mathbf{k}_2 = \mathbf{0}$ , which yields a bosonic factor of  $(N-2)$ , and the one

where  $\mathbf{k}_3 = \mathbf{k}_2 = \mathbf{0}$  and  $\mathbf{k}_4 = \boldsymbol{\kappa}_{\text{in}}$ , which has a bosonic factor of one,

$$\sum_{\mathbf{k}_2 \mathbf{k}_3 \mathbf{k}_4} \text{sf}_{\text{ex}} \langle \Psi_{\alpha}(\boldsymbol{\kappa}_{\text{in}}) | \hat{b}_{\mathbf{k}_3 + \mathbf{k}_4 - \mathbf{k}_2}^{\text{gr} \dagger} \hat{b}_{\mathbf{k}_2}^{\text{ex} \dagger} \hat{b}_{\mathbf{k}_3}^{\text{ex}} \hat{b}_{\mathbf{k}_4}^{\text{gr}} | \Psi_{\alpha}(\boldsymbol{\kappa}_{\text{in}}) \rangle_{\text{ex}}^{\text{sf}} = |c|^2 N [(N-2) + 1] = |c|^2 N(N-1). \quad (\text{A.21})$$

Together, this yields for the full matrix element (3.33) for the first state (3.31):

$$\begin{aligned} \text{sf}_{\text{ex}} \langle \Psi_{\alpha}(\boldsymbol{\kappa}_{\text{in}}) | \hat{H}_U | \Psi_{\alpha}(\boldsymbol{\kappa}_{\text{in}}) \rangle_{\text{ex}}^{\text{sf}} &= |c|^2 N \frac{U}{2N} (N+1)(N-2) + |c|^2 N \frac{U}{N} (N-1) \\ &= |c|^2 N \frac{U}{2N} (N^2 + N - 4). \end{aligned} \quad (\text{A.22})$$

The first term of (3.33) in the case of the second state (3.32) is non-vanishing only for  $\mathbf{k}_2 = \mathbf{k}_3 = \mathbf{k}_4 = \mathbf{0}$  and yields a bosonic factor of  $(N-1)(N-2)$ . For the second term, we only have a contribution for  $\mathbf{k}_3 = \mathbf{k}_2 = \boldsymbol{\kappa}_{\text{in}}$  and  $\mathbf{k}_4 = \mathbf{0}$  with a factor  $(N-1)$ . The full matrix element (3.33) for the second state (3.32) thus reads

$$\begin{aligned} \text{sf}_{\text{ex}} \langle \Psi_{\beta}(\boldsymbol{\kappa}_{\text{in}}) | \hat{H}_U | \Psi_{\beta}(\boldsymbol{\kappa}_{\text{in}}) \rangle_{\text{ex}}^{\text{sf}} &= |c|^2 N \frac{U}{2N} (N-1)(N-2) + |c|^2 N \frac{U}{N} (N-1) \\ &= |c|^2 N \frac{U}{2N} N(N-1). \end{aligned} \quad (\text{A.23})$$

#### A.4.2. Off-diagonal matrix elements of the on-site repulsion term

For the off-diagonal matrix elements, which are mixed from the first (3.31) and the second state (3.32), the first term in (3.33) is zero because it does not affect the excited-atom mode, which is different in the two states. Therefore, there is only a contribution from the second term. The annihilation operators are only nonzero for  $\mathbf{k}_4 = \mathbf{0}$  and  $\mathbf{k}_3 = \boldsymbol{\kappa}_{\text{in}}$ , and we only achieve an overlap for  $\mathbf{k}_2 = \mathbf{0}$ . Here, we only obtain a bosonic factor of  $\sqrt{N-1}$  from annihilation, as creation goes into previously unoccupied modes. In conclusion, this yields for the off-diagonal matrix elements:

$$\begin{aligned} \text{sf}_{\text{ex}} \langle \Psi_{\alpha}(\boldsymbol{\kappa}_{\text{in}}) | \hat{H}_U | \Psi_{\beta}(\boldsymbol{\kappa}_{\text{in}}) \rangle_{\text{ex}}^{\text{sf}} &= \text{sf}_{\text{ex}} \langle \Psi_{\beta}(\boldsymbol{\kappa}_{\text{in}}) | \hat{H}_U | \Psi_{\alpha}(\boldsymbol{\kappa}_{\text{in}}) \rangle_{\text{ex}}^{\text{sf}} \\ &= |c|^2 N \frac{U}{N} \sqrt{N-1}. \end{aligned} \quad (\text{A.24})$$

## A.5. Commutators of $\hat{\Sigma}^x(\boldsymbol{\kappa}_{\text{out}})$ and $\hat{\Sigma}^y(\boldsymbol{\kappa}_{\text{in}})$

### A.5.1. Calculation of the first ( $m = 1$ ) commutator

The first commutator (4.13) between the  $\hat{\Sigma}^x(\boldsymbol{\kappa}_{\text{out}})$  quasispin operator (1.64) and the  $\hat{\Sigma}^y(\boldsymbol{\kappa}_{\text{in}})$  quasispin operator (1.65) is given by

$$\begin{aligned} [\hat{\Sigma}^x(\boldsymbol{\kappa}_{\text{out}}), \hat{\Sigma}^y(\boldsymbol{\kappa}_{\text{in}})] &= \frac{1}{4i} \sum_{\mathbf{k}p, s_1 s_2} [\hat{a}_{\mathbf{k}, s_1}^{\text{ex} \dagger} \hat{a}_{\mathbf{k}-\boldsymbol{\kappa}_{\text{out}}, s_1}^{\text{gr}} + \text{H.c.}, \hat{a}_{\mathbf{p}, s_2}^{\text{ex} \dagger} \hat{a}_{\mathbf{p}-\boldsymbol{\kappa}_{\text{in}}, s_2}^{\text{gr}} - \text{H.c.}] \\ &= \frac{1}{4i} \sum_{\mathbf{k}p, s_1 s_2} \left( [\hat{a}_{\mathbf{k}, s_1}^{\text{ex} \dagger} \hat{a}_{\mathbf{k}-\boldsymbol{\kappa}_{\text{out}}, s_1}^{\text{gr}}, \hat{a}_{\mathbf{p}, s_2}^{\text{ex} \dagger} \hat{a}_{\mathbf{p}-\boldsymbol{\kappa}_{\text{in}}, s_2}^{\text{gr}}] + [\hat{a}_{\mathbf{k}, s_1}^{\text{ex}} \hat{a}_{\mathbf{k}-\boldsymbol{\kappa}_{\text{out}}, s_1}^{\text{gr} \dagger}, \hat{a}_{\mathbf{p}, s_2}^{\text{ex} \dagger} \hat{a}_{\mathbf{p}-\boldsymbol{\kappa}_{\text{in}}, s_2}^{\text{gr}}] \right. \\ &\quad \left. - [\hat{a}_{\mathbf{k}, s_1}^{\text{ex} \dagger} \hat{a}_{\mathbf{k}-\boldsymbol{\kappa}_{\text{out}}, s_1}^{\text{gr}}, \hat{a}_{\mathbf{p}, s_2}^{\text{ex}} \hat{a}_{\mathbf{p}-\boldsymbol{\kappa}_{\text{in}}, s_2}^{\text{gr} \dagger}] - [\hat{a}_{\mathbf{k}, s_1}^{\text{ex}} \hat{a}_{\mathbf{k}-\boldsymbol{\kappa}_{\text{out}}, s_1}^{\text{gr} \dagger}, \hat{a}_{\mathbf{p}, s_2}^{\text{ex} \dagger} \hat{a}_{\mathbf{p}-\boldsymbol{\kappa}_{\text{in}}, s_2}^{\text{gr}}] \right). \quad (\text{A.25}) \end{aligned}$$

Operators relating to different species  $\lambda \in \{\text{gr}, \text{ex}\}$  always commute. Thus, and due to the fact that two creation or annihilation operators (of the same species) always either commute (1.70) or anticommute (1.71), the first and the last commutator vanish. To calculate the remaining middle two commutators, we prepare

$$\begin{aligned} &\hat{a}_{\mathbf{p}, s_2}^{\text{ex} \dagger} \hat{a}_{\mathbf{p}-\boldsymbol{\kappa}_{\text{in}}, s_2}^{\text{gr}} \hat{a}_{\mathbf{k}, s_1}^{\text{ex}} \hat{a}_{\mathbf{k}-\boldsymbol{\kappa}_{\text{out}}, s_1}^{\text{gr} \dagger} \\ &= (\mp \delta_{\mathbf{k}p} \delta_{s_1 s_2} \pm \hat{a}_{\mathbf{k}, s_1}^{\text{ex}} \hat{a}_{\mathbf{p}, s_2}^{\text{ex} \dagger}) (\delta_{\mathbf{k}-\boldsymbol{\kappa}_{\text{out}}, \mathbf{p}-\boldsymbol{\kappa}_{\text{in}}} \delta_{s_1 s_2} \pm \hat{a}_{\mathbf{k}-\boldsymbol{\kappa}_{\text{out}}, s_1}^{\text{gr} \dagger} \hat{a}_{\mathbf{p}-\boldsymbol{\kappa}_{\text{in}}, s_2}^{\text{gr}}), \quad (\text{A.26}) \end{aligned}$$

where we have employed either bosonic commutation relations (1.70), coinciding with the upper written sign, or fermionic anticommutation relations (1.71), represented by the lower written sign. Now we can compute the second commutator in (A.25):

$$\begin{aligned} &[\hat{a}_{\mathbf{k}, s_1}^{\text{ex}} \hat{a}_{\mathbf{k}-\boldsymbol{\kappa}_{\text{out}}, s_1}^{\text{gr} \dagger}, \hat{a}_{\mathbf{p}, s_2}^{\text{ex} \dagger} \hat{a}_{\mathbf{p}-\boldsymbol{\kappa}_{\text{in}}, s_2}^{\text{gr}}] \\ &= \hat{a}_{\mathbf{k}, s_1}^{\text{ex}} \hat{a}_{\mathbf{k}-\boldsymbol{\kappa}_{\text{out}}, s_1}^{\text{gr} \dagger} \hat{a}_{\mathbf{p}, s_2}^{\text{ex} \dagger} \hat{a}_{\mathbf{p}-\boldsymbol{\kappa}_{\text{in}}, s_2}^{\text{gr}} - \hat{a}_{\mathbf{p}, s_2}^{\text{ex} \dagger} \hat{a}_{\mathbf{p}-\boldsymbol{\kappa}_{\text{in}}, s_2}^{\text{gr}} \hat{a}_{\mathbf{k}, s_1}^{\text{ex}} \hat{a}_{\mathbf{k}-\boldsymbol{\kappa}_{\text{out}}, s_1}^{\text{gr} \dagger} \\ &= -\delta_{\mathbf{k}-\boldsymbol{\kappa}_{\text{out}}, \mathbf{p}-\boldsymbol{\kappa}_{\text{in}}} \delta_{s_1 s_2} (\pm \hat{a}_{\mathbf{k}, s_1}^{\text{ex}} \hat{a}_{\mathbf{p}, s_2}^{\text{ex} \dagger} \mp \delta_{\mathbf{k}p}) + \delta_{\mathbf{k}p} \delta_{s_1 s_2} \hat{a}_{\mathbf{k}-\boldsymbol{\kappa}_{\text{out}}, s_1}^{\text{gr} \dagger} \hat{a}_{\mathbf{p}-\boldsymbol{\kappa}_{\text{in}}, s_2}^{\text{gr}} \\ &= -\delta_{\mathbf{k}-\boldsymbol{\kappa}_{\text{out}}, \mathbf{p}-\boldsymbol{\kappa}_{\text{in}}} \delta_{s_1 s_2} \hat{a}_{\mathbf{p}, s_2}^{\text{ex} \dagger} \hat{a}_{\mathbf{k}, s_1}^{\text{ex}} + \delta_{\mathbf{k}p} \delta_{s_1 s_2} \hat{a}_{\mathbf{k}-\boldsymbol{\kappa}_{\text{out}}, s_1}^{\text{gr} \dagger} \hat{a}_{\mathbf{p}-\boldsymbol{\kappa}_{\text{in}}, s_2}^{\text{gr}}. \quad (\text{A.27}) \end{aligned}$$

Via the Hermitian conjugate, i.e.,  $[\hat{A}^\dagger, \hat{B}^\dagger] = -[B^\dagger, A^\dagger] = -[\hat{A}, \hat{B}]^\dagger$ , we immediately obtain also the third commutator in (A.25) from (A.27),

$$\begin{aligned} [\hat{a}_{\mathbf{k},s_1}^{\text{ex}\dagger} \hat{a}_{\mathbf{k}-\boldsymbol{\kappa}_{\text{out}},s_1}^{\text{gr}}, \hat{a}_{\mathbf{p},s_2}^{\text{ex}} \hat{a}_{\mathbf{p}-\boldsymbol{\kappa}_{\text{in}},s_2}^{\text{gr}\dagger}] &= \delta_{\mathbf{k}-\boldsymbol{\kappa}_{\text{out}},\mathbf{p}-\boldsymbol{\kappa}_{\text{in}}} \delta_{s_1 s_2} \hat{a}_{\mathbf{k},s_1}^{\text{ex}\dagger} \hat{a}_{\mathbf{p},s_2}^{\text{ex}} \\ &\quad - \delta_{\mathbf{k}\mathbf{p}} \delta_{s_1 s_2} \hat{a}_{\mathbf{p}-\boldsymbol{\kappa}_{\text{in}},s_2}^{\text{gr}\dagger} \hat{a}_{\mathbf{k}-\boldsymbol{\kappa}_{\text{out}},s_1}^{\text{gr}}. \end{aligned} \quad (\text{A.28})$$

Inserting these two nonzero commutators (A.27) and (A.28) into the expression (A.25), we obtain the result (4.13) for the first commutator between  $\hat{\Sigma}^x(\boldsymbol{\kappa}_{\text{out}})$  and  $\hat{\Sigma}^y(\boldsymbol{\kappa}_{\text{in}})$ , i.e.,

$$\begin{aligned} [\hat{\Sigma}^x(\boldsymbol{\kappa}_{\text{out}}), \hat{\Sigma}^y(\boldsymbol{\kappa}_{\text{in}})] &= i \frac{1}{4} \sum_{\mathbf{k}\mathbf{p},s} (\delta_{\mathbf{k}-\boldsymbol{\kappa}_{\text{out}},\mathbf{p}-\boldsymbol{\kappa}_{\text{in}}} \hat{a}_{\mathbf{p},s}^{\text{ex}\dagger} \hat{a}_{\mathbf{k},s}^{\text{ex}} - \delta_{\mathbf{k}\mathbf{p}} \hat{a}_{\mathbf{k}-\boldsymbol{\kappa}_{\text{out}},s}^{\text{gr}\dagger} \hat{a}_{\mathbf{p}-\boldsymbol{\kappa}_{\text{in}},s}^{\text{gr}} + \text{H.c.}) \\ &= i \frac{1}{4} \sum_{\mathbf{p},s} (\hat{a}_{\mathbf{p},s}^{\text{ex}\dagger} \hat{a}_{\mathbf{p}-\boldsymbol{\kappa}_{\text{in}}+\boldsymbol{\kappa}_{\text{out}},s}^{\text{ex}} - \hat{a}_{\mathbf{p}-\boldsymbol{\kappa}_{\text{out}},s}^{\text{gr}\dagger} \hat{a}_{\mathbf{p}-\boldsymbol{\kappa}_{\text{in}},s}^{\text{gr}} + \text{H.c.}) \\ &= i \frac{1}{4} \sum_{\mathbf{p},s} (\hat{a}_{\mathbf{p}-\boldsymbol{\kappa}_{\text{out}},s}^{\text{ex}\dagger} \hat{a}_{\mathbf{p}-\boldsymbol{\kappa}_{\text{in}},s}^{\text{ex}} - \hat{a}_{\mathbf{p}-\boldsymbol{\kappa}_{\text{out}},s}^{\text{gr}\dagger} \hat{a}_{\mathbf{p}-\boldsymbol{\kappa}_{\text{in}},s}^{\text{gr}} + \text{H.c.}) \\ &= i \hat{\Sigma}_D^z(\boldsymbol{\kappa}_{\text{out}}, \boldsymbol{\kappa}_{\text{in}}), \end{aligned} \quad (\text{A.29})$$

with the definition (4.14). Note that we can always shift the indices of any term by an arbitrary reciprocal lattice vector (such as  $\boldsymbol{\kappa}_{\text{in}}$  or  $\boldsymbol{\kappa}_{\text{out}}$ ), as the summation runs over all reciprocal lattice vectors anyway.

### A.5.2. Calculation of the second ( $m = 2$ ) commutator

Now we calculate the second commutator (4.15), i.e., the commutator between the  $\hat{\Sigma}^x(\boldsymbol{\kappa}_{\text{out}})$  quasispin operator (1.64) and the result of the first commutator, that is the  $\hat{\Sigma}_D^z(\boldsymbol{\kappa}_{\text{out}}, \boldsymbol{\kappa}_{\text{in}})$  quasispin operator (4.14). Employing the relation  $[\hat{A} + \text{H.c.}, \hat{B} + \text{H.c.}] = ([\hat{A}, \hat{B} + \hat{B}^\dagger] - \text{H.c.})$ , we find

$$\begin{aligned} &[\hat{\Sigma}^x(\boldsymbol{\kappa}_{\text{out}}), \hat{\Sigma}_D^z(\boldsymbol{\kappa}_{\text{out}}, \boldsymbol{\kappa}_{\text{in}})] \\ &= \frac{1}{8} \sum_{\mathbf{k}\mathbf{p},s_1 s_2} [\hat{a}_{\mathbf{k},s_1}^{\text{ex}\dagger} \hat{a}_{\mathbf{k}-\boldsymbol{\kappa}_{\text{out}},s_1}^{\text{gr}} + \text{H.c.}, \hat{a}_{\mathbf{p}-\boldsymbol{\kappa}_{\text{out}},s_2}^{\text{ex}\dagger} \hat{a}_{\mathbf{p}-\boldsymbol{\kappa}_{\text{in}},s_2}^{\text{ex}} - \hat{a}_{\mathbf{p}-\boldsymbol{\kappa}_{\text{out}},s_2}^{\text{gr}\dagger} \hat{a}_{\mathbf{p}-\boldsymbol{\kappa}_{\text{in}},s_2}^{\text{gr}} + \text{H.c.}] \\ &= \frac{1}{8} \sum_{\mathbf{k}\mathbf{p},s_1 s_2} \left( [\hat{a}_{\mathbf{k},s_1}^{\text{ex}\dagger} \hat{a}_{\mathbf{k}-\boldsymbol{\kappa}_{\text{out}},s_1}^{\text{gr}}, \hat{a}_{\mathbf{p}-\boldsymbol{\kappa}_{\text{out}},s_2}^{\text{ex}\dagger} \hat{a}_{\mathbf{p}-\boldsymbol{\kappa}_{\text{in}},s_2}^{\text{ex}} + \hat{a}_{\mathbf{p}-\boldsymbol{\kappa}_{\text{in}},s_2}^{\text{ex}\dagger} \hat{a}_{\mathbf{p}-\boldsymbol{\kappa}_{\text{out}},s_2}^{\text{ex}}] \right. \\ &\quad \left. - [\hat{a}_{\mathbf{k},s_1}^{\text{ex}\dagger} \hat{a}_{\mathbf{k}-\boldsymbol{\kappa}_{\text{out}},s_1}^{\text{gr}}, \hat{a}_{\mathbf{p}-\boldsymbol{\kappa}_{\text{out}},s_2}^{\text{gr}\dagger} \hat{a}_{\mathbf{p}-\boldsymbol{\kappa}_{\text{in}},s_2}^{\text{gr}} + \hat{a}_{\mathbf{p}-\boldsymbol{\kappa}_{\text{in}},s_2}^{\text{gr}\dagger} \hat{a}_{\mathbf{p}-\boldsymbol{\kappa}_{\text{out}},s_2}^{\text{gr}}] - \text{H.c.} \right). \end{aligned} \quad (\text{A.30})$$



Using fundamental bosonic (upper sign) commutation relations (1.70) or fermionic (lower sign) anticommutation relations (1.71), we exemplarily calculate the first part of the first commutator in (A.30),

$$\begin{aligned}
 & \left[ \hat{a}_{\mathbf{k},s_1}^{\text{ex}\dagger} \hat{a}_{\mathbf{k}-\boldsymbol{\kappa}_{\text{out}},s_1}^{\text{gr}}, \hat{a}_{\mathbf{p}-\boldsymbol{\kappa}_{\text{out}},s_2}^{\text{ex}\dagger} \hat{a}_{\mathbf{p}-\boldsymbol{\kappa}_{\text{in}},s_2}^{\text{ex}} \right] \\
 &= \hat{a}_{\mathbf{k}-\boldsymbol{\kappa}_{\text{out}},s_1}^{\text{gr}} \left( \hat{a}_{\mathbf{k},s_1}^{\text{ex}\dagger} \hat{a}_{\mathbf{p}-\boldsymbol{\kappa}_{\text{out}},s_2}^{\text{ex}\dagger} \hat{a}_{\mathbf{p}-\boldsymbol{\kappa}_{\text{in}},s_2}^{\text{ex}} - \hat{a}_{\mathbf{p}-\boldsymbol{\kappa}_{\text{out}},s_2}^{\text{ex}\dagger} \hat{a}_{\mathbf{p}-\boldsymbol{\kappa}_{\text{in}},s_2}^{\text{ex}} \hat{a}_{\mathbf{k},s_1}^{\text{ex}\dagger} \right) \\
 &= \hat{a}_{\mathbf{k}-\boldsymbol{\kappa}_{\text{out}},s_1}^{\text{gr}} \left( \hat{a}_{\mathbf{k},s_1}^{\text{ex}\dagger} \hat{a}_{\mathbf{p}-\boldsymbol{\kappa}_{\text{out}},s_2}^{\text{ex}\dagger} \hat{a}_{\mathbf{p}-\boldsymbol{\kappa}_{\text{in}},s_2}^{\text{ex}} - \hat{a}_{\mathbf{p}-\boldsymbol{\kappa}_{\text{out}},s_2}^{\text{ex}\dagger} \left[ +\delta_{\mathbf{k},\mathbf{p}-\boldsymbol{\kappa}_{\text{in}}} \delta_{s_1 s_2} \pm \hat{a}_{\mathbf{k},s_1}^{\text{ex}\dagger} \hat{a}_{\mathbf{p}-\boldsymbol{\kappa}_{\text{in}},s_2}^{\text{ex}} \right] \right) \\
 &= -\delta_{\mathbf{k},\mathbf{p}-\boldsymbol{\kappa}_{\text{in}}} \delta_{s_1 s_2} \hat{a}_{\mathbf{p}-\boldsymbol{\kappa}_{\text{out}},s_2}^{\text{ex}\dagger} \hat{a}_{\mathbf{k}-\boldsymbol{\kappa}_{\text{out}},s_1}^{\text{gr}}, \tag{A.31}
 \end{aligned}$$

and the first part of the second commutator in (A.30), i.e.,

$$\begin{aligned}
 & \left[ \hat{a}_{\mathbf{k},s_1}^{\text{ex}\dagger} \hat{a}_{\mathbf{k}-\boldsymbol{\kappa}_{\text{out}},s_1}^{\text{gr}}, \hat{a}_{\mathbf{p}-\boldsymbol{\kappa}_{\text{out}},s_2}^{\text{gr}\dagger} \hat{a}_{\mathbf{p}-\boldsymbol{\kappa}_{\text{in}},s_2}^{\text{gr}} \right] \\
 &= \hat{a}_{\mathbf{k},s_1}^{\text{ex}\dagger} \left( \hat{a}_{\mathbf{k}-\boldsymbol{\kappa}_{\text{out}},s_1}^{\text{gr}} \hat{a}_{\mathbf{p}-\boldsymbol{\kappa}_{\text{out}},s_2}^{\text{gr}\dagger} \hat{a}_{\mathbf{p}-\boldsymbol{\kappa}_{\text{in}},s_2}^{\text{gr}} - \hat{a}_{\mathbf{p}-\boldsymbol{\kappa}_{\text{out}},s_2}^{\text{gr}\dagger} \hat{a}_{\mathbf{p}-\boldsymbol{\kappa}_{\text{in}},s_2}^{\text{gr}} \hat{a}_{\mathbf{k}-\boldsymbol{\kappa}_{\text{out}},s_1}^{\text{gr}} \right) \\
 &= \hat{a}_{\mathbf{k},s_1}^{\text{ex}\dagger} \left( \hat{a}_{\mathbf{k}-\boldsymbol{\kappa}_{\text{out}},s_1}^{\text{gr}} \hat{a}_{\mathbf{p}-\boldsymbol{\kappa}_{\text{out}},s_2}^{\text{gr}\dagger} \hat{a}_{\mathbf{p}-\boldsymbol{\kappa}_{\text{in}},s_2}^{\text{gr}} \mp \left[ \mp \delta_{\mathbf{k}\mathbf{p}} \delta_{s_1 s_2} \pm \hat{a}_{\mathbf{k}-\boldsymbol{\kappa}_{\text{out}},s_1}^{\text{gr}} \hat{a}_{\mathbf{p}-\boldsymbol{\kappa}_{\text{out}},s_2}^{\text{gr}\dagger} \right] \hat{a}_{\mathbf{p}-\boldsymbol{\kappa}_{\text{in}},s_2}^{\text{gr}} \right) \\
 &= \delta_{\mathbf{k}\mathbf{p}} \delta_{s_1 s_2} \hat{a}_{\mathbf{k},s_1}^{\text{ex}\dagger} \hat{a}_{\mathbf{p}-\boldsymbol{\kappa}_{\text{in}},s_2}^{\text{gr}}. \tag{A.32}
 \end{aligned}$$

The remaining parts of the commutators in (A.30) can be calculated analogously, as only  $\boldsymbol{\kappa}_{\text{in}}$  and  $\boldsymbol{\kappa}_{\text{out}}$  are exchanged in the indices. Altogether, and with the definition (4.16), we obtain the result (4.15):

$$\begin{aligned}
 & \left[ \hat{\Sigma}^x(\boldsymbol{\kappa}_{\text{out}}), \hat{\Sigma}_D^z(\boldsymbol{\kappa}_{\text{out}}, \boldsymbol{\kappa}_{\text{in}}) \right] \\
 &= -\frac{1}{8} \sum_{\mathbf{k}\mathbf{p},s_1 s_2} \left( \delta_{\mathbf{k},\mathbf{p}-\boldsymbol{\kappa}_{\text{in}}} \delta_{s_1 s_2} \hat{a}_{\mathbf{p}-\boldsymbol{\kappa}_{\text{out}},s_2}^{\text{ex}\dagger} \hat{a}_{\mathbf{k}-\boldsymbol{\kappa}_{\text{out}},s_1}^{\text{gr}} + \delta_{\mathbf{k},\mathbf{p}-\boldsymbol{\kappa}_{\text{out}}} \delta_{s_1 s_2} \hat{a}_{\mathbf{p}-\boldsymbol{\kappa}_{\text{in}},s_2}^{\text{ex}\dagger} \hat{a}_{\mathbf{k}-\boldsymbol{\kappa}_{\text{out}},s_1}^{\text{gr}} \right. \\
 &\quad \left. + \delta_{\mathbf{k}\mathbf{p}} \delta_{s_1 s_2} \hat{a}_{\mathbf{k},s_1}^{\text{ex}\dagger} \hat{a}_{\mathbf{p}-\boldsymbol{\kappa}_{\text{in}},s_2}^{\text{gr}} + \delta_{\mathbf{k}-\boldsymbol{\kappa}_{\text{out}},\mathbf{p}-\boldsymbol{\kappa}_{\text{in}}} \delta_{s_1 s_2} \hat{a}_{\mathbf{k},s_1}^{\text{ex}\dagger} \hat{a}_{\mathbf{p}-\boldsymbol{\kappa}_{\text{out}},s_2}^{\text{gr}} - \text{H.c.} \right) \\
 &= -\frac{1}{4} \sum_{\mathbf{p},s} \left( \hat{a}_{\mathbf{p},s}^{\text{ex}\dagger} \hat{a}_{\mathbf{p}-\boldsymbol{\kappa}_{\text{in}},s}^{\text{gr}} + \hat{a}_{\mathbf{p},s}^{\text{ex}\dagger} \hat{a}_{\mathbf{p}-2\boldsymbol{\kappa}_{\text{out}}+\boldsymbol{\kappa}_{\text{in}},s}^{\text{gr}} - \text{H.c.} \right) \\
 &= -\frac{i}{2} \left[ \hat{\Sigma}^y(\boldsymbol{\kappa}_{\text{in}}) + \hat{\Sigma}^y(2\boldsymbol{\kappa}_{\text{out}} - \boldsymbol{\kappa}_{\text{in}}) \right] = -i \hat{\Sigma}_D^y(\boldsymbol{\kappa}_{\text{out}}, \boldsymbol{\kappa}_{\text{in}}), \tag{A.33}
 \end{aligned}$$

where the quasispin  $Y$  operator (1.65) has been identified, and indices of individual terms have been shifted by reciprocal lattice vectors  $\pm\boldsymbol{\kappa}_{\text{in}}/\boldsymbol{\kappa}_{\text{out}}$  again in order to simplify the expression.

### A.5.3. Calculation of the third ( $m = 3$ ) commutator

Finally, let us calculate the third commutator (4.17), i.e., the commutator between the  $\hat{\Sigma}^x(\boldsymbol{\kappa}_{\text{out}})$  quasispin operator (1.64) and the result of the second commutator, that is the  $\hat{\Sigma}_D^y(\boldsymbol{\kappa}_{\text{out}}, \boldsymbol{\kappa}_{\text{in}})$  quasispin operator (4.16):

$$\begin{aligned} [\hat{\Sigma}^x(\boldsymbol{\kappa}_{\text{out}}), \hat{\Sigma}_D^y(\boldsymbol{\kappa}_{\text{out}}, \boldsymbol{\kappa}_{\text{in}})] &= \frac{1}{2}([\hat{\Sigma}^x(\boldsymbol{\kappa}_{\text{out}}), \hat{\Sigma}^y(\boldsymbol{\kappa}_{\text{in}})] + [\hat{\Sigma}^x(\boldsymbol{\kappa}_{\text{out}}), \hat{\Sigma}^y(2\boldsymbol{\kappa}_{\text{out}} - \boldsymbol{\kappa}_{\text{in}})]) \\ &= \frac{i}{2}(\hat{\Sigma}_D^z(\boldsymbol{\kappa}_{\text{out}}, \boldsymbol{\kappa}_{\text{in}}) + \hat{\Sigma}_D^z(\boldsymbol{\kappa}_{\text{out}}, 2\boldsymbol{\kappa}_{\text{out}} - \boldsymbol{\kappa}_{\text{in}})) \\ &= i\hat{\Sigma}_D^z(\boldsymbol{\kappa}_{\text{out}}, \boldsymbol{\kappa}_{\text{in}}), \end{aligned} \quad (\text{A.34})$$

where we first employed the result (4.13) of the first commutator and then made use of the property  $\hat{\Sigma}_D^z(\boldsymbol{\kappa}_{\text{out}}, 2\boldsymbol{\kappa}_{\text{out}} - \boldsymbol{\kappa}_{\text{in}}) = \hat{\Sigma}_D^z(\boldsymbol{\kappa}_{\text{out}}, \boldsymbol{\kappa}_{\text{in}})$ , which is clear from the definition (4.14).

## A.6. Commutators of $\hat{\Sigma}^x(\boldsymbol{\kappa}_{\text{in}})$ and $\hat{\Sigma}_J^y(\boldsymbol{\kappa}_{\text{in}})$

### A.6.1. Calculation of the first ( $m = 1$ ) commutator

In this subsection we are going to explicitly calculate the first commutator (4.34) between the usual  $\hat{\Sigma}^x(\boldsymbol{\kappa}_{\text{in}})$  quasispin operator (1.64) and the tunneling-evolved  $\hat{\Sigma}_J^y(\boldsymbol{\kappa}_{\text{in}})$  quasispin operator (4.30), i.e.,

$$\begin{aligned} &[\hat{\Sigma}^x(\boldsymbol{\kappa}_{\text{in}}), \hat{\Sigma}_J^y(\boldsymbol{\kappa}_{\text{in}})] \\ &= \frac{1}{4i} \sum_{\mathbf{k}\mathbf{p}, s_1 s_2} [\hat{a}_{\mathbf{k}, s_1}^{\text{ex}\dagger} \hat{a}_{\mathbf{k}-\boldsymbol{\kappa}_{\text{in}}, s_1}^{\text{gr}} + \text{H.c.}, \hat{a}_{\mathbf{p}, s_2}^{\text{ex}\dagger} \hat{a}_{\mathbf{p}-\boldsymbol{\kappa}_{\text{in}}, s_2}^{\text{gr}} \exp\{i\phi_{\mathbf{p}}^{\boldsymbol{\kappa}_{\text{in}}}(\Delta t)\} - \text{H.c.}] \\ &= \frac{1}{4i} \sum_{\mathbf{k}\mathbf{p}, s_1 s_2} \left( \exp\{i\phi_{\mathbf{p}}^{\boldsymbol{\kappa}_{\text{in}}}(\Delta t)\} ([\hat{a}_{\mathbf{k}, s_1}^{\text{ex}\dagger} \hat{a}_{\mathbf{k}-\boldsymbol{\kappa}_{\text{in}}, s_1}^{\text{gr}}, \hat{a}_{\mathbf{p}, s_2}^{\text{ex}\dagger} \hat{a}_{\mathbf{p}-\boldsymbol{\kappa}_{\text{in}}, s_2}^{\text{gr}}] \right. \\ &\quad \left. + [\hat{a}_{\mathbf{k}, s_1}^{\text{ex}} \hat{a}_{\mathbf{k}-\boldsymbol{\kappa}_{\text{in}}, s_1}^{\text{gr}\dagger}, \hat{a}_{\mathbf{p}, s_2}^{\text{ex}\dagger} \hat{a}_{\mathbf{p}-\boldsymbol{\kappa}_{\text{in}}, s_2}^{\text{gr}}] \right) \\ &\quad - \exp\{-i\phi_{\mathbf{p}}^{\boldsymbol{\kappa}_{\text{in}}}(\Delta t)\} ([\hat{a}_{\mathbf{k}, s_1}^{\text{ex}\dagger} \hat{a}_{\mathbf{k}-\boldsymbol{\kappa}_{\text{in}}, s_1}^{\text{gr}}, \hat{a}_{\mathbf{p}, s_2}^{\text{ex}} \hat{a}_{\mathbf{p}-\boldsymbol{\kappa}_{\text{in}}, s_2}^{\text{gr}\dagger}] \\ &\quad \left. + [\hat{a}_{\mathbf{k}, s_1}^{\text{ex}} \hat{a}_{\mathbf{k}-\boldsymbol{\kappa}_{\text{in}}, s_1}^{\text{gr}\dagger}, \hat{a}_{\mathbf{p}, s_2}^{\text{ex}} \hat{a}_{\mathbf{p}-\boldsymbol{\kappa}_{\text{in}}, s_2}^{\text{gr}\dagger}] \right). \end{aligned} \quad (\text{A.35})$$

Note that operators relating to different species  $\lambda \in \{\text{gr}, \text{ex}\}$  always commute. Thus, and due to the fact that two creation or annihilation operators (of the same species) always either commute (1.70) or anticommute (1.71), the first and the last commutator vanish. Employing bosonic commutation relations (1.70) or fermionic anti-

commutation relations (1.71) again, we prepare for the remaining two commutators:

$$\begin{aligned}
\hat{a}_{\boldsymbol{p},s_2}^{\text{ex}\dagger} \hat{a}_{\boldsymbol{p}-\boldsymbol{\kappa}_{\text{in}},s_2}^{\text{gr}} \hat{a}_{\boldsymbol{k},s_1}^{\text{ex}} \hat{a}_{\boldsymbol{k}-\boldsymbol{\kappa}_{\text{in}},s_1}^{\text{gr}\dagger} &= (\mp \delta_{\boldsymbol{k}\boldsymbol{p}} \delta_{s_1 s_2} \pm \hat{a}_{\boldsymbol{k},s_1}^{\text{ex}} \hat{a}_{\boldsymbol{p},s_2}^{\text{ex}\dagger}) (\delta_{\boldsymbol{k}\boldsymbol{p}} \delta_{s_1 s_2} \pm \hat{a}_{\boldsymbol{k}-\boldsymbol{\kappa}_{\text{in}},s_1}^{\text{gr}\dagger} \hat{a}_{\boldsymbol{p}-\boldsymbol{\kappa}_{\text{in}},s_2}^{\text{gr}}) \\
&= \delta_{\boldsymbol{k}\boldsymbol{p}} \delta_{s_1 s_2} \left( -\hat{a}_{\boldsymbol{k}-\boldsymbol{\kappa}_{\text{in}},s_1}^{\text{gr}\dagger} \hat{a}_{\boldsymbol{p}-\boldsymbol{\kappa}_{\text{in}},s_2}^{\text{gr}} \pm \hat{a}_{\boldsymbol{k},s_1}^{\text{ex}} \hat{a}_{\boldsymbol{p},s_2}^{\text{ex}\dagger} \mp 1 \right) + \hat{a}_{\boldsymbol{k},s_1}^{\text{ex}} \hat{a}_{\boldsymbol{p},s_2}^{\text{ex}\dagger} \hat{a}_{\boldsymbol{k}-\boldsymbol{\kappa}_{\text{in}},s_1}^{\text{gr}\dagger} \hat{a}_{\boldsymbol{p}-\boldsymbol{\kappa}_{\text{in}},s_2}^{\text{gr}} \\
&= \delta_{\boldsymbol{k}\boldsymbol{p}} \delta_{s_1 s_2} \left( \hat{n}_{\boldsymbol{p},s_1}^{\text{ex}} - \hat{n}_{\boldsymbol{p}-\boldsymbol{\kappa}_{\text{in}},s_1}^{\text{gr}} \right) + \hat{a}_{\boldsymbol{k},s_1}^{\text{ex}} \hat{a}_{\boldsymbol{k}-\boldsymbol{\kappa}_{\text{in}},s_1}^{\text{gr}\dagger} \hat{a}_{\boldsymbol{p},s_2}^{\text{ex}\dagger} \hat{a}_{\boldsymbol{p}-\boldsymbol{\kappa}_{\text{in}},s_2}^{\text{gr}}, \tag{A.36}
\end{aligned}$$

where the upper written sign coincides with the bosonic case and the lower written sign represents the fermionic case. As a result, we obtain the second commutator in (A.35),

$$\begin{aligned}
[\hat{a}_{\boldsymbol{k},s_1}^{\text{ex}} \hat{a}_{\boldsymbol{k}-\boldsymbol{\kappa}_{\text{in}},s_1}^{\text{gr}\dagger}, \hat{a}_{\boldsymbol{p},s_2}^{\text{ex}\dagger} \hat{a}_{\boldsymbol{p}-\boldsymbol{\kappa}_{\text{in}},s_2}^{\text{gr}}] &= \hat{a}_{\boldsymbol{k},s_1}^{\text{ex}} \hat{a}_{\boldsymbol{k}-\boldsymbol{\kappa}_{\text{in}},s_1}^{\text{gr}\dagger} \hat{a}_{\boldsymbol{p},s_2}^{\text{ex}\dagger} \hat{a}_{\boldsymbol{p}-\boldsymbol{\kappa}_{\text{in}},s_2}^{\text{gr}} - \hat{a}_{\boldsymbol{p},s_2}^{\text{ex}\dagger} \hat{a}_{\boldsymbol{p}-\boldsymbol{\kappa}_{\text{in}},s_2}^{\text{gr}} \hat{a}_{\boldsymbol{k},s_1}^{\text{ex}} \hat{a}_{\boldsymbol{k}-\boldsymbol{\kappa}_{\text{in}},s_1}^{\text{gr}\dagger} \\
&= -\delta_{\boldsymbol{k}\boldsymbol{p}} \delta_{s_1 s_2} \left( \hat{n}_{\boldsymbol{p},s_1}^{\text{ex}} - \hat{n}_{\boldsymbol{p}-\boldsymbol{\kappa}_{\text{in}},s_1}^{\text{gr}} \right), \tag{A.37}
\end{aligned}$$

and from the second commutator (A.37) we may also get the third commutator in (A.35) by swapping indices and using anticommutativity,

$$[\hat{a}_{\boldsymbol{k},s_1}^{\text{ex}\dagger} \hat{a}_{\boldsymbol{k}-\boldsymbol{\kappa}_{\text{in}},s_1}^{\text{gr}}, \hat{a}_{\boldsymbol{p},s_2}^{\text{ex}} \hat{a}_{\boldsymbol{p}-\boldsymbol{\kappa}_{\text{in}},s_2}^{\text{gr}\dagger}] = \delta_{\boldsymbol{k}\boldsymbol{p}} \delta_{s_1 s_2} \left( \hat{n}_{\boldsymbol{p},s_1}^{\text{ex}} - \hat{n}_{\boldsymbol{p}-\boldsymbol{\kappa}_{\text{in}},s_1}^{\text{gr}} \right). \tag{A.38}$$

Inserting these two nonzero commutators (A.37) and (A.38) into the expression (A.35), we immediately obtain the result (4.34) for the first commutator between  $\hat{\Sigma}^x(\boldsymbol{\kappa}_{\text{in}})$  and  $\hat{\Sigma}_J^y(\boldsymbol{\kappa}_{\text{in}})$ , i.e.,

$$\begin{aligned}
[\hat{\Sigma}^x(\boldsymbol{\kappa}_{\text{in}}), \hat{\Sigma}_J^y(\boldsymbol{\kappa}_{\text{in}})] &= -\frac{1}{4i} \sum_{\boldsymbol{p},s} \left( \exp \{ i \phi_{\boldsymbol{p}}^{\boldsymbol{\kappa}_{\text{in}}}(\Delta t) \} + \text{H.c.} \right) \left( \hat{n}_{\boldsymbol{p},s}^{\text{ex}} - \hat{n}_{\boldsymbol{p}-\boldsymbol{\kappa}_{\text{in}},s}^{\text{gr}} \right) \\
&= i \hat{\Sigma}_C^z(\boldsymbol{\kappa}_{\text{in}}), \tag{A.39}
\end{aligned}$$

with the definition (4.37).

### A.6.2. Calculation of the second ( $m = 2$ ) commutator

Now we calculate the second commutator (4.35), i.e., the commutator between the  $\hat{\Sigma}^x(\boldsymbol{\kappa}_{\text{in}})$  quasispin operator (1.64) and the result of the first commutator, that is the  $\hat{\Sigma}_C^z(\boldsymbol{\kappa}_{\text{in}})$  quasispin operator (4.37). Splitting up the commutator according to the

Hermitian conjugate parts yields:

$$\begin{aligned}
& [\hat{\Sigma}^x(\boldsymbol{\kappa}_{\text{in}}), \hat{\Sigma}_C^z(\boldsymbol{\kappa}_{\text{in}})] \\
&= \frac{1}{4} \sum_{\mathbf{k}, s_1, s_2} [\hat{a}_{\mathbf{k}, s_1}^{\text{ex} \dagger} \hat{a}_{\mathbf{k}-\boldsymbol{\kappa}_{\text{in}}, s_1}^{\text{gr}} + \text{H.c.}, \hat{n}_{\mathbf{p}, s_2}^{\text{ex}} - \hat{n}_{\mathbf{p}-\boldsymbol{\kappa}_{\text{in}}, s_2}^{\text{gr}}] \cos \{ \phi_{\mathbf{p}}^{\boldsymbol{\kappa}_{\text{in}}}(\Delta t) \} \\
&= \frac{1}{4} \sum_{\mathbf{k}, s_1, s_2} \cos \{ \phi_{\mathbf{p}}^{\boldsymbol{\kappa}_{\text{in}}}(\Delta t) \} \left( [\hat{a}_{\mathbf{k}, s_1}^{\text{ex} \dagger} \hat{a}_{\mathbf{k}-\boldsymbol{\kappa}_{\text{in}}, s_1}^{\text{gr}}, \hat{n}_{\mathbf{p}, s_2}^{\text{ex}} - \hat{n}_{\mathbf{p}-\boldsymbol{\kappa}_{\text{in}}, s_2}^{\text{gr}}] \right. \\
&\quad \left. + [\hat{a}_{\mathbf{k}, s_1}^{\text{ex}} \hat{a}_{\mathbf{k}-\boldsymbol{\kappa}_{\text{in}}, s_1}^{\text{gr} \dagger}, \hat{n}_{\mathbf{p}, s_2}^{\text{ex}} - \hat{n}_{\mathbf{p}-\boldsymbol{\kappa}_{\text{in}}, s_2}^{\text{gr}}] \right). \quad (\text{A.40})
\end{aligned}$$

The result of the commutators in (A.40) is obvious, as the combined number count  $\hat{n}_{\mathbf{p}, s_2}^{\text{ex}} - \hat{n}_{\mathbf{p}-\boldsymbol{\kappa}_{\text{in}}, s_2}^{\text{gr}}$  is only affected by the left part for  $\mathbf{k} = \mathbf{p}$  and  $s_1 = s_2$ , i.e.,

$$[\hat{a}_{\mathbf{k}, s_1}^{\text{ex} \dagger} \hat{a}_{\mathbf{k}-\boldsymbol{\kappa}_{\text{in}}, s_1}^{\text{gr}}, \hat{n}_{\mathbf{p}, s_2}^{\text{ex}} - \hat{n}_{\mathbf{p}-\boldsymbol{\kappa}_{\text{in}}, s_2}^{\text{gr}}] = -2\delta_{\mathbf{k}\mathbf{p}} \delta_{s_1 s_2} \hat{a}_{\mathbf{k}, s_1}^{\text{ex} \dagger} \hat{a}_{\mathbf{k}-\boldsymbol{\kappa}_{\text{in}}, s_1}^{\text{gr}}, \quad (\text{A.41})$$

$$[\hat{a}_{\mathbf{k}, s_1}^{\text{ex}} \hat{a}_{\mathbf{k}-\boldsymbol{\kappa}_{\text{in}}, s_1}^{\text{gr} \dagger}, \hat{n}_{\mathbf{p}, s_2}^{\text{ex}} - \hat{n}_{\mathbf{p}-\boldsymbol{\kappa}_{\text{in}}, s_2}^{\text{gr}}] = +2\delta_{\mathbf{k}\mathbf{p}} \delta_{s_1 s_2} \hat{a}_{\mathbf{k}, s_1}^{\text{ex}} \hat{a}_{\mathbf{k}-\boldsymbol{\kappa}_{\text{in}}, s_1}^{\text{gr} \dagger}. \quad (\text{A.42})$$

Inserting these two commutators (A.41) and (A.42) into the expression (A.40), we obtain the result (4.35),

$$\begin{aligned}
[\hat{\Sigma}^x(\boldsymbol{\kappa}_{\text{in}}), \hat{\Sigma}_C^z(\boldsymbol{\kappa}_{\text{in}})] &= -\frac{1}{2} \sum_{\mathbf{p}, s} \cos \{ \phi_{\mathbf{p}}^{\boldsymbol{\kappa}_{\text{in}}}(\Delta t) \} (\hat{a}_{\mathbf{p}, s}^{\text{ex} \dagger} \hat{a}_{\mathbf{p}-\boldsymbol{\kappa}_{\text{in}}, s}^{\text{gr}} - \hat{a}_{\mathbf{p}, s}^{\text{ex}} \hat{a}_{\mathbf{p}-\boldsymbol{\kappa}_{\text{in}}, s}^{\text{gr} \dagger}) \\
&= -i\hat{\Sigma}_C^y(\boldsymbol{\kappa}_{\text{in}}), \quad (\text{A.43})
\end{aligned}$$

with the definition (4.38).

### A.6.3. Calculation of the third ( $m = 3$ ) commutator

Finally, we calculate the third commutator (4.36), i.e., the commutator between the  $\hat{\Sigma}^x(\boldsymbol{\kappa}_{\text{in}})$  quasispin operator (1.64) and the result of the second commutator, that is the  $\hat{\Sigma}_C^y(\boldsymbol{\kappa}_{\text{in}})$  quasispin operator (4.38). The calculation is very similar to the calculation of the first commutator (A.35), as the same (lower-level) commutators, e.g.,

the commutators (A.37) and (A.38), appear. We then go on to calculate

$$\begin{aligned}
& [\hat{\Sigma}^x(\boldsymbol{\kappa}_{\text{in}}), \hat{\Sigma}_C^y(\boldsymbol{\kappa}_{\text{in}})] \\
&= \frac{1}{4i} \sum_{\mathbf{k}\mathbf{p}, s_1 s_2} \left[ \hat{a}_{\mathbf{k}, s_1}^{\text{ex} \dagger} \hat{a}_{\mathbf{k}-\boldsymbol{\kappa}_{\text{in}}, s_1}^{\text{gr}} + \text{H.c.}, \hat{a}_{\mathbf{p}, s_2}^{\text{ex} \dagger} \hat{a}_{\mathbf{p}-\boldsymbol{\kappa}_{\text{in}}, s_2}^{\text{gr}} - \text{H.c.} \right] \cos \{ \phi_{\mathbf{p}}^{\boldsymbol{\kappa}_{\text{in}}}(\Delta t) \} \\
&= \frac{1}{4i} \sum_{\mathbf{k}\mathbf{p}, s_1 s_2} \cos \{ \phi_{\mathbf{p}}^{\boldsymbol{\kappa}_{\text{in}}}(\Delta t) \} \times \\
&\quad \times \left( \left[ \hat{a}_{\mathbf{k}, s_1}^{\text{ex} \dagger} \hat{a}_{\mathbf{k}-\boldsymbol{\kappa}_{\text{in}}, s_1}^{\text{gr}}, \hat{a}_{\mathbf{p}, s_2}^{\text{ex} \dagger} \hat{a}_{\mathbf{p}-\boldsymbol{\kappa}_{\text{in}}, s_2}^{\text{gr}} \right] + \left[ \hat{a}_{\mathbf{k}, s_1}^{\text{ex}} \hat{a}_{\mathbf{k}-\boldsymbol{\kappa}_{\text{in}}, s_1}^{\text{gr} \dagger}, \hat{a}_{\mathbf{p}, s_2}^{\text{ex} \dagger} \hat{a}_{\mathbf{p}-\boldsymbol{\kappa}_{\text{in}}, s_2}^{\text{gr}} \right] \right. \\
&\quad \left. - \left[ \hat{a}_{\mathbf{k}, s_1}^{\text{ex} \dagger} \hat{a}_{\mathbf{k}-\boldsymbol{\kappa}_{\text{in}}, s_1}^{\text{gr}}, \hat{a}_{\mathbf{p}, s_2}^{\text{ex}} \hat{a}_{\mathbf{p}-\boldsymbol{\kappa}_{\text{in}}, s_2}^{\text{gr} \dagger} \right] - \left[ \hat{a}_{\mathbf{k}, s_1}^{\text{ex}} \hat{a}_{\mathbf{k}-\boldsymbol{\kappa}_{\text{in}}, s_1}^{\text{gr} \dagger}, \hat{a}_{\mathbf{p}, s_2}^{\text{ex} \dagger} \hat{a}_{\mathbf{p}-\boldsymbol{\kappa}_{\text{in}}, s_2}^{\text{gr}} \right] \right) \\
&= -\frac{1}{2i} \sum_{\mathbf{p}, s} \cos \{ \phi_{\mathbf{p}}^{\boldsymbol{\kappa}_{\text{in}}}(\Delta t) \} (\hat{n}_{\mathbf{p}, s}^{\text{ex}} - \hat{n}_{\mathbf{p}-\boldsymbol{\kappa}_{\text{in}}, s}^{\text{gr}}) = i \hat{\Sigma}_C^z(\boldsymbol{\kappa}_{\text{in}}), \tag{A.44}
\end{aligned}$$

where we have used the previously obtained results of the commutators (A.37, A.38) and the definition (4.37).

## A.7. Real and imaginary part of the phase sum

It has already been shown in section 2.3.1 that the phase sum (2.59),

$$\mathcal{J}_{\boldsymbol{\kappa}}(\Delta t) = \frac{1}{N} \sum_{\mathbf{p}} \exp \{ iJ/Z(T_{\mathbf{p}} - T_{\mathbf{p}-\boldsymbol{\kappa}})\Delta t \}, \tag{A.45}$$

can be approximated via Bessel functions (2.66) when the wave vector  $\boldsymbol{\kappa}$  is small compared to the inverse lattice spacing  $1/\ell$ , and the number of lattice sites per dimension is large,  $L \gg 1$ . As the resulting Bessel functions are real, it is evident that the imaginary part of (A.45) has to be negligible. This can also be demonstrated analytically. First, remember that the Fourier transform of the adjacency matrix (1.58) consists of a sum of cosine functions for the vector components,

$$T_{\mathbf{p}} = 2 \left[ \cos(p_x \ell) + \cos(p_y \ell) \right], \tag{A.46}$$

i.e., it is  $2\pi$ -periodic in  $p_x/y \ell$  and even, where  $T_{\mathbf{p}} = T_{-\mathbf{p}}$ . When we then redefine the summation index via  $\tilde{\mathbf{p}} = -\mathbf{p} + \boldsymbol{\kappa}$ , where  $\boldsymbol{\kappa}$  is a reciprocal lattice vector, the set of vectors for the summation over  $\tilde{\mathbf{p}}$  is technically altered accordingly. However, due to the  $2\pi$ -periodicity in (A.46), we can just as well sum over the same set as for  $\mathbf{p}$  before, i.e., over the first Brillouin zone. In a third step, we use the fact that sine is

an odd function. Altogether we find:

$$\begin{aligned}
 N \operatorname{Im} [\mathcal{J}_\kappa(\Delta t)] &= \sum_p \sin \{J/Z(T_p - T_{p-\kappa})\Delta t\} \\
 &= \sum_p \sin \{J/Z(T_{-p} - T_{-p+\kappa})\Delta t\} \\
 &= \sum_{\tilde{p}} \sin \{J/Z(T_{\tilde{p}-\kappa} - T_{\tilde{p}})\Delta t\} \\
 &= -\sum_{\tilde{p}} \sin \{J/Z(T_{\tilde{p}} - T_{\tilde{p}-\kappa})\Delta t\} = -N \operatorname{Im} [\mathcal{J}_\kappa(\Delta t)], \quad (\text{A.47})
 \end{aligned}$$

i.e.,  $\operatorname{Im}[\mathcal{J}_\kappa(\Delta t)] = 0$ . In conclusion, the phase sum (2.59) can be expressed solely via its real part, that is,

$$\mathcal{J}_\kappa(\Delta t) = \operatorname{Re} [\mathcal{J}_\kappa(\Delta t)] = \frac{1}{N} \sum_p \cos \{J/Z(T_p - T_{p-\kappa})\Delta t\}, \quad (\text{A.48})$$

a fact which we use in (4.49) in section 4.4.3.

# Bibliography

- [1] N. ten Brinke, R. Schützhold, “*Dicke superradiance as a nondestructive probe for quantum quenches in optical lattices*”, *Physical Review A* **92**, 013617 (2015).
- [2] N. ten Brinke, R. Schützhold, “*Dicke superradiance as nondestructive probe for the state of atoms in optical lattices*”, *European Physical Journal D* **70**, 102 (2016).
- [3] N. ten Brinke, R. Schützhold, D. Habs, “*Feasibility study of a nuclear exciton laser*”, *Physical Review A* **87**, 053814 (2013).
- [4] N. ten Brinke, M. Ligges, U. Bovensiepen, R. Schützhold, “*Multiple particle-hole pair creation in the Fermi-Hubbard model by a pump laser*”, submitted to *Physical Review B* (2016), arXiv:1602.00871.
- [5] P.S. Jessen, I.H. Deutsch, “*Optical lattices*” in *Advances in Atomic, Molecular, and Optical Physics*, vol. 37, edited by B. Bederson and H. Walther (Academic Press, 1996), pp. 95–138.
- [6] I. Bloch, “*Quantum gases in optical lattices*”, *Physics World* **17**, 25 (2004).
- [7] I. Bloch, “*Ultracold quantum gases in optical lattices*”, *Nature Physics* **1**, 23 (2005).
- [8] P.S. Jessen, C. Gerz, P.D. Lett, W.D. Phillips, S.L. Rolston, R.J.C. Spreeuw, C.I. Westbrook, “*Observation of quantized motion of Rb atoms in an optical field*”, *Physical Review Letters* **69**, 49 (1992).
- [9] A. Hemmerich, T.W. Hänsch, “*Two-dimensional atomic crystal bound by light*”, *Physical Review Letters* **70**, 410 (1993).
- [10] I. Bloch, J. Dalibard, W. Zwerger, “*Many-body physics with ultracold gases*”, *Reviews of Modern Physics* **80**, 885 (2008).
- [11] D. Jaksch, C. Bruder, J.I. Cirac, C.W. Gardiner, P. Zoller, “*Cold bosonic atoms in optical lattices*”, *Physical Review Letters* **81**, 3108 (1998).
- [12] D. Jaksch, P. Zoller, “*The cold atom Hubbard toolbox*”, *Annals of Physics* **315**, 52 (2005).

- [13] M. Raizen, C. Salomon, Q. Niu, “*New light on quantum transport*”, *Physics Today* **50**, 30 (1997).
- [14] M. Lewenstein, A. Sanpera, V. Ahufinger, *Ultracold Atoms in Optical Lattices: Simulating quantum many-body systems* (Oxford University Press, Oxford, 2012).
- [15] R.P. Feynman, “*Simulating physics with computers*”, *International Journal of Theoretical Physics* **21**, 467 (1982).
- [16] R.P. Feynman, “*Quantum mechanical computers*”, *Optics News* **11**, 11 (1985).
- [17] R.P. Feynman, “*Quantum mechanical computers*”, *Foundations of Physics* **16**, 507 (1986).
- [18] D. Jaksch, H.J. Briegel, J.I. Cirac, C.W. Gardiner, P. Zoller, “*Entanglement of atoms via cold controlled collisions*”, *Physical Review Letters* **82**, 1975 (1999).
- [19] O. Mandel, M. Greiner, A. Widera, T. Rom, T.W. Hänsch, I. Bloch, “*Controlled collisions for multi-particle entanglement of optically trapped atoms*”, *Nature* **425**, 937 (2003).
- [20] R. Raussendorf, H.J. Briegel, “*A one-way quantum computer*”, *Physical Review Letters* **86**, 5188 (2001).
- [21] S. Sachdev, *Quantum Phase Transitions*, Second Edition (Cambridge University Press, Cambridge, 2011).
- [22] M.P.A. Fisher, P.B. Weichman, G. Grinstein, D.S. Fisher, “*Boson localization and the superfluid-insulator transition*”, *Physical Review B* **40**, 546 (1989).
- [23] W. Zwerger, “*Mott–Hubbard transition of cold atoms in optical lattices*”, *Journal of Optics B: Quantum and Semiclassical Optics* **5**, S9 (2003).
- [24] K.V. Krutitsky, “*Ultracold bosons with short-range interaction in regular optical lattices*”, *Physics Reports* **607**, 1 (2016).
- [25] M. Greiner, O. Mandel, T. Esslinger, T.W. Hänsch, I. Bloch, “*Quantum phase transition from a superfluid to a Mott insulator in a gas of ultracold atoms*”, *Nature* **415**, 39 (2002).



- [26] T. Stöferle, H. Moritz, C. Schori, M. Köhl, T. Esslinger, “*Transition from a strongly interacting 1D superfluid to a Mott insulator*”, *Physical Review Letters* **92**, 130403 (2004).
- [27] I.B. Spielman, W.D. Phillips, J.V. Porto, “*Mott-insulator transition in a two-dimensional atomic Bose gas*”, *Physical Review Letters* **98**, 080404 (2007).
- [28] N.F. Mott, “*Metal-insulator transition*”, *Reviews of Modern Physics* **40**, 677 (1968).
- [29] M. Imada, A. Fujimori, Y. Tokura, “*Metal-insulator transitions*”, *Reviews of Modern Physics* **70**, 1039 (1998).
- [30] J. Hubbard, “*Electron correlations in narrow energy bands*”, *Proceedings of the Royal Society of London A: Mathematical, Physical and Engineering Sciences* **276**, 238 (1963).
- [31] T. Esslinger, “*Fermi-Hubbard physics with atoms in an optical lattice*”, *Annual Review of Condensed Matter Physics* **1**, 129 (2010).
- [32] M. Köhl, H. Moritz, T. Stöferle, K. Günter, T. Esslinger, “*Fermionic atoms in a three dimensional optical lattice: observing Fermi surfaces, dynamics, and interactions*”, *Physical Review Letters* **94**, 080403 (2005).
- [33] U. Schneider, L. Hackermüller, S. Will, T. Best, I. Bloch, T.A. Costi, R.W. Helmes, D. Rasch, A. Rosch, “*Metallic and insulating phases of repulsively interacting fermions in a 3D optical lattice*”, *Science* **322**, 1520 (2008).
- [34] R. Jördens, N. Strohmaier, K. Günter, H. Moritz, T. Esslinger, “*A Mott insulator of fermionic atoms in an optical lattice*”, *Nature* **455**, 204 (2008).
- [35] D. Greif, M.F. Parsons, A. Mazurenko, C.S. Chiu, S. Blatt, F. Huber, G. Ji, M. Greiner, “*Site-resolved imaging of a fermionic Mott insulator*”, *Science* **351**, 953 (2016).
- [36] Y. Kato, Q. Zhou, N. Kawashima, N. Trivedi, “*Sharp peaks in the momentum distribution of bosons in optical lattices in the normal state*”, *Nature Physics* **4**, 617 (2008).
- [37] J. Stenger, S. Inouye, A.P. Chikkatur, D.M. Stamper-Kurn, D.E. Pritchard, W. Ketterle, “*Bragg spectroscopy of a Bose-Einstein condensate*”, *Physical Review Letters* **82**, 4569 (1999).

- [38] D. Clément, N. Fabbri, L. Fallani, C. Fort, M. Inguscio, “*Exploring correlated 1D Bose gases from the superfluid to the Mott-insulator state by inelastic light scattering*”, *Physical Review Letters* **102**, 155301 (2009).
- [39] P.T. Ernst, S. Götze, J.S. Krauser, K. Pyka, D.S. Lühmann, D. Pfannkuche, K. Sengstock, “*Probing superfluids in optical lattices by momentum-resolved Bragg spectroscopy*”, *Nature Physics* **6**, 56 (2010).
- [40] N. Gemelke, X. Zhang, C.L. Hung, C. Chin, “*In situ observation of incompressible Mott-insulating domains in ultracold atomic gases*”, *Nature* **460**, 995 (2009).
- [41] A. Itah, H. Veksler, O. Lahav, A. Blumkin, C. Moreno, C. Gordon, J. Steinhauer, “*Direct observation of a sub-Poissonian number distribution of atoms in an optical lattice*”, *Physical Review Letters* **104**, 113001 (2010).
- [42] J.F. Sherson, C. Weitenberg, M. Endres, M. Cheneau, I. Bloch, S. Kuhr, “*Single-atom-resolved fluorescence imaging of an atomic Mott insulator*”, *Nature* **467**, 68 (2010).
- [43] M. Endres, M. Cheneau, T. Fukuhara, C. Weitenberg, P. Schauß, C. Gross, L. Mazza, M.C. Bañuls, L. Pollet, I. Bloch et al., “*Single-site- and single-atom-resolved measurement of correlation functions*”, *Applied Physics B* **113**, 27 (2013).
- [44] G.K. Campbell, J. Mun, M. Boyd, P. Medley, A.E. Leanhardt, L.G. Marcassa, D.E. Pritchard, W. Ketterle, “*Imaging the Mott insulator shells by using atomic clock shifts*”, *Science* **313**, 649 (2006).
- [45] H. Miyake, G.A. Siviloglou, G. Puentes, D.E. Pritchard, W. Ketterle, D.M. Weld, “*Bragg scattering as a probe of atomic wave functions and quantum phase transitions in optical lattices*”, *Physical Review Letters* **107**, 175302 (2011).
- [46] G. Birkl, M. Gatzke, I.H. Deutsch, S.L. Rolston, W.D. Phillips, “*Bragg scattering from atoms in optical lattices*”, *Physical Review Letters* **75**, 2823 (1995).
- [47] M. Weidemüller, A. Hemmerich, A. Görlitz, T. Esslinger, T.W. Hänsch, “*Bragg diffraction in an atomic lattice bound by light*”, *Physical Review Letters* **75**, 4583 (1995).

- [48] J. Ye, J.M. Zhang, W.M. Liu, K. Zhang, Y. Li, W. Zhang, “*Light-scattering detection of quantum phases of ultracold atoms in optical lattices*”, *Physical Review A* **83**, 051604 (2011).
- [49] J.S. Douglas, K. Burnett, “*Light scattering from ultracold atomic gases in optical lattices at finite temperature*”, *Physical Review A* **84**, 033637 (2011).
- [50] S. Slama, C. von Cube, M. Kohler, C. Zimmermann, P.W. Courteille, “*Multiple reflections and diffuse scattering in Bragg scattering at optical lattices*”, *Physical Review A* **73**, 023424 (2006).
- [51] C. Weitenberg, P. Schauß, T. Fukuhara, M. Cheneau, M. Endres, I. Bloch, S. Kuhr, “*Coherent light scattering from a two-dimensional Mott insulator*”, *Physical Review Letters* **106**, 215301 (2011).
- [52] I.B. Mekhov, C. Maschler, H. Ritsch, “*Cavity-enhanced light scattering in optical lattices to probe atomic quantum statistics*”, *Physical Review Letters* **98**, 100402 (2007).
- [53] I.B. Mekhov, C. Maschler, H. Ritsch, “*Probing quantum phases of ultracold atoms in optical lattices by transmission spectra in cavity quantum electrodynamics*”, *Nature Physics* **3**, 319 (2007).
- [54] I.B. Mekhov, C. Maschler, H. Ritsch, “*Light scattering from ultracold atoms in optical lattices as an optical probe of quantum statistics*”, *Physical Review A* **76**, 053618 (2007).
- [55] W. Chen, D. Meiser, P. Meystre, “*Cavity QED determination of atomic number statistics in optical lattices*”, *Physical Review A* **75**, 023812 (2007).
- [56] R. Landig, F. Brennecke, R. Mottl, T. Donner, T. Esslinger, “*Measuring the dynamic structure factor of a quantum gas undergoing a structural phase transition*”, *Nature Communications* **6**, 7046 (2015).
- [57] S. Rajaram, N. Trivedi, “*Photon counting as a probe of superfluidity in a two-band Bose-Hubbard system coupled to a cavity field*”, *Physical Review Letters* **111**, 243603 (2013).
- [58] M.J. Bhaseen, M. Hohenadler, A.O. Silver, B.D. Simons, “*Polaritons and pairing phenomena in Bose-Hubbard mixtures*”, *Physical Review Letters* **102**, 135301 (2009).

- [59] H. Zoubi, H. Ritsch, “*Quantum phases of bosonic atoms with two levels coupled by a cavity field in an optical lattice*”, *Physical Review A* **80**, 053608 (2009).
- [60] A.O. Silver, M. Hohenadler, M.J. Bhaseen, B.D. Simons, “*Bose-Hubbard models coupled to cavity light fields*”, *Physical Review A* **81**, 023617 (2010).
- [61] T.L. Dao, C. Kollath, I. Carusotto, M. Köhl, “*All-optical pump-and-probe detection of two-time correlations in a Fermi gas*”, *Physical Review A* **81**, 043626 (2010).
- [62] Q. Niu, I. Carusotto, A.B. Kuklov, “*Imaging of critical correlations in optical lattices and atomic traps*”, *Physical Review A* **73**, 053604 (2006).
- [63] S.N. Sanders, F. Mintert, E.J. Heller, “*Matter-wave scattering from ultracold atoms in an optical lattice*”, *Physical Review Letters* **105**, 035301 (2010).
- [64] K. Mayer, A. Rodriguez, A. Buchleitner, “*Matter-wave scattering from interacting bosons in an optical lattice*”, *Physical Review A* **90**, 023629 (2014).
- [65] R.H. Dicke, “*Coherence in spontaneous radiation processes*”, *Physical Review* **93**, 99 (1954).
- [66] N.E. Rehler, J.H. Eberly, “*Superradiance*”, *Physical Review A* **3**, 1735 (1971).
- [67] M.O. Scully, E.S. Fry, C.H.R. Ooi, K. Wódkiewicz, “*Directed spontaneous emission from an extended ensemble of  $N$  atoms: timing is everything*”, *Physical Review Letters* **96**, 010501 (2006).
- [68] M.O. Scully, “*Correlated spontaneous emission on the Volga*”, *Laser Physics* **17**, 635 (2007).
- [69] E.A. Sete, A.A. Svidzinsky, H. Eleuch, Z. Yang, R.D. Nevels, M.O. Scully, “*Correlated spontaneous emission on the Danube*”, *Journal of Modern Optics* **57**, 1311 (2010).
- [70] H.J. Lipkin, “*Coherent effects in transitions between states containing several nuclear excitons*” in *Multiple Facets of Quantization and Supersymmetry*, edited by M. Olshanetsky and A. Vainshtein (World Scientific, Singapore, 2002), pp. 128–150.

- [71] R. Wiegner, J. von Zanthier, G.S. Agarwal, “*Quantum-interference-initiated superradiant and subradiant emission from entangled atoms*”, *Physical Review A* **84**, 023805 (2011).
- [72] R.A. de Oliveira, M.S. Mendes, W.S. Martins, P.L. Saldanha, J.W.R. Tabosa, D. Felinto, “*Single-photon superradiance in cold atoms*”, *Physical Review A* **90**, 023848 (2014).
- [73] E. Akkermans, A. Gero, R. Kaiser, “*Photon localization and Dicke superradiance in atomic gases*”, *Physical Review Letters* **101**, 103602 (2008).
- [74] M.O. Scully, M.S. Zubairy, *Quantum Optics* (Cambridge University Press, Cambridge, 1997).
- [75] J.J. Sakurai, S.F. Tuan, *Modern Quantum Mechanics* (Addison-Wesley Pub. Co., Reading, Massachusetts, 1994).
- [76] R.J. Bettles, S.A. Gardiner, C.S. Adams, “*Cooperative ordering in lattices of interacting two-level dipoles*”, *Physical Review A* **92**, 063822 (2015).
- [77] S.L. Bromley, B. Zhu, M. Bishof, X. Zhang, T. Bothwell, J. Schachenmayer, T.L. Nicholson, R. Kaiser, S.F. Yelin, M.D. Lukin et al., “*Collective atomic scattering and motional effects in a dense coherent medium*”, *Nature Communications* **7**, 11039 (2016).
- [78] K.I. Petsas, A.B. Coates, G. Grynberg, “*Crystallography of optical lattices*”, *Physical Review A* **50**, 5173 (1994).
- [79] L. Santos, M.A. Baranov, J.I. Cirac, H.U. Everts, H. Fehrmann, M. Lewenstein, “*Atomic quantum gases in Kagomé lattices*”, *Physical Review Letters* **93**, 030601 (2004).
- [80] L.D. Landau, E.M. Lifshitz, *Quantum Mechanics: Non-Relativistic Theory*, Vol. 3, 3rd ed. (Pergamon Press, Oxford, 1977).
- [81] G.F. Gribakin, V.V. Flambaum, “*Calculation of the scattering length in atomic collisions using the semiclassical approximation*”, *Physical Review A* **48**, 546 (1993).
- [82] F. Bloch, “*Über die Quantenmechanik der Elektronen in Kristallgittern*”, *Zeitschrift für Physik* **52**, 555 (1929).

- [83] N.W. Ashcroft, N.D. Mermin, *Solid State Physics* (Harcourt College Publishers, Orlando, 1976).
- [84] C.J. Halboth, W. Metzner, “*Fermi surface of the 2D Hubbard model at weak coupling*”, *Zeitschrift für Physik B Condensed Matter* **102**, 501 (1997).
- [85] M.C. Gutzwiller, “*Effect of correlation on the ferromagnetism of transition metals*”, *Physical Review Letters* **10**, 159 (1963).
- [86] F. Queisser, K.V. Krutitsky, P. Navez, R. Schützhold, “*Equilibration and prethermalization in the Bose-Hubbard and Fermi-Hubbard models*”, *Physical Review A* **89**, 033616 (2014).
- [87] G.C. Wick, “*The evaluation of the collision matrix*”, *Physical Review* **80**, 268 (1950).
- [88] T.S. Evans, D.A. Steer, “*Wick’s theorem at finite temperature*”, *Nuclear Physics B* **474**, 481 (1996).
- [89] M. Abramowitz, I.A. Stegun, *Handbook of Mathematical Functions with Formulas, Graphs, and Mathematical Tables* (U.S. Govt. Print. Off., Washington, 1964).
- [90] L.D. Landau, E.M. Lifshitz, *Statistical Physics, Part 1*, Vol. 5, 3rd ed. (Pergamon Press, Oxford, 1980).
- [91] C.K.N. Patel, “*Continuous-wave laser action on vibrational-rotational transitions of CO<sub>2</sub>*”, *Physical Review* **136**, A1187 (1964).
- [92] W.B. Bridges, “*Laser oscillation in singly ionized argon in the visible spectrum*”, *Applied Physics Letters* **4**, 128 (1964).
- [93] S. Inouye, M.R. Andrews, J. Stenger, H.J. Miesner, D.M. Stamper-Kurn, W. Ketterle, “*Observation of Feshbach resonances in a Bose-Einstein condensate*”, *Nature* **392**, 151 (1998).
- [94] D.M. Stamper-Kurn, M.R. Andrews, A.P. Chikkatur, S. Inouye, H.J. Miesner, J. Stenger, W. Ketterle, “*Optical confinement of a Bose-Einstein condensate*”, *Physical Review Letters* **80**, 2027 (1998).

- [95] T. Volz, N. Syassen, D.M. Bauer, E. Hansis, S. Dürr, G. Rempe, “*Preparation of a quantum state with one molecule at each site of an optical lattice*”, *Nature Physics* **2**, 692 (2006).
- [96] S.A. Moses, J.P. Covey, M.T. Miecnikowski, B. Yan, B. Gadway, J. Ye, D.S. Jin, “*Creation of a low-entropy quantum gas of polar molecules in an optical lattice*”, *Science* **350**, 659 (2015).
- [97] D.N. Zubarev, “*Double-time Green functions in statistical physics*”, *Soviet Physics Uspekhi* **3**, 320 (1960).
- [98] V.L. Berezinskii, “*New model of the anisotropic phase of superfluid He<sup>3</sup>*”, *JETP Letters* **20**, 287 (1974).